

## Radon transport in sand : a laboratory study

**Citation for published version (APA):**

Spoel, van der, W. H. (1998). *Radon transport in sand : a laboratory study*. [Phd Thesis 1 (Research TU/e / Graduation TU/e), Applied Physics and Science Education]. Technische Universiteit Eindhoven.  
<https://doi.org/10.6100/IR508320>

**DOI:**

[10.6100/IR508320](https://doi.org/10.6100/IR508320)

**Document status and date:**

Published: 01/01/1998

**Document Version:**

Publisher's PDF, also known as Version of Record (includes final page, issue and volume numbers)

**Please check the document version of this publication:**

- A submitted manuscript is the version of the article upon submission and before peer-review. There can be important differences between the submitted version and the official published version of record. People interested in the research are advised to contact the author for the final version of the publication, or visit the DOI to the publisher's website.
- The final author version and the galley proof are versions of the publication after peer review.
- The final published version features the final layout of the paper including the volume, issue and page numbers.

[Link to publication](#)

**General rights**

Copyright and moral rights for the publications made accessible in the public portal are retained by the authors and/or other copyright owners and it is a condition of accessing publications that users recognise and abide by the legal requirements associated with these rights.

- Users may download and print one copy of any publication from the public portal for the purpose of private study or research.
- You may not further distribute the material or use it for any profit-making activity or commercial gain
- You may freely distribute the URL identifying the publication in the public portal.

If the publication is distributed under the terms of Article 25fa of the Dutch Copyright Act, indicated by the "Taverne" license above, please follow below link for the End User Agreement:

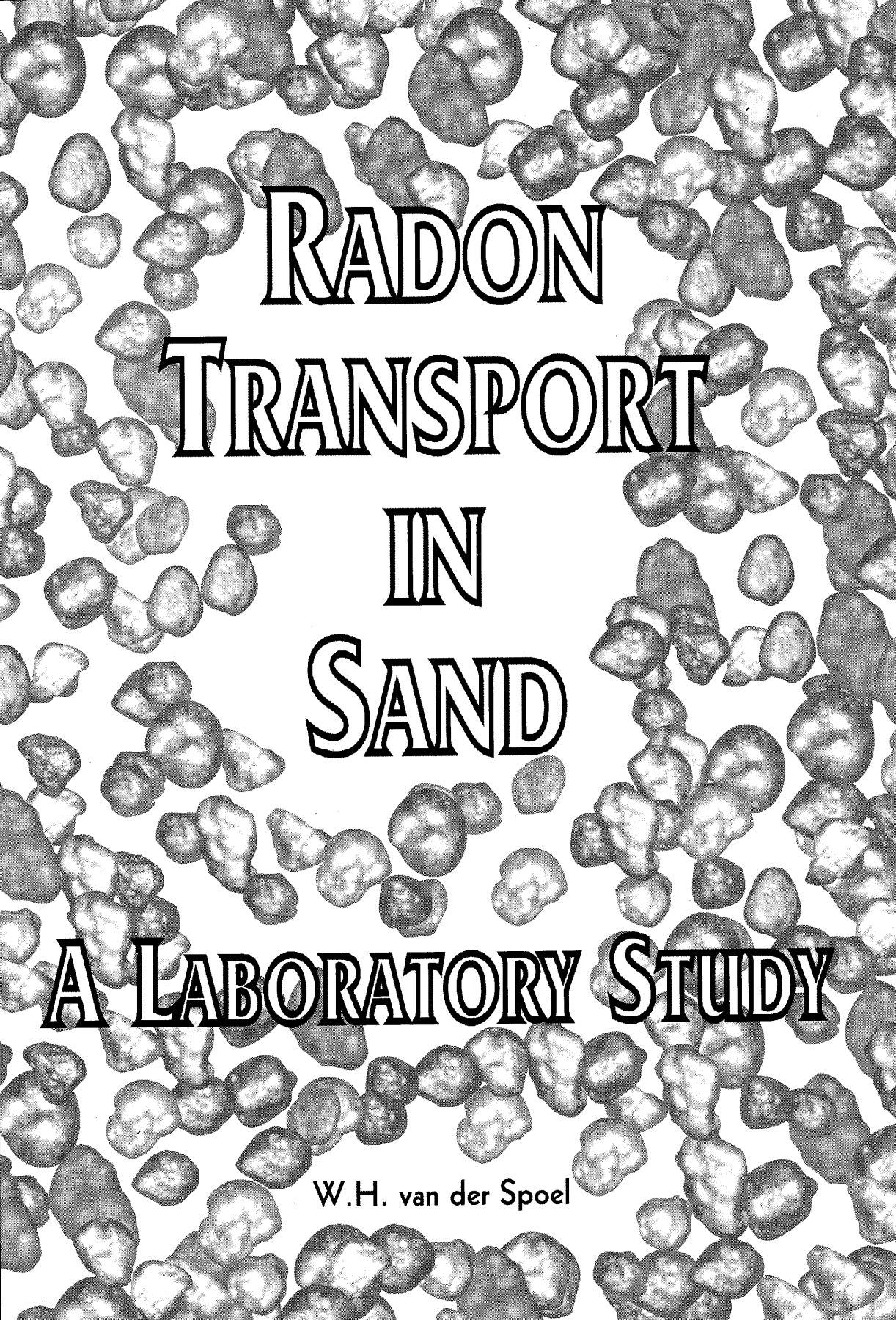
[www.tue.nl/taverne](http://www.tue.nl/taverne)

**Take down policy**

If you believe that this document breaches copyright please contact us at:

[openaccess@tue.nl](mailto:openaccess@tue.nl)

providing details and we will investigate your claim.

The background of the entire cover is a dense, grayscale microscopic image of sand grains. The grains are irregular in shape, ranging from small, rounded particles to larger, more angular and elongated ones. They are distributed throughout the frame, creating a textured, granular appearance. The lighting highlights the three-dimensional nature of the grains, with some appearing brighter and others in shadow.

**RADON  
TRANSPORT  
IN  
SAND**

**A LABORATORY STUDY**

W.H. van der Spoel

Radon Transport in Sand:

A Laboratory Study

Omslag: Zandkorreltjes, vergroting ca. 50×

CIP-DATA LIBRARY TECHNISCHE UNIVERSITEIT EINDHOVEN

Spoel, Willem Hendrik van der

Radon transport in sand: a laboratory study / by

Willem Hendrik van der Spoel. -

Eindhoven: Technische Universiteit Eindhoven, 1998. -

Proefschrift. -

ISBN 90-386-0647-8

NUGI 812

Trefw.: radon / poreuze media; transportverschijnselen / zand

Subject headings: radon / flow through porous media /  
sand / radioactivity.

Omslagontwerp : Fred van Os

Drukkerij : Stichting drukkerij C. Regenboog, Groningen, 1998

This work was conducted as part of the research programme of the Environmental Radioactivity Research and Consultancy Group (ERG) of the Kernfysisch Versneller Instituut (KVI) and was jointly financed by the Commission of the European Communities (CEC) (nuclear fission safety programme), the Dutch Ministry of Housing, Physical Planning and Environmental Protection (VROM) and ERG (KVI).



# Radon Transport in Sand: A Laboratory Study

PROEFSCHRIFT

ter verkrijging van de graad van doctor aan de  
Technische Universiteit Eindhoven, op gezag van  
de Rector Magnificus, prof.dr. M. Rem, voor  
een commissie aangewezen door het College voor  
Promoties in het openbaar te verdedigen op  
maandag 23 maart 1998 om 16.00 uur

door

Willem Hendrik van der Spoel

geboren te Ridderkerk

Dit proefschrift is goedgekeurd door de promotoren:

prof.dr. R.J. de Meijer

en

prof.dr.ir. M.E.H. van Dongen

Copromotor:

dr. E.R. van der Graaf

# Contents

<b>1</b>	<b>Introduction</b>	<b>1</b>
1.1	Radon transport	5
1.2	On this thesis	7
<b>2</b>	<b>Mathematical description for radon transport in porous materials</b>	<b>11</b>
2.1	Premises and elementary definitions	11
2.2	Soil-gas transport	12
2.3	Radon transport	13
2.3.1	Radon generation and decay	13
2.3.2	Radon diffusion and advection	14
2.3.3	Multi-phase time-dependent radon transport	15
2.3.4	Boundary conditions	18
2.3.5	Diffusion length	18
<b>3</b>	<b>Numerical model</b>	<b>21</b>
3.1	Introduction	21
3.2	Numerical method	22
3.2.1	Radon transport	22
3.2.2	Soil-gas transport	27
3.2.3	Boundary conditions	28
3.2.4	Interface positioning	29
3.2.5	Model implementation	30
3.3	Model comparison	31
3.3.1	One-dimensional problem	31
3.3.2	Two-dimensional problem	34
<b>4</b>	<b>Experimental</b>	<b>37</b>
4.1	Introduction	37
4.2	Laboratory facility	37
4.3	Radon-concentration determination	41
4.4	Homogeneity of the sand column	42
4.5	Sand properties	44
4.5.1	Grain size, density and porosity	44
4.5.2	Tortuosity	46
4.5.3	Radium content	47
4.5.4	Radon adsorption and desorption	47
4.5.5	Radon emanation coefficient	50

<b>5</b>	<b>Diffusive transport experiments</b>	<b>57</b>
5.1	Introduction . . . . .	57
5.2	Sand conditions . . . . .	57
5.3	Analytical diffusion model . . . . .	58
5.4	Experiments without a 'crawl space' . . . . .	60
5.5	Experiments with a 'crawl space' . . . . .	63
5.6	Conclusions . . . . .	70
<b>6</b>	<b>Diffusive and advective transport experiments</b>	<b>73</b>
6.1	Introduction . . . . .	73
6.2	Experiments with downward advective transport . . . . .	73
6.2.1	Model description . . . . .	74
6.2.2	Results and discussion . . . . .	76
6.3	Experiments with upward advective transport . . . . .	77
6.3.1	Two-dimensional modelling . . . . .	78
6.4	Experiments with pulsated advective transport . . . . .	83
6.5	Conclusions . . . . .	89
<b>7</b>	<b>Experiments with a sheet of foil on the sand surface</b>	<b>91</b>
7.1	Introduction . . . . .	91
7.2	The polyethylene foil . . . . .	92
7.3	Vessel experiments . . . . .	95
7.3.1	Undamaged foil without a crawl space . . . . .	95
7.3.2	Undamaged foil with a ventilated crawl space . . . . .	96
7.3.3	Undamaged foil with suction of air from the sand . . . . .	101
7.3.4	Undamaged foil with supply of air to the sand . . . . .	102
7.3.5	Damaged foil with a ventilated crawl space . . . . .	104
7.3.6	Damaged foil with suction of air from the sand . . . . .	107
7.3.7	Damaged foil with supply of air to the sand . . . . .	108
7.4	Conclusions and discussion . . . . .	109
<b>8</b>	<b>Experiments with a ground-water level</b>	<b>113</b>
8.1	Introduction . . . . .	113
8.2	Water-retention characteristics . . . . .	114
8.3	Radon diffusion coefficient . . . . .	116
8.4	Sampling technique - influence of pore water . . . . .	119
8.5	Experiments with the radon vessel . . . . .	122
8.5.1	Model calculations: experiments with a rising water level . . . . .	124
8.5.2	Model calculations: experiments with a falling water level . . . . .	128
8.5.3	Discussion . . . . .	130
8.6	Conclusions . . . . .	133
<b>9</b>	<b>Assessment, conclusions and general discussion</b>	<b>135</b>
9.1	The vessel experiments with room-dry sand in retrospect: an assessment . . . . .	135
9.2	Conclusions . . . . .	137
9.2.1	Input parameters . . . . .	137
9.2.2	Experiments with room-dry sand . . . . .	138
9.2.3	Experiments with a ground-water level . . . . .	139
9.2.4	Experiments with a foil covering the sand surface . . . . .	140

---

9.2.5	Main findings . . . . .	141
9.3	General discussion . . . . .	142
9.4	Outlook and recommendations for future developments . . . . .	146
9.4.1	Identifying the source of indoor radon . . . . .	146
9.4.2	Basic research . . . . .	147
9.4.3	Radon mitigation . . . . .	148
<b>A</b>	<b>Time-dependent diffusive transport in a rectangle</b>	<b>151</b>
<b>B</b>	<b>The radon-transparency instrument: mathematical formalism</b>	<b>155</b>
B.1	Radon concentration . . . . .	155
B.2	Count rate . . . . .	158
B.2.1	Detection efficiencies . . . . .	159
	<b>Bibliography</b>	<b>161</b>
	<b>Publications</b>	<b>169</b>
	<b>Nederlandse samenvatting</b>	<b>171</b>
	<b>Curriculum vitae</b>	<b>179</b>
	<b>Nawoord</b>	<b>181</b>



# Chapter 1

## Introduction

Natural materials consist of a variety of elements, from the lightest element hydrogen to the heaviest element uranium. Some of these elements are radioactive part of which belong to one of the four natural occurring decay series namely that of uranium ( $^{238}\text{U}$ ), thorium ( $^{232}\text{Th}$ ), actinium ( $^{235}\text{U}$ ) or potassium ( $^{40}\text{K}$ ). In nature the heavy radionuclides generally exist in trace amounts, e.g. the average crustal abundance of  $^{238}\text{U}$  is about  $2.3\text{ mg kg}^{-1}$  ( $28\text{ Bq kg}^{-1}$ ) [Emsley, 1989]. The distribution of these radioactive elements in the solid crust of the earth is however far from homogeneous and depends mainly on the mineral composition of the rock. High concentrations occur for example in minerals such as zircon and monazite. In contrast to solid rock, sediments like sand, clay and gravel originate from a large area and therefore the distribution of heavy elements in these materials is more homogeneous. In the Netherlands, sand and clay are the most predominantly occurring soil types with  $^{238}\text{U}$  concentrations of typically  $5 - 50\text{ Bq kg}^{-1}$  [Ackers, 1985].

The decay series of  $^{238}\text{U}$  is shown in Fig. 1.1. Since most of the decay products are metals, they are chemically bound to the rock material. The only exception being radon ( $^{222}\text{Rn}$ ), produced in the alpha-decay of radium ( $^{226}\text{Ra}$ ). The rate at which radon is produced per unit mass of material depends on the activity concentration of  $^{226}\text{Ra}$ . The  $^{226}\text{Ra}$ -activity concentration equals the activity concentration of all the other radionuclides if the decay series is in secular equilibrium. This equilibrium of activities is reached after about five times the half live of the longest living decay product in a series and as long as none of the products escape the material. For the decay series of  $^{238}\text{U}$  one sees that secular equilibrium is reached after a few million years, determined by the half live of  $^{234}\text{U}$ . Since this condition is usually met for Dutch natural materials, their  $^{226}\text{Ra}$  activity concentrations are also of the order of  $5 - 50\text{ Bq kg}^{-1}$  ( $5 - 50$  radon atoms are formed per second per kg material).

In the decay of  $^{238}\text{U}$  and most of its decay products  $\alpha$ -particles (equivalent to a helium nucleus) are emitted, indicated by a horizontal arrow in Fig. 1.1. Other radionuclides emit  $\beta$  particles (electrons and positrons), as indicated by a diagonal arrow in Fig. 1.1. Not shown in the figure is  $\gamma$  radiation (photons with a distinct energy) emitted in most  $\alpha$ - and  $\beta$  decay in the  $^{238}\text{U}$  series. Generally, these  $\gamma$  rays are penetrating enough, as opposed to  $\alpha$  - and to a lesser extent  $\beta$  - radiation, to reach a detector positioned in the vicinity of a sample. The  $^{226}\text{Ra}$ -activity concentration is usually obtained by means of  $\gamma$ -ray spectroscopy. Since most  $\gamma$ -rays in the series are emitted in the decay of  $^{214}\text{Bi}$  (bismuth) and  $^{214}\text{Pb}$  (lead), the activity concentrations of these radionuclides are usually measured. As part of the radon may escape a porous material, a sample must be first sealed (such that radon remains inside) for at least three weeks to establish secular

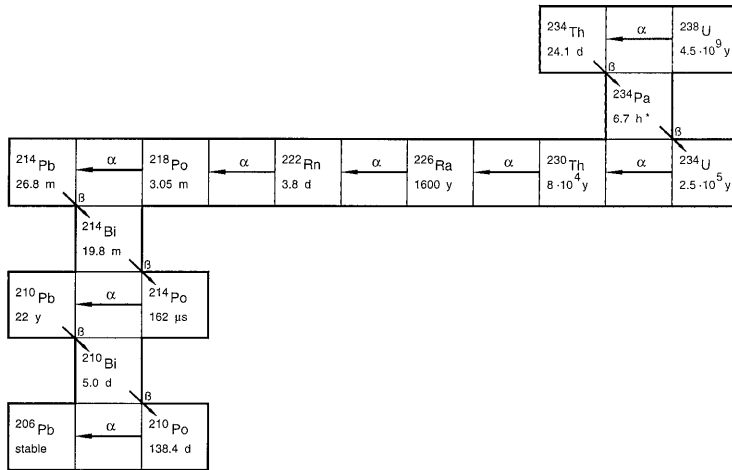


Figure 1.1: Simplified decay series of  $^{238}\text{U}$ . Only the highest abundances of the decay modes are shown.

equilibrium between  $^{226}\text{Ra}$  and its decay products (until  $^{210}\text{Pb}$ ) before the  $^{226}\text{Ra}$ -activity concentration can be obtained from  $\gamma$ -ray spectroscopy.

Radon, with a half-life of 3.825 days, is a noble gas. It is inert and hence has little affinity to get chemically bound. Upon being created in the decay of radium, the radon atom possesses a kinetic energy of 86 keV and travels a short distance before it is stopped. As rock and sediments generally have a porous structure, radon atoms may therefore also enter the pore space of the material<sup>1</sup>. In these pores, of which part is filled with a liquid (mixture) and the other part is filled with a gas (mixture), diffusion may transport radon over distances of typically 0.1 – 2 m before it decays. In addition, radon may also be carried along with a moving liquid or gas in the pores. This is usually called advective transport which may transfer radon over a wide range of distances, depending on the porosity (fraction of volume occupied by pores) and on the velocity of the moving fluid. It are these two transport processes, diffusion and advection in the pore-space of porous materials, which enable radon to escape from natural materials, viz. soil and porous building materials, into the earth's atmosphere and into the indoor environment.

Diffusion of radon, driven by radon concentration gradients, is most significant in the gas phase. The diffusion coefficient of radon in air ( $\approx 1.1 \cdot 10^{-5} \text{ m}^2 \text{ s}^{-1}$ ) is for example about  $10^4$  times larger than in water. As a result, the diffusion coefficient can vary over four orders of magnitude depending on the fraction of water saturation of the pores in a porous material. Advection, predominantly resulting from pressure-driven flow of pore gas, depends on the magnitude of pressure gradients and permeability (resistance to air-flow) of the material. The importance of advection with respect to diffusion can be large at even small pore-gas velocities. Suppose diffusion transports radon over 1 m during its half-life of nearly 4 days, then advective transport at a pore-air velocity of only

<sup>1</sup>Escape of radon from the solid material into the pore space is usually called radon emanation. The physical processes responsible for this escape are not fully understood yet. For Dutch building materials, typically 1%-25% of the radon atoms emanate into the pore space [Ackers, 1989].



1 cm per hour is of equal significance.

It should be remarked that, in addition to  $^{222}\text{Rn}$ , two other radon isotopes are produced in the other decay series. These are  $^{220}\text{Rn}$ , with a half-life of 55.6 s and originating from  $^{232}\text{Th}$ , and  $^{219}\text{Rn}$  with a half-life of 3.96 s and originating from  $^{235}\text{U}$ . Due to their short half-lives, the typical distances over which they are transported in porous materials is correspondingly shorter. As a result, their indoor and outdoor concentrations are usually much lower than for  $^{222}\text{Rn}$ . This thesis is restricted to  $^{222}\text{Rn}$  and therefore refers to this isotope if radon is mentioned in the text.

The radon concentration in the indoor environment can be high. Some decades ago, foreign surveys already indicated that the radon concentration in dwellings can be such that even the dose limits set for radiological workers is exceeded<sup>2</sup>. Triggered by these foreign surveys, the Dutch government initiated the research programme SAWORA (StralingsAspecten van WOonhygiëne en aanverwante Radiologische Aspecten; radiation aspects of domestic hygiene and related radiological aspects) in 1982 - 1986 which was aimed at determining the natural radiation background levels. The Dutch survey indicated an average indoor radon concentration<sup>3</sup> of  $22 \text{ Bq m}^{-3}$ , relatively low with respect to other countries, and an outdoor concentration of  $1\text{-}8 \text{ Bq m}^{-3}$ . Based on this result, it was estimated that 450-1800 fatal lung cancers per year occur due to radiation from radon progeny in the Netherlands [Vaas et al., 1991], mainly due to radon in the indoor environment.

Soil and porous building materials (mainly concrete) are considered to be major sources of indoor radon. The SAWORA programma indicated that radon in the crawl space originating from the soil (Dutch houses are commonly built with a crawl space) may be the most important source of indoor radon. This was based on the following findings [Put et al., 1986]:

- High radon concentrations were observed in some crawl spaces;
- Rooms at the first floor were found to have a lower radon concentration than those on the ground floor;
- No correlation between the indoor  $\gamma$ -activity and the radon concentration was found (this argument is only valid when the  $\gamma$ -activity is correlated with the radon exhalation rate of building materials); and
- Relative more dwellings with a high indoor radon concentration were found to be situated in areas with a higher outdoor radon concentration (i.e. higher radon exhalation rate from the soil).

The last finding is in accordance with earlier results obtained by Wolfs et al. [1984] who measured a strong correlation between the indoor and outdoor radon concentration in one particular dwelling. As the measurements during SAWORA were not sufficiently detailed for characterising the source of indoor radon, further research on radon transport, especially from the soil into dwellings, was recommended.

<sup>2</sup>The radioactive decay products of radon in air (rather than radon itself) are responsible for the health risk for humans. These progeny may adhere to particles in air that, in turn when inhaled, may attach to lung tissue. The smaller the particles, the deeper they penetrate the lung and the longer their residence time. The  $\alpha$ -particles, emitted in the decay of these radon progeny, damage the lung tissue and so may induce lung cancer.

<sup>3</sup>The initial value was  $29 \text{ Bq m}^{-3}$  but contained a systematic instrumental error of about  $7 \text{ Bq m}^{-3}$ .

The follow-up programme RENA (REguleerbare vormen van Natuurlijke Achtergrondstraling; controllable forms of natural background radiation) in 1987 - 1990 was directed at identifying sources, modelling of radon entry into houses and searching for means to lower radiation risks. Several dwellings with high radon concentrations were selected from the SAWORA database and investigated again, as well as (identical) nearby houses for comparison. These measurements showed that very high radon concentrations occur in the crawl space of houses with a high indoor radon concentration [Put, 1989]. It should be noted that, surprisingly, in one set of five houses in Maastricht a positive correlation between the crawl-space radon concentration (180 - 1060 Bq m<sup>-3</sup>) and the indoor radon concentration (30 - 80 Bq m<sup>-3</sup>) was observed, whereas a negative correlation was found in another set of five houses (crawl space: 620 - 750 Bq m<sup>-3</sup>, living room: 45 - 75 Bq m<sup>-3</sup>). As radon may easily flow through openings between the crawl space and the living room, the negative correlation may be caused by differences in leakage area of the ground floor. The role of the crawl space in the radon-infiltration process is however less clear in other studies involving houses with normal concentration levels. Measurements of the radon concentration in the crawl space and rooms on the ground - and first - floor in several houses in the city of Groningen revealed higher concentrations on the first floor than on the ground floor and in the crawl space [Van den Berg, 1990], clearly not in accordance with earlier observations.

As SAWORA indicated that radon entry into buildings is a complex problem in which many parameters play a role, also more detailed measurements were conducted to obtain a better insight in the problem. It was realised that short-term measurements (as opposed to long-term averages) were necessary to obtain more knowledge about the infiltration processes. In the framework of RENA, instruments were developed at the KVI (Kernfysisch Versneller Instituut) for measuring the (*in situ*) radon exhalation from materials and for measuring the time-dependent radon concentration in air in less than one-hour intervals. These instruments were applied in an extensive study on radon infiltration in a research house in Roden [Aldenkamp and Stoop, 1994]. In this study, time-varying and pressure-driven radon-source strengths, especially in the crawl space of the house, were observed. However, the nature of the processes responsible for the time-varying aspect could not be identified precisely. It was concluded that the understanding of the physical processes leading to pressure-dependent sources, both in soil and in building materials, remained partial and qualitative. It was therefore recommended to examine in even further detail the mechanisms that govern radon transport in porous media; in particular the dynamic processes. Also detailed studies outside the Netherlands have indicated that radon entry is a complicated process and that both diffusion and advection determine the radon concentration in houses [Åkerblom et al., 1984; Nero and Nazaroff, 1984; Nazaroff, 1988; Garbesi et al., 1993; Ward et al., 1993; Gadd and Borak, 1994; Arvela, 1995]. Generally, advective entry from the soil is believed to be the dominant transport mechanism in case high indoor radon concentrations are measured [Nazaroff, 1988; Garbesi and Sextro, 1989; Arvela, 1995; Ennemoser et al., 1995]. Since the source of indoor radon has not been fully characterised in such houses in the Netherlands, it is not clear whether this also accounts for the Dutch situation.

In this connection, it is interesting to mention that, despite the rather incomplete knowledge of radon infiltration into houses, it was estimated in 1991 that soil and building materials contribute about 60% (via infiltration) and 30% to the radon concentration in the living room, respectively [Vaas et al., 1991]. The remaining 10% comes from outdoor and largely originates from the soil as well. Policies that were developed within

the framework of the Dutch environmental policy plan (Nationaal Milieu Beleidsplan, NMP) for reducing the health risks of indoor radon were in a large part based on these estimated values. For this reason, the countermeasures for reducing the average radon concentration in houses mainly focussed on suppressing radon entry from the crawl space. Results of model calculations during the RENA programme [Van den Ham et al., 1991] showed that two cost-effective measures might be to increase the ventilation rate of the crawl space and/or to decrease the air permeability of the ground floor. In 1993 - 1994, in the framework of the research programme STRATEGO (STRALing TEen aanzien van de Gebouwde Omgeving; radiation in relation to buildings), the effectiveness of these two countermeasures has been investigated on a large scale (Stratego project 17). The average radon concentration in the (normally-ventilated) crawl space of 175 houses was found to be only  $43 \text{ Bq m}^{-3}$  [Schaap, 1996], in large contrast with the 'expected' value of  $300 \text{ Bq m}^{-3}$  [Bel, 1994]. It is therefore not so surprising that only a small (statistically insignificant) average reduction of radon concentration in the living rooms was measured for each countermeasure. If the average crawl-space radon concentration in the Netherlands is truly  $40 - 50 \text{ Bq m}^{-3}$ , this implies that only about 10% of the indoor radon concentration originates from the crawl space and that porous building materials are the major source of indoor radon. A recent investigation in houses built after 1984 indicates indeed a much larger contribution from building materials of about 70% and only 15% from the soil via the crawl space [RIVM, 1997]. The other 15% originates from outdoor. In addition, the survey indicated an average indoor radon concentration of  $29 \text{ Bq m}^{-3}$ , a rise of  $7 \text{ Bq m}^{-3}$  with respect to the value found for houses built before 1984 (SAWORA).

## 1.1 Radon transport

Whether the soil or building materials is the main contributor to indoor radon and whether advection is of importance, one of the prerequisites to predict and characterise radon entry rates into dwellings, and also to predict the effectiveness of possible countermeasures against radon infiltration, is a detailed and validated description of the mechanisms that govern radon transport in porous materials and into houses. In constructing such a description, the infiltration process may be considered to take place in two stages. As radon is formed inside a porous material and is transported through a network of pores in the material before it escapes (called radon exhalation) into a 'compartment' such as the living room, crawl space, cavity wall or outside, the transport of radon inside the porous material is often studied separately. After exhalation, radon may be transported with ventilation streams to other compartments, induced by e.g. temperature differences in a dwelling, wind effects and atmospheric pressure differences. These subjects usually comprise the second stage at which radon entry into houses is described. It should however be realised that in reality the two processes of radon transportation, i.e. inside and outside the porous material, are depending on each other and are varying in time. The eventual study and validation of radon transport in houses can therefore not be completely divided into these two components. On the other hand, as a first step in the validation process, one might study them independently and establish the necessary coupling at a later stage.

Next to a division with respect to pathways for radon transport, another subdivision can be made with regard to the research strategy. At one hand, validation of radon transport models may be carried out with *in situ* measurements. However, due to many influencing factors, this type of validation is difficult. Quantities that may influence

radon infiltration are, besides those given in the previous paragraph, concentration differences, volume and rate of ventilation of the crawl space, ground-water level, pore-water distribution, permeability, radium content and radon emanation coefficient of the porous material. It is not only hard to measure these quantities *in situ*, it is almost impossible to keep them constant during an experiment. Moreover, soil as it is found *in situ* is inhomogeneous due to mixing of different layers by geological and/or human activity, the influence of flora and fauna, etc. The complexity is even larger if one considers that diffusion is mainly governed by porosity but not strongly influenced by pore size or pore size distribution. Advection however is strongly dependent on pore size. Despite these difficulties, validation of radon transport models has mainly been attempted with measurements in complex situations [Schery et al., 1984; Garbesi et al., 1993; Aldenkamp and Stoop, 1994; Andersen et al., 1994; Robinson and Sextro, 1995]. With this method significant discrepancies were found between description and experiment. Tracing the causes of these discrepancies is difficult for such *in situ* situations since, as mentioned before, the number of (uncontrollable and time-varying) parameters that may have their influence is large. For example, results of experiments with test structures for identifying and characterising radon entry [Garbesi et al., 1993; Andersen et al., 1994; Robinson and Sextro, 1995], although well characterised, show that model calculations underestimate soil-gas entry rates. The cause of this is probably related to inhomogeneities and disturbances (cracks) of the surrounding soil, and also pressure-driven flow due to wind effects. Other studies show a better agreement between experiment and model, e.g. a study by Nielson et al. [1994] concerned a comparison of their RAETRAD model for steady-state radon transport with experiments at two test-cell structures. Their model calculations agreed within 20% with mean values of the measurements. However, several parameters in the radon-transport equations had to be estimated for some construction materials and gaps present in the test structures. A good agreement between model and experiment for field measurements was obtained by Clements and Wilkening [1974]. But, also in this study some parameters used in the model calculations had to be estimated<sup>4</sup>. One may therefore argue that a complete validation of the models was still not obtained.

At the other hand, to avoid many of the problems discussed above, validation may be conducted under well defined and controlled conditions. This approach constitutes the main basis for the study presented in this thesis. Therefore, a laboratory facility was built [Van der Graaf et al., 1992] which consists of a large cylindrical vessel<sup>5</sup> (height and diameter 2 m) homogeneously filled with sand with radially inserted measuring probes that allow measurement of radon concentrations in the pore gas at various depths under the sand surface. The vessel can be closed by lowering a stainless steel lid into a water filled moat surrounding the upper part of the vessel. The space under the lid above the sand simulates a crawl space.

In addition, a nearly one-dimensional air-flow pattern can be induced in the sand column. The situation under a house is then simulated where the crawl space is at a lower pressure than outside (generally caused by a temperature difference between in- and outdoor). Such a pressure difference may induce an air-flow through the soil from outside into the crawl space. The dynamic behaviour of the radon-source strength in the crawl space of the research house in Roden is largely believed to be caused by such an air-flow

<sup>4</sup>In addition to the field measurements, Clements and Wilkening [1974] obtained convincing experimental verification of the model with a laboratory set-up that consisted of a column of <sup>226</sup>Ra bearing sand. However, only a few experiments with this set-up are described in their paper.

<sup>5</sup>Throughout this thesis, the laboratory facility is frequently referred to as 'the radon vessel' or 'the vessel'.

[Aldenkamp and Stoop, 1994].

The framework of the validation process is schematically shown in Fig. 1.2. Starting from a well known initial condition (simple geometry and soil type, no ground water and no lid on the vessel) the complexity of the situation is increased step by step. After each step a series of measurements are carried out and the results are compared with transport model calculations. Only when the models satisfactorily describe the measured radon concentrations, the complexity is increased. In case of discrepancies between models and measurements, the models should be adjusted or extended. The advantage of this strategy is that experiment and model are being compared after each step, in which only one parameter is varied. With this procedure the cause

of possible discrepancies is traceable and it is clear where to focus on in the modelling. In addition, another advantage is that after each step a model with a well-known domain of validity becomes available. An important aspect concerns the determination of the parameters needed for modelling radon transport in the vessel. As outlined before, there are many influencing parameters such as porosity, pore-water content, permeability, diffusion coefficient etc. It is emphasized that all these quantities were determined from *independent* experiments. In other words, the radon-vessel experiments were not used to derive any of the involving parameters.

As soil was previously considered to be the major contributor to indoor radon in the Netherlands, the radon vessel was specifically designed to simulate radon transport in soil under a crawl-space house. The main objective of the study is however to validate a description of radon transport in porous materials. Since sand is less complex than building materials, the study of sand is an initial step to investigate building materials in a later stage. With regard to the earlier made subdivision, it is emphasized that this study is limited to research on radon transport inside porous materials. The other part of the infiltration process that should be taken into account when a complete house is considered, i.e. exchange of radon between compartments and related topics, see e.g. Aldenkamp and Stoop [1994], is only dealt with sideways.

## 1.2 On this thesis

In chapter 2 of this thesis the physics of radon transport in porous materials is outlined. The derivation is made such that the mathematical equations remain applicable for multi-phase transport in inhomogeneous media. In this respect, the description is 'broader' than necessary to account for the transport phenomena studied with the radon vessel. This presentation is nevertheless chosen to leave the possibility open of examining the sensitivity of the model calculations to certain parameters which, for example, at first instance are believed to have a negligible influence in the radon vessel. Similar descriptions have earlier been presented by others. The presentation has however been customized

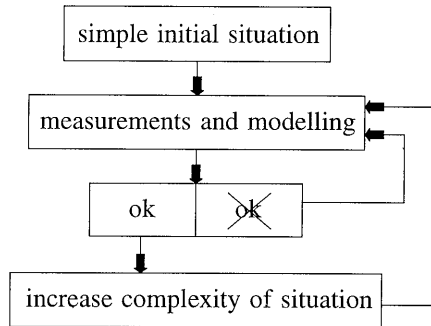


Figure 1.2: The framework of the research strategy.

according to personal preferences and a description for transient radon adsorption to solid surfaces has been included.

In the validation process, measured concentrations in the vessel are compared with expected concentrations according to the transport model. In some cases, the expected values can be obtained from an analytical solution of the applying differential equation. However, in those circumstances in which an analytical solution becomes extremely difficult to find, numerical simulations are necessary for calculating the expected concentrations. As such cases occur in this study, a two-dimensional numerical model for time-dependent radon transport is discussed in chapter 3.

Chapter 4 covers the experimental methods and techniques. The laboratory facility is described in detail, as well as procedures for measuring radon concentrations in the vessel. As mentioned, the radon-transport parameters of the sand were measured independently. These additional experiments are described in this chapter as well. Since the emphasis is on (relatively-)dry sand, chapter 4 forms more or less the basis for the vessel experiments with dry sand discussed in the following two chapters. The determination of radon-transport parameters necessary for modelling transport with moisturised sand are discussed in chapter 8 that is fully dedicated to the influence of pore water.

The research with the vessel started with studying pure diffusive transport in dry sand without the lid on the vessel. This corresponds to the most simple conditions that can be investigated because the boundary conditions are simple and well known. Thereafter, the complexity was slightly increased by conducting similar experiments with the lid installed at several different heights on the vessel (simulating a crawl space). Finally, the effect of forced ventilation of the crawl space was investigated. The results of these experiments and the comparison with analytical model calculations are discussed in chapter 5.

Experiments with combined diffusive and advective transport in dry sand constitute the following logical step in the validation process and are discussed in chapter 6. Also in this chapter a subdivision is made with regard to the complexity of the situation. In one case, the transport processes can be described analytically and are therefore presented first. In the other experiments two-dimensional radon transport takes place, meaning that application of the numerical model becomes expedient. Finally, experiments with time-dependent advective transport are discussed. As different instruments were used for measuring the rapidly changing radon concentrations, the experimental techniques are briefly presented as well.

Next, a technique for reducing radon entry into the crawl space has been investigated. In the technique, the crawl space floor is covered with a membrane which acts as a barrier for radon transport from the soil into the crawl space. *In situ* studies have shown that predicting the effectiveness of foil coverage in reducing the radon entry is hampered by uncertainties in the radon-transport parameters of the underlying soil and by unidentified transport through or along the membrane [Nazaroff and Doyle, 1985; Andersen et al., 1996]. To reduce the uncertainties in modelling the effectiveness of such a membrane-based technique, experiments have been made with the radon vessel in which the sand column is covered with a sheet of polyethylene foil. These experiments are described in chapter 7.

The experiments with a ground-water level set at various heights in the radon vessel are discussed in chapter 8. Introduction of water to the pore space of the sand largely increases the complexity for radon transport because several input parameters are influenced by the presence of pore water. Because this influence depends on the fraction of water saturation of the pores, additional experiments were conducted to determine this

dependence. In addition, the method to assess the water-content distribution in the sand is outlined in chapter 8. Although only experiments with pure diffusive transport were studied and so only one-dimensional transport occurred, the measured concentrations are compared with numerical calculations. The dependence of several transport parameters on the height in the sand column requires this type of modelling.

In chapter 9 the results with the vessel are reviewed and discussed. Recommendations for future research are presented as well. The results of this work are discussed in a broader framework like building materials and applicability in 'real' houses.





## Chapter 2

# Mathematical description for radon transport in porous materials

In this chapter, the mathematical equations for radon transport in isotropic porous materials will be derived and discussed. The description is made for a three-phase system, i.e. for a porous medium containing a solid, liquid and gas phase. Although most experiments with the radon vessel were performed with dry sand, this approach is chosen because the equations for dry porous media form a subset of the more complex description for a three-phase system. Similar descriptions for multi-phase radon transport have been used by Rogers and Nielson [1991b, 1993] and Andersen [1992].

This chapter contains three sections. Elementary soil quantities that are used in the description of radon transport are given in section 2.1, followed by a derivation of the soil-gas transport equation in section 2.2. The equation for radon transport which includes the four basic processes of radon generation, decay, diffusion and advection is derived in section 2.3.

### 2.1 Premises and elementary definitions

In this chapter, soil is considered to consist of three phases, i.e. solid, water and air phase. In principle, radon transport in porous media may be described on a microscopic level, focussing on transport within one phase on a scale smaller than the soil grains. This approach, however, requires an exact description of the geometrical configuration on a microscopical level. Since such a description is very complex to develop and since we are more interested in measurable quantities that only vary on a macroscopic scale, the transport problem is transformed from the microscopic level to a macroscopic one conform the so-called 'continuum approach' [Bear, 1991]. A full delineation of the method is beyond the scope of this thesis, so the discussion of the method will be confined to basic elements that are necessary or useful in the description of a macroscopical model for radon transport in porous media.

In the macroscopical approach, a Representative Elementary soil Volume (REV)  $\delta V$  ( $\text{m}^3$ ) is defined that may be considered as the sum of contributions from the volumes ( $\delta V_s$ ,  $\delta V_w$ ,  $\delta V_a$ ) of the solid, water and air phase, respectively:

$$\delta V = \delta V_s + \delta V_w + \delta V_a. \quad (2.1)$$

The size of a REV must be such that volumetric averages are statistically meaningful. On the other hand, the REV should be small enough as to prevent smearing or smoothing of

details and variations within a porous domain that may be of interest. In the continuum approach, quantities such as pore-air radon-activity concentration, porosity, water content etc. are averaged over  $\delta V$ , and assigned to a point  $(x, y, z)$  centred at  $\delta V$ .

The volume of pore space  $\delta V_p$  within the REV may be subdivided into three components, denoting pore space occupied by interconnected pores ( $\delta V_{cp}$ ), dead-end pores ( $\delta V_{dp}$ ) and isolated pores ( $\delta V_{ip}$ ):

$$\delta V_p = \delta V_{cp} + \delta V_{dp} + \delta V_{ip} = \delta V_w + \delta V_a. \quad (2.2)$$

In addition, the porosity  $\epsilon$ , air-filled porosity  $\epsilon_a$  and water-filled porosity  $\epsilon_w$ , are defined as:

$$\epsilon = \frac{\delta V_p}{\delta V}; \quad (2.3)$$

$$\epsilon_a = \frac{\delta V_a}{\delta V}; \quad (2.4)$$

$$\epsilon_w = \frac{\delta V_w}{\delta V}. \quad (2.5)$$

$$(2.6)$$

The fraction of water saturation of the pores,  $m$ , is defined as:

$$m = \frac{\epsilon_w}{\epsilon}. \quad (2.7)$$

## 2.2 Soil-gas transport

Gases in soil can be displaced by bulk movement of the soil-air phase in response to differences in air pressure. These pressure differences can be induced by wind, rainfall, temperature and ventilation effects. In this work it is assumed that soil gas only moves in response to pressure differences imposed at the boundaries (this may be regarded as ventilation). Besides, for modelling purposes, it is also easier to work in terms of a pressure field (resembles a velocity potential) rather than in terms of the velocity components. For the pressure gradients applied in the radon vessel ( $< 10 \text{ Pa m}^{-1}$ ), Darcy's Law [Darcy, 1856] may be used to describe gas flow in a porous medium:

$$\vec{q} = -\frac{K}{\mu}(\nabla P_a - \rho_a \vec{g}) \quad (2.8)$$

where

- $\vec{q}$  = bulk flux density of soil gas ( $\text{m}^3 \text{m}^{-2} \text{s}^{-1}$ );
- $K$  = intrinsic permeability ( $\text{m}^2$ );
- $\mu$  = dynamic viscosity of air ( $1.83 \cdot 10^{-5} \text{ Pa s}$ , at  $T = 293 \text{ K}$ );
- $P_a$  = air pressure (Pa);
- $\rho_a$  = density of air ( $\text{kg m}^{-3}$ ); and
- $\vec{g}$  = acceleration of gravity ( $\text{m s}^{-2}$ ).

By introducing the symbol  $P$  for the pressure disturbance field, defined by  $\nabla P = \nabla P_a - \rho_a \vec{g}$ , Eq. 2.8 can be written as

$$\vec{q} = -\frac{K}{\mu} \nabla P. \quad (2.9)$$

Substitution of this equation into the equation of continuity for gas flow through a porous medium [Bird et al., 1960],

$$\epsilon_a \frac{\partial \rho_a}{\partial t} = -\nabla \cdot (\rho_a \vec{q}), \quad (2.10)$$

and assuming a constant air density (i.e.  $\rho_a$  independent of  $P$ , valid in our case because the pressure differences are less than 0.02% of atmospheric pressure), the continuity equation 2.10 can be simplified to

$$\nabla \cdot \left( \frac{K}{\mu} \nabla P \right) = 0. \quad (2.11)$$

## 2.3 Radon transport

### 2.3.1 Radon generation and decay

Radon ( $^{222}\text{Rn}$ ) is formed in the decay of its parent: radium ( $^{226}\text{Ra}$ ). In general, radium may be present in both solid material and in the liquid (water) phase. However, for the sand present in the radon vessel, it is justified to assume that radium is only present in the solid grains because so-called leaching of radium (i.e. radium transport from the solid to the liquid phase) has not been observed in our experiments. Therefore, production of radon in the liquid phase is neglected in this chapter.

First, radon production and decay in the REV  $\delta V$  are considered. The rate of change of the number of radon atoms within  $\delta V$ ,  $\frac{dN^{Rn}}{dt}$ , is determined by radon decay and generation of radon in the decay of radium present in  $\delta V_s$ . Since the radium activity per unit solid volume is given by  $\rho_s C^{Ra}$  ( $\text{Bq m}^{-3}$ ), where  $\rho_s$  ( $\text{kg m}^{-3}$ ) is the density of the solid phase and  $C^{Ra}$  ( $\text{Bq kg}^{-1}$ ) is the radium activity per unit mass, the following relation is obtained:

$$\frac{dN^{Rn}}{dt} = -\lambda N^{Rn} + \rho_s C^{Ra} \delta V_s, \quad (2.12)$$

where  $\lambda$  ( $\text{s}^{-1}$ ) is the decay constant of radon. Using the relation  $\delta V_s = (1 - \epsilon)\delta V$  and  $(1 - \epsilon)\rho_s = \rho_b$ , where  $\rho_b$  ( $\text{kg m}^{-3}$ ) is the bulk density of dry material, Eq. 2.12 can be written as:

$$\frac{dN^{Rn}}{dt} = -\lambda N^{Rn} + \rho_b C^{Ra} \delta V. \quad (2.13)$$

To find the rate of change of the number of radon atoms in the *air-filled* pore space within  $\delta V$ ,  $\frac{dN_a^{Rn}}{dt}$ , one needs to consider that only a fraction of the radon produced in the solid material will escape (emanate) into the pore-air space. Introducing the symbol  $\eta_a$  ( $0 \leq \eta_a \leq 1$ ) for the coefficient of emanation into the air-filled pore space, Eq. 2.13 can be transformed into

$$\frac{dN_a^{Rn}}{dt} = -\lambda N_a^{Rn} + \eta_a \rho_b C^{Ra} \delta V. \quad (2.14)$$

Multiplying this equation with  $\lambda$  and using the relation

$$C_a = \frac{\lambda N_a^{Rn}}{\delta V_a} = \frac{\lambda N_a^{Rn}}{\epsilon_a \delta V}, \quad (2.15)$$

where  $C_a$  ( $\text{Bq m}^{-3}$ ) is the radon-activity concentration in the air-filled pore space within  $\delta V$ , results in

$$\epsilon_a \frac{dC_a}{dt} = -\epsilon_a \lambda C_a + \eta_a \rho_b \lambda C^{Ra}. \quad (2.16)$$

The equation for radon generation and decay in the *water-filled* pore space can be derived in the same manner, and is given by

$$\epsilon_w \frac{dC_w}{dt} = -\epsilon_w \lambda C_w + \eta_w \rho_b \lambda C^{Ra}, \quad (2.17)$$

where  $C_w$  ( $\text{Bq m}^{-3}$ ) is the radon-activity concentration in the water-filled pore space:

$$C_w = \frac{\lambda N_w^{Rn}}{\delta V_w} = \frac{\lambda N_w^{Rn}}{\epsilon_w \delta V}, \quad (2.18)$$

and  $\eta_w$  is the fraction of radon atoms that emanates into the water-filled pore space ( $0 \leq \eta_w \leq 1$ ;  $0 \leq \eta_a + \eta_w \leq 1$ ).

Finally, radon may be adsorbed to the solid surfaces of the soil grains. The balance equation for adsorbed radon is given by

$$\rho_b \frac{dC_s}{dt} = -\rho_b \lambda C_s + \eta_s \rho_b \lambda C^{Ra}, \quad (2.19)$$

where  $C_s$  ( $\text{Bq kg}^{-1}$ ) is the adsorbed radon activity per unit dry mass (note that previous definitions of radon-activity concentration refer to bulk volume instead of mass) and  $\eta_s$  is the fraction of radon atoms that directly emanate into the 'adsorbed phase'.

### 2.3.2 Radon diffusion and advection

Diffusion in isotropic media is based on Fick's law which states that the rate of transfer of a diffusing substance through a unit area is proportional to the concentration gradient normal to this area. In terms of the bulk diffusive-flux density of radon activity in the air-filled pore space,  $\vec{j}_{d,a}$  ( $\text{Bq m}^{-2} \text{s}^{-1}$ ), we may write:

$$\vec{j}_{d,a} = -\epsilon_a \tau_a D_a \nabla C_a, \quad (2.20)$$

where the superscript  $d$  is a reference to diffusion,  $D_a$  ( $\approx 1.1 \cdot 10^{-5} \text{ m}^2 \text{ s}^{-1}$ ) is the diffusion coefficient for radon in air, and  $\tau_a$  is the tortuosity for transport in the air phase. The latter is an empirical factor that accounts for the fact that the flow channels are not straight, the pore cross-section vary and also for the presence of dead-end and isolated pores. Note that some others use the inverse value,  $\tau_a^{-1}$ , for the tortuosity [Nazaroff et al., 1988; Mason and Malinauskas, 1983]. An advantage of the definition presented here is its bounded value:  $0 \leq \tau_a \leq 1$ . For dry coarse sand with a narrow grain-size distribution, it is reasonable to assume that  $\tau_a$  is almost fully determined by the varying cross-section of pores and by the fact that the flow channels are not straight.

In addition to transport in the air-filled pore space, we have diffusion in the water phase. In the same manner as described above, the bulk diffusive-flux density of radon activity in the water-filled pore space,  $\vec{j}_{d,w}$  ( $\text{Bq m}^{-2} \text{ s}^{-1}$ ) is written as

$$\vec{j}_{d,w} = -\epsilon_w \tau_w D_w \nabla C_w, \quad (2.21)$$

where  $D_w$  ( $\text{m}^2 \text{s}^{-1}$ ) is the diffusion coefficient for radon in water and  $\tau_w$  is the tortuosity for transport in the water phase. It should be noted here that a physical interpretation of the tortuosity as described by Eq. 2.20 and Eq. 2.21 is rather problematic when a partly-saturated medium is considered. Suppose the water distribution is such that both the water phase and air phase only consists of isolated parts (a situation which may occur locally). As a result, there are no transport pathways in the porous structure such that radon remains in one of the two phases, i.e. for transport the radon atoms have to pass through air-filled as well as water-filled parts. Since diffusion through the material does take place under such conditions, one can not interpret  $\tau_a$  and  $\tau_w$  as parameters which only account for the fact that the flow channels are not straight and have a varying cross-section because they would be zero then. Therefore, it is actually not valid to describe macroscopic diffusive transport on the basis of independent components for the water and air phase. It is nevertheless possible to derive an effective radon transport equation on basis of the transport equation for each phase. One only needs to bear in mind that these transport equations, from which the effective equation is composed, are not accompanied by a clear physical interpretation for partly-saturated porous media.

Transport of radon activity caused by the bulk movement of soil gas is usually called advective transport. The bulk advective-flux density of radon activity in the air-filled pore space,  $\vec{j}_{a,a}$  ( $\text{Bq m}^{-2} \text{s}^{-1}$ ), is obtained by multiplying Eq. 2.9 by the pore-air radon-activity concentration:

$$\vec{j}_{a,a} = C_a \vec{q} = -C_a \frac{K}{\mu} \nabla P. \quad (2.22)$$

As in the case of diffusive transport, advective transport of radon in the water phase may take place. However, since all measurements have been done with either dry sand or moisturised sand in absence of bulk movement of pore water, this component of radon transport is discarded in this thesis.

### 2.3.3 Multi-phase time-dependent radon transport

For describing time-dependent combined diffusive and advective radon transport in the air-filled pore space, the equation of continuity (mass conservation) for gas in a porous medium, Eq. 2.10, may be applied to the radon-activity concentration in the air phase:

$$\epsilon_a \frac{\partial C_a}{\partial t} = -\nabla \cdot (\vec{j}_{d,a} + \vec{j}_{a,a}). \quad (2.23)$$

In addition to - and independent of - these two transport components, the rate of change of the air-filled radon-activity concentration is also determined by radon decay and radon generation, as given by Eq. 2.16, and exchange of radon with the water phase and solid surfaces. The continuity equation for radon in the air phase, using Eqs. 2.11, 2.20 and 2.22, may be written as

$$\epsilon_a \frac{\partial C_a}{\partial t} = \nabla \cdot (\epsilon_a \tau_a D_a \nabla C_a) + \frac{K}{\mu} \nabla P \cdot \nabla C_a - \epsilon_a \lambda C_a + \eta_a \rho_b \lambda C^{Ra} - T_{a \rightarrow w} + T_{w \rightarrow a} - T_{a \rightarrow s} + T_{s \rightarrow a}, \quad (2.24)$$

where  $T_{a \rightarrow w}$  and  $T_{a \rightarrow s}$  ( $\text{Bq m}^{-3} \text{s}^{-1}$ ) denote the rate of transfer of radon activity per unit volume from the air-filled pore space to the water-filled pore space and solid surfaces, respectively. Reversely,  $T_{w \rightarrow a}$  and  $T_{s \rightarrow a}$  ( $\text{Bq m}^{-3} \text{s}^{-1}$ ) denote the rate of transfer of radon

activity per unit volume from the water-filled pore space and solid surfaces to the air-filled pore space.

In the same manner the transport equation for the water-filled pore space, neglecting transfer from and to solid surfaces, is given by

$$\epsilon_w \frac{\partial C_w}{\partial t} = \nabla \cdot (\epsilon_w \tau_w D_w \nabla C_w) - \epsilon_w \lambda C_w + \eta_w \rho_b \lambda C^{Ra} + T_{a \rightarrow w} - T_{w \rightarrow a}. \quad (2.25)$$

The assumption of negligible radon adsorption to wet surfaces is supported by experimental results [Rogers and Nielson, 1991b; Schery and Whittlestone, 1989] which show an exponentially decreasing adsorbed fraction of radon activity with pore water content. Since these experiments were conducted using sand with added activated charcoal, a porous material known to adsorb radon, the comparison with pure sand is actually not fully legitimate. However, experiments with pure sand (see chapter 4) do indicate that adsorption to wet surfaces may be neglected.

Finally, it is assumed that adsorbed radon forms an immobile fraction, i.e. surface diffusion is neglected. The balance equation for adsorbed radon is therefore given by Eq. 2.19 including transfer from and to the air phase:

$$\rho_b \frac{\partial C_s}{\partial t} = -\rho_b \lambda C_s + \eta_s \rho_b \lambda C^{Ra} + T_{a \rightarrow s} - T_{s \rightarrow a}. \quad (2.26)$$

The situation can be simplified if the rate of transfer between phases is fast. We have such a balanced transfer between phases if the typical time scales involved are much smaller than in other radon transport processes. For radon partitioning between air and water, diffusion in water ( $D = 1.2 \cdot 10^{-9} \text{ m}^2 \text{ s}^{-1}$  [Broecker and Peng, 1974]) is probably the slowest component with a characteristic time scale of about 10 s for diffusion over a typical pore length of 100  $\mu\text{m}$ . Since the other time scales for radon transport are estimated to be much larger under moderate conditions, the assumption of balanced transfer between the air and water phase ( $T_{a \rightarrow w} = T_{w \rightarrow a}$ ) appears justified. The partitioning between air and water may therefore in the present experiments be described by Henry's law:

$$C_w = LC_a, \quad (2.27)$$

where  $L$  is the Ostwald coefficient (dimensionless form of Henry's constant) [Clever, 1979]. The value of  $L$  is 0.26 at 293 K and its sensitivity to temperature is about  $0.007 \text{ K}^{-1}$  (at 293 K).

For the radon distribution between air and solid surfaces, adsorption- and desorption rates must be considered. The transfer coefficients  $T_{a \rightarrow s}$  and  $T_{s \rightarrow a}$  can be written as:

$$T_{a \rightarrow s} = \alpha_{a \rightarrow s} \epsilon_a C_a \quad (2.28)$$

$$T_{s \rightarrow a} = \alpha_{s \rightarrow a} \rho_b C_s \quad (2.29)$$

where  $\alpha_{a \rightarrow s}$  is the adsorption rate ( $\text{s}^{-1}$ ) and  $\alpha_{s \rightarrow a}$  is the desorption rate ( $\text{s}^{-1}$ ). Typical time scales involved are represented by the reciprocal values  $\alpha_{a \rightarrow s}^{-1}$  and  $\alpha_{s \rightarrow a}^{-1}$  (s). In this perspective, two circumstances can be distinguished based on the criterion whether radon adsorption and desorption are fast or not with respect to other transport processes. For completeness, these two cases will be discussed.

### Case 1: Fast transfer from and to the solid phase

In this case, typical time scales of transfer between the air and adsorbed phase are short with respect to other transport processes. Hence, we have a balanced transfer at any time and position, i.e.  $T_{a \rightarrow s} = T_{s \rightarrow a}$ . Equating Eqs. 2.28 and 2.29 shows that the adsorbed radon-activity concentration is linearly proportional to the gas-phase radon concentration:

$$C_s = k_a C_a, \quad (2.30)$$

where  $k_a$  ( $\text{m}^3 \text{kg}^{-1}$ ) is the radon surface-adsorption coefficient, given by:

$$k_a = \frac{\epsilon_a \alpha_{a \rightarrow s}}{\rho_b \alpha_{s \rightarrow a}}. \quad (2.31)$$

The three separate equations for transport in the air, water and adsorbed phase may be coupled to form a single (effective) equation for radon transport. Adding Eqs. 2.24, 2.25 and 2.26 and using Eqs. 2.27 and 2.30 to express  $C_w$  and  $C_s$  in terms of  $C_a$ , results in an effective equation for transport in the air-filled pore space:

$$\beta \frac{\partial C_a}{\partial t} = \nabla \cdot (D \nabla C_a) + \frac{K}{\mu} \nabla P \cdot \nabla C_a - \beta \lambda C_a + S, \quad (2.32)$$

where  $\beta$  is the partition-corrected porosity (term suggested by Andersen [1992]):

$$\beta = \epsilon_a + L \epsilon_w + \rho_b k_a = \epsilon(1 - m + Lm) + \rho_b k_a, \quad (2.33)$$

$S$  is the production rate of radon activity per unit bulk volume ( $\text{Bq m}^{-3} \text{s}^{-1}$ ):

$$S = \eta \rho_b \lambda C^{Ra}, \quad (2.34)$$

in which  $\eta$  is the sum of fractions of emanation into the air-, water- and adsorbed phase:

$$\eta = \eta_a + \eta_w + \eta_s, \quad (2.35)$$

and  $D$  is the bulk diffusion coefficient, which can be interpreted to have a component for transport in the air- and water phase:

$$D = \epsilon_a \tau_a D_a + L \epsilon_w \tau_w D_w. \quad (2.36)$$

It is realised that Eq. 2.32 only describes radon transport in unsaturated soil because  $C_a$  is a non-existing quantity for saturated soil. Yet, Eq. 2.32 can be used for saturated soil by simply replacing  $C_a$  with  $\frac{C_w}{L}$ .

Finally, for convenience, the bulk radon-activity flux density  $\vec{j}$  ( $\text{Bq m}^{-2} \text{s}^{-1}$ ) is introduced:

$$\vec{j} = \vec{j}_{d,a} + \vec{j}_{d,w} + \vec{j}_{a,a} = -D \nabla C_a - C_a \frac{K}{\mu} \nabla P. \quad (2.37)$$

### Case 2: Dynamic transfer from and to the solid phase incorporated

If dynamic transfer from and to the solid phase has to be taken into account, i.e. (de)adsorption is not fast with respect to other transport processes, only Eqs. 2.24 and

2.25 for transport in the air- and water phase may be coupled. Using Eqs. 2.28 and 2.29, the effective equation for transport in the air-filled pore space is given by:

$$(\epsilon_a + L\epsilon_w) \frac{\partial C_a}{\partial t} = \nabla \cdot (D\nabla C_a) + \frac{K}{\mu} \nabla P \cdot \nabla C_a - (\epsilon_a + L\epsilon_w) \lambda C_a + (\eta_a + \eta_w) \rho_b \lambda C^{Ra} - \alpha_{a \rightarrow s} \epsilon_a C_a + \alpha_{s \rightarrow a} \rho_b C_s, \quad (2.38)$$

and is coupled to the equation for the adsorbed phase:

$$\rho_b \frac{\partial C_s}{\partial t} = -\rho_b \lambda C_s + \eta_s \rho_b \lambda C^{Ra} + \alpha_{a \rightarrow s} \epsilon_a C_a - \alpha_{s \rightarrow a} \rho_b C_s. \quad (2.39)$$

Note that in equilibrium ( $\frac{\partial C_a}{\partial t} = \frac{\partial C_s}{\partial t} = 0$  and  $C_s = k_a C_a$ ), a single transport equation, identical to Eq. 2.32, is obtained by substitution of Eq. 2.39 into Eq. 2.38.

Practically all the analysis in this thesis is based on the description given for fast transfer between the phases, because adsorption may be neglected for the conditions studied with the laboratory facility. In the following, the discussion will therefore be limited to application of the effective radon-transport equation 2.32. The equations for dynamic transfer will only find application in the experiments for determining the radon (de)adsorption characteristics of the sand. Adsorption and desorption processes may however play an important role in other soil types such as clay.

### 2.3.4 Boundary conditions

Application of the effective radon-transport equation requires defining boundary conditions for both radon flux and radon concentration (in the forthcoming, the term ‘radon-activity’ will be abbreviated to ‘radon’ for convenience). For an interface between two different media, the boundary conditions are continuity of pore-air radon concentration,  $C_a$ , and continuity of bulk radon-flux density at the two interfaces, as given by Eq. 2.37<sup>1</sup>. If one of the two media at the interface is impermeable for radon, the boundary condition reduces to  $\vec{j} \cdot \vec{n} = 0$  (Neumann type), where  $\vec{n}$  is the unit vector normal to the impermeable plane. In the same manner, the continuity equation for gas flow (Eq. 2.11) requires continuity of bulk air-flux density, given by Eq. 2.9, which reduces to  $\vec{q} \cdot \vec{n} = 0$  for a boundary that is impermeable to air-flow. We may also have boundaries where the radon concentration or pressure is prescribed (Dirichlet type).

### 2.3.5 Diffusion length

An often used variable in the radon literature is the diffusion length of radon in soil. The physical meaning of this variable can be well illustrated by considering the equilibrium radon concentration profile in a semi-infinite homogeneous sand column due to pure diffusive transport. For this one-dimensional problem, using  $z$  as spatial variable ( $0 \leq z \leq \infty$ ), Eq. 2.32 reduces to

$$D \frac{d^2 C_a}{dz^2} - \beta \lambda C_a + S = 0. \quad (2.40)$$

<sup>1</sup>This is in contrast with the interface condition adopted by Rogers and Nielson [1991b], where continuity of the ‘pore-average’ radon flux,  $\vec{j}_e$ , is advocated as the appropriate one.



Imposing the boundary condition  $C_a = 0$  at  $z = 0$ , the solution of this differential equation is:

$$C_a(z) = \frac{S}{\beta\lambda} \left(1 - e^{\left(\frac{-z}{\ell}\right)}\right), \quad (2.41)$$

where  $\ell$  is the diffusion length:

$$\ell = \sqrt{\frac{D}{\beta\lambda}} = \sqrt{\frac{D_e}{\lambda}}, \quad (2.42)$$

in which the effective diffusion coefficient  $D_e$  is introduced:

$$D_e = \frac{D}{\beta} = \frac{D}{\epsilon_a + L\epsilon_w + \rho k_a}. \quad (2.43)$$

The diffusion length is traditionally interpreted as the characteristic distance travelled by the radon atoms during one half-life. However, this interpretation may be deceptive in some cases, as will be discussed in chapter 7.



# Chapter 3

## Numerical model

### 3.1 Introduction

In the previous chapter, a differential equation for radon<sup>1</sup> transport in porous materials was derived. Considering the aim of this study, i.e. validation of a radon-transport model, the strategy of comparing measured and calculated radon concentrations requires solutions of the radon transport equation. Because, in principle, experiments which allow analytical solutions provide insight, this type of experiments is preferred. However, the derivation of a closed-form expression can be extremely complex, especially when two-dimensional modelling is required. For such cases, numerical modelling is a good alternative for analysing experimental results. Therefore, analytical modelling will be used for cases which can be described by one-dimensional transport. On the other hand, if the situation in the radon vessel is such that the radon concentration varies in two directions (and in time), two-dimensional numerical modelling will be used for describing transport processes.

This chapter focusses on a numerical method to solve the radon-transport equation 2.32 for a two-dimensional geometry. Although this numerical model is not fully used until the experiments with advective transport are analysed (chapter 6), it is discussed here because the matter is closely related to the mathematical description in the previous chapter. The kind of numerical method covered is known as the ‘control-volume method’ (receding under the method of Finite Differences) and can be found in many textbooks on this subject, e.g. [Ames, 1977; Anderson et al., 1984; Patankar, 1980]. Other numerical approaches such as the Finite Element Method or methods based on a pure mathematical discretisation (Taylor-series expansion) of the governing differential equation may be used as well. The control-volume method is chosen for several reasons: 1) the resulting solution implies that the conservation of mass (radon-activity) is satisfied over any part of the calculation domain including one or more control volumes; 2) the underlying ideas are easy to understand; 3) the discretisation allows a direct physical interpretation and 4) implementation into a programme code is relatively simple and easy to maintain and debug. Although widely covered in the literature<sup>2</sup> the method is rather extensively outlined in section 3.2 because several facets are handled somewhat differently than usual, especially the manner in which advective fluxes are approximated. In addition, a correction has been incorporated to minimize discretisation errors for advection-dominated

---

<sup>1</sup>As mentioned in chapter 2, throughout this thesis ‘radon’ is used as an abbreviation for ‘radon-activity’

<sup>2</sup>Similar numerical procedures for radon transport, although different in some details and only for the equilibrium state, are discussed by Andersen [1992] and Loureiro [1987].

conditions, outlined in section 3.2.4. Above all, it also offers a useful interpretation and visualisation of the radon-transport processes.

To verify the performance of the numerical method, a comparison with analytical solutions is made in section 3.3.

## 3.2 Numerical method

### 3.2.1 Radon transport

The numerical method used for solving the radon-transport equation is based on the so-called control-volume approach. In this approach, the continuous problem domain is replaced by a finite-difference mesh or grid, with a control volume about each grid point (node or nodal point). The nodes are located in the centre of the control volumes (in first instance), except at the geometric boundaries where they are situated at the boundary itself (see section 3.2.3). The dependent variables, i.e. radon concentration  $C_a$  and pressure  $P$ , represent the values at the nodes, but can also be regarded to represent the average value in a control volume since there is only one grid point in each control volume. With respect to radon transport, the aim of the method is to find the concentration at time  $t + \Delta t$  at each node, given the concentrations at time  $t$ . By considering a 'mass-balance' for the radon concentration in each control volume, a set of equations is obtained in which each unknown represents the radon concentration at a different node at time  $t + \Delta t$ . The procedure for solving this set of equations is shortly outlined in section 3.2.5. The numerical method for finding the pressure at each node is slightly different but may be considered as a 'subset' of the method for radon transport. The numerical method for radon transport will therefore be elucidated first.

As a starting point for finding the mass-balance equation for the radon-activity within a control volume, the effective radon-transport equation 2.32 is considered. Using Eqs. 2.11 and 2.37 and replacing  $C_a$  with  $C$  for convenience, Eq. 2.32 can be rewritten as

$$\beta \frac{\partial C}{\partial t} = -\nabla \cdot \vec{j} - \beta \lambda C + S. \quad (3.1)$$

Using Gauss theorem

$$\int_G \nabla \cdot \vec{j} dG = \iint_S \vec{j} \cdot \vec{n} dS, \quad (3.2)$$

where  $S$  is the closed surface surrounding a volume  $G$  and  $\vec{n}$  is the unit vector normal to the plane of  $S$  pointing outward, integration of Eq. 3.1 over  $G$  and from  $t$  to  $t + \Delta t$  yields

$$\beta \int_G (C^{t+\Delta t} - C^t) dG = - \int_t^{t+\Delta t} \iint_S \vec{j} \cdot \vec{n} dS dt + \int_t^{t+\Delta t} \int_G (-\beta \lambda C + S) dG dt, \quad (3.3)$$

where  $C^t$  and  $C^{t+\Delta t}$  refer to the radon concentration at time  $t$  and  $t + \Delta t$ . How this equation is used to form the mass-balance equation, may be well demonstrated by considering a node somewhere inside the problem domain, indicated by the letter  $p$  in Fig. 3.1.

The grid is established on the  $x, y$ -domain with the type of coordinate system, e.g. cartesian or cylindrical, to be chosen later. Adjacent nodes of  $p$  are denoted by the letters

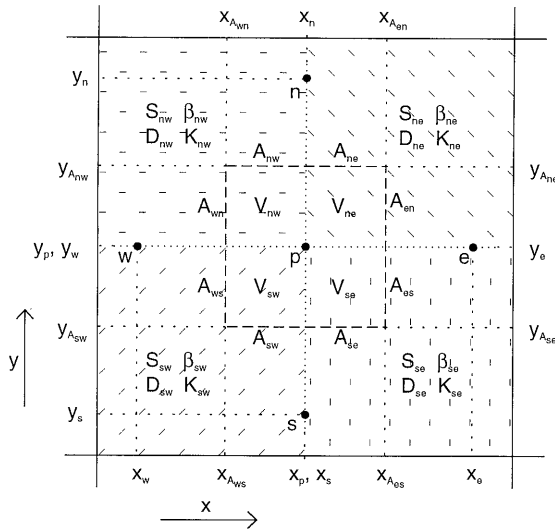


Figure 3.1: Sketch of the situation around control volume  $V_p$  at nodal point  $p$ . Nomenclature of radon-transport parameters, control-volume interfaces, volumes, nodal points and associated coordinates in the  $x, y$ -domain.

$w, e, s$  and  $n$  to indicate their position (west, east, south and north) relative to  $p$ . The interfaces of the control volume at node  $p$  are shown by dashed lines. The grid is set up such that nodal points coincide with junctures between two different media, indicated by a dotted line in Fig. 3.1 (an alternative method which positions the control-volume interfaces exactly on these junctures is discussed in section 3.2.5). Each of the four segments of the control volume at node  $p$  is parameterised by the radon-production term  $S$ , partition corrected porosity  $\beta$ , permeability  $K$ , bulk diffusion coefficient  $D$ , radon decay constant  $\lambda$  and volume  $V$ . These parameters are indexed by the letters  $ne, nw, sw$  and  $se$  to indicate the segment (north-east, north-west, south-west and south-east) to which they apply. The surface areas of interfaces between segments of adjacent control volumes are denoted by  $A$  with subscripts  $ne, nw, wn, ws, sw, se, es$ , and  $en$  to indicate their position relative to node  $p$ . The diffusion coefficient  $D$  and permeability  $K$  are additionally indexed by  $x$  or  $y$  to indicate their components into these directions (being principal axes of diffusion and advection [Crank, 1956]). The radon-activity in the pore-air space  $C$  and the pressure  $P$  are assumed to exist at the nodal points and are therefore indexed by the nodal index only. For convenience, the following quantities are introduced: total volume  $V_p$  (sum of segment volumes) of the control volume at node  $p$ ; control-volume-averaged partition-corrected porosity  $\beta_p$ ; and bulk radon-production rate  $S_p$ :

$$V_p = V_{ne} + V_{nw} + V_{sw} + V_{se}, \quad (3.4)$$

$$\beta_p = \frac{V_{ne}\beta_{ne} + V_{nw}\beta_{nw} + V_{sw}\beta_{sw} + V_{se}\beta_{se}}{V_p}, \quad (3.5)$$

$$S_p = \frac{V_{ne}S_{ne} + V_{nw}S_{nw} + V_{sw}S_{sw} + V_{se}S_{se}}{V_p}. \quad (3.6)$$

By replacing the volume  $G$  in Eq. 3.3 by the volume  $V_p$  at node  $p$  and assuming that 1) the bulk radon-flux density is constant over segment interfaces between adjacent control volumes; 2)  $\beta$  and  $S$  may be replaced by their volume-averaged equivalents  $\beta_p$  and  $S_p$ ; and 3)  $C_p$  represents both the radon concentration at node  $p$  and the spatially averaged concentration within the volume  $V_p$ , Eq. 3.3 can be written as:

$$\begin{aligned} \beta_p V_p (C_p^{t+\Delta t} - C_p^t) = & \\ - \int_t^{t+\Delta t} (-A_{ws}j_{ws} - A_{wn}j_{wn} + A_{es}j_{es} + A_{en}j_{en} - A_{sw}j_{sw} - A_{se}j_{se} + A_{nw}j_{nw} + A_{ne}j_{ne}) dt & \\ - \beta_p \lambda V_p \int_t^{t+\Delta t} C_p dt + V_p S_p \Delta t, & \quad (3.7) \end{aligned}$$

where

- $C_p^{t+\Delta t}$  = pore-air radon concentration ( $\text{Bq m}^{-3}$ ) at time  $t + \Delta t$  at node  $p$ ;
- $C_p^t$  = pore-air radon concentration ( $\text{Bq m}^{-3}$ ) at time  $t$  at node  $p$ ;
- $A_{nw}$  = surface area ( $\text{m}^2$ ) of the 'north-west' interface between node  $p$  and  $n$ ;
- $A_{ne}$  = surface area ( $\text{m}^2$ ) of the 'north-east' interface between node  $p$  and  $n$ ;
- $j_{nw}$  = bulk radon-flux density ( $\text{Bq m}^{-2} \text{s}^{-1}$ ) through  $A_{nw}$  from node  $p$  to  $n$ ;
- $j_{ne}$  = bulk radon-flux density ( $\text{Bq m}^{-2} \text{s}^{-1}$ ) through  $A_{ne}$  from node  $p$  to  $n$ ;
- $A_{sw}$  = surface area ( $\text{m}^2$ ) of the 'south-west' interface between node  $p$  and  $s$ ;
- $A_{se}$  = surface area ( $\text{m}^2$ ) of the 'south-east' interface between node  $p$  and  $s$ ;
- $j_{sw}$  = bulk radon-flux density ( $\text{Bq m}^{-2} \text{s}^{-1}$ ) through  $A_{sw}$  from node  $s$  to  $p$ ; and
- $j_{se}$  = bulk radon-flux density ( $\text{Bq m}^{-2} \text{s}^{-1}$ ) through  $A_{se}$  from node  $s$  to  $p$ .

The surface areas and bulk flux densities in the west-east direction are defined accordingly.

As a next step towards obtaining the algebraic mass-balance equation, the integrands in Eq. 3.7 may be evaluated at some reference time  $t = t + \theta \Delta t$  ( $0 \leq \theta \leq 1$ ) where  $\theta$  determines to which extent the old ( $t$ ) and new ( $t + \Delta t$ ) time level is taken into account. For example, the decay term (second term at the right-hand side of Eq. 3.7) is evaluated as:

$$-\beta_p \lambda V_p \int_t^{t+\Delta t} C_p dt = -\beta_p \lambda V_p \Delta t (\theta C_p^{t+\Delta t} + (1 - \theta) C_p^t). \quad (3.8)$$

When  $\theta = 1$ , the time differencing is called fully implicit, whereas  $\theta = 0$  refers to an explicit time differencing scheme. It is easily seen that Eq. 3.8 is exact if the rate of change of concentration is constant within the time interval  $\Delta t$  and  $\theta = 0.5$  (Crank-Nicolson differencing). The optimum value (with respect to numerical accuracy) of  $\theta$  however depends on the relative importance of the several transport processes, grid spacing and the time step  $\Delta t$ .

The term representing bulk flux of radon (first term at the right-hand side of Eq. 3.7) is evaluated in the same manner as the decay term. As an example, the expression for the change of radon activity in the volume  $V_p$  due to radon flux through the south interface (expressions for other interfaces are similar, but note the change of sign for the north and east side) is given by

$$+ A_{sw}\Delta t \left( \theta(j_{d,sw}^{t+\Delta t} + j_{a,sw}^{t+\Delta t}) + (1-\theta)(j_{d,sw}^t + j_{a,sw}^t) \right) \\ + A_{se}\Delta t \left( \theta(j_{d,se}^{t+\Delta t} + j_{a,se}^{t+\Delta t}) + (1-\theta)(j_{d,se}^t + j_{a,se}^t) \right) \quad (3.9)$$

where the bulk flux densities ( $\text{Bq m}^{-2} \text{s}^{-1}$ ) from node  $s$  to  $p$  have been divided in a diffusive and advective part:  $j_d$  and  $j_a$  with the superscript indicating the moment in time and the additional subscript the interface. For example  $j_{d,sw}^{t+\Delta t}$  is the bulk diffusive-flux density through the south-west interface  $A_{sw}$  at time  $t + \Delta t$ . In the numerical model, the flux density through an interface is related to the concentration at the two nodal points involved. As an example, and referring to the diffusive term in Eq. 2.37, the diffusive-flux densities  $j_{d,sw}$  and  $j_{d,se}$  (advective transport is discussed later) through the south-west and south-east interface into the control volume at  $p$  at time  $t$  (the equations relating to other interfaces are practically identical, except for indices) is approximated by

$$j_{d,sw}^t = -D_{sw}^y \left( \frac{C_p^t - C_s^t}{y_p - y_s} \right) \quad (3.10)$$

$$j_{d,se}^t = -D_{se}^y \left( \frac{C_p^t - C_s^t}{y_p - y_s} \right) \quad (3.11)$$

and similarly at time  $t + \Delta t$  by

$$j_{d,sw}^{t+\Delta t} = -D_{sw}^y \left( \frac{C_p^{t+\Delta t} - C_s^{t+\Delta t}}{y_p - y_s} \right) \quad (3.12)$$

$$j_{d,se}^{t+\Delta t} = -D_{se}^y \left( \frac{C_p^{t+\Delta t} - C_s^{t+\Delta t}}{y_p - y_s} \right) \quad (3.13)$$

where  $y_p$  and  $y_s$  are the  $y$ -coordinate of the nodal points  $p$  and  $s$ , respectively.

The procedure for approximating the advective flux through the south interface is not as straightforward as for the diffusive flux. First, advection through an interface is induced by pressure differences between nodal points. As a consequence, to be able to model advective radon transport, the pressure at the nodal points has to be known in advance. The calculation of these pressures involves a numerical procedure which, in principle, corresponds to the procedure for modelling steady-state diffusive transport of radon in which production and decay are ignored. For the moment, the pressure at the nodal points may be considered as given in the present discussion on advective radon transport. The procedure for calculating the pressure is discussed in section 3.2.2. Secondly, the finite-difference scheme for advective transport is expected to depend only on the bulk air flux and radon concentration, as described by Eq. 2.22. However, to avoid numerical problems in case advective transport is dominating over diffusive transport (e.g. occurrence of negative concentrations due to numerical dispersion), a scheme is adapted such that it will also depend on the relative importance of the respective transport processes. In the following, only advective transport at time  $t$  will be considered because the equations at the new time level (weighted by the factor  $\theta$ , see Eq. 3.9) are simply obtained by

replacing the superscripts  $t$  by  $t + \Delta t$ . The attention will also be limited to the west part of the south interface, for the equations relating to the south-east part of this interface are simply obtained by replacing the index  $sw$  by  $se$ .

The finite-difference scheme for the advective-flux density through the south-west interface at time  $t$  is given by

$$j_{a,sw}^t = q_{sw} \left( (1 - \alpha_{sw}) C_s^t + \alpha_{sw} C_p^t \right), \quad (3.14)$$

where  $q_{sw}$  is the bulk air-flux density ( $\text{m}^3 \text{m}^{-2} \text{s}^{-1}$ ) through the south-west interface  $A_{sw}$  from node  $s$  to node  $p$  and  $\alpha_{sw}$  is a parameter which accounts for the relative importance of diffusion and advection. Notice that the bulk air-flux density  $q_{sw}$ , defined by Eq. 3.27 in the discussion of the pressure-field calculation, is independent of time because only steady-state pressure fields are considered. In further explaining the use of  $\alpha_{sw}$ , we introduce the grid Peclet number  $Pe$  for convenience. For the south-west interface, this non-dimensional parameter is defined as

$$Pe_{sw} = \frac{q_{sw}(y_p - y_s)}{D_{sw}^y}, \quad (3.15)$$

and denotes the ratio of intensities of advection and diffusion. Diffusion dominates for  $|Pe| < 1$ , while advection in the positive (negative)  $x$  or  $y$ -direction dominates for  $Pe > 1$  ( $Pe < -1$ ). The parameter  $\alpha_{sw}$  is defined such that the total, i.e. diffusive plus advective, approximated radon-flux density equals the exact (analytical) one-dimensional equilibrium total radon flux through the south-west interface for a situation without production and decay [Patankar, 1980]. An additional advantage of this method is the independence of the approximated total-flux density on the location of the interface between nodal points<sup>3</sup>. The expression for  $\alpha_{sw}$  is given by

$$\alpha_{sw} = \frac{e^{-Pe_{sw}}}{e^{-Pe_{sw}} - 1} + \frac{1}{Pe_{sw}}, \quad (3.16)$$

which comprises that  $0 \leq \alpha_{sw} \leq 1$ . In what fashion the difference scheme 3.14 is affected by  $\alpha_{sw}$  may be clarified by considering advection-dominated transport in the positive  $y$ -direction ( $Pe_{sw} \gg 1$ ), in which case  $\alpha_{sw}$  approaches to zero. According to Eq. 3.14, the radon flux into the control volume at  $p$  through the south-west interface is then fully determined by the radon concentration at node  $s$ ; a result which is preferred from a physical point of view. Vice versa, for advection-dominated transport in the opposite direction,  $\alpha_{sw}$  approaches unity ( $Pe_{sw} \ll -1$ ) in which case radon transport from node  $p$  to node  $s$  is fully determined by the concentration at node  $p$ .

The approximated advective flux as defined by Eq. 3.14 needs a different formulation for the opposite interface of node  $p$  because (replacing subscripts  $sw$  by  $nw$  in Eqs. 3.14 and 3.15) the weighting factor  $\alpha_{nw}$  should be such that the advective flux is determined by the concentration at the node from where the gas is flowing. The adapted definition for  $\alpha_{nw}$  is:

$$\alpha_{nw} = \frac{e^{Pe_{nw}}}{e^{Pe_{nw}} - 1} - \frac{1}{Pe_{nw}}, \quad (3.17)$$

which represents Eq. 3.16 where  $Pe_{sw}$  is substituted by  $-Pe_{nw}$ . The definitions for  $\alpha$  for the west- and east direction correspond to those for the south- and north direction, respectively.

<sup>3</sup>This is not the case if the radon concentration is linearly or quadratically interpolated. The interpolation adopted here results in the so-called exponential scheme.



With Eqs. 3.8 to 3.17 and the corresponding expressions for other interfaces of the control volume at node  $p$ , the ‘mass-balance’ equation 3.7 can be written as an algebraic equation involving the unknown radon concentrations  $C^{t+\Delta t}$  and known concentrations  $C^t$  at the five nodes. Since we have such an equation for each node present in the problem domain, a set of equations is obtained from which the unknown variables,  $C^{t+\Delta t}$  at each node, can be solved. In the successive time step of the numerical procedure, the concentrations  $C^{t+\Delta t}$  are known, allowing the formulation of a set of equations for the unknown concentration at time  $t + 2\Delta t$ . This procedure may be continued to find the radon concentration in each nodal point as function of time.

The numerical procedure also provides a means for quickly finding the *equilibrium* radon concentration in each node, i.e. the solution of differential equation 3.1 in which the left-hand side is zero. The integration over time may be discarded in this case, which simplifies Eq. 3.7 to

$$-(-A_{ws}j_{ws} - A_{wn}j_{wn} + A_{es}j_{es} + A_{en}j_{en} - A_{sw}j_{sw} - A_{se}j_{se} + A_{nw}j_{nw} + A_{ne}j_{ne}) - \beta_p \lambda V_p C_p^t + V_p S_p = 0. \quad (3.18)$$

This algebraic mass-balance equation may be verified to represent the equation for a time-marching problem in which  $\theta = 1$  and  $\Delta t \gg \lambda^{-1}$ , and the superscripts  $t + \Delta t$  are interpreted as a reference to equilibrium values. As a consequence, equilibrium concentrations are immediately obtained after solving one set of algebraic equations.

Finally, the surface areas of control-volume interfaces remain to be defined. They depend on the type of coordinate system imposed on the problem domain. Only a cartesian- and cylindrical coordinate system are considered. In the former case, the surface areas and volume of, for example, the north-east segment are given by:

$$A_{en} = L_z |y_{A_{ne}} - y_p|, \quad (3.19)$$

$$A_{ne} = L_z |x_{A_{en}} - x_p|, \quad (3.20)$$

$$V_{ne} = L_z |y_{A_{ne}} - y_p| \cdot |x_{A_{en}} - x_p| \quad (3.21)$$

and accordingly for the other segments, where  $L_z$  is the control-volume length in the  $z$ -direction. For a cylindrical coordinate system, the grid coordinates  $x$  and  $y$  represent  $r$  and  $z$  in the conventional  $(r, z, \theta)$  notation. Since only axial-symmetrical problems are considered, the polar angle  $\theta$  is discarded in the numerical model. The following relations for the north-east segment apply for cylindrical coordinates:

$$A_{en} = 2\pi x_{A_{en}} |y_{A_{ne}} - y_p|, \quad (3.22)$$

$$A_{ne} = \pi |x_{A_{en}}^2 - x_p^2|, \quad (3.23)$$

$$V_{ne} = \pi |x_{A_{en}}^2 - x_p^2| \cdot |y_{A_{ne}} - y_p| \quad (3.24)$$

and similarly for other segments.

### 3.2.2 Soil-gas transport

As mentioned previously, the (disturbance) pressure at the nodal points has to be known in advance to model advective radon transport. Referring to Eq. 2.10 and assuming a constant air density, the continuity equation for gas flow is

$$-\nabla \cdot \vec{q} = 0. \quad (3.25)$$

This equation clearly resembles the (equilibrium) diffusion equation  $\nabla \cdot \vec{j}_d = 0$ . The corresponding soil-gas mass-balance equation for the control volume at node  $p$  may therefore be formed on the basis of Eq. 3.18 where advection, decay and production are discarded and the bulk diffusive radon-flux density is replaced by the bulk air-flux density  $q$  ( $\text{m}^3 \text{m}^{-2} \text{s}^{-1}$ ) ( $q$  is positive for transport in the positive  $x$  or  $y$ -direction):

$$-(-A_{ws}q_{ws} - A_{wn}q_{wn} + A_{es}q_{es} + A_{en}q_{en} - A_{sw}q_{sw} - A_{se}q_{se} + A_{nw}q_{nw} + A_{ne}q_{ne}) = 0. \quad (3.26)$$

As an example, the air-flux density through the south-west interface into the control volume at  $p$  is approximated with a procedure that is comparable with the one for diffusive radon transport (Eq 3.11):

$$q_{sw} = -\frac{K_{sw}^y}{\mu} \left( \frac{P_p - P_s}{y_p - y_s} \right). \quad (3.27)$$

The pressure at the nodal points is thus obtained by solving once a set of algebraic equations.

### 3.2.3 Boundary conditions

As mentioned before, a special treatment is necessary for control volumes that are situated near a geometrical border. A 'boundary node' is established on the control volume interface that coincides with the border of the problem domain (only borders for which either  $x = \text{constant}$  or  $y = \text{constant}$  are considered). This boundary node may be regarded to represent an infinitesimal thin 'boundary control volume' such that previously defined finite-difference schemes remain applicable. This greatly facilitates the formulation of the boundary finite-difference schemes.

A first category of geometrical boundaries is formed by those that are impermeable for diffusive radon transport. For this type, diffusive transport across the boundary is simply discarded. For advective transport, the parameter  $\alpha$  is set to zero for air-flow into the domain and set to unity for air-flow out of the domain<sup>4</sup>. In addition, the radon concentration at the boundary node is specified by the radon concentration of incoming air.

The second category concerns boundaries through which diffusive transport may take place. The radon concentration is set to a constant value at these boundary nodes. The diffusive and advective radon-flux density across these boundaries is approximated by identical equations as for internal nodal points. One only needs to take into account the negligible thickness of the boundary control volume.

The treatment of boundaries in the pressure-field calculation strongly resembles the procedure for diffusive radon transport. Gas flow is discarded for boundaries that are impermeable for air-flow. On the other hand, the boundary-node pressure is set to a constant value for boundaries through which air-flow may take place. Notice that pressure differences inside a problem domain are only created if at least two boundary nodes are at different pressure.

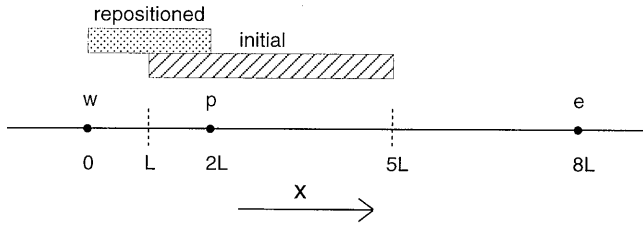


Figure 3.2: Repositioning of the control-volume at nodal point  $p$ . Initial (hatched) and repositioned (dotted) control volume in case of advection-dominated transport in the positive  $x$ -direction.

### 3.2.4 Interface positioning

The control-volume interfaces were previously considered to exist at the centres between nodal points. Although this seems a logical choice, it may yield inaccurate results in case of advection-dominated transport when the distances between adjacent nodal points are not equal. The basis of this problem mainly lies in the presence of a source term in the equations for radon transport. Consider a (one-dimensional) region with  $x$  as coordinate and nodal points  $w$  at  $x = 0$ ,  $p$  at  $x = 2L$  and  $e$  at  $x = 8L$ , as shown in Fig. 3.2. The control-volume interfaces are centred between nodal points at  $x = L$  and  $x = 5L$ . In equilibrium, and for negligible diffusion and decay with respect to advection, the transport equation is approximated by  $-v\frac{\partial C}{\partial x} + S = 0$ , where  $v$  is the bulk velocity in the  $x$ -direction ( $v \gg \lambda L$  and  $vL \gg D$ ). By imposing the boundary condition  $C = C_0$  at  $x = 0$ , the radon concentration is given by  $C(x) = C_0 + \frac{Sx}{v}$ .

Since in the numerical model, according to Eq. 3.14, the advective flux entering the control volume at node  $p$  is fully determined by the radon concentration  $C_w$  at node  $w$ , this flux will be  $vC_0$ . Similarly, the advective flux leaving the control volume at  $p$  is determined by the radon concentration at  $p$ , and is given by  $vC(2L)$ . The net rate at which radon concentration leaves the control volume is thus  $vC(2L) - vC_0$ . Since this loss rate is counterbalanced by the production rate within the control volume at  $p$ ,  $(5L - L)S = 4LS$ , a value  $C(2L) = C_0 + \frac{4LS}{v}$  is computed for the radon concentration at node  $p$ . If  $C_0 = 0$ , this is a factor two larger than the true value; an off-set which is caused by taking into account the production of radon in the region  $3L < x < 5L$ . Since this part of the control volume is situated 'down stream' of nodal point  $p$ , it does not contribute to the radon concentration at node  $p$  and should be discarded. As a correction, the control-volume interfaces may be positioned closer to the nodal point at the 'upstream' side. In the example at hand, a shift of the interfaces at  $x = L$  and  $x = 5L$  to  $x = 0$  and  $x = 2L$ , respectively, results in a calculated radon concentration  $C(2L) = C_0 + \frac{2LS}{v}$  at  $p$ , corresponding with the correct value.

In two dimensions, the situation is slightly more complex, because a region between four nodal points must be taken into consideration. As an example, consider the region between nodal points  $p$ ,  $e$ ,  $n$  and the one north of  $e$  (east of  $n$ ). The calculation of the control-volume segment interface positions should account for the relative importance

<sup>4</sup>For a boundary at the south interface, for example, this result may be verified by considering  $\alpha_{sw}$  in the limit  $D_{sw}^y \downarrow 0$ .

of diffusion and advection between adjacent nodes. The coordinates of the segment interfaces  $A_{en}$  and  $A_{ne}$  are evaluated as:

$$x_{A_{en}} = x_p + (1 - \bar{\alpha}_{en})|x_e - x_p|; \quad (3.28)$$

$$y_{A_{ne}} = y_p + (1 - \bar{\alpha}_{ne})|y_n - y_p|, \quad (3.29)$$

where  $\bar{\alpha}_{en}$  denotes the average of  $\alpha_{en}$  (node  $p$ ) and  $\alpha_{es}$  (node  $n$ ) and where  $\bar{\alpha}_{ne}$  denotes the average of  $\alpha_{ne}$  (node  $p$ ) and  $\alpha_{nw}$  (node  $e$ ). This procedure is not based on a theoretical ground but rather on an intuitive elaboration of the method for approximating the advective radon-flux density. Note that the interfaces are centred between nodal points for pure diffusive transport.

### 3.2.5 Model implementation

The numerical model has been implemented in the PASCAL programming language using the Borland Pascal 7.0 compiler for PC-compatible computer systems. As a first step in the programme, nodal points are defined (max. 7000) and control-volume interfaces are subsequently positioned centrally between nodal points for calculating the pressure field. Each row (representing one control volume) in the set of algebraic equations for soil-gas transport contains five unknowns (except for control volumes at a boundary) and is ordered such that a penta-diagonal matrix is obtained. This system is solved with a direct method by first converting the matrix into an upper triangular matrix using Gaussian elimination, followed by backward substitution. To correct for possible truncation errors, Gauss-Seidel iteration (with optionally over-relaxation) is applied [Ames, 1977]. It should be remarked that these truncation errors are usually extremely small.

The bulk air-flux densities across interfaces are subsequently calculated from the pressure field and used in the procedure for repositioning the control-volume interfaces, as described in section 3.2.4. The (time-dependent) radon concentrations are then calculated as described in section 3.2.1, starting from a given initial radon-concentration field. The mass balance equations for radon transport also form a system of equations with generally five unknowns in each row and is solved by Gaussian elimination and backward substitution. In the first time step of the radon-concentration field calculation, the row multipliers are stored in memory to speed up calculation of subsequent (equal) time steps.

### Alternative method

Although the preceding fully relied on the assumption of having fixed positions of nodal points, an alternative method for establishing the grid consists of locating and fixing the control-volume interfaces (such that they coincide with junctures between two different media) and, depending on the relative strength of diffusion and advection, repositioning the nodal points within the control volumes. An advantage of this procedure is the homogeneous control volume which simplifies the formulation of several finite-difference schemes (e.g. transport in the north-south direction is not divided into a west- and east part). It also gives a better numerical simulation in case  $\beta$  or  $S$  strongly vary from one medium to another. This is most evident at an interface between a radium-free and a radon-producing medium. The method that fixes the nodal points at junctures between media, averages  $S$  and  $\beta$  over the control volumes (Eqs. 3.5 and 3.6), and thereby causes radon production in the radium-free part. Considerable errors may be introduced if the radium-free medium represents a crack through which radon is quickly transported while

radon is slowly transported in the radon-producing medium. This problem does not arise when control-volume interfaces are exactly located on junctures between different media. A drawback of this method, on the other hand, is that when a calculated concentration field at some time  $t$  is to be used as an initial field in a situation with a different pressure field. This requires an interpolation technique for estimating the concentrations at time  $t$  at the new nodal point positions. Therefore, the most suited method depends on the situation studied. In this work, the method that fixes the nodal points is most frequently used because

- the positions where radon concentrations will be calculated are known in advance;
- transition to another pressure field is easily made; and
- it yields more accurate results near boundaries of the problem domain for diffusion-dominated transport, as will be outlined in the following section.

A situation in which the alternative method is applied is discussed in chapter 7.

### 3.3 Model comparison

For accuracy tests, results of the numerical models were compared with analytical solutions in two situations: 1) One-dimensional steady-state combined diffusive and advective transport and 2) Two-dimensional time-dependent diffusive transport. For optimal similarity with the radon-vessel experiments, it is favourable to have a test case with two-dimensional combined diffusive and advective transport, preferably in a cylindrical coordinate system. Unfortunately, such analytical solutions are complex and difficult to derive. On the other hand, the two test situations give an indication of the order of magnitude of the accuracy to be expected.

#### 3.3.1 One-dimensional problem

The first test case concerns one-dimensional advective radon transport through a homogeneous column of porous medium. To obtain similarity with the radon vessel experiments, the length ( $d$ ) of the medium is set at 2.56 m (to facilitate mesh refining in powers of two) and the (imaginary) surface area at  $\pi \text{ m}^2$  (for calculation of the total air-flow). The analogy is further enhanced by using the parameters of the sand as given in Table 5.1. The radon concentration at both ends of the column is set to zero (Dirichlet boundary conditions). The governing differential equation for this problem, with advective transport in the direction of the positive  $z$ -axis, is given by the one-dimensional stationary counterpart of Eq. 2.32 with  $v > 0$ :

$$D \frac{d^2 C}{dz^2} - v \frac{dC}{dz} - \beta \lambda C + S = 0, \quad (3.30)$$

where  $v$  is bulk air flux ( $\text{m s}^{-1}$ ). The boundary conditions imply zero concentration at both ends of the medium:

$$C = 0, \quad \text{at } z = 0 \text{ and } z = d. \quad (3.31)$$

The analytical solution of the problem is given by:

$$C = \frac{S}{\beta \lambda} \left( \frac{(1 - e^{\omega_2 d}) e^{\omega_1 z} - (1 - e^{\omega_1 d}) e^{\omega_2 z}}{e^{\omega_2 d} - e^{\omega_1 d}} + 1 \right), \quad (3.32)$$

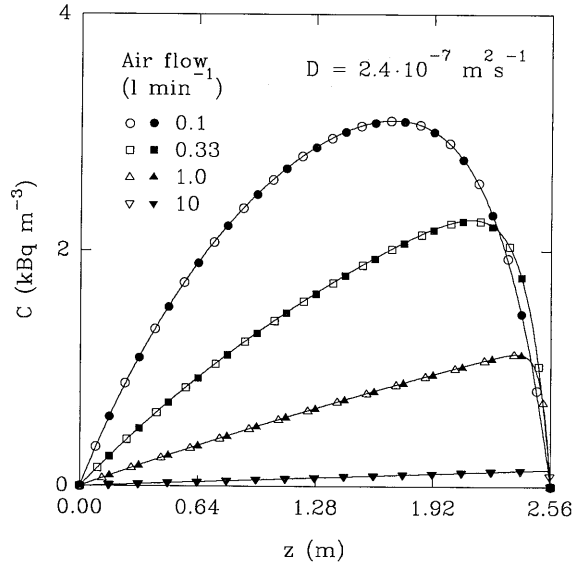


Figure 3.3: Numerically calculated pore-air radon concentrations  $C$  ( $\text{kBq m}^{-3}$ ) using the ‘fixed-node’ method (filled markers) and ‘fixed-interface’ method (open markers) and corresponding analytical solutions (solid lines) for four different flow rates passing through a 2.56 m porous column (radius 1 m) with zero radon concentration at both ends. Note that open and closed markers coincide for a flow  $J = 10 \text{ l min}^{-1}$ .

with  $\omega_{1,2}$  defined as:

$$\omega_{1,2} = \frac{v}{2D} \pm \sqrt{\left(\frac{v}{2D}\right)^2 + \frac{\beta\lambda}{D}}. \quad (3.33)$$

Model test calculations are conducted for three different bulk diffusion coefficients<sup>5</sup>:  $D = 2.4, 0.24$  and  $0.024$  ( $\cdot 10^{-6}$ )  $\text{m}^2 \text{s}^{-1}$ , and with four different air-flows:  $J = 0.1, 0.33, 1.0$  and  $10 \text{ l min}^{-1}$ , corresponding to values of  $v = 0.53, 1.8, 5.3$  and  $53$  ( $\cdot 10^{-6}$ )  $\text{m s}^{-1}$ . In addition, the tests are carried out with 6 different grid spacings  $\Delta z = 0.5, 1, 2, 4, 8$  and  $16$  cm on an equally-spaced grid (except for control volumes adjacent to boundaries which are about 2 times smaller than the others).

In Fig. 3.3 the analytical (solid lines) solution and results of the numerical ‘fixed-node’ (filled markers) and ‘fixed-interface’ (open markers) method are plotted as function of  $z$  for all flows tested for  $D = 2.4 \cdot 10^{-7} \text{ m}^2 \text{ s}^{-1}$  and a grid spacing of 16 cm. The repositioning of nodal points in the fixed-interface method is well illustrated by comparing the relative distance between open and closed markers at different flow rates. From the comparison it can be concluded that there is no noticeable difference over the full range of  $z$  between the results of the two methods of calculation over an air-flow range of two orders of magnitude.

<sup>5</sup>A value of  $2.4 \cdot 10^{-6} \text{ m}^2 \text{ s}^{-1}$  applies for dry sand in the vessel.

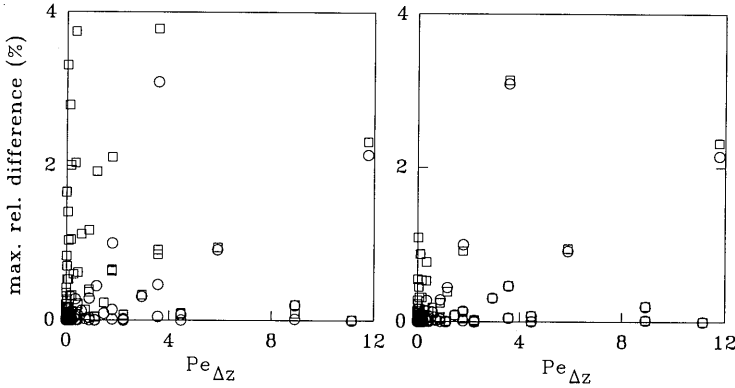


Figure 3.4: Left part: maximum relative difference between analytical and numerical solutions in each of the  $3 \times 4 \times 6 = 72$  one-dimensional test cases as function of grid Peclet number for the ‘fixed-node’ method (circles) and ‘fixed-interface’ method (squares). Identical data are displayed in the right part except that two nodal points adjacent to the boundaries  $z = 0$  and  $z = 2.56$  have been omitted in the calculations.

As mentioned before, the grid Peclet number

$$Pe_{\Delta z} = \frac{v\Delta z}{D}, \quad (3.34)$$

is a useful parameter for characterising transport processes. When  $Pe_{\Delta z} < 1$  the radon concentration varies smoothly. However, for larger  $Pe_{\Delta z}$  a sudden drop of radon concentration occurs near  $z = d$ , caused by the Dirichlet boundary condition. The maximum difference (%) in the entire mesh between the analytical and numerical solution (all test cases) as function of the grid Peclet number is presented in the left part of Fig. 3.4 for the fixed-node (circles) and interface (squares) method. Large maximum differences are observed for low grid Peclet numbers and the fixed-interface method. These differences, however, only occur at the two nodal points near  $z = 0$  and  $z = 2.56$ . If these two nodal points are discarded, the maximum differences are  $< 1.1\%$  for all cases except at  $Pe_{\Delta z} \approx 4$  (3.5%) and  $Pe_{\Delta z} \approx 12$  (2.2%), see right part of Fig. 3.4. The results indicate a much better performance of the fixed node method for diffusion dominated transport. Since this may be due to a finer grid near boundaries, the fixed-interface method was also tested with a similar (but not identical) local grid refinement. This did not improve the performance and even gave higher differences for moderate  $Pe_{\Delta z}$ . The solutions are apparently very sensitive to the positions of the grid points and control-volume interfaces near the boundaries of the problem domain.

In view of the radon-vessel experiments, the grid Peclet number of the numerical calculations may be restricted according to a maximum allowed difference of 2%, corresponding to the relative error at which radon concentrations are determined in the radon vessel. This imposes no constraints on the grid Peclet number for both methods (discarding solutions close to boundaries in the fixed-interface method) if one accepts a slightly higher maximum difference occasionally (as occurred in 2 of the 72 cases)

### 3.3.2 Two-dimensional problem

The second test case concerned two-dimensional time-dependent diffusive radon transport in a homogeneous isotropic porous medium. A cartesian  $(x, y)$  coordinate system is used in the calculations. The medium is assumed to exist in a rectangle ( $0 \leq x \leq a$ ;  $0 \leq y \leq b$ ). The boundary conditions imply zero radon concentration at three sides of the rectangle ( $x = 0$ ,  $x = a$  and  $y = b$ ) and zero radon flux (Neumann boundary condition) at the remaining side ( $y = 0$ ). As initial condition, zero radon concentration is imposed in the whole rectangle. The analytical solution of this problem is derived in appendix A.

Again, to obtain similarity with the radon-vessel experiments, the length and width of the medium is set at 2 m and the parameters of the sand (Table 5.1) are utilised for the porous medium. Model calculations are carried out with two different bulk diffusion coefficients: 2.4 and  $0.24 \cdot 10^{-6} \text{ m}^2 \text{ s}^{-1}$  (referred to as test case 1 and 2). In addition, the number of control volumes is varied from 8 ( $\Delta x = \Delta y = 25 \text{ cm}$ ) to 64 ( $\Delta x = \Delta y = 3.125 \text{ cm}$ ) in each direction with a factor two refinement near boundaries. The time-dependent concentrations are calculated until the maximum value in the rectangle has reached half of the maximum steady-state concentration  $C_{eq}$  to assure that possible errors introduced by making a finite time-step in the numerical calculations are noticed in the solution. This corresponds with a time  $t = 10 \text{ h}$  for the first test case ( $C_{eq} = 518 \text{ Bq m}^{-3}$ ), and a time  $t = 60 \text{ h}$  for the second test case ( $C_{eq} = 2700 \text{ Bq m}^{-3}$ ). The time differencing of the mass-balance equations is based on a time-centred implicit method (Crank-Nicolson differencing,  $\theta = 0.5$ ). The number of time steps is varied from 1 to 1024.

A contour plot of the radon concentration ( $\text{Bq m}^{-3}$ ) is presented in the left part of Fig. 3.5 to give an idea of the concentration field after 10 h (case 1). The concentration has a maximum of  $260 \text{ Bq m}^{-3}$  in the middle of the impermeable boundary  $y = 0$ , and decreases monotonously to zero at the other boundaries.

The method that fixes the nodal points will be discussed first. It is observed that the maximum relative difference (between the analytical and numerical solution) is less than 2% when the non-dimensional parameter  $\nu = \frac{S \Delta t \ell}{C_{eq} \Delta x} < 1$  ( $\ell$  is diffusion length, defined by Eq. 2.42). The constraint  $\nu < 1$  implies that reliable modelling calculations are obtained for large  $\Delta t$  (concentration field calculated within less than 8 time steps) and large  $\Delta x$ . A strange consequence is a worse performance when a finer grid spacing is applied. However, when a much smaller  $\Delta t$  is considered (number of time steps larger than 30), a finer grid does improve the results as long as  $\nu < 1$ .

The *average* relative difference is usually much smaller than the maximum relative difference, especially when a fine grid spacing is used. This is illustrated in the right part of Fig. 3.5, where the relative difference (%) is presented in a contour plot as function of  $x$  and  $y$ . These results are obtained with a numerical calculation in which  $D = 2.4 \cdot 10^{-6} \text{ m}^2 \text{ s}^{-1}$ ,  $\Delta t = 2250 \text{ s}$  and  $\Delta x = \Delta y = 0.0625 \text{ m}$ , corresponding with  $\nu = 1.1$ . The results in Fig. 3.5 (right part) show that the maximum differences (up to 0.35%) only occur in a small area close to the corners  $(0, b)$  and  $(a, b)$ , exactly where the solution has a maximum curvature in both  $x$  and  $y$ .

The test results also indicate a proportionality of numerical errors to the square of the grid spacing  $\Delta x$ , as well as to the square of the time step  $\Delta t$ . This is in accordance with error analysis of similar numerical approaches to the heat equation [Anderson et al., 1984; Carnahan et al., 1969]. It should be remarked that the  $O(\Delta t^2)$  error dependence is only visible by inspection of the absolute differences at small  $\Delta x$  and large  $\Delta t$ , while the  $O(\Delta x^2)$  dependence is only observed at small  $\Delta t$  values.



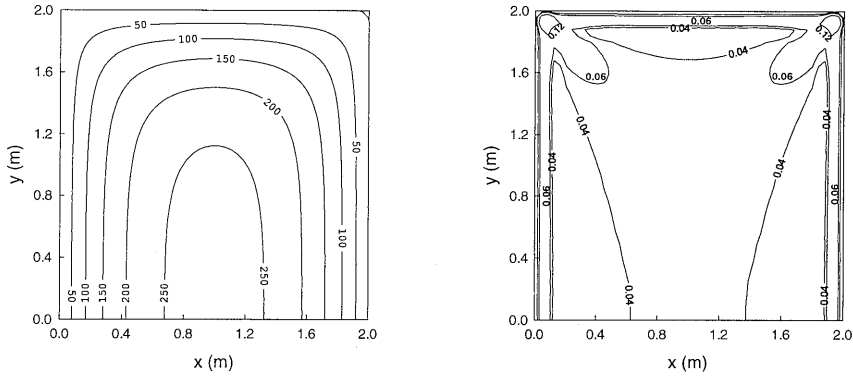


Figure 3.5: Left part: contour plot of analytically calculated radon concentrations ( $\text{Bq m}^{-3}$ ) at  $t = 10$  h as function of  $x$  and  $y$  (m) in a rectangle of  $2 \times 2 \text{ m}^2$ . Right part: relative difference (%) between two-dimensional analytical and numerical results (fixed-node method) as function of  $x$  and  $y$  for a calculation with time step  $\Delta t = 2250$  s and grid spacing  $\Delta x = \Delta y = 0.0625$  m. Relative deviation at the boundaries is nil. Results in both plots are obtained with a diffusion coefficient of  $2.4 \cdot 10^{-6} \text{ m}^2 \text{ s}^{-1}$  and parameters listed in Table 5.1.

The alternative method which fixes the control-volume interfaces is less accurate. At small  $\Delta t$  and  $D = 2.4 \cdot 10^{-6} \text{ m}^2 \text{ s}^{-1}$ , the maximum relative error with a coarse grid spacing of 25 cm is about 3.5%, while the error is still about 2% with a fine spacing of 3.125 cm. The basis of this behaviour lies in the different grid which is established near boundaries.

As the fixed-node method is the most accurate of the two, this method is used for modelling the vessel experiments (except for one type discussed in chapter 7). The previously mentioned constraint  $\nu < 1$  implies a maximum allowed time step of about 7200 s at a grid spacing of 5 cm. The situation in practise is however complicated by several aspects: experiments with time-dependent combined diffusive *and* advective transport are conducted and modelled (chapter 6); the finite-difference grid is refined near positions where high concentration gradients occur; the calculations are done in a cylindrical coordinate system; and a block-wise homogenous problem domain is considered (contains more than one type of porous medium). For these reasons, it is not so relevant to define a constraint on basis of a test case with pure diffusive transport in a homogeneous medium and with an equally-spaced grid in a cartesian coordinate system. Nevertheless, the comparisons in this section show that numerical errors are generally  $< 2\%$  and that model calculations are optimal for small grid spacing and small  $\Delta t$ . Therefore, the grid spacing and time step in the model calculations of radon transport in the vessel are refined until the results do not significantly differ from previous results, i.e. for a calculation with a coarser grid or larger time step. The utilised grid spacing and time step are therefore thought to be an optimization of numerical accuracy and computing time.



# Chapter 4

## Experimental

### 4.1 Introduction

To validate the radon-transport model presented in chapter 2, measurements on radon transport have been made under well-defined and controlled conditions. For this purpose, a laboratory facility was built which consists of a large cylindrical vessel with radially inserted measuring probes that allow measurement of radon concentrations in the pore space of the soil at various depths. The vessel has been filled with nearly pure sand<sup>1</sup> obtained from settling in a tank with a constant water flow. Its narrow grain-size distribution and small transition range from saturated pores to dry pores in a partly water-saturated sand column approach relatively simple conditions. In view of the adopted research strategy of starting with simple conditions and increasing the complexity step by step, this sand is the optimal choice of soil type for this study of radon transport. The laboratory facility will be described in section 4.2, followed by a description of the procedures and equipment for measuring the pore-air radon concentration in section 4.3. An assessment of the homogeneity of the sand column is discussed in section 4.4. Finally, the experiments for determining properties of the sand that are of importance for radon transport, such as grain-size distribution, density, porosity, tortuosity, radium content, radon adsorption and desorption rates, and radon emanation coefficient are discussed in section 4.5.

### 4.2 Laboratory facility

The laboratory facility, shown in perspective in Fig. 4.1, consists of a cylindrical stainless steel vessel (height and diameter 2 m; bottom slightly curved for strength) surrounded by a stainless steel moat filled with water, acting as a water seal. The vessel can be closed by lowering a stainless steel lid into the moat. When the vessel is filled with soil the space under the lid simulates a crawl space. The lid rests on three supports in the moat, which can be manually adjusted in height. At the adjustment points the height of the lid above the rim of the vessel is indicated on scales. With this construction the distance between the sand surface and the lid can be varied from 6 cm to 70 cm.

The vessel has four legs, which are adjustable in length for positioning purposes. The dimensions of the vessel are of the order of the diffusion length of radon in dry soil, 1-2 m. They are an optimisation of reducing boundary effects and the maximum

---

<sup>1</sup>Ankersmit classified filter sand, Ankersmit, Deventer, The Netherlands.

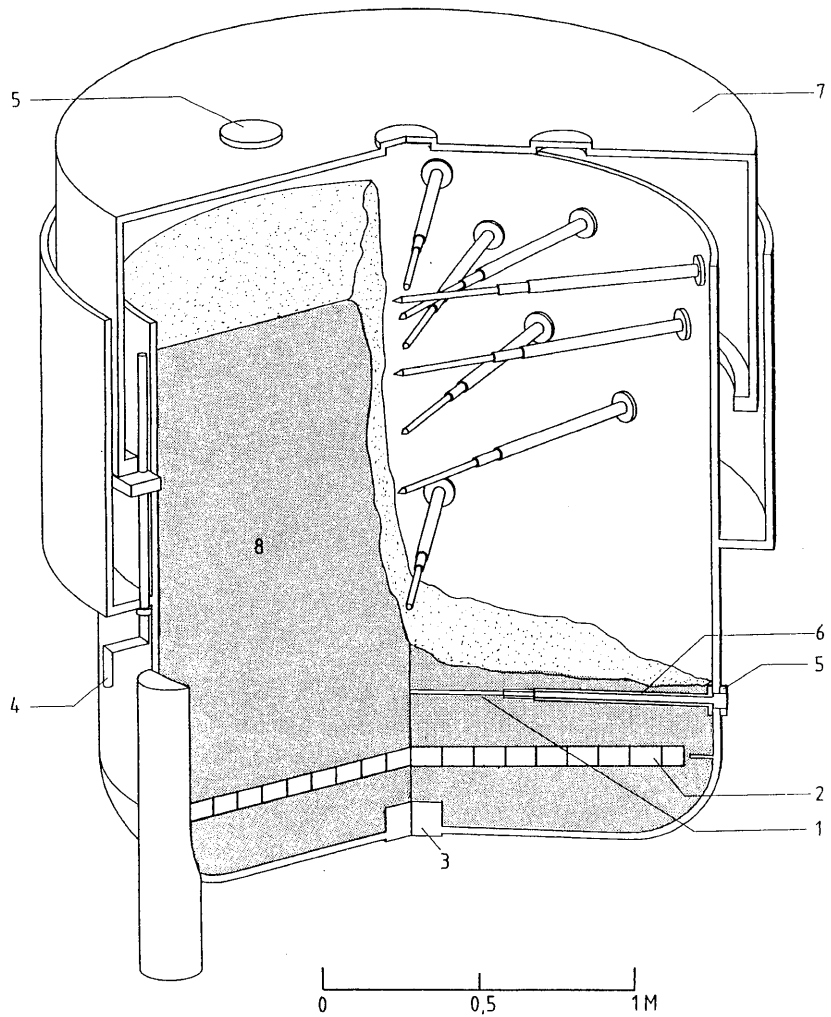


Figure 4.1: Schematic presentation of the radon vessel. 1) probe; 2) perforated cylindrical box; 3) water inlet/outlet; 4) adjustment point for height of the lid; 5) flange; 6) sleeve; 7) lid; 8) soil.

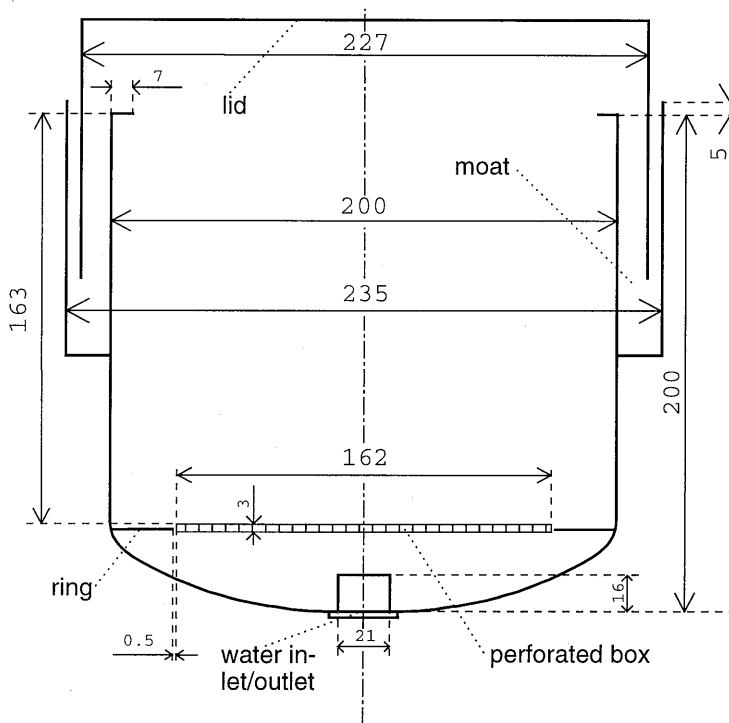


Figure 4.2: Vertical cross-section of the radon vessel through the symmetry axis. Dimensions are given in centimeters.

permissible weight and height with regard to the experimental room. In Fig. 4.2 a vertical cross-section of the vessel through the symmetry axis is shown. The vessel has been orientated such that the tilt angle of the symmetry axis of the vessel is less than  $0.06^\circ$  [Van der Graaf, 1992]. Considering other deviations from the ideal situation of a cylindrical symmetric column, the error induced by a possible tilt is negligible.

At nine different heights flanged ports are constructed in the vessel wall. Radially mounted on these flanges are 70 cm long sleeves. They penetrate the vessel at distances of 10, 15, 20, 30, 40, 60, 80, 120 and 150 cm below the upper rim of the vessel. During the filling of the vessel with sand these sleeves were closed with dummy probes. After filling, these probes were replaced by multi-functional probes for measuring the pore-air radon concentration and pore-water pressure at the centre of the vessel. These (hollow) probes have a length of 105 cm and penetrate the soil for the first 70 cm via the sleeves. Owing to this construction their deviation from the ideal position in the vessel is less than 5 mm. The rear end of each measuring probe consists of a flange that fits onto the flange of the port.

The head of the probe, shown in Fig. 4.3, has a pointed tip to facilitate penetration of the probe into the soil and has an air filter and a ceramic filter. The position of the probes is such that the vertical symmetry axis of the vessel intersects the probe heads between the two filters. The air filter consists of a layer of five perforated metal sheets with an

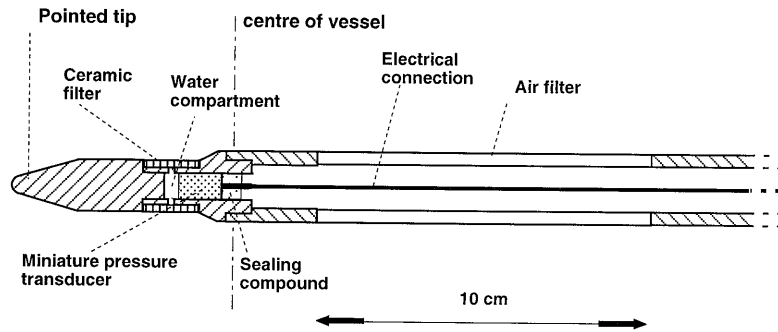


Figure 4.3: Schematic sketch of the head end of a probe.

effective pore diameter of  $2\ \mu\text{m}$  and prevents sand grains from entering the hollow inner part of the probe. The inside of the probe is connected to a plastic tube, mounted on a connector in the rear-end flange of each probe that is connected to a flange in the vessel wall. In case the flange is situated in the moat of the vessel, the plastic tube is led outside the vessel via the bottom of the moat. For determining the radon concentration, pore-air surrounding the air filter may be sampled from the sand by drawing air from the plastic tube. In addition, a pressure transducer is placed inside the head of a probe. Capillary suction induced by the sand pores introduces, via the ceramic filter, a negative pressure on a water-filled compartment sealed with a pressure transducer. The measured pressure difference can be related to the water content of the sand by using the corresponding water-retention curve (see chapter 8). However, due to instrumental difficulties, this measuring technique for determining the water content has not been used in this study.

For the study of pressure-driven radon transport, a cylindrical box (diameter 1.62 m, height 3 cm) consisting of two parallel, perforated stainless steel plates covered with a stainless steel gauze (effective pore size  $35\ \mu\text{m}$ ) and mounted on a frame of perforated glass-fibre grating is placed at a distance of 1.63 m below the sand surface. A small diameter tube is led through the centre of the bottom of the vessel and is connected to the centre of the perforated box for either supplying air to or withdrawing air from the box. Since a circular metal ring (width 18.5 cm, inner diameter 1.63 m) is constructed inside the vessel at the location where the concave bottom is attached, exactly adjacent to the cylindrical box, a small 0.5 cm gap is left in between. As a result, radon originating from below the box can practically only enter the sand above by transport through the box (and vice versa).

Through water inlet/outlets in the bottom flange at the centre of the vessel, water can be introduced in - or removed from - the sand via a perforated cylinder. This cylinder is covered with cloth to prevent loss of sand through the openings. A water pressure transducer mounted on the bottom flange of the vessel is used to measure the height of the water level in the vessel. The openings in the bottom flange may also be sealed to prevent leakage of radon.

## 4.3 Radon-concentration determination

Pore-air radon concentrations in the sand column were generally measured by sampling utilising the nine multifunctional probes. Nine pistons were constructed (length 30 cm, inner diameter 7 cm) to sample all nine probes quickly in sequence. Sampling is normally started at the upper probe and subsequently at successively deeper probes. This procedure allows determination of a so-called radon profile in the sand, i.e. the pore-air radon concentration in the sand as function of height. A short, small diameter flexible plastic tube is connected to the piston opening and sealed with a (normally-closed) male quick connector<sup>2</sup>. Since corresponding (normally-closed) female connectors are fitted on the plastic air tubes of the probes, the pistons can be quickly connected and disconnected. After grab sampling, the pistons are left undisturbed for at least 10 minutes to allow thoron (<sup>220</sup>Rn) to decay. The air inside each piston is then transferred to an evacuated scintillation flask<sup>3</sup> via a filter. Since radon and thoron daughters are intercepted by this filter, <sup>222</sup>Rn is the only alpha-particle emitting nuclide that may enter the flask. The filling is continued until about 102% of atmospheric pressure. Some air is then allowed to escape to equilibrate pressures.

The scintillation flask<sup>4</sup> consists of a light-tight cylinder with a transparent window at one end and one or two air inlets/outlets on the back plane. The inside of the cylinder and the back plane are covered with ZnS(Ag). When hit by an alpha particle, this material responds by emitting a flash of scintillation light which can be detected by a photo-multiplier tube. The Lucas cells are normally positioned in front of the photomultiplier tube of a portable radiation monitor<sup>5</sup>. Since seven radiation monitors and about twenty-three Lucas cells are in use, the relative efficiencies of the monitors and cells were determined to eliminate systematic errors introduced by using different combinations of monitor and cell [Van der Graaf et al., 1994]. The relative standard deviation in the measured radon concentration is less than 2%. The absolute uncertainty is approximately 10%.

Since initially we only have <sup>222</sup>Rn in a Lucas cell, the alpha activity will gradually increase due to ingrowth of radon daughters <sup>218</sup>Po and <sup>214</sup>Po, see Fig. 1.1. Due to a short decay constant of 3.05 min of <sup>218</sup>Po, secular equilibrium with <sup>222</sup>Rn is reached after circa 15 min. However, the <sup>214</sup>Po activity increases at a much slower rate due to a half life of 26.8 min and 19.8 min for <sup>214</sup>Pb and <sup>214</sup>Bi, respectively (Fig. B.1 in appendix B shows the ingrowth of alpha activity). As a result, secular equilibrium between all three alpha-emitting nuclides is reached after about three hours. To minimize possible errors (due to a different counting efficiency for each nuclide), the activity in the cells is measured during equilibrium. Therefore, the pulses obtained during the first three hours are discarded. The number of pulses are registered in one-hour intervals during a 24 hours period. This period may be shorter in cases with, for example, a short time interval between two radon-profile measurements. When all probes are sampled, nine Lucas cells are filled of which five are directly measured. Routinely, the remaining four cells are measured the following day. For each probe the same combination of piston, Lucas cell and Pylon monitor is used. These procedures are generally followed but may occasionally be deviated from if the circumstances require that.

To determine the minimum allowed sample volume such that a representative radon

<sup>2</sup>Swagelock SS-QC4.

<sup>3</sup>Pylon 100A and 300A Scintillation Flasks, Pylon Electronics Inc., Ottawa, Canada.

<sup>4</sup>Commonly referred to as Lucas cell after a first description by Lucas [1957].

<sup>5</sup>Pylon AB-5 Radiation Detectors.

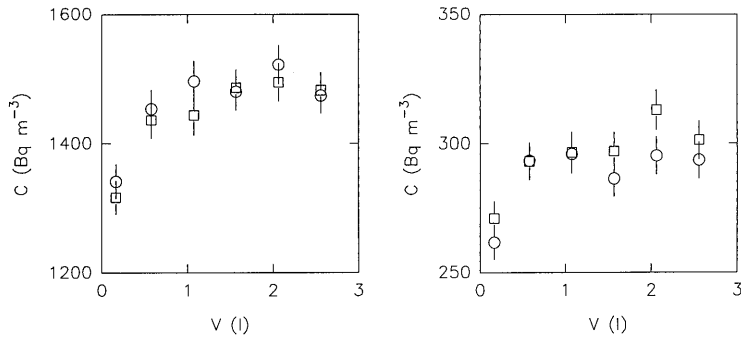


Figure 4.4: Radon concentration  $C$  (Bq m<sup>-3</sup>) as function of air volume sampled with the radially inserted probe at 150 cm depth (left part) and at 20 cm depth (right part) for two measurement series (circular and square markers).

concentration is still obtained, the functional relation between sample volume and radon concentration has been measured, see Fig. 4.4. The radon concentration increases with increasing air volume due to the void space in the probes (approximately 0.3 litre). Thereafter, a more or less constant radon concentration as function of air volume is observed. Based on this radon-concentration ‘plateau’, starting at about 0.5 l, it was decided to discard the first 0.5 l and to utilise the second 0.5 l for determining the radon concentration. When all nine probes are sampled, about 9 litre of pore gas is removed from the sand. Regarding the total air volume inside the sand column, which is approximately 2 m<sup>3</sup> for dry sand, the disturbance of the radon-concentration profiles due to sampling is likely to be negligible. Difficulties that may arise at high pore-water contents are discussed in chapter 8.

#### 4.4 Homogeneity of the sand column

To obtain a relatively homogeneous soil column the vessel has been filled gradually with layers of 15-20 cm. After each sand layer, the water level in the vessel was raised and lowered a few times to allow the sand to settle in a close-packed configuration. After filling was completed, the sand column was flushed with an air-flow of 50 l min<sup>-1</sup> (5% rel. humidity) via the perforated box through the column for more than a week. Afterwards, the sand column was left undisturbed for about 5 months, allowing gravitational downward transport and evaporation of remaining pore water.

To assess the homogeneity of the column, pressure fields in the sand were measured. An air-flow of 44.4 l min<sup>-1</sup> was induced in the sand column (without the lid installed) by pressurising the perforated cylindrical box close to the bottom of the vessel. Pressure differences between the surface of the sand and different positions in the sand were measured by vertically entering a small-diameter probe (inner and outer diameter 4 and 6 mm, length 160 cm) in the sand from the surface. The tip of the probe has four small perforations while the other end is connected to a differential pressure transducer. Imposing a cylindrical coordinate system  $(r, \theta, z)$  on the vessel geometry, pressure measurements were carried out at 6 radii, 14 heights and 3 sections ( $\theta = 0^\circ, 120^\circ$



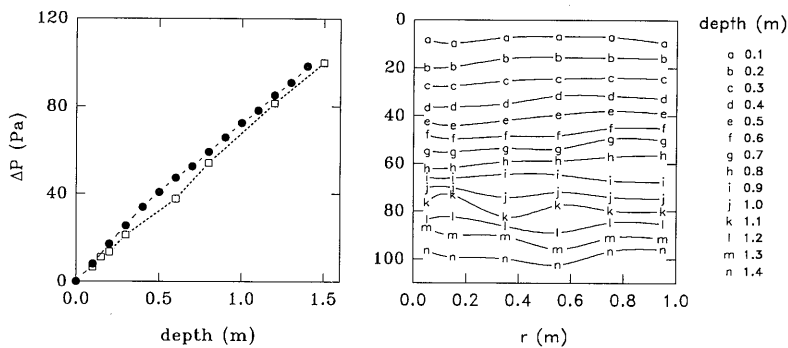


Figure 4.5: Left part: Pressure difference  $\Delta P$  (Pa) as function of depth in the sand. Closed circles represent the arithmetic mean of pressure differences measured at one depth with the small-diameter probe (data shown in the right part). Open squares represent the pressure differences measured with the radially inserted probes (flow  $42.41 \text{ min}^{-1}$ ). Right part: Pressure differences  $\Delta P$  (Pa) between positions ( $r$ , depth) in the sand and the surface of the column at one section, measured with an air flow of  $44.41 \text{ min}^{-1}$ . Lines connect data points at the same depth. Experimental uncertainties ( $1\sigma$ ) are within markers.

and  $240^\circ$ ). Fig. 4.5 (right part) shows the results of measurements at the section opposite to the location of the probes (all probes are positioned within an angle  $\theta$  of  $90^\circ$ ). In the ideal case of a homogeneous (one-dimensional) sand column, the lines in this figure would be horizontal and equidistant. In this respect considerable deviations are observed at approximately 1.1 m below the sand surface. Also, in the ideal case the pressure difference would increase proportionally with depth. Fig. 4.5 (left part) shows the pressure difference as a function of depth. Each data point (closed circles) in this figure represents the arithmetic mean of the pressure measured at six radii at one depth of the section shown in the right part of the figure. It is seen that the pressure difference increases somewhat faster with depth in the top layer of the column than in the middle and bottom layer. This suggests a lower permeability of the top layer than of the deeper layers.

An additional assessment of the homogeneity was performed by measuring the pressure difference between the surface of the sand column and the perforated tip of the radially inserted probes with an air-flow of  $42.41 \text{ min}^{-1}$  induced through the column by pressurising the perforated box. The results, presented in Fig. 4.5 (left part, open squares, no overlap with the closed circles due to a 5% smaller air-flow), do not support the previous observation of a faster increasing pressure difference in the top layer of the sand. They rather show that the sand column is more homogeneous than could be concluded from the data obtained with the small diameter probe. A possible explanation is that the perforated tip of the small-diameter probe may become obstructed by sand grains while it is being driven into the sand column. This may have caused the observed phenomenon of a smaller increase of the pressure difference at larger depths and may also have caused the fluctuations in the radial direction at larger depths.

It should be mentioned that the vessel is actually not a one-dimensional system since the perforated cylindrical box (diameter 1.62 m) does not overlay the whole area of the

sand column (diameter 2.00 m). Two-dimensional numerical calculations of the pressure field show that deviations from the ideal one-dimensional case at the axis of the column vary between 1% at 1.4 m depth to 3% near the surface of the sand column. Near the wall of the vessel these deviations are 6% and 4%, respectively (numerical values being lower). For the data presented in the left part of Fig. 4.5 (open squares) which have been measured at the central axis of the vessel, these deviations are negligible. On the other hand, with respect to the pressure differences measured near the wall of the vessel and which are presented in the right part, the 6% deviation at 1.4 m depth may not be discarded. However, with respect to the measured variations of the pressure difference at one depth, which are larger than 6%, this change is not significant. Also the arithmetic mean of the pressure differences measured at six radii at one depth, is influenced by the two-dimensional effect. However, for every depth down to 1.4 m this effect on the arithmetic mean is approximately 3%. As a consequence, to first order the measured pressure difference still increases proportionally to depth. In other words, two-dimensional effects can be ignored and inhomogeneities in the sand column are indicated by deviations from a linearly increasing pressure with depth.

Another point of concern is the humidity of the sand column during the measurements since about 60 litre of water was removed from the bottom of the vessel about a year later. However, the measured water-retention curve of the sand (see chapter 8) indicates a low and constant pore-water fraction ( $\approx 9\%$ ) at 50 cm or more above the saturated sand near the bottom. As a consequence, the sand column must have been rather dry and homogeneous (considering the air-filled porosity) to a depth of 1.5 m; the region of the pressure measurements. In addition, as the sand column is 'interrupted' by the perforated box with no water retention capability, the water content above the box might also have been lower.

In conclusion, from the maximum difference between each datapoint and a linear fit to the data for the two datasets presented in the left part of Fig. 4.5, it is estimated that deviations from the ideal homogeneous situation are less than 10%. Based on this finding, the maximum allowed differences in the validation process between modelled and measured radon concentrations in the vessel is 10%.

## 4.5 Sand properties

The properties of the sand that are of importance for radon transport and radon generation have been measured in separate experiments. In principle, referring to Eq. 2.32, for the study of radon transport in porous materials it is sufficient to know the partition-corrected porosity, tortuosity and radon production rate. However, referring to Eqs. 2.34 and 2.35, it is more constructive to analyse the radon production rate on the basis of more elementary quantities like density, radon emanation coefficient and radium content. For example, conditions like water content and compaction of soil are directly related to changes of the emanation coefficient and (air-filled) porosity, respectively. Therefore, these basic parameters will be used in the analysis instead of only the radon production rate.

### 4.5.1 Grain size, density and porosity

The grain-size distribution was measured by dry sieving. The results, presented in Fig. 4.6, show that the mass fractions are reasonably symmetrically distributed around 300  $\mu\text{m}$  with a slightly longer tail to larger diameters. Assuming a lognormal distribution

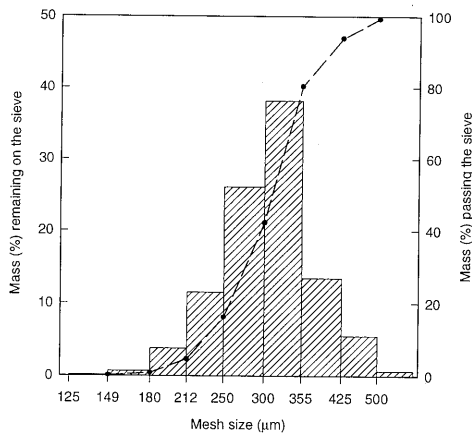


Figure 4.6: Grain-size distribution of the sand. Bars indicate mass fraction remaining on the sieve with corresponding mesh size (left vertical axis); dashed curve connects data points indicating the total mass fraction passing the sieve (right vertical axis). The horizontal axis is on a logarithmic scale.

(the hypothesis of a lognormal distribution can not be rejected using a significance level of 5%) the estimated values for the geometric mean and geometric standard deviation are  $305 \mu\text{m}$  and 1.2, respectively.

The porosity  $\epsilon$  was determined using the mass increase of a dry cylindrical sand sample (height  $\approx 5 \text{ cm}$ ; diameter  $15 \text{ cm}$ ) due to water saturation (see chapter 8 for a description of the instrument). It was observed that saturating and drying the sample several times compacted the sand notably. A dry sample with an initial porosity of 0.38, could finally attain a porosity of 0.33. Since the vessel has been gradually filled with layers sand of 15-20 cm and the water level has been raised and lowered a few times after each layer, such compaction probably also occurred during the filling of the vessel. However, the weight of the sand on top may have counteracted the compaction of the sand at the bottom of each new layer. On the other hand, this may have caused a smaller initial porosity. In the light of these uncertainties, it was decided to use a porosity at the low end of the measured range:  $0.340 \pm 0.010$ .

For an accurate determination of the specific density (mass per unit solid phase), a  $500 \pm 0.25 \text{ ml}$  ( $20^\circ\text{C}$ ) volumetric flask was partly filled with a mass  $M_s$  (kg) of sand and subsequently filled up with a mass  $M_w$  (kg) of water ( $20^\circ\text{C}$ ). The specific density  $\rho_s$  ( $\text{kg m}^{-3}$ ) of the sand is calculated using the relation

$$\frac{M_w}{\rho_w} + \frac{M_s}{\rho_s} = V_f, \quad (4.1)$$

where  $\rho_w$  is the density of water at  $20^\circ\text{C}$  and  $V_f$  is the volume ( $\text{m}^3$ ) of the flask. This experiment was repeated several times, giving an average specific density of  $2634 \pm 10 \text{ kg m}^{-3}$ . Specific density measurements of sieved samples with a grain-size range of 210-250, 250-300, 300-355 and 355-420  $\mu\text{m}$  indicate that smaller grains have a slightly higher density [Meschendorp, 1994]. The difference with unsieved sand ( $<0.2\%$ )

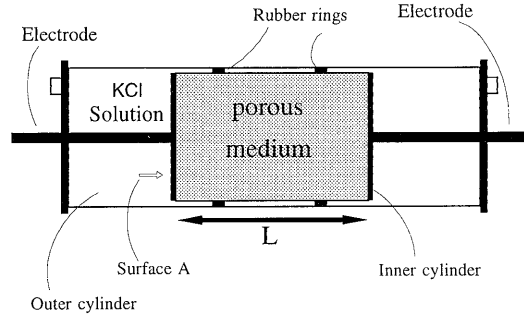


Figure 4.7: Schematic presentation of device to measure the tortuosity.

is virtually negligible. As the bulk density  $\rho_b$  is related to the specific density  $\rho_s$  according to  $\rho_b = (1 - \epsilon)\rho_s$ , a value of  $1740 \pm 50 \text{ kg m}^{-3}$  is found for the bulk density of the sand.

#### 4.5.2 Tortuosity

The tortuosity of the sand was determined using electrical conductivity measurements [Van der Grinten, 1987; Meschendorp, 1994]. The analogy which exists between diffusion and flux of electricity has been described in [Klinkenberg, 1951]. The device to measure tortuosity is pictured in Fig. 4.7. It consists of two concentric perspex cylinders. The inner cylinder, containing the sand sample, is closed with two metal gauzes. The outer cylinder is closed with perspex flanges, which have feed-throughs for electrodes connected to the metal gauzes of the inner cylinder. The device is filled with a 0.01 M KCl solution. Experiments were carried out with and without a sample in the inner cylinder. In both cases, the electrical resistances, denoted as  $R_s$  and  $R_0$ , were measured by applying an alternating voltage with a frequency of 1000 Hz. The electrical resistance without a sample can be written as

$$R_0 = \frac{L}{A\sigma}, \quad (4.2)$$

where  $L$  (m) is the length of the inner cylinder,  $A$  ( $\text{m}^2$ ) is the surface area of the inner cylinder and  $\sigma$  ( $\Omega^{-1}\text{m}^{-1}$ ) is the conductivity of the solution. With a porous medium in the inner cylinder, the surface area  $A$  is multiplied by the porosity  $\epsilon$  and the length  $L$  is corrected for the tortuosity, giving for the electrical resistance  $R_s$  with a porous medium:

$$R_s = \frac{L}{\epsilon\tau A\sigma}. \quad (4.3)$$

Combining Eqs. 4.2 and 4.3 results in

$$\tau = \frac{R_0}{\epsilon R_s}. \quad (4.4)$$

The resistances  $R_0$  and  $R_s$  were measured by varying the alternating voltage from 0 to 1000 mV in steps of 200 mV and measuring the accompanying alternating current. By

a least-squares fit of Ohm's law to the data,  $R_0$  and  $R_s$  were obtained. No significant frequency dependence between  $10^2$  Hz and  $10^4$  Hz was observed. Measurements of the porosity dependence of the classified filter sand indicate that tortuosity varies from 0.635 to 0.642 (uncertainty approximately 1%) when porosity is in the range  $0.338 < \epsilon < 0.375$ . In the calculation of the tortuosity it is assumed that all pores in the medium are filled with the saline solution. If this is not the case the measured  $\tau$  will be smaller than the true value. Since the cylinder was filled slowly with the solution and experiments were started one day later, presumably no air was trapped inside the material. A tortuosity of  $0.640 \pm 0.010$  is assumed for the sand in the vessel.

### 4.5.3 Radium content

For an approximate determination of the radium content, sand samples of about one litre were placed in Marinelli beakers and positioned over a hyper-pure germanium detector<sup>6</sup> inside a lead shielding and analysed for the gamma-activities of several lines of radon daughters  $^{214}\text{Pb}$  and  $^{214}\text{Bi}$ . The  $^{226}\text{Ra}$  content was calculated assuming secular equilibrium, which resulted in  $3.68 \pm 0.13 \text{ Bq kg}^{-1}$  (statistical error). Since emanated radon could escape the sand sample during these measurements the actual radium content may be 20% higher (taken into consideration the measured value of the emanation coefficient). It must be emphasized that knowing the exact value of the radium content and emanation coefficient is not so relevant. For this study on radon transport, only the product of the radium content and emanation coefficient is of crucial importance since this product (which is actually measured) determines the production rate of radon in the pore space of the sand.

### 4.5.4 Radon adsorption and desorption

The radon adsorption and desorption characteristics of the sand were measured with 'build-up and flush' experiments. Basically, in such an experiment a high pore-air radon concentration is established in a small sand column. After equilibrium has been reached in the radon partitioning between the air, water and adsorbed phase, the column is quickly flushed with radon-free nitrogen. By measuring the radon concentration of the effluent flow as function of time, information about the radon adsorption and desorption rates  $\alpha_{s \rightarrow a}$  and  $\alpha_{a \rightarrow s}$  can be inferred.

### Experimental

In the experiments, two 50 cm PVC cylinders (inner diameter 9.25 cm) are filled with sand. The back and front side of each cylinder has a feed through (including a filter to obstruct the sand grains) to which a small diameter plastic tube may be connected. A closed loop between both cylinders and a container with a radon source is established and air is circulated with an electrical pump at a rate of approximately  $1 \text{ l min}^{-1}$  through the system for about four weeks. This period is sufficient to attain equilibrium radon transfer between the phases. Before disconnecting the pump and radon source, an evacuated Lucas cell is filled with air from the system to determine the initial radon concentration  $C_a(t = 0)$  in the air-filled pore space. Thereafter, a radon-free nitrogen flow of  $0.5 \text{ l min}^{-1}$  is induced through each column (starting at  $t = 0$ ) utilising a mass flow controller<sup>7</sup> for

<sup>6</sup>EG&G ORTEC GEM Series HPGe coaxial detector system.

<sup>7</sup>MKS MFC 1179A, MKS Instruments, Inc.

each column separately. The two flows are joined at the exhaust side of the columns. At regular intervals, some gas from the exhaust flow is transferred to a Lucas cell to determine the radon concentration of the effluent gas as function of time. A 'build-up and flush' experiment was carried out with oven-dry sand ( $m = 0$ ) and room-dry sand. In the latter case, the pore-water content is in the range  $(1 - 3) \cdot 10^{-3} \text{ m}^3 \text{ m}^{-3}$ : the hygroscopic water content of the sand between 20% and 70% relative humidity at 20 °C (see Table 4.2).

### Model description

The transport equation for the adsorbed phase, Eq. 2.39, forms the basis for analysing the data. Several simplifications can, fortunately, be made. First, since each column is flushed once in 2.4 min, the pore-air radon concentration at  $t > 10$  min is such that transfer from the air phase to the solid phase may be ignored with respect to the reversed process. Secondly, since the experiment takes only a few hours, radon decay may be ignored. Thirdly, the radon production rate of the sand may be neglected due to the high initial concentration. As an additional simplification, we assume that the adsorption and desorption rates  $\alpha_{s \rightarrow a}$  and  $\alpha_{a \rightarrow s}$  can each be represented by one constant value. Then, Eq. 2.39 is simplified to

$$\frac{\partial C_s}{\partial t} = -\alpha_{s \rightarrow a} C_s, \quad (4.5)$$

and may be regarded to apply for each position in a column. The initial adsorbed concentration  $C_s(t = 0)$  can be obtained from the measured initial air-filled radon concentration  $C_a(t = 0)$  using Eqs. 2.30 and 2.31:

$$C_s(t = 0) = \frac{\epsilon_a \alpha_{a \rightarrow s} C_a(t = 0)}{\rho_b \alpha_{s \rightarrow a}}. \quad (4.6)$$

Application of this initial condition for solving the differential equation 4.5 is actually complicated by the fact that Eq. 4.5 only holds for  $t > 10$  min. As a first order correction for the non-instantaneous removal of pore-air radon, a delay of 144 s is introduced corresponding with the period necessary to flush a column once. The adsorbed concentration ( $t > 10$  min) is therefore approximated by:

$$C_s(t) = \frac{\epsilon_a \alpha_{a \rightarrow s} C_a(t = 0)}{\rho_b \alpha_{s \rightarrow a}} \exp(-\alpha_{s \rightarrow a}(t - 144)). \quad (4.7)$$

The rate of (negative) change of adsorbed concentration,  $-\frac{dC_s(t)}{dt}$ , multiplied by the total mass  $M_s$  of the sand, yields the total radon production rate ( $\text{Bq s}^{-1}$ ) in the air-filled pore space. The time-dependent effluent radon concentration is finally obtained by dividing by the gas-flow rate  $F$ :

$$C_{\text{eff}}(t) = \frac{M_s \epsilon_a \alpha_{a \rightarrow s} C_a(t = 0)}{\rho_b F} \exp(-\alpha_{s \rightarrow a}(t - 144)). \quad (4.8)$$

### Results and discussion

The total mass  $M_s$  of the sand in the columns was measured as  $11.318 \pm 0.005$  kg; corresponding with a density  $\rho_b$  of  $1680 \pm 30 \text{ kg m}^{-3}$  (experimental uncertainty mainly determined by estimated uncertainty in cylinder volume) and an air-filled porosity  $\epsilon_a$

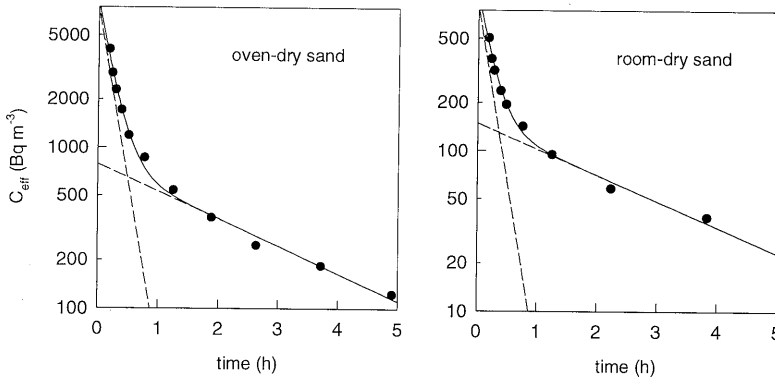


Figure 4.8: Measured effluent radon concentration  $C_{\text{eff}}$  ( $\text{Bq m}^{-3}$ ) as function of time for oven-dry sand (left part) and room-dry sand (right part). Statistical uncertainties ( $1\sigma$ ) are within markers. Solid lines represent a fitted (two-term) exponential function of which each term is indicated by dashed lines.

of  $0.361 \pm 0.007$ . Furthermore, the initial air-filled radon concentration was  $2.94 \pm 0.07 \text{ MBq m}^{-3}$  and  $1.16 \pm 0.03 \text{ MBq m}^{-3}$  in the experiment with room-dry and oven-dry sand, respectively. The measured effluent radon concentrations as function of time are presented in Fig. 4.8.

As expected from Eq. 4.8, a continually decreasing concentration is measured. However, an (single-valued) exponentially decreasing concentration as described by the model is not observed in both experiments. As alternative, a superposition of two independent desorption processes (of which each is given by Eq. 4.8), written as

$$C_{\text{eff}}(t) = \frac{M_s \epsilon_a C_a(t=0)}{\rho_b F} (\alpha_{a \rightarrow s1} \exp(-\alpha_{s1 \rightarrow a}(t - 144)) + \alpha_{a \rightarrow s2} \exp(-\alpha_{s2 \rightarrow a}(t - 144))), \quad (4.9)$$

where  $s1$  and  $s2$  refer to a different adsorption surface, was fitted to the data with  $\alpha_{a \rightarrow s1}$ ,  $\alpha_{s1 \rightarrow a}$ ,  $\alpha_{a \rightarrow s2}$ , and  $\alpha_{s2 \rightarrow a}$  ( $\text{s}^{-1}$ ) as free parameters. The results, shown in Table 4.1 and by solid lines in Fig. 4.8 (dashed lines represent each fitted term in Eq. 4.9) are seen to describe the data fairly well.

An interesting aspect in comparing the results with room-dry and oven-dry sand is the same fitted desorption-rate constants (gradient of dashed lines in Fig. 4.8). Apparently, the presence of a thin water film on the sand grains<sup>8</sup> does not influence the rate of desorption. On the other hand, since the effluent concentrations are much higher with oven-dry sand, the presence of water affects the rate of adsorption. If the water film is not homogeneously distributed around the grains such that dry-surface parts remain, these results indicate that radon adsorbs to these surface parts only. In that case, the increased adsorption is completely caused by the larger area of dry surfaces.

In view of this hypothesis - only radon adsorption to dry surfaces - the observation of having two different desorption-rate constants is a remarkable one. It may suggest

<sup>8</sup>A 5.66 kg sand sample (porosity 0.36) with a pore-water content of  $2 \cdot 10^{-3}$  contains about 2.5 gr water. Spread over  $43 \text{ m}^2$  (assuming spherical grains with a radius of  $150 \mu\text{m}$ ), this amount of water is contained in a layer of circa 60 nm, corresponding with hundreds of layered molecules.

that desorption occurs from the PVC wall and the aluminum back and front side of a column. However, their influence has been observed to be negligible in an experiment with an 7.5 cm inner perspex tube instead of sand. As another explanation, the energy of adsorption may be different for each adsorption site due to the complex structure of a sand-grain surface. In view of this supposition, it is actually surprising that a model description using two different desorption-rate constants reproduces the experimental data quite well. On the other hand, the high values of  $\chi_{\text{red}}^2$  suggest that more desorption rates (possibly dependent on the adsorbed concentration  $C_s$ ) may be involved in the process.

It should be remarked that above-mentioned conclusions can only be drawn if the initially present radon has been completely removed after 10 min. Complete removal can be appreciated by comparing the measured effluent and initial concentrations in the two experiments. Higher effluent concentrations are measured with oven-dry sand than with room-dry sand. Since a three times lower concentration was present in the oven-dry sand initially, this certainly indicates a negligible influence of remaining radon in the air-filled pore space.

Finally, the possibility should be addressed that radon may diffuse through the sand grains. Radon which has entered the sand grains by diffusion, may again diffuse out of the grains when the column is being flushed with radon-free gas. This process largely depends on the intragranular diffusion coefficient. Reported values for the diffusion constant of argon in rock-forming minerals are extremely small. Tanner [1964] refers to values ranging from  $10^{-31}$  to  $10^{-69} \text{ m}^2 \text{ s}^{-1}$ . Even if the largest value of  $10^{-31} \text{ m}^2 \text{ s}^{-1}$  would apply to radon in sand grains, matrix diffusion may be fully ignored. In addition, Krishnaswami and Seidemann [1987] found negligible leakage of argon<sup>9</sup> from rock forming minerals. It should be noted that these findings refer to diffusion of an inert gas which has been produced inside the matrix. Diffusion of 'external' gas may take place along other pathways in the grains, resulting in a different diffusion coefficient. If so, the process of diffusion may be important. From the present experiments it is however not feasible to distinguish between intragranular diffusion and surface adsorption.

The experimental results indicate an equilibrium radon adsorption coefficient  $k_a$  of  $(9.4 \pm 0.6) \cdot 10^{-7}$  and  $(1.45 \pm 0.10) \cdot 10^{-5} \text{ m}^3 \text{ kg}^{-1}$  for room-dry and oven-dry sand, respectively. The results agree well with experimental results for sand obtained by Schery and Whittlestone [1989] who found  $k_a < 3 \cdot 10^{-5} \text{ m}^3 \text{ kg}^{-1}$  and data presented by Rogers and Nielson [1991b] which suggest  $k_a \approx 1 \cdot 10^{-5} \text{ m}^3 \text{ kg}^{-1}$ . Radon adsorption should be taken into account for completely dry sand because, in equilibrium, about 7% of the radon activity in the pore-space is adsorbed to surfaces<sup>10</sup> (or diffused into the grains). For room-dry sand, the adsorbed activity only amounts 0.4% and may thus be neglected.

#### 4.5.5 Radon emanation coefficient

The radon emanation coefficient  $\eta$  (the total fraction of radon atoms that escape from a mineral grain, see Eq. 2.35), is known to be sensitive to the moisture content of the porous medium. Therefore, an experimental study of the effect of moisture on the emanation coefficient of the sand was performed. The measurements for pore-water contents  $> 2\%$  were carried out with a 'closed-can method' using two identical instruments. Each instrument consisted of a closed cylinder (diameter 20 cm, height 32 cm) of which the

<sup>9</sup> <sup>39</sup>Ar and <sup>38</sup>Ar produced by neutron activation and <sup>40</sup>Ar produced in the decay of <sup>40</sup>K.

<sup>10</sup> The ratio of radon activity adsorbed to surfaces and in the air-filled pore space is calculated (see Eqs. 2.30 and 4.6) as  $\frac{\rho_h C_s}{\epsilon_a C_a} = \frac{\alpha_{a \rightarrow s1}}{\alpha_{s1 \rightarrow a}} + \frac{\alpha_{a \rightarrow s2}}{\alpha_{s2 \rightarrow a}} = \frac{k_a \rho_h}{\epsilon_a}$ .



Table 4.1: Results of fitting Eq. 4.9 to the measured effluent radon concentration with room-dry sand and oven-dry sand with free parameters  $\alpha_{a \rightarrow s1}$ ,  $\alpha_{s1 \rightarrow a}$ ,  $\alpha_{a \rightarrow s2}$ , and  $\alpha_{s2 \rightarrow a}$  ( $\text{s}^{-1}$ ). Indicated uncertainties refer to external errors.

	experiment with room-dry sand	experiment with oven-dry sand
$\alpha_{a \rightarrow s1}$	$(1.5 \pm 0.3) \cdot 10^{-6}$	$(3.5 \pm 0.5) \cdot 10^{-5}$
$\alpha_{s1 \rightarrow a}$	$(1.4 \pm 0.2) \cdot 10^{-3}$	$(1.4 \pm 0.4) \cdot 10^{-3}$
$\alpha_{a \rightarrow s2}$	$(3.4 \pm 0.4) \cdot 10^{-7}$	$(4.6 \pm 0.5) \cdot 10^{-6}$
$\alpha_{s2 \rightarrow a}$	$(1.04 \pm 0.15) \cdot 10^{-4}$	$(1.09 \pm 0.10) \cdot 10^{-4}$
$\chi_{\text{red}}^2$	9	19

lower half was filled with a sand sample of about 8 kg. After a period of four weeks, when the radon concentration inside the cylinder has virtually reached its equilibrium value, air from the void space above the sand was sampled with a piston. The radon concentration of the air sample was measured with the same equipment as used in the vessel experiments. These measurements were carried out with a range of moisture contents, obtained by simply pouring known amounts of water on top of the sand sample.

In the closed-can method, the radon emanation coefficient is calculated using the steady-state solution of the analytical diffusion model discussed hereafter in section 5.3. It is presented in the next chapter because the model is predominantly applied for analysing the radon-vessel experiments with time-dependent diffusive transport. Following the nomenclature in section 5.3, the closed cylinder with the sand sample may be regarded as a one-dimensional system, consisting of a homogeneous sand column of height  $h_s$  (16 cm) and a void space of height  $h_{cs}$  (16 cm) above. The equilibrium radon concentration  $C_v$  in the void space is given by (Eq. 5.5 with  $z = h_s$ ,  $\lambda_v = 0$  and  $t \rightarrow \infty$ ):

$$C_v = \frac{S}{\beta\lambda} \left[ 1 - \frac{\cosh\left(\frac{h_s}{\ell}\right)}{\cosh\left(\frac{h_s}{\ell}\right) + \frac{D}{\ell h_{cs}\lambda} \sinh\left(\frac{h_s}{\ell}\right)} \right], \quad (4.10)$$

where the partition-corrected porosity  $\beta$  is given by Eq. 2.33, the diffusion length  $\ell$  by Eq. 2.42 and the radon production rate  $S$  by Eq. 2.34:

$$S = \eta\rho_b\lambda C^{Ra}.$$

Since radon adsorption may be neglected, the partition-corrected porosity is only determined by the porosity and pore-water content. The dependence of the bulk diffusion coefficient on pore-water content  $m$  has been measured. These measurements are outlined in chapter 8 covering the vessel experiments with a ground-water level. A fitted correlation function (Eq. 8.3) is used for the radon-diffusion coefficient as function of pore-water fraction:

$$D = \epsilon\tau_a D_a \exp(a_1(m + m^5)).$$

A ‘flush and adsorb method’ (FAM) was used for water contents  $< 2\%$ . Later, several extensions and improvements have been introduced to the experimental set-up. A description of the instrument will be given as it was used for determining the emanation

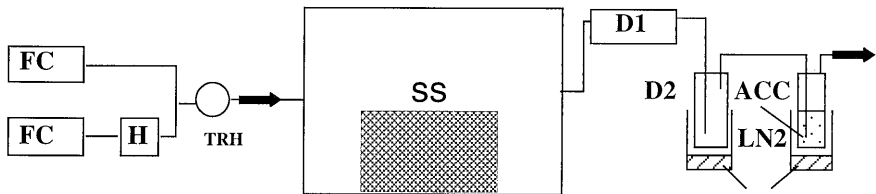


Figure 4.9: Schematic drawing of the instrument used in the 'flush and adsorb method'. FC: nitrogen-flow controller; H: humidifier; TRH: temperature and relative humidity sensor; SS: sand sample; D1: silica-gel dryer; D2: water trap; LN2: liquid nitrogen; ACC: activated charcoal.

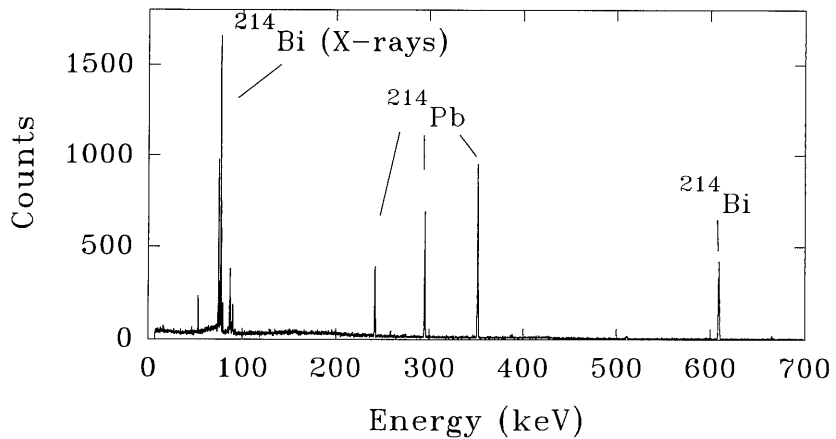


Figure 4.10: Spectrum (8096 channels) taken with the low-background planar gamma-ray detector for 17.1 g ACC with an adsorbed-radon activity of 38 Bq and a measuring (live) time of 10 h.

coefficient of the sand<sup>11</sup>. In short, the instrument consists of a stainless steel box with a sealed lid. The outer dimensions are  $0.66 \times 0.46 \times 0.31 \text{ m}^3$ . Inside the box a (radon-producing) sample (SS in Fig. 4.9) can be placed. Radon-free nitrogen gas is supplied through a small-diameter opening in the left wall of the box. To prevent changes in the conditioned moisture content of the sample during experiments, the humidity of the ingoing nitrogen flow is controlled by a humidifier (H in Fig. 4.9). The temperature and relative humidity of the ingoing flow are measured with combined temperature and humidity sensors (TRH in Fig. 4.9) of which the output voltages are connected to a datalogger for registering hourly averages. The (radon-bearing) exhaust nitrogen gas that leaves the box through an opening at the right wall is led through a pre-dryer (D1 in Fig. 4.9) consisting of a column of silica-gel (length 50 cm, diameter 9.3 cm) and a water trap (D2 in Fig. 4.9) consisting of a tube cooled with nitrogen vapour. Thereafter, the dried flow is led through a radon adsorber consisting of a glass test-tube (height 20 cm, diameter 3 cm) filled with charcoal pellets and cooled to nitrogen-vapour temperature (ACC in Fig. 4.9). The water vapour is removed from the exhaust flow to prevent ice-accretion in the charcoal bed. The radon activity that is accumulated on the charcoal depends on the time of adsorption, which is usually 24 h or more. After adsorption, the charcoal pellets are transferred from the test-tube into a 5 cm diameter standard pill-box. The radon activity on the charcoal pellets is determined using gamma-ray spectroscopy. The gamma-ray activity of several radon-daughters is measured in the energy window from 0 to 700 keV with a low-background planar gamma-ray detector<sup>12</sup>. In Fig. 4.10 a spectrum is shown measured with the gamma-ray detector for 17.1 g ACC (the amount needed to fill the standard pill-box geometry) with an adsorbed-radon activity of 38 Bq and a measuring time of 10 h. The spectrum shows among others the 242, 295 and 352 keV gamma-rays from  $^{214}\text{Pb}$ , the 609 keV gamma-ray from  $^{214}\text{Bi}$  and  $\text{K}_{\alpha 1}$  (77.1 keV) and  $\text{K}_{\alpha 2}$  (74.8 keV) X-rays from  $^{214}\text{Bi}$ .

To relate the measured gamma-ray activity to the radon activity on the charcoal, three radon sources were prepared consisting of different quantities of sand originating from the former uranium mining operation at Wismut, Germany. This sand has a high radium and low thorium content. Each source was placed in a 5 litre stainless steel leaktight cylinder (at 50% relative humidity, 20°C) to determine the radon source strength ( $\text{Bq s}^{-1}$ ) according to the conventional closed-can method described above. With the 'calibrated' sources 14 adsorbed activities were measured in which one of the sources was placed in the box. A nitrogen flow rate of approximately  $0.71 \text{ min}^{-1}$  (50% RH; 20°C) was led through the box and radon was adsorbed on 17.1 g of activated charcoal. The results of these calibration experiments, presented in Fig. 4.11, show a completely linear relation between the net count rate in the gamma-energy window from 0-700 keV and the adsorbed radon activity as calculated from the calibrated source strengths (relative error < 1%) [Van der Graaf et al., 1995]. The procedure for calculating the radon source strength ( $\text{Bq s}^{-1}$ ) of a sample is described by Van der Graaf et al. [1997]<sup>13</sup>.

To measure the emanation coefficient of the sand for low pore-water contents, four open plastic boxes ( $0.21 \times 0.15 \times 0.06 \text{ m}^3$ ) were each filled with about 2 kg sand (sample height 4 cm) and placed inside the stainless steel box. The relative humidity of the incoming flow was set at different values to attain a range of pore-water contents, see

<sup>11</sup>This largely corresponds to a description given by Van der Graaf et al. [1995].

<sup>12</sup>EG&G ORTEC LO-AX Series HPGe coaxial low-energy photon spectrometer.

<sup>13</sup>More precisely, the exhalation rate ( $\text{Bq m}^{-2} \text{ s}^{-1}$ ) is calculated in this document. The source strength is obtained by multiplying by the surface area of a sample.

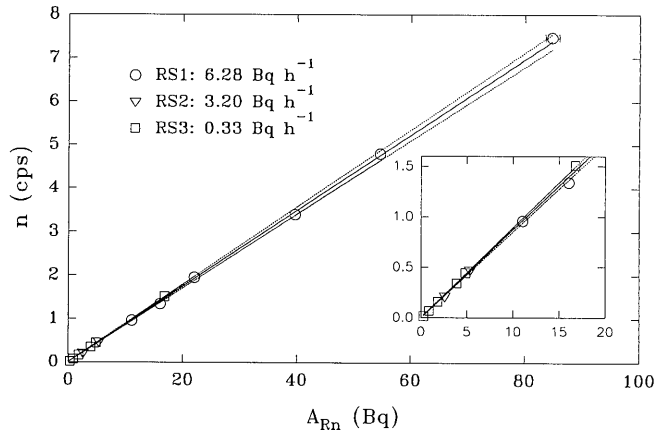


Figure 4.11: Net count rate  $n$  (cps) in the energy window 0-700 keV against the adsorbed radon activity  $A_{Rn}$  (Bq) as calculated from the adsorption time and the radon source strength ( $\text{Bq h}^{-1}$ ) of three different sources RS1, RS2 and RS3. The solid line represents a linear fit to the data with the 95% confidence indicated by dashed lines.

Table 4.2. In addition, one experiment was carried out in which a cup of liquid water was introduced in the metal box and the incoming flow was set at maximum relative humidity (95%). This increased the pore-water content to  $(7.5 \pm 0.2) \cdot 10^{-3}$ . Pore-water contents were determined by weighing each sample before and after each experiment. The adsorption- and measuring time were both at least 48 h (adsorbed radon activity approximately 2 Bq). Emanation coefficients are calculated with:

$$\eta = \frac{S_s}{\lambda M_s C^{Ra}}, \quad (4.11)$$

where  $S_s$  is the source strength of a sample ( $\text{Bqs}^{-1}$ ) and  $M_s$  (kg) its mass. Note that *all* emanated radon is assumed to escape the sample. This is a valid assumption for the sand samples used in this study due to the large radon-diffusion coefficient.

The measured emanation coefficient as function of pore-water content is shown in Fig. 4.12. A sharp rise in emanation coefficient from 0.13 to 0.28 is seen as the pore moisture content is increased from zero to only 0.5%. For higher moisture contents, the emanation coefficient decreases slightly to about 0.24 and seems to increase again for moisture contents higher than 15%<sup>14</sup>. The mechanisms by which moisture affects the radon emanation coefficient is only partly understood and has been reviewed by Tanner [1980]. Qualitatively it can be stated that in a dry porous medium a reasonable fraction of the radon atoms that escape from a grain due to recoil bury themselves in another grain. Since the recoil range in water is much smaller ( $0.1 \mu\text{m}$ ) than in air ( $63 \mu\text{m}$ ) [Nazaroff et al., 1988], addition of water to the pore space inhibits this mechanism by which the emanation coefficient is increased. This process is probably responsible for the measured

<sup>14</sup>Actual emanation coefficients may be about 20% lower due to a systematic error in the method for determining the radium content.

Table 4.2: Relative humidity (rel. error estimated at 5%) and corresponding pore-water content of the sand. The '>95' case refers to a situation with liquid water inside the box.

rel. humidity (%)	pore-water content ( $\cdot 10^{-3} \text{ m}^3 \text{ m}^{-3}$ )
0	$0.0 \pm 0.2$
20	$0.9 \pm 0.2$
50	$1.8 \pm 0.2$
88	$4.0 \pm 0.2$
95	$5.0 \pm 0.2$
> 95	$7.5 \pm 0.2$

increase of the emanation coefficient in the range  $0 < m < 0.004$ . In this context, it is remarkable that a pore-water content of 0.004 corresponds with a water-film thickness on the sand grains of circa  $0.12 \mu\text{m}$  (assuming spherical grains with a diameter of  $300 \mu\text{m}$  and a uniform film thickness), in good agreement with the radon recoil range in water.

The measured variation of the emanation coefficient in the range  $m > 1\%$  constitutes a complication since a decreasing emanation coefficient with increasing moisture content is not supported by a known physical process. A difficulty with the closed-can method is however the non-uniform water distribution in the sand sample. For low moisture contents the sand on top might have been wetter than the sand close the bottom, while the reverse might have been the case for large moisture contents. Such an inhomogeneity is an important aspect which should be reckoned with in these experiments. In principle, these difficulties can be avoided by using a smaller sample, but the low radon production rate of the sand ( $< 1 \cdot 10^{-2} \text{ Bq kg}^{-1} \text{ h}^{-1}$ ) impedes a precise radon concentration determination when the sample is small. As yet, the measured variation of emanation coefficient for  $m > 1\%$  is believed to be caused by a inhomogeneous water content distribution in the sand samples.

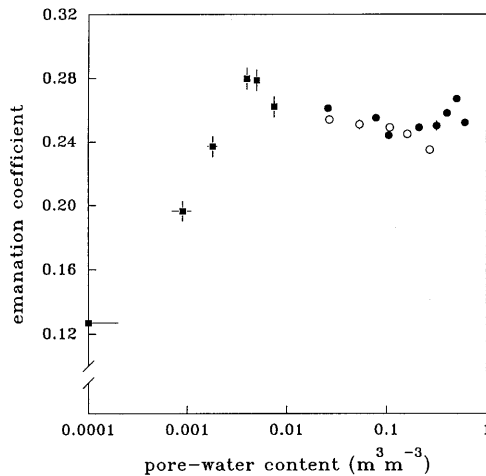


Figure 4.12: Results of measurements of the emanation coefficient of the sand as function of pore-water content. Results of the 'closed-can method' are indicated with circular marker (open and closed markers indicate which of the two identical instruments was used). Results of the 'flush and adsorb method' are depicted by square markers. Error bars indicate statistical errors ( $1\sigma$ ).

This concludes the discussion of the radon-transport parameters that are necessary for modelling radon transport in dry sand. The foundation has thus been laid for analysing the radon-vessel experiment conducted with dry sand (chapter 5, 6 and 7). Some additional parameters that are needed for modelling transport in moisturised sand are discussed in chapter 8.

# Chapter 5

## Diffusive transport experiments

### 5.1 Introduction

In this chapter the results of a set of measurements with pure diffusive transport in room-dry sand are presented and compared with analytical solutions of the governing differential equation. By eliminating advective radon transport, more or less simple experimental situations are examined which may be regarded as the first steps in the validation process. Most measurements concern time-dependent diffusive transport with initially nearly zero radon concentration in the sand column. First, the sand conditions during the experiments with room-dry sand will be discussed in section 5.2, followed by a description of the analytical diffusion model in section 5.3. The experiments without the lid on the vessel are considered to embody one of the most simple situations that can be studied and are discussed in section 5.4. Section 5.5 covers the experiments with the lid installed on the vessel at several several different heights simulating a crawl space. Finally, conclusions are drawn in section 5.6.

### 5.2 Sand conditions

As outlined in the previous chapter, most sand properties such as density, tortuosity and porosity could be determined with fair precision. A main difficulty in the experiments with room-dry sand however deals with the uncertainty in pore-water content. After the vessel had been completely filled in December 1991, the sand was dried by inducing an air-flow of  $50 \text{ l min}^{-1}$  (5% rel. humidity) through the column for more than a week. Afterwards, the sand column was left undisturbed (without the lid) for more than a year before starting the experiments with diffusive transport. Gravitational downward transport and evaporation of remaining pore water during this period further dried the sand. This process, however, may not have lowered the water content to such an extent that only hygroscopic water remained in the pores. In addition, during experiments with the lid installed, the water-saturated air in the crawl space might have moisturised the sand again. Therefore, the exact moisture content is not precisely known and might even vary with height and time. Although the pore-water content of the sand is expected to be  $< 5 \cdot 10^{-3} \text{ m}^3 \text{ m}^{-3}$  (except at the bottom in the first experiment without the lid installed, see section 5.4), which we might label as 'precisely known', the sensitivity of the radon emanation coefficient to the moisture content in this range, see Fig. 4.12, forms the main uncertainty. For example, an absolute change in moisture content of only  $1 \cdot 10^{-4} \text{ m}^3 \text{ m}^{-3}$  ( $34 \mu\text{g}$  water in a litre of bulk sand) is accompanied by a 2% change in

Table 5.1: Parameters of room-dry sand in the vessel as used in model calculations.

Bulk density	$\rho_b$	$1740 \pm 50 \text{ kg m}^{-3}$
Tortuosity	$\tau_a$	$0.640 \pm 0.010$
Radium content	$C^{Ra}$	$3.68 \pm 0.13 \text{ Bq kg}^{-1}$
Air-filled porosity	$\epsilon_a$	$0.340 \pm 0.010$
Partition-corrected porosity	$\beta$	$0.340 \pm 0.010$
Emanation coefficient	$\eta$	0.22

emanation coefficient. This complicates the situation for radon transport considerably because of the possible variation of emanation coefficient with height in the vessel. As the pore-water content of the sand in the vessel could not be measured, it is also not feasible to model a position-dependent emanation coefficient. Besides, such analysis would require application of a numerical transport model, whereas analytical solutions are preferred for validating purposes. In the light of these considerations, the emanation coefficient will be assumed independent of height.

Which value to use for the emanation coefficient depends on the (average) moisture content of the sand. As an approximation, it is assumed that only hygroscopic water remained in the sand. Based on the measured average relative humidity of the air in the experimental room, which is 30%, a water content of circa  $1.2 \cdot 10^{-3} \text{ m}^3 \text{ m}^{-3}$  is inferred from Table 4.2, which gives an emanation coefficient of about 0.22 (see Fig. 4.12).

In the previous chapter, the radon adsorption coefficient for room-dry sand was determined at  $(9.4 \pm 0.6 \cdot 10^{-7}) \text{ m}^3 \text{ kg}^{-1}$ . This value may not represent the adsorption coefficient of the sand in the vessel because of a possibly different moisture content. Fortunately, it is not of crucial importance to know the adsorption coefficient precisely since the influence of adsorption is small. If the measured value would apply to the situation in the vessel, the partition-corrected porosity  $\beta$  would be 0.5% higher than the air-filled porosity. As the influence of a varying emanation coefficient with height is considered to be the major source of error, followed by an uncertainty of 3% in the porosity of the sand, it appears justified to neglect the effect of adsorption on the partition-corrected porosity. For the same reasons, the effect of pore water (0.12%) on  $\beta$  may also be neglected. As a result, the numerical value of  $\beta$  equals the value of porosity:  $0.34 \text{ m}^3 \text{ m}^{-3}$ .

An overview of the parameters to be used in the model calculations for room-dry sand are given in Table 5.1 (with statistical uncertainties). Absolute errors, which are not so much of interest for this study of radon transport, are considerably higher for the  $^{226}\text{Ra}$  content (20%) and emanation coefficient (20%).

### 5.3 Analytical diffusion model

Diffusive transport of radon in the vessel can be described by a one-dimensional model. Some aspects do deteriorate the condition of full one-dimensionality, such as the concave bottom, the perforated box (not covering the full cross-sectional area) and the metal ring surrounding the box, but these are considered to have a minor influence as will be



discussed later. Moreover, the perforated box may be ignored due to its small volume (1%) with respect to the total sand volume. The vessel may thus be represented by a one-dimensional (2 m diameter) soil column of height  $h_s$  inside a closed casing leaving an air column of height  $h_{cs}$  above the soil, as schematically sketched in Fig. 5.1. Leakage or controlled ventilation may be present in the air column.

The one-dimensional counterpart of equation 2.32 for homogeneous soil, using  $z$  as spatial coordinate, neglecting advective transport and influence of pore-water, is given by (writing  $C$  for  $C_a$  for convenience):

$$\beta \frac{\partial C}{\partial t} = \epsilon_a \tau_a D_a \frac{\partial^2 C}{\partial z^2} - \beta \lambda C + S. \quad (5.1)$$

To solve Eq. 5.1 for  $C(z)$  three boundary conditions imposed by the set-up are included. 1) Since the bottom of the soil column is impermeable for radon, no radon flux is present at this position:

$$\frac{\partial C}{\partial z} = 0, \quad z = 0; \quad t \geq 0. \quad (5.2)$$

2) It is assumed that air in the air column is well mixed at all times. This, because a) diffusion of radon in air is fast (diffusion nearly neutralizes concentration differences over a distance of 50 cm in 6 hours), b) some mixing is introduced due to intake and exhaust of crawl-space air for radon concentration determination and c) free-convection is probably present in the crawl space. Besides, the analysis is much less complex when diffusion in the crawl space is not incorporated in the model. Mixing of crawl-space air can be assured by using a fan. However, it was decided to avoid air-flows to rule out generation of pressure differences over the surface of the sand. Such pressure differences would deteriorate the condition of pure diffusion. Based on the above-mentioned assumptions, the rate of change of radon concentration in the air column above the soil equals the flux due to diffusion into this volume minus the rate of removal, either by decay, leakage or ventilation. This concentration balance may be applied at the surface of the soil column:

$$\frac{\partial C}{\partial t} = -\frac{\epsilon_a \tau_a D_a}{h_{cs}} \frac{\partial C}{\partial z} - (\lambda + \lambda_v) C, \quad z = h_s; \quad t \geq 0, \quad (5.3)$$

where  $h_{cs}$  (m) is the height and  $\lambda_v$  ( $s^{-1}$ ) is the leakage or ventilation rate of the air column. 3) Starting from a situation with no radon activity in the soil pore space, one can formulate the initial condition

$$C = 0, \quad 0 \leq z \leq h_s; \quad t = 0. \quad (5.4)$$

With these boundary conditions Eq. 5.1 is solved using the method of Laplace transformation [Crank, 1956]. The following expression for the radon concentration as a function of  $z$  and  $t$  was derived:

$$C(z, t) = \frac{S}{\beta \lambda} \left( 1 - \frac{\cosh\left(\frac{z}{\ell}\right)}{\cosh\left(\frac{h_s}{\ell}\right) + \frac{\epsilon_a \tau_a D_a}{\ell h_{cs} (\lambda + \lambda_v)} \sinh\left(\frac{h_s}{\ell}\right)} - \frac{e^{-\lambda t}}{1 + \frac{h_{cs}}{\beta h_s} \delta_{\lambda_v, 0}} + \lambda \sum_{n=0}^{\infty} \frac{\cos(k_n z) e^{p_n t}}{G(p_n)} \right) \quad (5.5)$$

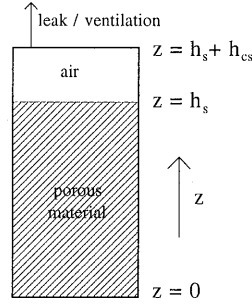


Figure 5.1: Schematic presentation of the system used for one-dimensional modelling.

with  $k_n$  the positive roots of

$$\epsilon_a \tau_a D_a k \tan(k h_s) + \frac{h_{cs} \epsilon_a \tau_a D_a k^2}{\beta} - h_{cs} \lambda_v = 0, \quad (5.6)$$

and with

$$p_n = -\frac{\epsilon_a \tau_a D_a}{\beta} k_n^2 - \lambda, \quad (5.7)$$

$$G(p_n) = p_n \left[ \left( \frac{p_n + \lambda}{p_n + \lambda + \lambda_v} \right) \left( 1 + \frac{\epsilon_a h_s}{2 h_{cs}} \right) - \frac{h_{cs} h_s (p_n + \lambda + \lambda_v)}{2 \epsilon_a \tau D_a} - \frac{1}{2} \right] \cos(k_n h_s), \quad (5.8)$$

and where  $\ell$  is the diffusion length (Eq. 2.42):

For the situation with an open top of the casing (air column with infinite height), the radon concentration at the surface of the sand ( $z = h_s$ ) is assumed to be zero:

$$C(z) = 0 \quad z = h_s; \quad t > 0. \quad (5.9)$$

Using this boundary condition instead of Eq. 5.3 the solution of Eq. 5.1 is

$$C(z, t) = \frac{S}{\beta \lambda} \left( 1 - \frac{\cosh\left(\frac{z}{\ell}\right)}{\cosh\left(\frac{h_s}{\ell}\right)} + \lambda \sum_{n=0}^{\infty} \frac{2(-1)^n \cos(k_n z) e^{p_n t}}{p_n h_s k_n} \right), \quad (5.10)$$

with

$$k_n = \frac{\pi}{2 h_s} (2n + 1), \quad (5.11)$$

and  $p_n$  given by Eq. 5.7.

## 5.4 Experiments without a ‘crawl space’

Two experiments were carried out without the lid on the vessel. A nearly zero radon concentration in the pore space of the sand was established by continuously flushing the column with an air-flow of  $50 \text{ l min}^{-1}$  (through the perforated box) during at least a day. Thereafter, the ingrowth of radon concentration was followed by sampling from the nine probes at regular intervals. Since about 60 litres of water could be removed from the bottom of the vessel just after completing the first experiment, a second identical experiment was performed 15 months later to assess whether the presence of this pore water influenced the measurements without a crawl space.

The time evolution of the radon concentration after stopping the flow is presented in Fig. 5.2 for the first (left part) and second (right part) experiment. For clarity, only a few of the measured radon profiles are shown in this figure. It is seen that the measured concentrations are well reproduced in the second experiment. The solid lines represent calculations based on Eq. 5.10 using the parameters listed in Table 5.1 and an effective column height  $h_s$  of 1.86 m, inferred from a calculation of the volume of the vessel<sup>1</sup>.

Two notable deviations concerning the measured radon profiles need some attention. First, the measured concentrations at the lowest two probes ( $z=0.36$  and  $z=0.66$ )<sup>2</sup> are

<sup>1</sup>The effective height is less than 2 m (the height of the sand at the centre) due to the concave bottom.

<sup>2</sup>Effective probe heights, deduced from their depth below the sand surface.

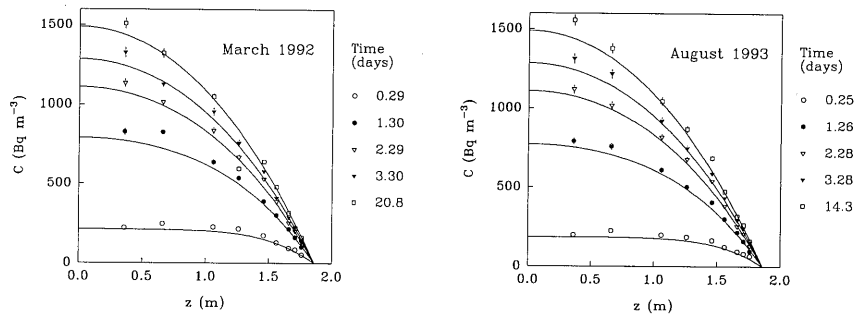


Figure 5.2: Results of the two experiments without a crawl space with diffusive radon transport. Radon concentration  $C$  ( $\text{Bq m}^{-3}$ ) is given as function of  $z$ -coordinate for different times  $t$  after flushing for experiment 1 (left part) and experiment 2 (right part). Solid lines represent calculated curves with input parameters given in Table 5.1. Error bars ( $1\sigma$ ) indicate experimental uncertainties.

higher than calculated. Since the measured concentration profile follows a reasonably smooth curve, the discrepancy at these heights might be due to the simplification of a flat bottom, made in the analytical one-dimensional model. However, when 2D numerical calculations are done with a curved bottom for the vessel, the differences with the analytical results are small and predict even lower concentrations at  $z=0.36$  (caused by the volume of the perforated box, present in the 2D numerical model, in which no radon is produced). Another cause may be the presence of moisture in the sand close to the bottom of the vessel. In that case the pore-air radon concentration is increased due to a higher emanation coefficient and also by the partitioning of radon between the water and air phase. However, as the second measured concentrations do not significantly differ from the first measured concentrations, it may be concluded that the pore water near the bottom hardly influenced the conditions for radon transport. This may not be so striking if one realises that 60l corresponds to a 6 cm layer of saturated sand. The effect on the radon concentration 30 cm higher (in fact more, due to the curved bottom) is then expected to be small.

Secondly, the measured concentration at the fifth probe from the top ( $z = 1.46$ ) clearly constitutes a deviation in the concentration profile. This is not only the case in the experiments without a crawl space but also in practically most subsequent experiments. Unfortunately, an explanation can not be given for this effect.

Next to these comments concerning some of the probes, an overall underestimation of the calculations is noticed. This is most obvious for profiles measured within two days after stopping the flow. This discrepancy is partly due to the remaining radon ( $C \neq 0$  at  $t = 0$ ). A flow rate of  $50 \text{ l min}^{-1}$  (estimated radon concentration  $5 \text{ Bq m}^{-3}$ ) ventilates the column once in 40 min. During this interval a pore-air radon concentration of  $20 \text{ Bq m}^{-3}$  is established by production in the sand, giving a total initial concentration of  $25 \text{ Bq m}^{-3}$ . Although this initially present radon quickly disappears from the column by diffusion, it has some effect (about 8%) on the profiles measured after 6-7h, but it hardly influences other profiles. In this respect, it is interesting to notice a larger

difference between experiment and model for the profile measured after 1.3 d than for the first one, indicating that remaining radon can not be the only cause of these differences. In addition to a non-zero initial condition, the radon concentration in the experimental room also influences the radon concentration in the sand. As this concentration in the well-ventilated room has been measured<sup>3</sup> at  $10 \text{ Bq m}^{-3}$ , the off-set in the measured concentrations in the sand due to ambient radon is however small.

Also, the influence of atmospheric pressure differences should be addressed. During a barometric pressure drop radon-rich pore air leaves the sand column due to expansion. Vice versa, during a barometric pressure rise radon-poor ambient air enters the sand column due to compression. This phenomenon is referred to as the barometric pump effect. A typical (large) pressure fluctuation over one day, which is of the order of 1-2%, induces a vertical displacement at the top of the column of 2-4 cm and will affect mainly the upper sand column. In some cases, these air displacements may have a large effect on radon transport processes. In the experiments without a crawl-space the effect is however small as a result of fast diffusive transport<sup>4</sup> and low radon concentrations in the upper part of the column.

As yet, the disagreement can not be explained by the influence of conditions or processes which are not incorporated in the model. On the other hand, one might argue an effect of inhomogeneities, but these are thought to cause a variance in measured concentrations instead of an overall offset. Also model parameters may be varied such that an optimal agreement between model and experiment is obtained. One could for example take a slightly higher value for the emanation coefficient. However, this would constitute a rather inconvenient process if such a 'fitting procedure' is conducted after each experiment with the vessel. Because different radon-transport characteristics may appear after each experiment, it seems wise to continue using the model parameters as given in Table 5.1 in the analysis of subsequent experiments with room-dry sand for the time being. It is only after completing a whole set of measurements that well-founded conclusions may be drawn about any incorrectness of transport parameters used so far. Therefore, the observed differences in the experiments without a crawl space will be left as they are for the moment.

Nevertheless, it may be remarked here that increased calculated concentrations at positions close to the bottom, i.e. a better agreement between model and experiment, can be obtained by using a lower effective diffusion coefficient for radon. This may be realised by either using a lower tortuosity or lower diffusion coefficient for radon in air. The first parameter should actually not be adapted because it has been measured in an independent experiment and, with respect to experimental procedures, is considered to be a lower bound value. The value of the diffusion coefficient for radon in air is available from the literature but is not a precisely known quantity. Several values, varying about 10%, are being used (Tanner [1964]:  $(1.0 - 1.2) \cdot 10^{-5} \text{ m}^2 \text{ s}^{-1}$ ; Søggaard-Hansen and Damkjær [1987]:  $1 \cdot 10^{-5} \text{ m}^2 \text{ s}^{-1}$ ; Rogers and Nielson [1991a]:  $1.1 \cdot 10^{-5} \text{ m}^2 \text{ s}^{-1}$ ; Revzan et al. [1993]:  $1.2 \cdot 10^{-5} \text{ m}^2 \text{ s}^{-1}$ ). Tanner refers to, among others, Hirst and Harrison [1939] who obtained a precise value of  $(1.20 \pm 0.04) \cdot 10^{-5} \text{ m}^2 \text{ s}^{-1}$  (mean value with std. error of four experiments, atm. pres., 15 °C). They claim that the difficulty of adhesion of radon to surfaces, which resulted in a lower measured diffusion coefficient in previous experiments, was overcome in their experiments. The results of Hirst and Harrison [1939] suggest a 10% higher diffusion rate of radon in air than used in the calculations ( $1.1 \cdot 10^{-5} \text{ m}^2 \text{ s}^{-1}$ ). Contrary to

<sup>3</sup>Concerns one measurement; the true concentration in the room may of course vary in time.

<sup>4</sup>The typical distance for radon diffusion in the sand is 45 cm in one day.

what we were aiming at, this would have a negative effect on the correspondence between measurement and model. Anyhow, it is important to remark that the real value of the diffusion coefficient may be somewhat lower.

## 5.5 Experiments with a 'crawl space'

### Time-dependent diffusive transport without forced ventilation

Three experiments were carried out with the lid installed at effective heights of 9, 50 and 92 cm simulating a crawl space. During these experiments a small-diameter outlet tube connected the crawl space with the outside air to equilibrate the pressure in the crawl space with respect to barometric pressure (a barometric pressure drop of 1.8 kPa will lift the lid of the vessel if the system is completely closed). The radon concentration in the crawl space was measured continuously.

The influence of uncontrolled ventilation due to atmospheric pressure variations has to be included in the analysis in the experiments with a crawl space. Hourly averaged values of the atmospheric pressure were used to calculate the average ventilation parameter  $\lambda_v$  ( $s^{-1}$ ) during each experiment. The volume of exchange air that enters or leaves the crawl space through the small-diameter tube within one hour is approximated by multiplying the relative change of atmospheric pressure in one hour by the total air volume inside the vessel. Dividing this exchange volume by the crawl-space volume gives the ventilation rate ( $h^{-1}$ ). For averaging, these values are summed and divided by the duration of the experiment:

$$\lambda_v = \frac{1}{2} \cdot \frac{1}{3600 n} \cdot \frac{\epsilon_a h_s + h_{cs}}{h_{cs}} \sum_{i=1}^n \frac{|P_i - P_{i-1}|}{P_{i-1}} \quad (5.12)$$

where  $n$  is the duration of the experiment (h) and  $P_i$  is the atmospheric pressure at  $t = i$  h. The factor two in the denominator is included to account for the fact that only entering air may be considered as ventilation<sup>5</sup>. The calculated values of  $\lambda_v$  are 3.3, 1.8 and 0.8 ( $\cdot 10^{-7} s^{-1}$ ) for the experiments with a 9, 50 and 92 cm crawl space, respectively. The results of these experiments are presented in Figs. 5.3, 5.4 and 5.5, respectively. The solid lines in these figures represent calculations based on Eq. 5.5 and using the parameters of Table 5.1. The barometric pressure during the experiments is also included in these figures.

For 'crawl-space heights' of 9 and 50 cm the model calculations agree well with the measurements during the first five days. But later, when the equilibrium state is being reached, the calculations start to overestimate the experimental data. This in contrast with results of the experiment with a 92 cm crawl space which indicate a good correspondence between measurement and model with a slight underestimation at larger depths. These observations indicate that a physical phenomenon in the vessel may occur which has mainly an influence at small crawl-space heights.

The water-filled moat surrounding the vessel may have this influence since radon dissolves in water and 'leaks' out of the crawl space. The loss of radon into the water-filled moat may be regarded as an additional leakage parameter  $\lambda_w$  ( $s^{-1}$ ). Assuming that radon

<sup>5</sup>Practically identical ventilation rates are obtained when only time intervals with an increasing atmospheric pressure are considered and the factor two is omitted.

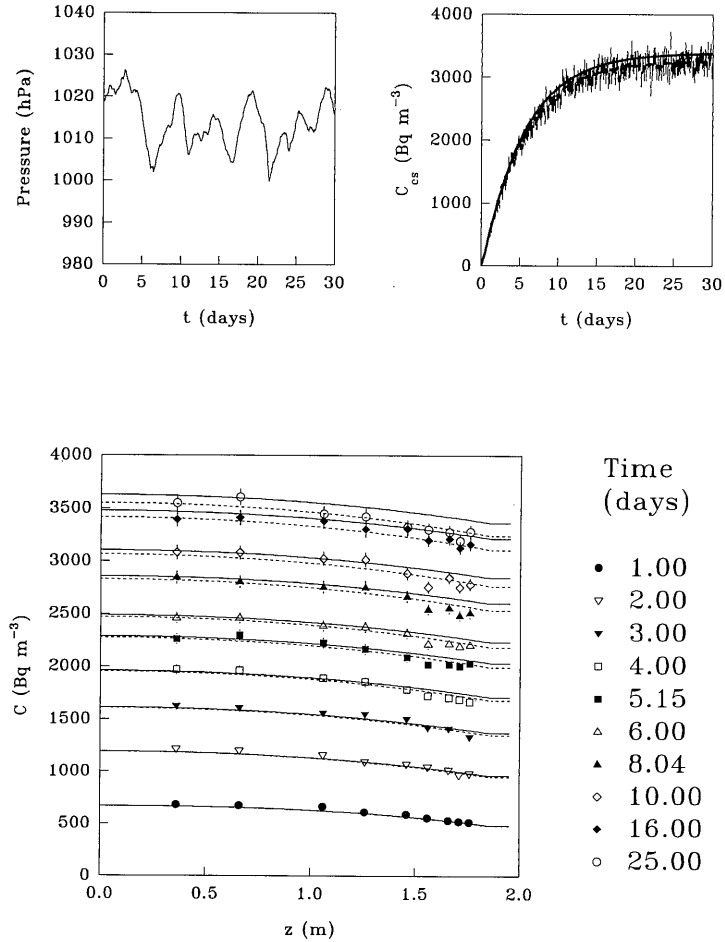


Figure 5.3: Results of the experiment with diffusive transport and a crawl space of 9 cm. Hourly averaged atmospheric pressure during the experiment (left top). Radon concentration  $C_{cs}$  (Bq m<sup>-3</sup>) in the crawl space volume as function of time  $t$  after flushing (right top). Radon concentration  $C$  (Bq m<sup>-3</sup>) as function of  $z$ -coordinate for different times  $t$  after flushing (bottom). Lines represent calculated curves with input parameters given in Table 5.1 including ventilation due to barometric pressure variations (solid lines) and loss of radon into the water-filled moat (dashed lines). Error bars ( $1\sigma$ ) indicate experimental uncertainties.

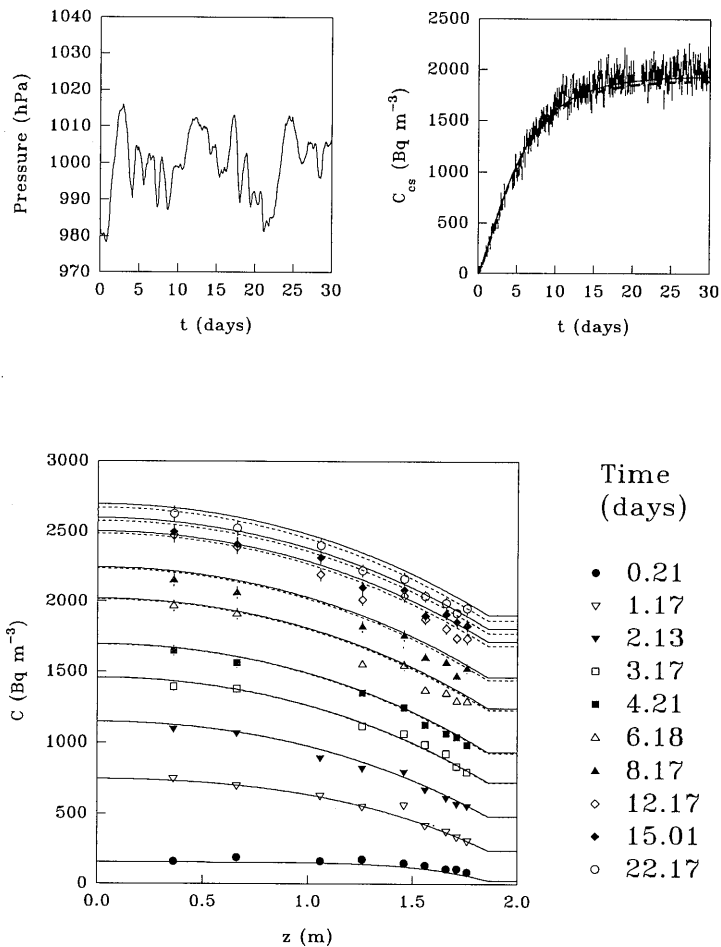


Figure 5.4: Results of experiment with diffusive transport and a crawl space of 50 cm. See also Fig. 5.3.

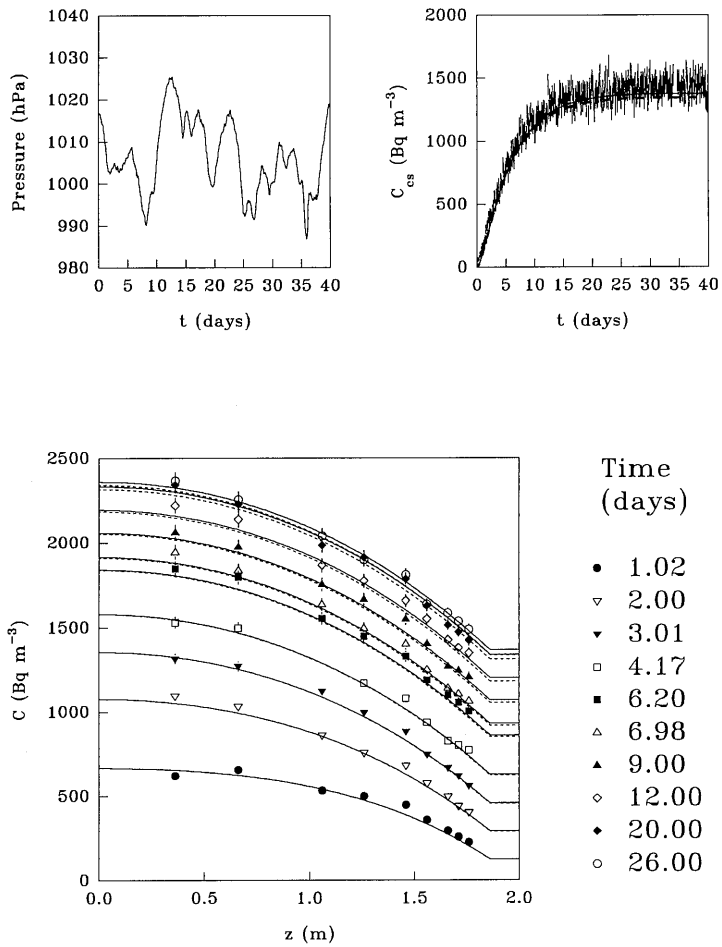


Figure 5.5: Results of experiment with diffusive transport and a crawl space of 92 cm. See also Fig. 5.3.



transport in the water is governed by diffusion only, the radon concentration as function of depth  $y$  (m) in the water is

$$C_w = LC_{cs} \exp\left(-\frac{y}{l_w}\right), \quad (5.13)$$

where

- $C_w$  =  $^{222}\text{Rn}$ -activity concentration in water ( $\text{Bq m}^{-3}$ );
- $L$  = radon distribution coefficient (Ostwald coefficient, equals 0.26 at  $20^\circ \text{C}$ );
- $C_{cs}$  = crawl-space radon-activity concentration ( $\text{Bq m}^{-3}$ );
- $l_w$  = diffusion length in water,  $\sqrt{D_w/\lambda}$  (m);
- $D_w$  = diffusion coefficient for radon in water ( $1.2 \cdot 10^{-9} \text{ m}^2 \text{ s}^{-1}$  [Broecker and Peng, 1974]).

For the radon activity that leaves the crawl-space volume  $V_{cs}$  per unit time, we may write

$$V_{cs} \frac{\partial C_{cs}}{\partial t} = -AD_w \left. \frac{\partial C_w}{\partial y} \right|_{y=0} = ALL_w \lambda C_{cs}, \quad (5.14)$$

where  $A$  ( $0.87 \text{ m}^2$ ) is the surface of the water in contact with crawl-space air. In comparing the loss of radon into the water-filled moat with loss of radon due to ventilation, the quantity  $\frac{ALL_w \lambda}{V_{cs}}$  may be regarded as the leakage parameter  $\lambda_w$ . For experiments with a 9, 50 and 92 cm crawl space  $\lambda_w$  is 4.1, 0.7 and 0.4 ( $\cdot 10^{-8} \text{ s}^{-1}$ ), respectively. Since these values are small with respect to the calculated ventilation rates earlier, diffusion of radon through water does not contribute significantly to the ventilation rate of the crawl space.

Another process disregarded so far concerns loss of radon in the moat due to free-convective mixing of water. It is illustrative to consider this phenomenon in a layer of water between two (infinite) parallel vertical plates at a distance  $d$  apart having different temperatures. Water-density variations due to temperature variations give rise to differences in gravitational force per unit volume, which brings the water into motion. If it is assumed that the water motion is only in the vertical direction, the transport of heat between the two plates is only by conduction in the horizontal direction. As a result the temperature of the water decreases linearly from the higher to the lower temperature plate. To estimate the associated water velocities the Boussinesq approximation [Tritton, 1988] is used in which the inertia forces are omitted since only steady-state vertical motion is assumed. The equation of motion for the vertical velocity  $v(x)$  ( $\text{m s}^{-1}$ ) is then given by

$$\nu \frac{\partial^2 v}{\partial x^2} - g\alpha \Delta T = 0 \quad (5.15)$$

where

- $x$  = horizontal coordinate (m);
- $\nu$  = kinematic viscosity of water ( $1 \cdot 10^{-6} \text{ m}^2 \text{ s}^{-1}$ );
- $g$  = gravitational acceleration ( $9.8 \text{ m s}^{-2}$ );
- $\alpha$  = coefficient of expansion of water ( $2 \cdot 10^{-4} \text{ K}^{-1}$  at  $20^\circ \text{C}$ );
- $\Delta T$  = temperature difference from reference (K).

The system is symmetric if the water at the mid-plane between the two plates is at reference temperature. As boundary condition, zero velocity at the surface of the two

plates is imposed. The solution  $v(x)$  of Eq. 5.15 may be integrated to obtain the mean velocity  $\bar{v}$  in one of the vertical directions:

$$\bar{v} = \frac{g\alpha\Delta T d^2}{96\nu} \quad (5.16)$$

A temperature difference of only  $0.001^\circ\text{K}$  between two plates 10 cm apart gives water transport with a mean velocity of  $1\cdot 10^{-4} \text{ m s}^{-1}$ , showing that minor temperature variations give rise to fast mixing of water with respect to mixing of radon by diffusion only. Although this approximation does not describe the complex real situation because (1) vertical dimensions are not accounted for, (2) inertia forces should be included, and (3) a boundary layer type of flow will probably occur, the estimated water velocities are so large that such a conclusion may be drawn without doubt.

To assess the magnitude of the water mixing and to quantify the loss of radon from the crawl space, the radon concentration  $C_{\text{mo}}$  in the water at the bottom of the moat (water height 58 cm, movable lid at lowest position), see Fig. 5.6, and the concentration at the water surface in contact with crawl-space air (derived from the crawl-space radon concentration  $C_{\text{cs}}$  using Henry's Law) were measured. For analysing these data, a simple model is considered for radon transport in the water-filled moat. Based on the assumption that the mixing of radon can be described by a diffusion process, the steady-state diffusion equation was considered for a one-dimensional geometry (using  $x$  as coordinate) representing the moat. In this model, the water surface in contact with crawl-space air is positioned at  $x = 0$ , the midpoint between the bottom of the moat and the lower edge of the lid is located at  $x = 0.515 \text{ m}$  and the water surface in contact with ambient air at  $x = 2 \cdot 0.515 = 1.03 \text{ m}$ . The boundary conditions imply zero radon concentration

at  $x = 1.03$  and the measured concentrations at  $x = 0$  ( $803 \text{ Bq m}^{-3}$ ) and  $x = 0.515$  ( $180 \text{ Bq m}^{-3}$ ). The fourth boundary condition implies continuity of radon flux at  $x = 0.515$ . A difficulty in this one-dimensional representation concerns the difference in (horizontal) cross-sectional area of the water column in the inner ( $0.87 \text{ m}^2$ ) and outer part ( $0.25 \text{ m}^2$ ) of the moat. Moreover, as a consequence of this difference, the magnitude of the free-convective mixing may be different in the two water columns. At first instance, according to Eq. 5.16, the convective velocity in the outer part will be smaller because of a smaller distance  $d$ . However, since a boundary layer type of flow is likely to occur, the magnitude of the mixing flows ( $\text{m}^3 \text{ s}^{-1}$ ) in both columns are probably comparable. As a result, the mean convective velocity (mixing flow divided by cross-sectional area) in the

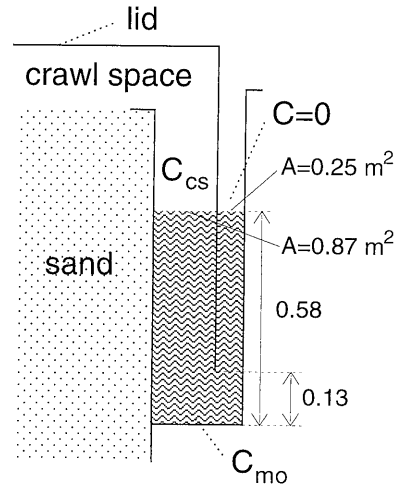


Figure 5.6: Schematic vertical cross-section of the water-filled moat surrounding the vessel. Position of measured radon concentrations in the crawl space and in the moat are indicated by  $C_{\text{cs}}$  and  $C_{\text{mo}}$ , respectively.

outer part will be a factor  $0.87/0.25 = 3.5$  larger than in the inner part. It is assumed that the diffusion coefficient scales with the mean convective velocity.

With these boundary conditions and assumptions, the value of the diffusion coefficient in the inner part of the moat was found to be  $2.7 \cdot 10^{-7} \text{ m}^2 \text{ s}^{-1}$  (and a factor 3.5 higher for the outer part), corresponding with a diffusion length for radon of 0.36 m, a factor 15 larger than the diffusion length in still water. When this result is incorporated in the calculation of the leakage parameter  $\lambda_w$  due to loss of radon into the water for the experiments with a 9, 50 and 92 cm crawl space (each with a different one-dimensional representation of the moat due different water- and crawl-space heights), a value of 5.4, 1.0 and 0.8 ( $\cdot 10^{-7} \text{ s}^{-1}$ ) is found, respectively. Calculations including these ventilation rates (next to atmospheric pressure induced ventilation) are depicted by dashed lines in Figs. 5.3, 5.4 and 5.5. By doing so, the agreement with the probe data is seen to improve somewhat for the experiments with a 9 cm and 50 cm crawl space, but seen to worsen slightly for the experiment with a 92 cm crawl space. In addition, the crawl-space data are better reproduced for a 9 cm crawl space, but are poorer reproduced in the other two cases: An overall improved situation is therefore not obtained by introducing leakage of radon in the water-filled moat. Nevertheless, the improved agreement for the experiment most sensitive to such leakage, i.e. the one with the smallest crawl space, shows that it should be included in the calculations.

### Equilibrium diffusive transport with forced ventilation

In the final experiment with pure diffuse transport the *equilibrium* radon concentration was measured as function of height ( $z$ ) at different ventilation rates for a 50 cm crawl space. In this experiment, a measured flow of nearly radon-free air was continuously forced into the crawl space through an opening at one side of the lid, while at the other side a small diameter outlet tube of several meters length was connected to allow escape of crawl-space air. These measurements were carried out with air-flows of 0.25, 0.5, 1.0, 2.0, 4.3 and  $8.91 \text{ min}^{-1}$ , corresponding with a ventilation rate of 2.65, 5.3, 10.6, 21, 46 and  $94 (\cdot 10^{-6}) \text{ s}^{-1}$ .

The measured concentrations as function of height are presented in the left part of Fig. 5.7 while the measured radon concentrations in the crawl space as function of the ventilation rate are presented in the right part. The solid lines in this figure represent results of model calculations based on Eq. 5.5 using the parameters listed in Table 5.1. In these experiments  $\lambda_v$  is equal to the (forced) ventilation rate, assuming no uncontrolled ventilation due to e.g. barometric pressure variations. This condition is met for the smallest ventilation rate (the case most sensitive for this effect) if the barometric pressure did not increase faster than  $4.2 \text{ hPa h}^{-1}$  during the experiment. Since the fastest barometric pressure variation observed was  $1.5 \text{ hPa h}^{-1}$ , it is concluded that uncontrolled ventilation of the crawl space did not occur.

As can be seen an almost perfect agreement is obtained between model calculations and measurement. From Fig. 5.7 (right part) it is evident that even a very small ventilation rate of once a day ( $= 1.2 \cdot 10^{-5} \text{ s}^{-1}$ ) reduces for this vessel geometry the crawl space concentration by a factor five with respect to an initial situation without ventilation. Further increase in the ventilation rate only reduces the concentration marginally. For practical purposes this implies that knowledge of the natural ventilation is necessary to calculate the effect of forced ventilation, and that mitigation of a crawl space with a 'normal' natural ventilation rate by forced ventilation will be rather limited.

Finally, it is interesting to notice an underestimation of model calculations for positions

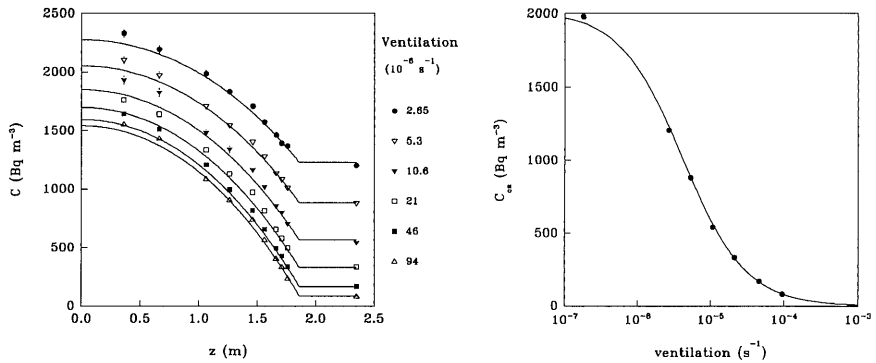


Figure 5.7: Results of experiment with different forced crawl-space ventilation rates. Left part: equilibrium radon concentration  $C$  (Bq m<sup>-3</sup>) as function of  $z$ -coordinate for different ventilation rates  $\lambda_v$ . Right part: Equilibrium radon concentration in the crawl space  $C_{cs}$  (Bq m<sup>-3</sup>) as function of crawl-space ventilation rate. Solid lines represent calculated curves with input parameters given in Table 5.1. Experimental uncertainties ( $1\sigma$ ) are within markers.

close to the bottom of the vessel, as is observed in the experiment with a 92 cm crawl space and those without a crawl space. The radon concentration profiles in all these experiments are characterised by a high diffusive flux towards the surface of the sand column (the spatial derivative of the radon concentration is large). So, improved calculated profiles can be obtained by using a lower effective radon-diffusion coefficient. On the other hand, this will yield lower crawl-space concentrations: a highly undesirable effect considering the results of the experiments with a 50 cm and 92 cm crawl space. Therefore, the results so far do not give explicit cause for reconsidering the value of the diffusion coefficient.

## 5.6 Conclusions

It may be concluded that the experiments with pure diffusive transport and room-dry sand are well described by model calculations using one set of input parameter inferred from *independently* measured parameters. The maximum differences between model and experiment are less than 10%. These differences may be explained by processes or situations inside the vessel which are hard to control and difficult to measure. Especially the dependence of the emanation coefficient on moisture content complicates the situation with room-dry sand considerably. In this light, the assumption of a constant radon generation rate in the whole sand column in the model calculations may be a too rough approximation. However, since the data are reasonably well described by a constant emanation coefficient, there is not yet a clear reason to abandon this approximation.

These experiments have further indicated that small temperature variations in the moat surrounding the vessel will generate a water circulation that transports radon from the space under the lid to the outside. Another result, which has more practical implications, is the fact that small ventilation rates in the space under the lid have a large effect on the radon concentration in that space. Under normal conditions the natural

---

ventilation in real crawl spaces is likely to be at least of the order of  $10^{-5} \text{ s}^{-1}$  ( $\approx 0.04 \text{ h}^{-1}$ ) and increasing the ventilation rate by forced ventilation will have a rather limited effect on the radon concentration.



# Chapter 6

## Diffusive and advective transport experiments

### 6.1 Introduction

In the previous chapter experiments with only diffusive transport were conducted. Since their results were well described by model calculations, the next steps are made to increase the complexity.

In this chapter the results of a set of measurements with combined diffusive and advective transport in room-dry sand are discussed. The measurements concern steady-state as well as time-dependent combined advective and diffusive transport. Advective transport was induced by supplying air to the perforated box (upward air-flow in the sand column) or withdrawing air from the box (downward air-flow). As the situation with advective transport is hard to describe analytically, except for steady-state conditions with a downward air-flow, most measurements are compared with results of the two-dimensional numerical model presented in chapter 3. The parameters of the sand as listed in Table 5.1 are again used in these model calculations.

The experiments may be subdivided into three parts. The first, discussed in section 6.2 and which can be described analytically, covers steady-state downward advective transport without a crawl space. Secondly, the experiments with steady-state upward advective transport, with and without a crawl space, are covered in section 6.3. And thirdly, experiments with time-dependent advective transport are presented in section 6.4. As each of the three type of experiments required their own experimental techniques, procedures and analysing methods, these matters will be described in the respective sections. Finally, conclusions are drawn in section 6.5.

### 6.2 Experiments with downward advective transport

In this experiment steady-state radon concentrations were measured as function of height in the vessel without a crawl space and a downward air-flow induced by withdrawing air from the perforated circular box, located at a depth of 1.63 m. Radon-concentration profiles were measured at flow rates  $J$  of 0.1, 0.2, 0.4 and  $0.8 \text{ l min}^{-1}$ , regulated by a mass-flow controller (MFC)<sup>1</sup>. Similar to the diffusive transport experiments, the radon transport processes in the sand are still in one direction in this case. As a consequence, analytical

---

<sup>1</sup>Brooks 5850E MFC, 0 - 1 l min<sup>-1</sup>.

one-dimensional modelling may be applied for comparison with the experimental results. For convenience, this model is made somewhat more general such that it can also be used for analysing the upcoming similar experiment with an upward air-flow.

### 6.2.1 Model description

The one-dimensional steady-state counterpart of equation 2.32 for homogeneous soil, using  $z$  as spatial coordinate and neglecting influence of pore-water, is given by (writing  $C$  for  $C_a$  for convenience):

$$\epsilon_a \tau_a D_a \frac{d^2 C}{dz^2} - v \frac{dC}{dz} - \beta \lambda C + S = 0 \quad (6.1)$$

where  $v$  ( $\text{m s}^{-1}$ ) is bulk air (Darcy's) velocity (see also Eq. 2.9):

$$v = -\frac{K}{\mu} \nabla P. \quad (6.2)$$

For the vessel geometry one needs to consider that advective transport of radon can only take place in the region above the perforated box (located between  $z = d_1 = 0.20$  m and  $z = d_2 = 0.23$  m) because the bottom of the vessel ( $z = 0$ ) acts as an impermeable boundary. Air which is supplied to the box will leave the vessel through the surface of the sand column at  $z = 1.86$  m. Vice versa, air taken from the box originates from pore-air in the sand above the box. Therefore, the  $z$ -domain is split into two regions: one below the box ( $0 \leq z \leq d_1$ ) where we have diffusive transport only (Eq. 6.1 with  $v = 0$ ) and a region above the box where Eq. 6.1 is the governing equation. Note that a downward air-flow is associated with a negative velocity  $v$ . The two coupled differential equations for each region were solved with boundary conditions, illustrated in Fig. 6.1, that reflect the situation of the vessel without lid and combined advective and diffusive transport. The following boundary conditions apply:

- 1) The bottom of the vessel ( $z = 0$ ) is impermeable for radon transport:

$$\frac{\partial C}{\partial z} = 0, \quad z = 0. \quad (6.3)$$

- 2) The radon concentration at the surface of the sand ( $h_s = 1.86$  m) is set at the measured value in the (well ventilated) experimental room:  $C(h_s) = C_h = 10 \text{ Bq m}^{-3}$ .

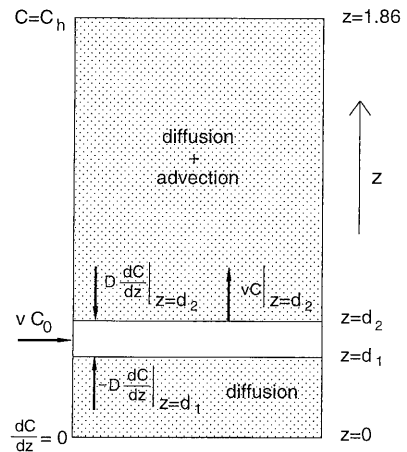


Figure 6.1: One-dimensional representation of the vessel with boundary conditions for a situation in which air is supplied to the perforated box and without the lid installed on the vessel.



- 3) Radon in the box is completely mixed:  $C(d_1) = C(d_2)$ .
- 4) The last boundary condition is found by considering a mass balance for the perforated box. The exact representation of this mass balance depends on whether air is drawn from - or supplied to - the box via the small-diameter tube connected to the centre of the box and led outside the vessel via the bottom. In the case air is supplied, the diffusive and advective flux (due to the radon concentration  $C_0$  of the supplied air, estimated at  $5 \text{ Bq m}^{-3}$ ) of radon concentration into the perforated box is in equilibrium with radon decay and advective flux out of the box:

$$\epsilon_a \tau_a D_a \left( \left. \frac{dC}{dz} \right|_{z=d_2} - \left. \frac{dC}{dz} \right|_{z=d_1} \right) + vC_0 = \lambda C(d_1)(d_2 - d_1) + vC(d_2). \quad (6.4)$$

On the other hand, if air is drawn from the perforated box the advective fluxes entering and leaving the box are equal. Therefore, the boundary condition for this situation is Eq. 6.4 with omission of the advective terms  $vC_0$  and  $vC(d_2)$ .

The radon concentration  $C(z)$  in the region between the box and the surface of the sand can be written as:

$$C(z) = A(e^{\omega_1 z} - e^{\omega_2 z}) + B(e^{\omega_1 z} + e^{\omega_2 z}) + \frac{S}{\beta\lambda}, \quad z \geq d_2, \quad (6.5)$$

where  $A$  and  $B$  are constants that follow from the boundary conditions:

$$B = \frac{S}{N\beta\lambda} \left( -\frac{v}{\lambda} + \frac{\beta v C_0}{S} - d_2 + d_1 \right) G e^{w_1 h_s} + (1 - \beta\ell^2 \omega_1 G) \left( 1 - \frac{\beta\lambda C_h}{S} \right) e^{w_1 d_2}, \quad (6.6)$$

$$A = \left( C_h - \frac{S}{\beta\lambda} \right) e^{-w_1 h_s} - B e^{(w_2 - w_1) h_s}, \quad (6.7)$$

where

$$N = (1 - \beta\ell^2 G w_2) e^{(w_2 d_2 + w_1 h_s)} - (1 - \beta\ell^2 G w_1) e^{(w_2 h_s + w_1 d_2)}, \quad (6.8)$$

$$G = \left( d_2 - d_1 + \frac{v}{\lambda} + \beta\ell \tanh\left(\frac{d_1}{\ell}\right) \right)^{-1}, \quad (6.9)$$

$$w_{1,2} = \frac{v}{2\epsilon_a \tau_a D_a} \pm \sqrt{\left( \frac{v}{2\epsilon_a \tau_a D_a} \right)^2 + \frac{\beta\lambda}{\epsilon_a \tau_a D_a}}, \quad (6.10)$$

and  $\ell$  is the diffusion length (Eq. 2.42):

$$\ell = \sqrt{\frac{\epsilon_a \tau_a D_a}{\beta\lambda}}. \quad (6.11)$$

The expression for  $B$ , Eq. 6.6, was derived for the situation with an upward air-flow. The solution for a reversed air-flow is found by discarding the terms containing the velocity  $v$  in Eqs. 6.6 and 6.9.

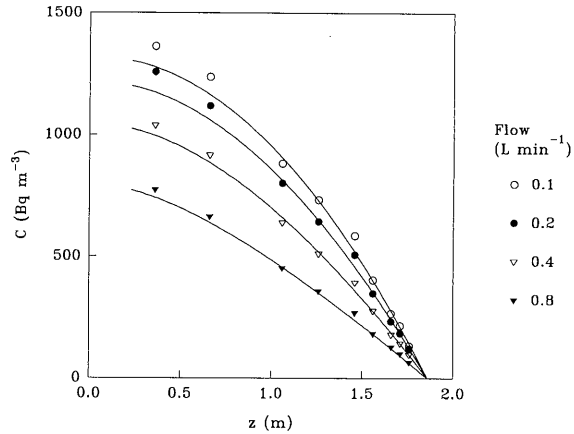


Figure 6.2: Radon concentration  $C$  ( $\text{Bq m}^{-3}$ ) as function of height  $z$  (m) for different values of the air-flow rate  $J$  ( $\text{l min}^{-1}$ ) for experiments with combined diffusive and advective transport without a crawl space and with a downward air-flow. Solid lines represent calculated values from the analytical 1D model utilising parameters of the sand as given in Table 5.1.

It should be remarked that, at first instance, the permeability  $K$  seems to be a relevant parameter since, according to Eq. 6.2, it determines the air-flow rate through the sand at a given pressure difference over the column. However, since the air-flow was set using a mass-flow controller in the experiments with advective transport and since only the bulk air velocity  $v$  is needed to model advective transport of radon<sup>2</sup>, the permeability of the sand is not of great importance for this study (assuming a homogeneous column). Nevertheless, the permeability of the sand was measured using several techniques to obtain an idea of its magnitude [Van der Graaf et al., 1992, 1993]. For example, from the pressure-field measurements in the sand, performed to assess to homogeneity of the sand column (see section 4.4 and in particular Fig. 4.5), follows a permeability of about  $6 \cdot 10^{-11} \text{ m}^2$  using a dynamic viscosity of  $1.83 \cdot 10^{-5} \text{ Pa}\cdot\text{s}$  for air.

### 6.2.2 Results and discussion

The measured radon-concentration profiles together with results of the analytical model are shown in Fig. 6.2. It is seen that the agreement with experiment is good, particularly for the experiments with the highest flow rates. Remarkable is the effect of lower modelled concentrations close to the bottom of the vessel, as has also been observed in the first set of measurements with diffusive transport (chapter 5). Several possible causes of this difference were given (influence of curved bottom, presence of pore water, a lower diffusion coefficient in air than modelled) of which only the possibility of a lower diffusion coefficient, which was extensively discussed in section 5.4, was not rejected. In this context it is interesting to see that, upon examination of the results of the experiment at hand,

<sup>2</sup>Air velocities are obtained by dividing the measured flow rate  $J$  by the surface area of the sand ( $3.14 \text{ m}^2$ ).

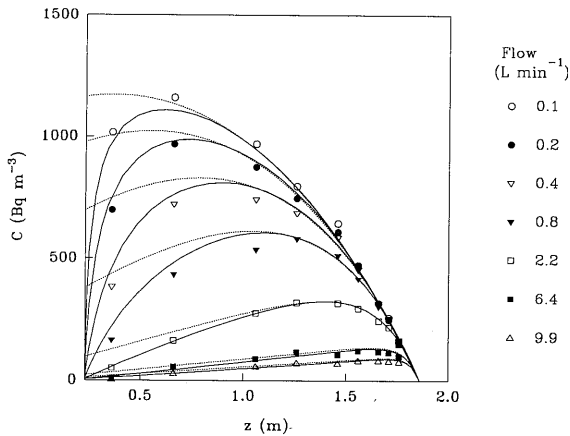


Figure 6.3: Radon concentration  $C$  ( $\text{Bq m}^{-3}$ ) as function of height  $z$  (m) for different values of the air-flow rate  $J$  ( $\text{l min}^{-1}$ ) for experiments with combined diffusive and advective transport without a crawl space and with an upward air-flow. Dashed and solid lines represent calculations with an analytical one-dimensional model and numerical 2D-model, respectively, utilising input parameters as given in Table 5.1.

this difference diminishes when advective transport starts to dominate. This is a further indication that the discrepancies may be caused by a too high value of the diffusion coefficient. Another point of interest, for which an explanation can not be given either, is the higher measured concentration with the fifth probe ( $z=1.46$ ), also observed in the previous measurements. The fact that this effect also occurs in this series of experiments with advective transport indicates systematic deviations which, unfortunately, can not be identified precisely.

### 6.3 Experiments with upward advective transport

In these experiments radon-poor air was supplied to the box and steady-state profiles were measured. In case of the experiment without the lid an air-flow rate  $J$  was induced of 0.1, 0.2, 0.4 and 0.8, 2.2, 6.4 and 9.9  $\text{l min}^{-1}$  using the MFC for  $J < 11 \text{ l min}^{-1}$  and a gas-flow meter (GFM)<sup>3</sup> for the flows exceeding the MFC full range. The results of this experiment, presented in Fig. 6.3, illustrate that even a very small air-flow drastically alters the radon profile in the sand due to introduction of radon free air in the perforated box; a position where the radon concentration is normally high. Instead of a gradual decrease in radon concentration from the bottom to surface of the column, a maximum in the concentration is found. The position of this maximum shifts to the surface of the vessel for higher flow rates. Results of calculations with the analytical one-dimensional model (Eq. 6.5) are indicated by dashed lines in Fig. 6.3. Large differences are observed for the lowest two probes, where the calculations are significantly *higher* than the measured

<sup>3</sup>Meterfabriek Dordrecht, 0 – 50  $\text{l min}^{-1}$ .

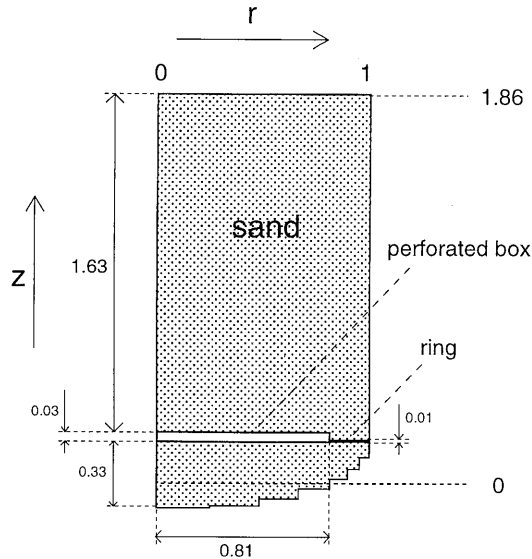


Figure 6.4: Schematic presentation of the radon vessel without the lid, used in 2D-model calculations. Dimensions are in metres.

values. This behaviour is caused by the fact that the situation with an upward air-flow (pressurised perforated box) can no longer be described by a one-dimensional model. This can most easily be appreciated by inspection of the radon concentration inside the box when radon-poor air is forced through the box at the centre of its bottom plate. The concentration at this position will be nearly zero but increases in the radial direction due to diffusive influx of radon through the surfaces of the box. This implies that in the model also a radial coordinate has to be taken into account. As a consequence, the two-dimensional numerical model is mandatory to analyse the results of the experiments with an upward air-flow.

### 6.3.1 Two-dimensional modelling

The two-dimensional problem domain (in a cylindrical coordinate system), reflecting the radon vessel without the lid, is depicted in Fig. 6.4. Typical characteristics of the vessel geometry that may be incorporated, as opposed to one-dimensional modelling, concern the radial dimensions of the perforated box, the 18.5 cm wide ring (situated at the same height) and the curved bottom. The latter is approximated in a step-wise manner (7 steps) such that only boundaries with either  $z = \text{constant}$  or  $r = \text{constant}$  are established. Other aspects which are considered in the numerical model are:

- The outer wall of the perforated box (at  $r = 0.81$  m) is modelled as an impermeable boundary and is directly attached to the wide ring, i.e. the free space of 5 mm between these two objects is ignored. This is justified by negligible concentration differences observed for calculations including and excluding the gap. Advantage of ignoring the gap is the possibility of imposing a relatively coarse grid at this

position, resulting in faster calculations.

- The perforated box is treated as a porous medium for which 1) the (partition-corrected) porosity is set to unity, 2) the diffusion coefficient equals the radon-diffusion coefficient in free air, 3) the radon production rate is zero and 4) the permeability is about  $10^6$  times higher than the permeability of the sand. The latter number is rather arbitrary since the permeability of the perforated box has not been measured. It is however expected to be much higher than the permeability of the sand. Since calculated concentrations are almost completely insensitive of the value of permeability of the box (taking a  $K$ -value which is an order in magnitude higher or lower shows changes of less than 0.1% in the calculated radon concentrations), it is irrelevant to know its exact value.
- In view of the (penetrated) glass-fibre grating in the box, the air-flow is probably turbulent because of the intermittent blockages of the grating and different positions of the openings. As a result, the value of the diffusion coefficient for radon is not well known too. The turbulence may cause a higher (effective) diffusivity (depending on the air-flow rate), but on the other hand, it may be lowered due to the intermittent blockage of the grating (tortuous path). Taking a value which represents diffusion in free air is a compromise. In this context, it should be remarked that Darcy's Law may not hold for the perforated box and that more complex transport equations should be used for exact modelling. However, since the applied type of modelling gives satisfying results, as will be shown, there is actually no need to pass on to a more complicated description.
- The pressure field is calculated with boundary conditions implying zero pressure at the top of the sand column and a positive pressure at the centre of the perforated box. As the induced flow rate through the sand with these boundary pressures (obtained from numerically integrating the flow rate through each boundary control volume at the sand surface) may not reflect the true air-flow rate, the complete pressure field is corrected afterwards by multiplying the field with the ratio between the experimental value and the calculated value of the air-flow rate.
- The radon concentration at the sand surface is set at the concentration in the experimental room ( $10 \text{ Bq m}^{-3}$ ). The concentration at the centre of the box is set at the concentration of incoming air:  $5 \text{ Bq m}^{-3}$ . The true concentrations may differ  $10 \text{ Bq m}^{-3}$  at maximum. As the calculations are rather insensitive to these values, e.g. the concentration in the middle and in the centre of the vessel is raised  $1 - 5 \text{ Bq m}^{-3}$  when the incoming flow is  $10 \text{ Bq m}^{-3}$  instead of  $5 \text{ Bq m}^{-3}$  (the concentration is not raised by  $5 \text{ Bq m}^{-3}$  because most of the incoming radon is transported to larger radii in the vessel), this uncertainty is however of no great importance.
- For optimal accuracy of the calculations, the mesh is refined near positions with high radon concentration gradients. As a consequence, the grid spacing varies from 2 mm near the centre of the perforated box ( $r = 0, z = 0.20 - 0.23 \text{ m}$ ) to 5 cm at other positions. This mesh is also used in all subsequent numerical calculations.

The radon concentrations at the central axis, calculated with the 2D numerical model, are indicated by solid lines in Fig. 6.3. The supposition of a two-dimensional effect is clearly demonstrated by the much better correspondence with the experimental results

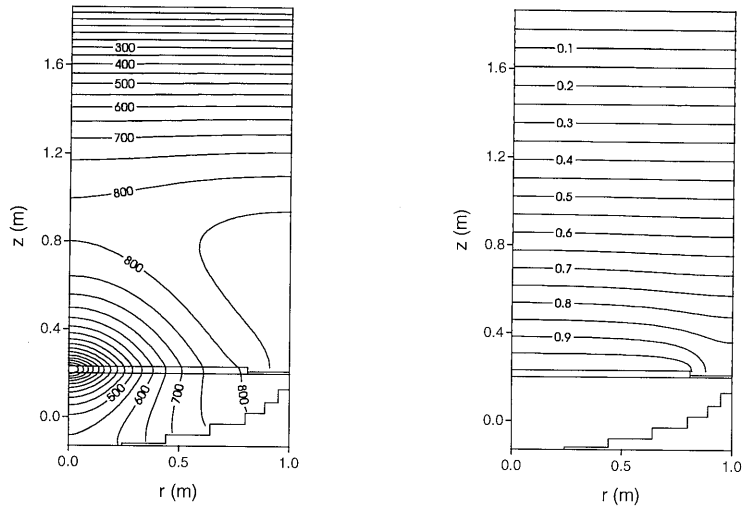


Figure 6.5: Left part: Results of 2D-model calculations of the radon concentration ( $\text{Bq m}^{-3}$ ) in the radon vessel with an air-flow rate of  $0.41 \text{ min}^{-1}$  induced through the sand column. Right part: Pressure field in the sand above the perforated box. The pressure at the centre of the perforated box is 1 Pa and 0 Pa at the top of the sand column.

(especially for the lowest probe) than is obtained with the 1D model. That radon transport indeed takes place in two directions is well illustrated by a contour plot of the radon concentration in the sand in the  $(r, z)$ -plane, shown in the left part of Fig. 6.5 for a flow rate of  $0.41 \text{ min}^{-1}$ . The lowest concentrations occur at the centre of the perforated box where radon-poor air enters the vessel. From that point on, the concentration increases in all directions and reaches a maximum near the wall of the vessel at an effective height<sup>4</sup> of circa 0.6 m. A ‘saddle point’ is observed at  $r = 0$  and  $z = 0.9 \text{ m}$ , corresponding with the maximum of the solid line in Fig. 6.3 representing the radon concentration profile with a flow rate of  $0.41 \text{ min}^{-1}$ .

From the calculated concentration field one might think that the incoming radon-poor air spreads out in a spherically manner in the vessel. This is however not the case. In the right part of Fig. 6.5, the pressure field inside the sand is shown for a situation with a pressure of 1 Pa in the centre of the perforated box (flow rate  $0.361 \text{ min}^{-1}$ ). The pressure field is seen to be horizontally stratified except for the region just above the ring (the pressure is practically constant at 1 Pa between the bottom of the vessel and the box). In other words, the air-flow through the sand is mainly in the vertical direction and, considering the air velocity, almost uniformly distributed over the radius. In contrast with the situation in the sand, the pressure field in the perforated box is *vertically* stratified, see Fig. 6.6, which implies a radial air-flow. The low resistance to air-flow of the box allows such a radial spreading of the incoming air over its total volume that the inflow into the sand becomes nearly uniformly distributed over the upper box surface. The pressure

<sup>4</sup>The use of effective heights as adopted in the 1D modelling is continued in the 2D calculations. As a result, the sand surface is at 1.86 m and the bottom of the vessel at -0.13 m in the centre.

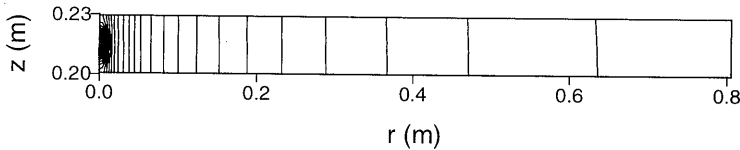


Figure 6.6: Pressure field in the perforated box in steps of  $2 \cdot 10^{-6}$  Pa. The pressure is 1 Pa at the middle of the centre of the box ( $r = 0$ ) and 0.9990 Pa near the outer radius ( $r = 0.8$ ).

differences inside the box are very small due to its high permeability: the pressure drop in the radial direction is of the order of 0.1%. It is for this reason that the pressure field in the sand approaches a one-dimensional pattern. The box may be considered to function as a ‘radon pump’. Advection in the box transports radon to the outside of the vessel and diffusion in the sand returns it back to the centre. In the meantime, of course, we also have advective and diffusive losses at the sand surface.

Returning to the results presented in Fig. 6.3, a remarkable phenomenon which needs some attention is the concentration at the fifth probe ( $z = 1.46$  m). The ratio of the measured and calculated radon concentration at the probe height as function of the air-flow rate is shown in Fig. 6.7. At low flow rates (up to  $0.81 \text{ min}^{-1}$ ) the calculated concentration underestimates, as usual for this probe, the measured value. At higher flow rates, however, the opposite occurs: the calculated concentration becomes higher than measured. An explanation for this observation may be that, during sampling with this probe, mainly air from *below* the probe is drawn from the sand. If this is true, the question rises whether similar phenomena occur at the other probes as well. Upon examination of the results with the lowest probe, this might very well be the case. Usually, higher measured concentrations than calculated are obtained with this probe in experiments with a decreasing concentration towards the surface of the sand, while the opposite is now observed when the concentration gradient is reversed (an exception is formed by the results with a flow rate of  $0.11 \text{ min}^{-1}$ ). It is difficult to indicate why preferential sampling from below the probe would take place. Downward compaction of the sand column may have caused a region of less-compacted sand below the probe. It could also be that the top part of the air-filter has become partly obstructed by fine sand grains.

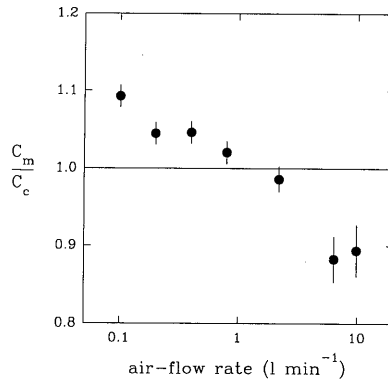


Figure 6.7: Ratio of the measured  $C_m$  and calculated  $C_c$  radon concentration at  $z = 1.46$  as function of air-flow rate  $J$  ( $1 \text{ min}^{-1}$ ), see also Fig. 6.3.

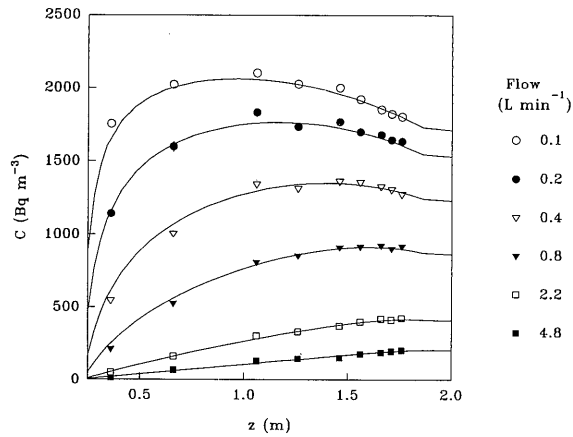


Figure 6.8: Radon concentration  $C$  ( $\text{Bq m}^{-3}$ ) as function of height  $z$  (m) for different values of the air-flow rate  $J$  ( $\text{l min}^{-1}$ ) for experiments with combined diffusive and advective transport with a 50 cm crawl space and with an upward air-flow. Solid lines represent calculations with the numerical 2D-model and input parameters as given in Table 5.1.

### Experiments with a crawl space

To increase the complexity of the situation to some degree, similar experiments with an upward air-flow were carried out with the lid placed on the vessel, simulating a crawl space with an effective height of 50 cm. With this geometry, steady-state radon concentration profiles were measured with flow rates  $J$  of 0.1, 0.2, 0.4, 0.8, 2.2 and 4.8  $\text{l min}^{-1}$ . During these experiments a pressure-control system was installed on the lid of the vessel. The system consisted of a differential pressure transducer, a control valve and a programmable electronic unit. The system was programmed to open the control valve on the lid when the pressure difference between the vessel and outside exceeded 1.5 hPa. The valve was closed when this pressure difference dropped below 0.5 hPa (minimum pressure range within instrumental resolution). Since air was continuously supplied through the perforated box at the bottom of the vessel, the air pressure in the vessel gradually increased. The valve was automatically opened when the pressure difference reached the limit of 1.5 hPa, allowing escape of crawl-space air and inducing a rapidly decreasing pressure difference to 0.5 hPa, after which the valve was closed. The valve opened each 40 min at the lowest applied flow rate of 0.1  $\text{l min}^{-1}$  and was almost continuously open at the highest flow rate of 4.8  $\text{l min}^{-1}$ . With this method uncontrolled ventilation of the crawl space due to barometric pressure changes (several tens of hPa) was almost completely suppressed for all flow rates studied.

The measured radon-concentration profiles are presented in Fig. 6.8 together with values calculated with the 2D-model (solid lines in this figure). The two sets of concentrations are in good agreement. Also here the above mentioned behaviour at the fifth and lowest probe is observed.

For houses it is generally assumed that advective transport into a crawl space enhances the entry rate and radon concentration. This seems to be in contrast with the results



of these experiments which indicate that already a small air-flow reduces the radon concentration in the crawl space (compare Fig. 6.8 with equilibrium in Fig. 5.4). However, it must be realized that the natural ventilation rate of a crawl space is usually in the order of several times per day. This deviates with the situation of an unventilated crawl space in this experiment. Calculations show that in a situation with a forced ventilation rate, comparable in magnitude to the natural ventilation rate found in real crawl spaces, the crawl space concentration would have increased during advective transport (at small flow rates). Also, the dimensions of the vessel are still small with respect to real houses. Radon-free air enters the vessel at a distance of only 1.6 m from the crawl space and advective transport takes place over the whole column. Consequently, it is easily depleted. For the situation under a house, where the crawl space is usually at lower pressure with respect to the outside pressure, advective transport takes place over the whole distance from the outside soil to the crawl-space floor. In addition, depletion of the soil will not easily occur due to diffusive supply of radon from the deeper layers. The influence of advective transport in the more realistic situation under a house is further discussed chapter 9.

## 6.4 Experiments with pulsated advective transport

For validating time-dependent advective transport, several experiments were carried out with a pulsed air-flow through the sand column (with a 50 cm crawl space). In these experiments an upward air-flow was induced in the column for a certain time interval. Thereafter, the air-flow was turned off for an equal time interval. The sum of these two intervals constitutes the period of the pulsed air-flow experiments. The pressure-control system was only installed during the interval with advective transport. In the subsequent interval, when air was not supplied to the perforated box, the control valve was closed. To prevent overflow of water from the moat into the sand, the control unit was programmed to open the valve only in case of a large increase of atmospheric pressure. As this situation did not occur during any of the experiments, uncontrolled ventilation of the crawl space was prevented.

Two continuous radon meters (CRM's) [Aldenkamp and Stoop, 1994] were installed, see Fig 6.9, to measure the radon concentration in the crawl space as well as the concentration between the probes located at 1.06 m and 1.26 m (i.e. at a depth of 80 cm and 60 cm below the sand surface, respectively). A horizontal separation between the sampling inlet and return would have been preferred since a vertical separation affects the radon concentration profile to a higher degree. However, to avoid disturbance of the

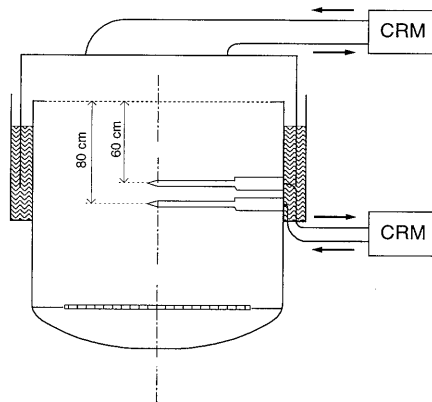


Figure 6.9: Schematic sketch of the vessel and continuous radon monitors in the experiments with time-dependent advective transport.

Table 6.1: Overview of the measurement with time-dependent advective transport.

exp. nr.	air-flow rate ( $l \text{ min}^{-1}$ )	period (days)	number of periods measured
04lm4d	0.4	4	3.0
10lm2d	1.0	2	3.0
10lm4d	1.0	4	4.0
10lm7d	1.0	7	2.7

homogeneity of the sand column, it was decided to use two adjacent probes as sampling points instead of introducing vertically inserted probes at different radii.

The measuring technique of these continuous radon monitors is based on detection of emitted scintillation light in a nine-sector scintillation flask (volume 3 litres) with a photomultiplier tube. The CRM's were used in quasi-continuous mode, meaning that a sample of air was taken at the beginning of a cycle, while light pulses were only counted during the rest of the cycle. The scintillation flasks were flushed with a flow rate of  $2l \text{ min}^{-1}$  for 5 minutes whereafter light pulses were counted during 25 minutes. Radon concentrations were calculated with an algorithm which takes into account the presence of alpha-emitting radon daughters from previous cycles. As a consequence, the time resolution of determining the radon concentration with the CRM's was 30 minutes. The intake and exhaust of one CRM were connected to the probes located at 1.26 m and 1.06 m, respectively. The intake and exhaust of the other CRM were connected to openings on the lid, approximately 1 m apart.

The experiments with time-dependent advective transport were carried out with a period of 4 days at a flow rate of  $0.4l \text{ min}^{-1}$ , and with periods of 2, 4 and 7 days at a flow rate of  $1l \text{ min}^{-1}$ . The conditions of the four experiments with time-dependent transport are summarized in Table 6.1. For each experiment at least three periods were obtained during which the radon concentration varied periodically around a certain constant value (semi steady-state situation), with exception of the 10lm7d experiment in which 2.7 periods were obtained. In addition to the measurements with the CRM's, radon-concentration profiles in the vessel were measured at the end of the intervals (just before the air-flow was switched) in the experiment with a period of 7 days and a flow rate of  $1l \text{ min}^{-1}$ .

Usually, radon concentrations in the radon-vessel experiments are measured using other radon monitors and cells than the CRM's. To eliminate systematic errors introduced by using other equipment, the efficiencies of the CRM's were determined relative to the standard radon monitor and cell to which all radon concentrations are referred. This was carried out by connecting the two CRM's and the reference monitor and cell to the crawl space, ventilated with a flow rate of  $0.25l \text{ min}^{-1}$ . The steady-state radon concentration was measured for almost one week, allowing a precise determination ( $\pm 1\%$ ) of the relative efficiencies for a constant radon concentration.

Fig. 6.10 presents the results of the experiment with a period of 4 days and an air-flow rate of  $0.4l \text{ min}^{-1}$  (04lm4d), showing the radon concentration  $C_{cs}$  ( $\text{Bq m}^{-3}$ ) in the crawl space (top), the radon concentration  $C_p$  ( $\text{Bq m}^{-3}$ ) at 60 cm below the sand surface (bottom). When the measured concentrations at the two different positions are compared,

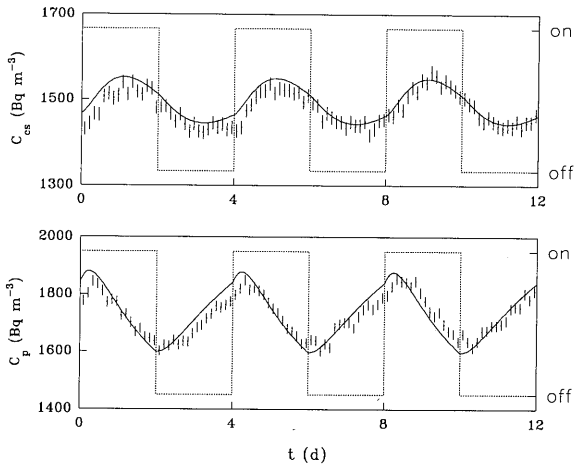


Figure 6.10: Radon concentration  $C_{cs}$  ( $\text{Bq m}^{-3}$ ) in the crawl space (top) and radon concentration  $C_p$  ( $\text{Bq m}^{-3}$ ) 60 cm below the sand surface (bottom), both as function of time for an experiment with a pulsed air-flow of  $0.41 \text{ min}^{-1}$  and a period of 4 days. The air-flow switched on at  $t = 0$ , as indicated on the right vertical axis and the dashed lines. Solid lines represent calculated curves using the numerical 2D-model with input parameters given in Table 5.1.

a first observation may be the difference between the shape of the two responses. The concentration in the sand resembles a saw-toothed wave, while the concentration in the crawl space varies more smoothly. The smoothly oscillating behaviour of the crawl space concentration is mainly caused by diffusive smearing of the 'low-radon pulse' entering the vessel at 163 cm below the sand surface. This smoothing becomes less pronounced when positions closer to the perforated box are considered, i.e. at a depth of 60 cm. Diffusion (and radial expansion of the pulse) also lowers the amplitude of the radon concentration oscillation. At 60 cm depth we have an amplitude of nearly  $300 \text{ Bq m}^{-3}$ , while in the crawl space it has decreased to about  $100 \text{ Bq m}^{-3}$ .

Considering the phase of the periodical variation of radon concentration, it is noticed that the crawl-space radon concentration is delayed with respect to the signal at 60 cm depth. The time-lag between the respective maxima and minima of the two curves (i.e. position of a maximum or minimum of the 'crawl-space' curve compared with the position of the respective maximum or minimum of the '60 cm depth' curve) are not equal. The time difference between the minima is approximately 1.2 days, while the time difference between the maxima is less: about 0.9 days. The time lags are partly caused by the time it takes to transport the radon pulse through the sand. The time lags are in reasonable correspondence with the time needed to transport pore-air over a 60 cm distance (pore-air velocity at  $0.41 \text{ min}^{-1}$  is  $54 \text{ cm day}^{-1}$ ), but precise values depend largely on the spatial distribution of the radon concentration in the vessel. Moreover, between respective maxima of the radon concentration we have combined diffusive and advective transport, while between minima we have diffusive transport only.

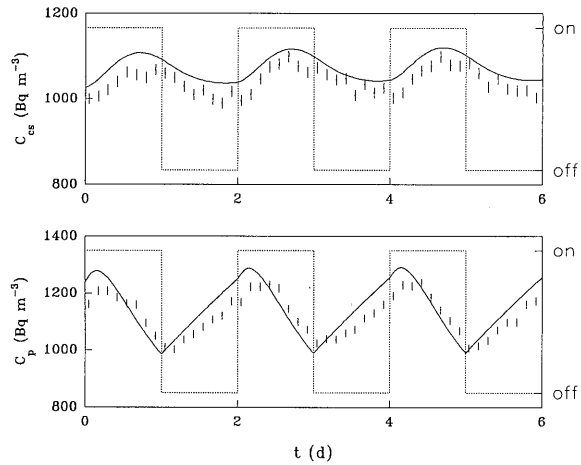


Figure 6.11: See Fig. 6.10, but with an air-flow rate of  $1.01 \text{ min}^{-1}$  and a period of 2 days. The air-flow switched on at  $t = 0$ .

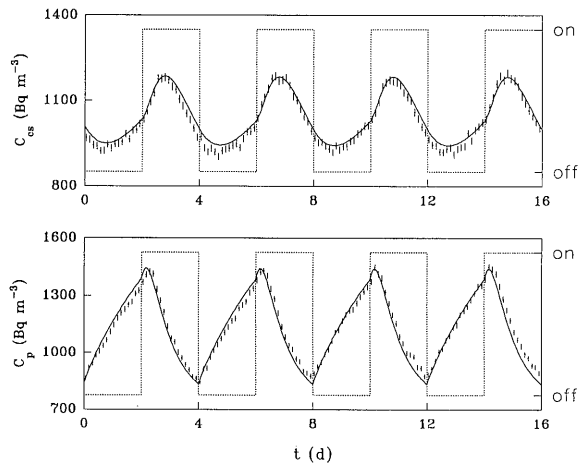


Figure 6.12: See Fig. 6.10, also with a period of 4 days but with an air-flow rate of  $1.01 \text{ min}^{-1}$ . The air-flow switched off at  $t = 0$ .

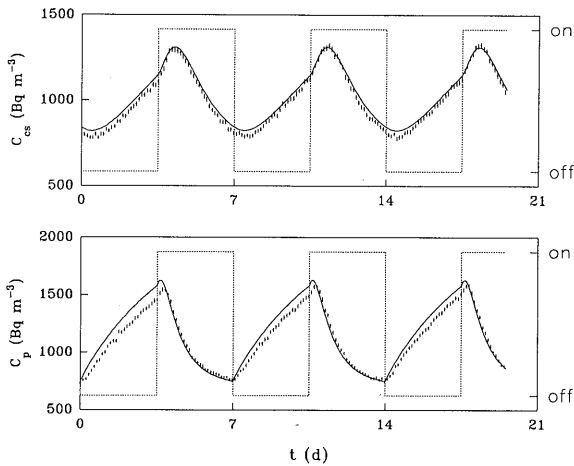


Figure 6.13: See Fig. 6.10, but with an air-flow rate of  $1.01 \text{ min}^{-1}$  and a period of 7 days. The air-flow switched off at  $t = 0$ .

Figs. 6.11, 6.12 and 6.13 show the same quantities as Fig. 6.10, but for the experiments with a flow rate of  $1.01 \text{ min}^{-1}$  and a period of 2, 4 and 7 days, respectively. The results of these experiments show a similar behaviour as in the first experiment, presented in Fig. 6.10. The crawl-space radon concentration as function of time has a lower amplitude and shows a more smooth behaviour than the radon concentration at 60 cm depth. Also in these experiments the crawl-space radon concentration lags the concentration at 60 cm depth. An additional feature is seen in Fig. 6.13 where the results are presented of the experiment with a period of 7 days. In this case the period of the pulsed air-flow is long enough to allow  $C_p$  approach the equilibrium value during periods with the air-flow turned on. This is not so surprising since pore-air is transported over almost 5 meter in the sand within a period of 3.5 days. Figs. 6.11, 6.12 and 6.13 also show that the average concentration is hardly influenced by the period of the pulsed air-flow. When extrapolating to high frequencies, we conclude that the equilibrium concentrations with a continuous flow rate of half magnitude must be nearly equal to the average concentrations in the pulsed-flow experiments. This finding is supported by the results of the experiments with steady advective transport, shown in Fig. 6.8.

The solid lines in the graphs showing  $C_{cs}$  and  $C_p$  denote results of 2D numerical calculations. The time steps in the numerical calculations were chosen such that 80 steps constituted one period of a pulsed air-flow experiment. For example,  $\Delta T = 4320 \text{ s}$  for the experiment with a period of 4 days. It is realised that this choice does not meet the requirement  $\nu < 1$ , see section 3.3.2, at positions close to the centre of the perforated box. The refinement of the grid at this position, which is accompanied by an (unwanted) increase of  $\nu$ , is necessary to keep the grid Peclet number, Eq. 3.15, as low as possible during periods with advective transport. Also, further refinement of the time step  $\Delta T$  did not significantly change the solution at positions in the vessel which are of interest for comparison with experimental results (in the crawl space and about 60 cm below the surface of the sand). Therefore, the choice of time step and grid spacing is thought to be

an optimization of numerical accuracy and computing time.

In general (Figs. 6.10 to 6.13), it is observed that the concentrations calculated with the 2D-model agree well with the measured concentrations considering amplitude, phase and absolute value. The best agreement concerns the amplitude. The absolute value of the crawl space data slightly deviates, with the measured concentrations being fractionally lower than calculated. However, it is not so meaningful to discuss this in further detail since the discrepancies in absolute value are of similar magnitude as observed in previous experiments with stationary advection, and are well within the 10% range. The data also indicate a negligible influence of atmospheric pressure fluctuations. Experiment 10lm4d (Fig. 6.12) namely shows the best agreement between experimental and modelling results while the strongest atmospheric pressure variations (alternatively raising and falling 25 hPa every 4 days) occurred during this experiment.

The phase of the signal also differs somewhat, mainly for the radon concentration at 60 cm below the sand surface. These small aberrations are not strongly correlated with the air-flow rate and/or period of the pulsed flow. The phase shift for the radon concentration at 60 cm below the sand surface varies from experiment to experiment, but seems to be more pronounced for the measurements with a higher air-flow rate. The calculated concentrations are ahead of the measured concentrations by at least several hours. The time lag is larger during the intervals with the air-flow turned off than in the cycle with advective transport. A plausible explanation for this phenomenon may be that air taken from the pore volume at 60 cm depth, is being returned at a depth of 80 cm. This pumping disturbs the actual radon-concentration distribution when the concentrations at 60 and 80 cm depth are different.

The disturbance of the radon concentration field at  $z=1.06$  and  $1.26$  m is illustrated in Fig. 6.14, where the measured radon profiles during the 10lm7d experiment at moments of changing the air-flow are presented. The radon concentration at  $z=1.06$  m is lower than calculated for the profile taken just after the cycle with diffusive transport (upper curve in Fig. 6.14). Since the CRM withdraws air from the sand at  $z=1.26$ , and returns the air at  $z=1.06$ , relatively radon-poor air is introduced at  $z=1.06$ , caused by the negative concentration gradient between these two positions. The reversed is true just after a cycle with the air flow turned on (lower curve). Then, relatively radon-rich air at  $z = 1.26$  m is transported by the CRM to  $z=1.06$  m. When the transport processes in the sand are very slow, this disturbance may persist and therefore influence the measured concentration considerably. We may have such a situation during periods with diffusive transport only. On the other hand, the disturbance is suppressed during periods with advective transport due to the quick

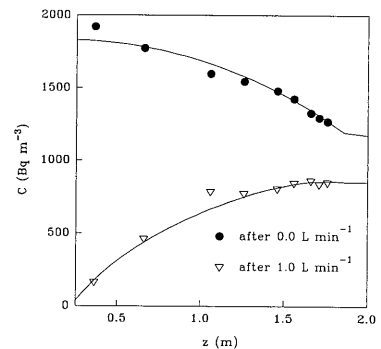


Figure 6.14: Radon concentration  $C$  ( $\text{Bq m}^{-3}$ ) as function of height  $z$  (m) for the experiment with an air-flow rate of  $1.0 \text{ l min}^{-1}$  and a period of 7 days. Upper profile after the interval without an air-flow (at  $t = 3.5, 10.5$  and  $17.5$  days) and lower profile after the interval with air-flow (at  $t = 0, 7$  and  $14$  days), see also Fig. 6.13.

refreshment of pore air from other layers. As a result, a shorter time lag is observed when the air-flow is turned on.

In conclusion, the experiments with time-dependent advective transport have indicated that the measured concentrations are well reproduced by the 2D finite-difference model, especially concerning amplitude and phase of the signal. Small systematic deviations in the absolute value (5% at most) are noticeable, but are still small when compared to deviations observed in previous experiments.

## 6.5 Conclusions

The steps towards more complex conditions made in this chapter, i.e. combined diffusive and advective transport, have revealed several aspects of radon transport in the vessel. First, downward advective transport in the vessel does not complicate the situation to a large extent since the transport processes remain one-dimensional. These experiments truly complied with the strategy to vary only one parameter, i.e. the advective component. The situation with upward advective transport is however far more 'disturbed' with respect to previously studied conditions because of two-dimensional effects which start to play a role. Inevitably, numerical simulations had to be conducted for comparison with model predictions. Both steps of introducing advection and two-dimensional transport could be made without many difficulties, i.e. the calculations are in good agreement with the experimental results. In addition, the complexity was even further increased by studying time-dependent advective transport instead of equilibrium conditions. Also these experiments were well reproduced by the numerical model calculations. As the modelling results of the experiments discussed in this chapter are rather sensitive to the value of the porosity because the pore-air velocity, which depends on porosity, largely determines the influence of advection with respect to diffusion, these findings also suggest that the value of 0.34 (initially estimated uncertainty 0.01) represents the true value in the vessel well, provided that the other parameters are representative as well.

The method of increasing the complexity of the experiments step by step has proven to be fruitful. We may conclude that the experiments have shown that, within the uncertainties of the controlled conditions, combined diffusive and (pulsated) advective radon transport in room-dry sand and into a crawl space can be reproduced within 10% by model calculations on the basis of known transport processes and *independently* measured parameters. In other words, the radon-transport model presented in chapter 2 has been validated for two-dimensional transport in a homogeneous room-dry sand column.





# Chapter 7

## Experiments with a sheet of foil on the sand surface

### 7.1 Introduction

One of the techniques to reduce radon entry into crawl-space houses is coverage of the crawl space floor with a membrane. The membrane acts as a barrier for radon transport from the soil into the crawl space and therefore may reduce the radon concentration in the crawl space and living rooms. To improve the reduction even further, the technique may be applied in combination with forced ventilation of the crawl space as a whole, with suction of air from the region below the foil, or with (de)pressurisation of the crawl space. Especially the withdrawal of air from the space between the soil and an impermeable barrier (e.g. a concrete floor of a slab-on-grade house or a concrete slab or a foil on the crawl-space floor) has been proven to be an effective radon mitigation technique [Osborne et al., 1989; Swedjemark and Mäkitalo, 1990; Henschel, 1992; Osborne and Harrison, 1992; Ennemoser et al., 1995; Van der Graaf et al., 1997]. On the other hand, a comparison with modelling results of the effectiveness of such impermeable layers has scarcely been performed.

A study of the effectiveness of a membrane-based technique has been carried out for a Dutch situation (high ground-water level and low-indoor radon concentration) in a research house [Andersen et al., 1996]. Part of that study concerned detailed two-dimensional numerical modelling of radon transport through and along the membrane. Andersen et al. [1996] showed a discrepancy between the expected reduction of the radon concentration in the crawl space and the observed reduction. In order to match the calculations with observed concentrations, the value of the radon-diffusion coefficient of the membrane had to be 3 orders of magnitude higher than the measured value. These findings demonstrate uncertainties in modelling the effectiveness of this type of countermeasure for radon infiltration. This may be due to uncertainties in the value of radon transport parameters of the underlying soil but, considering the large difference between the measured and modelled diffusion coefficient of the foil, unidentified transport through or along the foil may also be an important factor. Also, the measured transport properties of the (small-scale) foil may not be representative for the true (large-scale) situation in a house.

In addition to the findings by Andersen et al. [1996], Nazaroff and Doyle [1985] observed an order-of-magnitude discrepancy between the estimated diffusive flux through a sheet of foil covering the crawl-floor of a research house and that necessary to account

for the calculated entry rate. As an explanation for the higher measured radon entry than expected, Nazaroff and Doyle [1985] suggested that radon migration from the soil into the crawl space is not dominated by diffusion in that particular house.

To obtain a better knowledge of radon-transport processes from the soil into a crawl space of which the ground is covered with sheets of foil, and to reduce the uncertainties in modelling the effectiveness of such a membrane-based technique, experiments have been made with the radon vessel in which the room-dry sand column is covered with a sheet of polyethylene foil<sup>1</sup>. These experiments are described in this chapter, as well as the additional experiments to determine the transport parameters of the polyethylene foil (section 7.2). The effect of having the foil on the surface of the sand was studied under the following conditions and are each covered separately in subsections in section 7.3:

- Undamaged foil without the lid installed (no crawl-space situation).

The following experiments were performed with a 9 cm high crawl space:

- Undamaged foil with ventilation of the crawl space,
- Undamaged foil with suction of air from the sand column,
- Undamaged foil with supply of air to the sand column.

In addition, the effect of a 5 cm diameter opening in the centre of the foil was studied. Such an opening alters the conditions of the experiments significantly and may better reflect the true situation where leakage along - or through openings in - the foil are likely to occur. These 'damaged foil' experiments were carried out under the following conditions, all with a 9 cm high crawl space:

- Damaged foil with and without ventilation of the crawl space,
- Damaged foil with suction of air from the sand column.
- Damaged foil with supply of air to the sand column.

Finally, conclusions are drawn in section 7.4.

## 7.2 The polyethylene foil

One of the prerequisites to describe radon transport in the vessel in the 'foil experiments' is knowledge of the relevant transport parameters for radon in the polyethylene foil. If the foil is assumed to be impermeable for air-flow and contains no detectable radium, the only parameters of concern are the thickness of the foil and the effective diffusion coefficient for radon. The thickness of the foil was measured as  $(2.33 \pm 0.02) \cdot 10^{-4}$  m.

The radon-diffusion coefficient of the foil has been measured with the 'radon-transparency set-up'. This instrument, schematically shown in Fig. 7.1, consists of a leak-tight cylindrical lower ( $V_1$ ) and upper ( $V_2$ ) compartment (height 16 cm, diameter 20 cm; stainless-steel wall and aluminium bottom and top flanges) separated by a sheet of foil. The lower compartment contains a radon source; the upper compartment is empty. The alpha activity in both compartments is measured with 5 cm diameter scintillation flasks (length 15 cm), which are mounted on a 5 cm diameter circular opening in the

<sup>1</sup>Tonzon Nederland, Enschede, The Netherlands.

cylindrical wall of each compartment. This large surface area assures fast transport of radon to the measuring volume of the cells. The cells are separated from the compartments with a 5 cm diameter glass-fibre filter which prevents transport of radon progeny between the compartments and the flasks. The opposite sides of the flasks are closed with a transparent window and positioned in front of the photomultiplier tube of a radiation monitor<sup>2</sup>.

At the start of an experiment, the lower and upper compartment are flushed with radon-poor ambient air. Exhaust air from the lower compartment, of which the radon concentration is relatively high due to production of radon in this compartment, is led to the upper compartment to equalize radon concentrations in the set-up<sup>3</sup>. After stopping the air-flow, the alpha activity in both compartments is measured by registering the number of pulses in consecutive intervals of one hour.

An analytical expression for the time-dependent radon concentration in both compartments was derived by solving the one-dimensional diffusion equation for radon in the foil with appropriate boundary conditions. Given the radon concentration as function of time in each compartment and the relative efficiencies for radon and

radon daughters, an expression for the time-dependent count rate is obtained. Integration over one hour periods finally gives an expression for the count rate in one hour intervals. The efficiencies for the two alpha-emitting radon daughters  $^{218}\text{Po}$  and  $^{214}\text{Po}$  relative to the efficiency for  $^{222}\text{Rn}$ , as well as the efficiency of the two scintillation flasks relative to each other were measured in independent experiments. The mathematical formalism and additional measurements are covered in detail in Appendix B<sup>4</sup>.

The measured count rate in each interval (one hour) as function of time after flushing is shown in Fig. 7.2 for both compartments. The count rates for the two compartments are highly different, which indicate that the transport of radon from lower to upper compartment is obstructed by the foil. The solid lines in Fig. 7.2 result from a least-squares fit of the analytical model to the data ( $\chi_{\text{red}}^2=0.8$ ) with the radon-diffusion coefficient of the foil, the radon-source strength in the lower compartment and initial radon concentration as free parameters. For the diffusion coefficient,  $D_f$ , was found  $(1.02 \pm 0.04) \cdot 10^{-11} \text{ m}^2 \text{ s}^{-1}$  at  $20 \pm 2^\circ\text{C}$ . This value<sup>5</sup> is in good agreement with the value

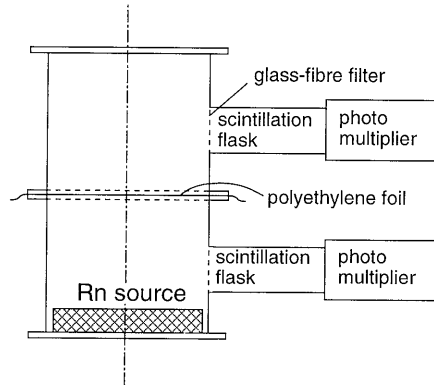


Figure 7.1: Sketch of the instrument for measuring the radon diffusion coefficient of a foil.

<sup>2</sup>Pylon AB-5 Radiation Detectors, Pylon Electronics Inc., Ottawa, Canada.

<sup>3</sup>If the compartments are flushed in the reverse order, or independently, a radon concentration gradient will be present over the foil at the start of the experiment. This complicates the initial conditions.

<sup>4</sup>The mathematical formalism is described for a (more general) situation with a slab a radium-bearing material as separating medium between the two compartments. Such experiments are discussed in chapter 8. In applying the model for a foil as separating material, the (partition-corrected) porosity and tortuosity are set to unity and  $D_0$  is replaced by the diffusion coefficient  $D_f$  of the foil.

<sup>5</sup>It is interesting to consider the radon-diffusion length in the foil. The diffusion length,  $\sqrt{D_f/\lambda} = 2.2 \cdot 10^{-3} \text{ m}$ , is about 10 times larger than the thickness of the foil, suggesting that most radon atoms

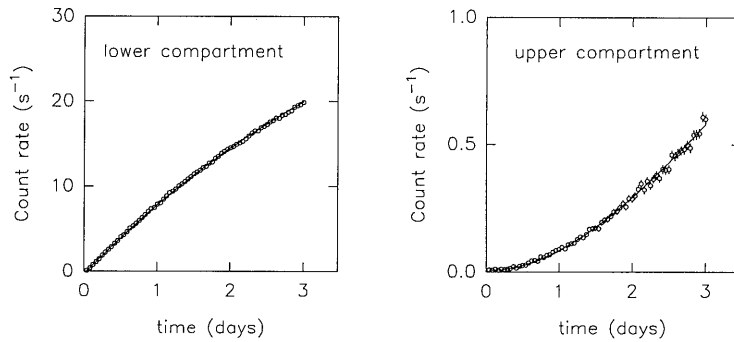


Figure 7.2: Measured count rate ( $\text{s}^{-1}$ ) in one-hour intervals as a function of time for the two compartments. Solid lines represent a least-squares fit of the analytical model to the data. Note the different scale of the vertical axis.

found by Nazaroff and Doyle [1985] for a polyethylene foil:  $(0.65 \pm 0.20) \cdot 10^{-11} \text{ m}^2 \text{ s}^{-1}$  at  $11.4 \pm 1.7^\circ\text{C}$  and  $(1.61 \pm 0.20) \cdot 10^{-11} \text{ m}^2 \text{ s}^{-1}$  at  $25.1 \pm 1.2^\circ\text{C}$  and is in reasonable agreement with the value found by Hakl et al. [1991]:  $7.1 \cdot 10^{-12} \text{ m}^2 \text{ s}^{-1}$ . It is, however, almost three times larger than found for an older polyethylene foil of the same manufacturer [Van der Spoel, 1994].

It is realised that  $D_f$  is an effective parameter to which others refer as the permeability constant [Jha et al., 1982; Haraya and Hwang, 1992; Wojcik, 1991; Hakl et al., 1991] or permeation coefficient [Labeled et al., 1992]. Other physical processes than diffusion are lumped into this parameter. One of these is the solubility of radon in polyethylene. If the solubility is low, the concentration in the foil at the interface between air and foil is then a fraction of the concentration in air. This results in a lower effective diffusion coefficient  $D_f$  than the true diffusion coefficient of radon in polyethylene. Other processes that influence the effective diffusion coefficient are adsorption of radon on the polyethylene surface and the presence of small pinholes in the foil. Since diffusion of radon in air is usually much larger than in polyethylene, pinholes enlarge the effective diffusion coefficient. However, one of the objectives of the radon-vessel experiments with a foil-covered sand surface is to verify whether measured concentrations can be reproduced by model calculations that make use of independently measured transport parameters of the foil. Only if the model calculations disagree with experimental results, it is meaningful to consider whether this type of modelling oversimplifies the true situation and if a more complicated model should be preferred. In this context it is at first instance sufficient to work in terms of effective parameters.

will pass through the foil before they decay. As a consequence, one might conclude that the foil should be nearly transparent for radon transport. This strongly contradicts the observation that most of the transport of radon from the lower to the upper compartment is obstructed by the foil. The reason for this paradox is that the usual interpretation of the diffusion length as 'the typical distance travelled by the radon atoms during one half-life' (see page 19), although correct, is rather deceptive in this case: the radon flux through the foil entering the upper compartments depends primarily on the diffusion coefficient, and not on the fraction of radon atoms that decay within the foil.

## 7.3 Vessel experiments

A 2 m diameter, one-piece circular sheet of foil was attached with 6 cm wide PVC-tape to the 7 cm wide inner metal rim of the vessel. Since the sand surface is about 1 cm below this metal rim, the foil is not in direct contact with the sand close to the rim. The foil rests, however, at the sand surface close to the centre. At first instance there seemed to be a good contact between metal rim and foil. However, the tape slowly released at positions where the foil had been creased. Extra tape was used at these places to minimize leakage along the foil.

A complication with the radon-vessel foil experiments is the influence of barometric pressure variations. If the vessel is completely sealed, a pressure difference would almost continuously exist over the foil due to fluctuations in barometric pressure. The foil will be pressed on the sand surface or will puff up, depending on the pressure difference over the foil. As this is an unwanted effect, a radon-tight air-filled plastic bag<sup>6</sup> was connected to an opening at the bottom of the vessel. Expansion or compression of air inside the vessel is then expected to swell or shrink the plastic bag, suppressing pressure differences over the foil. An additional advantage of the bag is the minimized loss of radon out of the radon vessel. However, the bag remained empty during the experiment without the lid, even after a barometric pressure drop. Apparently, the resistance to air-flow into - and out of - the vessel was extremely low, allowing the plastic bag to be emptied by the pressure of its own weight. The location of the leakage was not identified, but most likely it occurred through small air gaps where the foil was taped on the metal ring. So, an air-tight connection between the foil and the vessel was probably not established.

### 7.3.1 Undamaged foil without a crawl space

Based on the measured value of the diffusion coefficient of the foil, it is expected that most of the radon will remain in the pore space of the sand when the sand column is covered with the foil. However, this is only true if the leakage along the foil is negligible. The aim of the first experiment was to obtain an indication to what extent the foil, mounted on the vessel, served as a barrier for radon transport and to examine the influence of leakage along the foil. Therefore, equilibrium radon concentrations in the sand were measured without the lid on the vessel. Without a foil, radon concentrations are very low near the surface of the sand. With the foil, the concentrations near the sand surface are expected to be much higher.

The measured equilibrium concentrations as function of height in the vessel are shown in Fig. 7.3. The concentrations hardly vary with height and have an arithmetic mean value of  $3868 \pm 19 \text{ Bq m}^{-3}$ . The situation is totally different from the case without the foil, where the concentration increases from nearly zero at the surface of the sand, to about  $1600 \text{ Bq m}^{-3}$  at the bottom, see Fig 5.2. Clearly, the foil inhibits most of the radon exhalation from the sand, reducing the exhalation rate at the surface of the column to a large extent (about factor 25).

It is interesting to compare the measured average concentration with a calculated value. Using the independently measured values of the sand given in Table 5.1, the maximum equilibrium concentration is  $4138 \text{ Bq m}^{-3}$  for a situation without leakage and without diffusive loss through the foil. The measured value of  $3868 \text{ Bq m}^{-3}$  is 6.5% lower, which is due to diffusive loss through the foil and leakage of radon due to barometric

<sup>6</sup>Cole-Parmer Tedlar gas-sampling bag, 24" x 24".

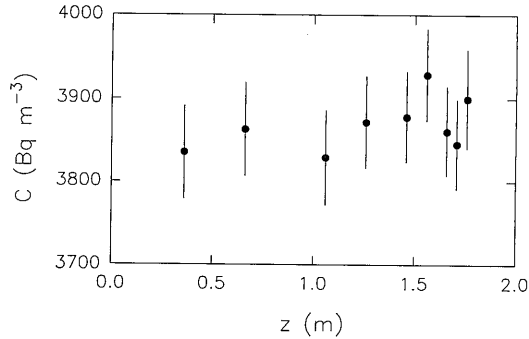


Figure 7.3: Measured radon concentration  $C$  ( $\text{Bq m}^{-3}$ ) as a function of the height  $z$  (m) in the vessel for the experiment with undamaged foil and without a crawl space. Error bars indicate statistical uncertainties.

pressure fluctuations. The diffusive loss can be approximated by  $\frac{AD_f\Delta C}{d}$  ( $\text{Bq s}^{-1}$ ), where  $A$  is the surface area of the foil ( $3.14 \text{ m}^2$ ),  $\Delta C$  is the concentration difference over the foil ( $3868 \text{ Bq m}^{-3}$ ), and  $d$  is the thickness of the foil. This results in a loss of  $5.3 \cdot 10^{-4} \text{ Bq s}^{-1}$ , which is 3.1% of the radon production rate of the sand (the sand volume of  $5.84 \text{ m}^3$  corresponds with a radon production rate of  $1.73 \cdot 10^{-2} \text{ Bq s}^{-1}$ ). The remaining 3.5% is probably caused by leakage of radon out of the vessel due to atmospheric pressure variations. This leakage may be calculated with a method which is similar to the type of calculation for the ventilation rate of the crawl space in the experiments with diffusive transport only, see Eq. 5.12. For the present case, the average leakage parameter  $\lambda_{\text{leak}}$  ( $\text{s}^{-1}$ ) for the whole vessel is obtained with:

$$\lambda_{\text{leak}} (\text{s}^{-1}) = \frac{1}{2} \cdot \frac{1}{3600 n} \sum_{i=1}^n \frac{|P_i - P_{i-1}|}{P_{i-1}} \quad (7.1)$$

where  $n$  is the duration of the experiment (h) and  $P_i$  is the atmospheric pressure at  $t = i$  h. This yields a ventilation rate for the whole sand column of  $6.8 \cdot 10^{-8} \text{ s}^{-1}$  and corresponds to 3.1% of the loss (due to decay) without leakage. As this value is in good agreement with the above-mentioned expected value of 3.5%, it may be concluded that the additional leakage is almost fully caused by the atmospheric pressure fluctuations. For this experiment, the diffusive loss through the large-scale foil can apparently be described on the basis of a measured small-scale diffusion coefficient of the foil. The subsequent experiments with a crawl space investigate whether this also holds for more complex situations.

### 7.3.2 Undamaged foil with a ventilated crawl space

In the second experiment and in all subsequent experiments, the lid was installed on the vessel simulating a crawl space with an effective height of 9 cm. In the present experiment, the crawl space was ventilated with an air-flow of  $6 \text{ l h}^{-1}$ , which corresponds with a ventilation rate of  $5.8 \cdot 10^{-6} \text{ s}^{-1}$  (once in two days). Crawl-space height and ventilation rate are very small with respect to more realistic values for houses. These

low values were chosen to effectuate easily measurable crawl-space radon concentrations. It is true that even higher concentrations are obtained by fully eliminating ventilation of the crawl space. However, such conditions introduce more uncertainties with respect to radon loss out of the crawl space since a fraction of the radon atoms in the crawl space dissolves in the water-filled moat surrounding the vessel. This loss is probably influenced by variations of the ambient temperature, causing the loss to fluctuate in time. The relative influence of these variations is suppressed by ventilation of the crawl space. A small air-flow of  $6 \text{ l h}^{-1}$  through the crawl space already reduces these uncontrolled variations to at most 6%.

In contrast to the previous experiment without a crawl space, the plastic bag was not connected to the bottom of the vessel. The somewhat lower radon concentration at larger depths in the experiment without a crawl space (Fig. 7.3) may indicate leakage of radon near the bottom of the vessel. Therefore, it was decided to close the bottom of the vessel and connect a small diameter plastic tube (of 2 m length to minimize diffusive loss) to an opening on the lid to force air-flows, caused by barometric pressure variations, to pass through small gaps between foil and upper metal rim of the vessel. Such conditions may give difficulties (e.g. pure diffusive transport through - and along - the foil can not be studied), but, on the other hand, a definite advantage is the certainty that the atmospheric pressure induced air-flows occur at the top of the sand column.

In the second experiment, radon concentrations in the crawl space were measured at eight-hour intervals during a period of six weeks (radon concentration profiles in the sand were not measured). In addition, atmospheric-pressure values were measured each 15 minutes and averaged over one-hour intervals. The measured crawl-space radon concentration (in the following, 'crawl-space' is sometimes omitted for convenience)  $C_{cs}$  ( $\text{Bq m}^{-3}$ , open circles) and atmospheric pressure (hPa) are presented as function of time (Julian days) in the lower and upper part of Fig. 7.4, respectively. Clearly there is an anti-correlation between radon concentration and atmospheric pressure.

To get a more quantitative understanding of the radon transport processes, it is expedient to compare the experimental results with model calculations. For the present experiment a simplistic 'mass-balance' model can be used to describe the time evolution of the radon concentration in the crawl space. In principle, such a model consists of a differential equation for the radon activity in the crawl space and, as part of the model, will include the rate of change of atmospheric pressure. Because the atmospheric pressure was measured in discrete one-hour time intervals (i.e. not continuously), an approximation to the differential equation is made in terms of one-hour time steps. Further, the following assumptions are taken into account:

- The radon concentration below the foil has a constant value, equal to the measured value in the previous experiment:  $3868 \text{ Bq m}^{-3}$ .
- The radon concentration of the incoming (ventilation) air is constant and is estimated at  $5 \text{ Bq m}^{-3}$ .
- The diffusive radon flux through the foil into the crawl space is proportional to the radon concentration difference over the foil.
- The effective ventilation rate of the crawl space due to loss of radon in the water-filled moat is constant:  $5.4 \cdot 10^{-7} \text{ s}^{-1}$ , see page 69.
- The crawl-space air is well mixed.

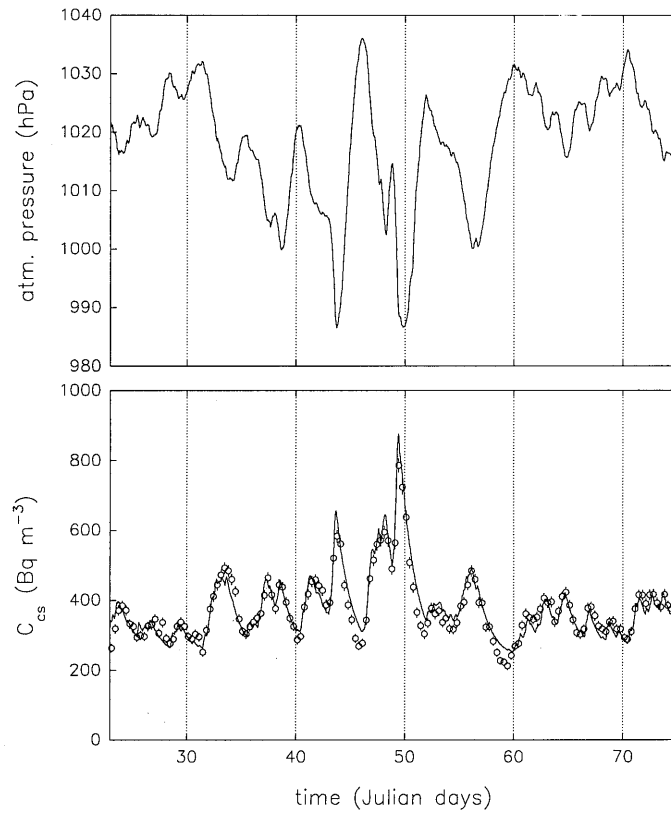


Figure 7.4: Results of the experiment with undamaged foil and a 9 cm ventilated crawl space ( $6\text{ l h}^{-1}$ ). Atmospheric pressure (hPa, upper part) and crawl-space radon concentration  $C_{cs}$  ( $\text{Bq m}^{-3}$ ) with statistical error bars (lower part) as function of time (Julian days). The relative uncertainty in atmospheric pressure is negligible; the absolute uncertainty is 2 hPa. Solid line in lower part results from a calculation with the simplistic mass-balance model, given by Eqs. 7.2 and 7.3.



- The effect of density variations due to barometric pressure fluctuations on radon concentration is ignored (i.e. the radon concentration in a geometric volume is calculated).

For a barometric pressure rise,  $P^{i+1} - P^i \geq 0$ , the model is mathematically expressed by:

$$V_{cs} \frac{C_{cs}^{i+1} - C_{cs}^i}{\Delta T} = QC_0 + \frac{D_f A}{d} (C_{ps} - C_{cs}^i) - [P_t V_{ps} + (Q - P_t (V_{ps} + V_{cs})) + (\lambda + \lambda_w) V_{cs}] C_{cs}^i \quad (7.2)$$

and for a barometric pressure drop,  $P^{i+1} - P^i \leq 0$ , by:

$$V_{cs} \frac{C_{cs}^{i+1} - C_{cs}^i}{\Delta T} = QC_0 + \frac{D_f A}{d} (C_{ps} - C_{cs}^i) - P_t V_{ps} C_{ps} - [(Q - P_t (V_{ps} + V_{cs})) + (\lambda + \lambda_w) V_{cs}] C_{cs}^i \quad (7.3)$$

in which  $P_t$  ( $s^{-1}$ ) is the relative rate of change of atmospheric pressure:

$$P_t = \frac{P^{i+1} - P^i}{P^i \Delta T} \quad (7.4)$$

and in which

$P^i$	= atmospheric pressure at $t = i$ h (hPa);
$V_{cs}$	= crawl-space volume ( $0.286 \text{ m}^3$ );
$V_{ps}$	= pore-space volume of the sand column ( $1.99 \text{ m}^3$ );
$C_{cs}^i$	= crawl-space radon concentration at $t = i$ h ( $\text{Bq m}^{-3}$ );
$C_{ps}$	= pore-space radon concentration below the foil ( $3868 \text{ Bq m}^{-3}$ );
$C_0$	= radon concentration of ventilation air ( $5 \text{ Bq m}^{-3}$ );
$Q$	= ventilation flow ( $6 \text{ l h}^{-1} = 1.66 \cdot 10^{-6} \text{ m}^3 \text{ s}^{-1}$ );
$\Delta T$	= time step (3600 s);
$\lambda$	= $^{222}\text{Rn}$ decay constant ( $2.1 \cdot 10^{-6} \text{ s}^{-1}$ );
$\lambda_w$	= ventilation due to loss in the water-filled moat ( $5.4 \cdot 10^{-7} \text{ s}^{-1}$ );
$D_f$	= radon diffusion coefficient of the foil ( $1.02 \cdot 10^{-11} \text{ m}^2 \text{ s}^{-1}$ );
$A$	= surface area of the sand column ( $3.14 \text{ m}^2$ );
$d$	= foil thickness ( $2.33 \cdot 10^{-4} \text{ m}$ ).

The term at the left-hand side of Eqs. 7.2 and 7.3 represents the rate of change of radon activity in the crawl space during a barometric pressure rise and drop, respectively. This change may be expressed as the difference per unit time of radon activity entering and leaving the crawl space (latter part is given between square brackets). The first two terms at the right-hand side represent the incoming radon activity per unit time due to ventilation and diffusive flux through the foil. The last term in both equations represents decay and loss of radon into the water-filled moat. The other terms representing air-flows induced by atmospheric pressure variations need some more elucidation. The in- and outflowing radon activities are schematically sketched in Fig. 7.5.

During an atmospheric pressure rise, the first two terms between square brackets in Eq. 7.2 express the outflowing radon activity per unit time to the sand and out of the vessel (ventilation air). It should be mentioned that Eq. 7.2 only describes the situation as long as ambient air does not enter the crawl space ( $Q > P_t (V_{ps} + V_{cs})$ ). With an air-flow of  $6 \text{ l h}^{-1}$ , the maximum allowed pressure rise is about  $2.6 \text{ hPa h}^{-1}$ . Such a fast rise did not occur during the experiment. The situation is slightly different for

an atmospheric pressure drop. Then, the third term at the right-hand side of Eq. 7.3 represents incoming radon activity from the sand below the foil, while the escaping activity from the vessel is expressed by the first term between square brackets. Part of this term,  $Q - P_t(V_{ps} + V_{cs})$ , corresponding to the second term between square brackets in Eq. 7.2, represents the ventilation flow leaving the crawl space with superimposed an atmospheric-pressure induced air-flow.

The solid line in the lower part of Fig. 7.4 results from a calculation with the ‘mass-balance’ model. The agreement with the experimental data is extremely good. Small deviations are visible at times following a sharp barometric pressure peak (e.g. at day 46, 52 and 59). An explanation for this might be a decrease of radon concentration below the foil due to flow of relative radon-poor crawl-space air to the sand. Diffusive supply from lower regions in the sand is probably not fast enough to equalize the accompanying concentration differences in the sand. As a result, a lower concentration gradient temporarily exists over the foil causing in a smaller diffusive radon flux to the crawl space. Since the calculations are reasonably sensitive to the value of the radon-diffusion coefficient of the foil - a 10% varied diffusion coefficient gives a 7% change in the crawl-space radon concentration - we may conclude that the measured small-scale diffusion coefficient of the foil represents the value of a much larger piece of foil well.

It is also interesting to consider the overall effect of barometric pressure variations on the crawl-space radon concentration. For a constant atmospheric pressure, the equilibrium concentration  $C_{eq}$  is easily calculated utilizing Eq. 7.2 or Eq. 7.3 where  $P_t = 0$ :

$$C_{eq} = \frac{QC_0 + \frac{D_f A}{d} C_{ps}}{\frac{D_f A}{d} + (\lambda + \lambda_w)V_{cs} + Q} = 214 \text{ Bq m}^{-3}. \quad (7.5)$$

As this value is even lower than the minimum measured value, the conclusion can be drawn that fluctuations in barometric pressure increase the average crawl-space radon concentration. For the present geometry, the average increment is approximately 60%. This ‘barometric pumping’ depends on many parameters such as permeability, radon-diffusion coefficient and ground-water level of the underlying soil. These dependencies (especially on permeability) have been studied by Tsang and Narasimhan [1992] for different geometries and frequencies of the atmospheric pressure variations. Their numerical simulations of a comparable case (only diffusion and an impermeable basement floor with a 1 cm crack) indicated an increasing relative influence with increasing permeability. Moreover, cracks in the soil may considerably enlarge the soil volume as ‘seen’ by a crawl space. Therefore, also considering the complex interplay of the various parameters, general guidelines with respect to the influence of barometric pressure variations on crawl-space radon concentration (even for a situation without continuous advective transport) are difficult to formulate. In any case, radon transport models that only include diffusive transport should be used with caution to estimate the average

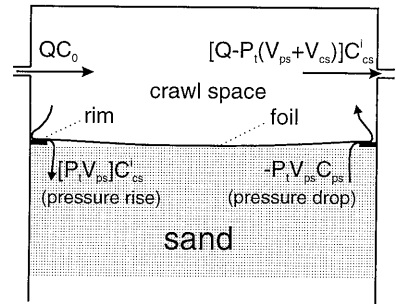


Figure 7.5: Schematic representation of the crawl space and in- and outflowing radon activities due to ventilation and barometric pressure variations.

crawl-space radon concentration, also when there is no net flow across the foil.

### 7.3.3 Undamaged foil with suction of air from the sand

As a next step, experiments were carried out with an advective flow through the sand. The previous experiment showed that advective transport from sand to crawl space increases the radon concentration. One of the techniques to counteract this flow of radon-rich air to the crawl space is suction of air from below the foil. This method is being put into practice in the US [Osborne and Harrison, 1992] and has been studied in 25 houses in the Netherlands [Van der Graaf et al., 1997].

Considering the radon vessel, there are several methods for removing air from the sand: using the perforated-tip of one of the probes or using the circular perforated box at 1.63 m below the sand surface. Disadvantage of the former method is the complex pressure field induced in the sand. For this reason the second option was chosen. The box spreads the intake of air over a much larger horizontal area in the sand. As a result, a nearly one-dimensional pressure field is established in a large part of the sand column. An air-flow rate of  $3\text{ l h}^{-1}$  was applied. At this flow rate, crawl-space air only escapes the vessel during an atmospheric pressure drop which is faster than  $1.5\text{ hPa h}^{-1}$  (did not occur during the experiment). Except for the applied flow rate, no additional ventilation of the crawl space was induced. A schematic sketch of the experiment is shown in Fig. 7.6.

The measured radon concentrations are shown in the bottom-left part of Fig. 7.7. In comparison to the set of data obtained in the previous experiment, the average concentration has decreased with 40% to approximately  $220\text{ Bq m}^{-3}$ . However, the crawl-space ventilation rates were different. For corresponding ventilation rates, the reduction of the crawl-space radon concentration would have been even larger. Another observation is the weaker anti-correlation between atmospheric pressure (top-left part of Fig. 7.7) and radon concentration. As mentioned before, this relates to the suppressed flow of radon-rich air to the crawl space due to the forced flow in the reverse direction.

Also for this experiment a relatively simple ‘mass-balance’ model can be used to describe the crawl-space radon concentration. The derivations and assumptions are similar to those discussed in the previous model. The adaption concerns the addition of a continuous flow of crawl-space air to the sand, and discarding the ventilation flow. The following equation is obtained for an increasing as well as decreasing atmospheric pressure (one equation is sufficient because a flow from sand to crawl space did not occur):

$$V_{cs} \frac{C_{cs}^{i+1} - C_{cs}^i}{\Delta T} = \frac{D_f A}{d} (C_{ps} - C_{cs}^i) + (Q_w + P_t(V_{ps} + V_{cs}))C_{out} - [(Q_w + P_t V_{ps}) + (\lambda + \lambda_w)V_{cs}] C_{cs}^i \quad (7.6)$$

where  $Q_w$  ( $\text{m}^3\text{ s}^{-1}$ ) is the flow rate at which air is withdrawn from the perforated box and  $C_{out}$  is the radon concentration in the experimental room, measured at  $10\text{ Bq m}^{-3}$ . The advective fluxes entering and leaving the crawl space are depicted in Fig. 7.6. Note that the dynamic influence of atmospheric pressure variations is simply superimposed on the forced flow. A complication is however formed by the unknown value of  $C_{ps}$ . The previous value can not be used because radon-rich air is continuously withdrawn from the sand, which lowers the pore-air radon concentration. Since  $C_{ps}$  was not measured, an estimation is made on basis of a mass balance for the radon activity in the sand column. In equilibrium and for a constant atmospheric pressure, the incoming radon activity in the pore space of the sand may be equated with the outgoing activity:

$$SV_{ps} + Q_w C_{cs} = \frac{D_f A}{d} (C_{ps} - C_{cs}) + Q_w C_{ps} + \lambda C_{ps} V_{ps} \quad (7.7)$$

where  $S$  is the  $^{222}\text{Rn}$  production rate ( $8.7 \cdot 10^{-3} \text{ Bq m}^{-3} \text{ s}^{-1}$ ) in the pore-space of the sand. Substituting the measured average crawl-space radon concentration ( $220 \text{ Bq m}^{-3}$ ) for  $C_{cs}$  in Eq. 7.7 leaves only  $C_{ps}$  unknown, giving  $3400 \text{ Bq m}^{-3}$ .

The solid line in Fig. 7.7 (bottom left) represents the radon concentration calculated with the mass-balance model. These results agree with the measured concentrations as far as the influence of barometric pressure variations is concerned: the amplitude of the fluctuations in the calculated and measured data are equal. However, the average concentration differs significantly, with the calculations being about 20-25% higher. Several reasons for this deviation may be given. Probably the largest effect is a lower diffusive entry through gaps along - or pinholes in - the foil in the presence of a pressure difference over the foil. The induced air-flow changes the radon concentration profile in these air channels (this effect is not incorporated in the mass-balance model) such that the diffusive flux is strongly decreased. Considering the observed difference between calculations and measurements, one might conclude that about 20-25% of the diffusive flux through the foil passes through small openings, either in or along the foil. However, the superb agreement between model and measurement in the previous experiment suggests a negligible diffusive flux through openings along the foil (note that the effect of pure diffusion through pinholes in the foil is lumped into the measured diffusion coefficient  $D_f$ ). This is an extra indication for the presence of pinholes in the foil. Only in situations where diffusive transport through these pinholes dominates over advective transport, which is more the case in the previous experiment without forced flow, the measured value for  $D_f$  is a valid parameter for describing radon transport. In this respect, it is interesting to revert to the observation of higher modelled concentrations directly after a barometric pressure rise in the previous experiment, see Fig 7.4. For the same reason as described above, this might be due to the presence of pinholes in the foil. The presence of such micro openings hinders the use of a simple mass-balance model in cases with a continuous advective transport to the high-radon side of the foil. Additional information on the number and size of the pinholes and openings along the foil is then necessary for a correct description of radon transport.

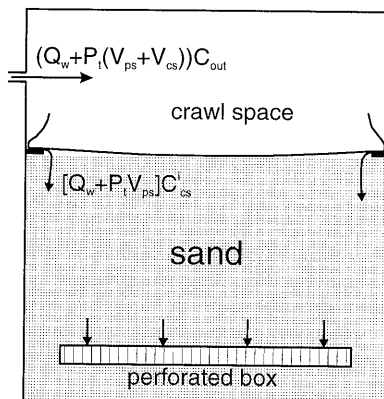


Figure 7.6: Schematic representation of the crawl space and in- and outflowing radon activities due to withdrawal of air from the sand via the perforated box and barometric pressure variations.

### 7.3.4 Undamaged foil with supply of air to the sand

A reversed forced flow through the sand column results in a continuous advective transport from sand to crawl space. This is definitely not a mitigation technique and as such not of interest for practical applications. Yet, the experiment has been carried out because the conditions can be simulated with a relatively simple mass-balance model (a decreased diffusive flux through openings along - and in - the foil is present but hardly noticed

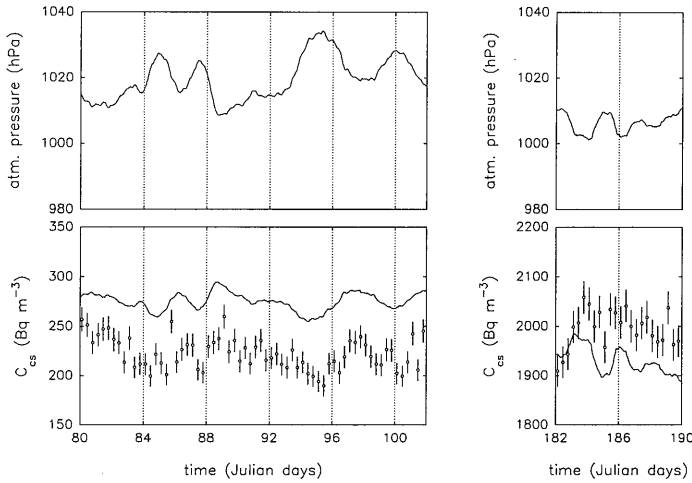


Figure 7.7: Left part: Results of the experiment with undamaged foil and withdrawal of air at a flow rate of  $3\text{ l h}^{-1}$  from the pore space of the sand via the perforated box at 1.63 m below the sand surface. See also Fig. 7.4. The solid line in the lower part represents the results of a simplistic mass-balance model, given by Eq. 7.6. Right part: Results of the experiment with undamaged foil and supply of air at a flow rate of  $2.5\text{ l h}^{-1}$  to the sand via the perforated box. The solid line in the lower part results from a simplistic mass-balance calculation, given by Eq. 7.8.

in this experiment because of a relatively high advective flux towards the crawl space). A more thorough understanding of radon transport processes may be obtained without much extra (modelling) effort.

To describe the radon concentration in the crawl space as function of time in this experiment, the following equation is used (one equation is sufficient because a flow from crawl space to sand did not occur):

$$V_{cs} \frac{C_{cs}^{i+1} - C_{cs}^i}{\Delta T} = \frac{D_f A}{d} (C_{ps} - C_{cs}^i) + (Q_s - P_t V_{ps}) C_{ps} - [(Q_s - P_t (V_{ps} + V_{cs})) + (\lambda + \lambda_w) V_{cs}] C_{cs}^i \quad (7.8)$$

where  $Q_s$  ( $\text{m}^3 \text{s}^{-1}$ ) is the flow rate ( $2.5\text{ l h}^{-1}$ ) at which air is supplied to the perforated box (for optimal correspondence, all the measurements were planned to be performed with flow rates of 3 and  $6\text{ l h}^{-1}$ ; unfortunately, an instrumental off-set decreased the flow rates to 2.5 and  $5\text{ l h}^{-1}$  in this and all subsequent experiments). The advective fluxes entering and leaving the crawl space are schematically shown in Fig. 7.8. The radon concentration in the sand  $C_{ps}$ , which is unknown, is estimated with a procedure similar to the one discussed in the previous section. Equating source and sink terms for the radon activity in the sand column gives:

$$S V_{ps} + Q_s C_0 = \frac{D_f A}{d} (C_{ps} - C_{cs}) + Q_s C_{ps} + \lambda C_{ps} V_{ps} \quad (7.9)$$

where the measured average crawl-space radon concentration ( $2000\text{ Bq m}^{-3}$ , see bottom-

right part of Fig. 7.7) is substituted for  $C_{cs}$ . This results in a value of  $3540 \text{ Bq m}^{-3}$  for the radon concentration in the sand column.

From the measured and calculated radon concentrations, presented in Fig. 7.7 (bottom right), is seen that the continuous transport of radon-rich air from the sand to the crawl space increases the radon concentration substantially, raising the average value to about  $2000 \text{ Bq m}^{-3}$ . Still, there is a mitigative effect of having the sheet of foil on the sand because the crawl-space radon concentration is, according to a numerical simulation, in the order of  $3000 \text{ Bq m}^{-3}$  for a corresponding situation without the foil. The results of calculations using Eq. 7.8, presented in the same figure, are in satisfactory agreement with the experimental data. Therefore, the use of a simple mass-balance model seems to be justified for cases with advective transport from sand to crawl space. However, one should be careful in translating the results of this radon vessel experiment to a true situation. As a consequence of having such a high crawl-space radon concentration in the vessel, a smaller concentration gradient will exist over the foil. Therefore, the radon concentration is less sensitive to the diffusive flux through the foil. Moreover, a decreased diffusive flux through pinholes is hardly noticed because it is only a small component of the combined advective and diffusive flux. In real situations, this component may have more influence due to a higher concentration gradient over the foil.

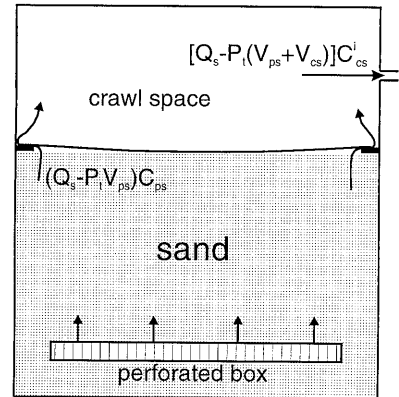


Figure 7.8: Schematic representation of the crawl space and in- and outflowing radon activities due to supply of air to the sand via the perforated box and barometric pressure variations.

### 7.3.5 Damaged foil with a ventilated crawl space

If a sheet of foil is used as radon mitigation technique in a house, damages may be inflicted during the installation. In broader sense, any path for direct flow of air along the foil may be considered as a 'damage'. Therefore, holes, imperfect seams and attachments, cracks and fissures can all be reduced to the same denominator. To study the effect of such a direct flow path, the preceding experiments with a crawl space were repeated with a 5 cm diameter opening in the centre of the foil.

The measured radon concentrations in a ventilated crawl space without forced flow through the sand column are presented in Fig. 7.9 (bottom-left part). There are two notable differences with the corresponding experiment with intact foil (see Fig. 7.4). In the first place, the average concentration has increased about a factor 1.7. Secondly, the correlation with atmospheric pressure is less pronounced. The latter is in fact a result of the former. With a 5 cm opening, a steady diffusive flux to the crawl space dominates over advective fluxes due to atmospheric pressure variations. Besides, the atmospheric pressure was relatively constant during the measuring period. The loss of data around day 113 is due to a memory overflow of the equipment.

Unfortunately, it is impossible to analyse the situation with an opening in the foil

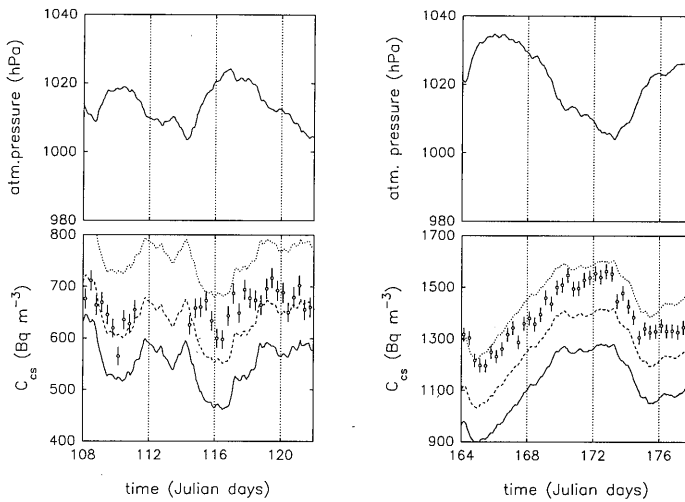


Figure 7.9: Results of the experiment with a damaged foil and a 9 cm crawl space ventilated with an air-flow of  $5\text{ l h}^{-1}$  (left part) and without ventilation (right part). See also Fig. 7.4. Some data points are missing round day 113 due to a memory overflow of the equipment. The three lines in the two lower parts of the figure represent calculations with a two-dimensional numerical model that includes the effect of barometric pressure variations on radon transport. The solid, dashed and dotted line refer to a calculation with an air-layer between the sand surface and the foil with a thickness of 0, 2 and 8 mm, respectively.

with a simple mass-balance model. For analysis, one has to turn to more complex numerical methods as outlined in chapter 3. However, one of the assumptions in this numerical model is the incompressibility of air. This raises a problem because exactly those variations of atmospheric pressure have a large influence on the crawl-space radon concentration in the experiments with a sheet of foil. Therefore, the 2D model can not be used in a straightforward manner. To include the effect of atmospheric pressure variations, two different methods may be followed to extend the model. In the first method, and after a model description by Edwards and Bates [1980], a transport equation for the radon-activity density (which includes diffusion, advection, decay and production) is coupled with the (non-linear) continuity equation for the total air density. The latter is predominantly ‘driven by’ atmospheric pressure variations and describes the transport of the total air density in a porous medium. The spatial variation of air density induces transport of air in the porous medium, resulting in advective transport of radon. Analytically, this method gives an exact description for radon transport (assuming either isothermal or adiabatic expansion and compression). However, in finding a numerical approach to the analytical equations, a severe difficulty is encountered. The numerical problems are not only introduced by the non-linear behaviour of one of the equations, but also by the completely different typical time-scales involved in the two coupled equations. A time scale of about one day seems appropriate for radon transport. This stands in large contrast with the typical time scale for air-density transport being of the order of

seconds (an air-pressure pulse is transported at about  $1 \text{ m s}^{-1}$  in the sand). Consequently, extremely small time steps are necessary for precise numerical modelling of a pressure pulse through the sand. This demands too much computing time (the method is more interesting to apply - and should be applied - if the two time scales are of the same order, i.e. for porous media with a much lower permeability).

In the alternative method, a numerical approach to the linearised continuity equation is made. This introduces negligible errors (estimated  $<1\%$ ) because the atmospheric pressure fluctuations are small relative to the absolute pressure. In addition, the fact of two totally different time scales is exploited by assuming an instantaneously responding air pressure in the whole sand column to atmospheric pressure changes (calculation of transport of a pressure pulse in the sand is bypassed).

The linearised continuity equation for a dry porous medium is written as [Clements and Wilkening, 1974] (neglecting influence of gravity):

$$\frac{\epsilon_a}{\bar{P}_a} \frac{\partial P_a}{\partial t} = \nabla \cdot \left( \frac{K}{\mu} \nabla P_a \right), \quad (7.10)$$

where  $\bar{P}_a$  is the mean atmospheric pressure (Pa). In the numerical approach, convective air-flows in the sand and crawl space are calculated for a linearly increasing or decreasing air pressure within a certain period. Since the atmospheric pressure was measured in one-hour intervals, the left-hand side of Eq. 7.10 is *a priori* known and is assumed constant during this interval. Moreover, this procedure is applied for each region in the vessel, in accordance with the assumed instantaneous response. As a result, Eq. 7.10 reduces to a steady-state diffusion equation with a source/sink term. This equation may be solved using the control-volume method outlined in chapter 3. In this case, the calculations are done with the 'fixed-interface' method because it is easier to extend this programme code with finite-difference expressions<sup>7</sup> for Eq. 7.10. The boundary conditions are also similar to those used for radon transport. A no-flow condition at impermeable boundaries and a constant value for the air pressure at the boundary where air can enter and leave the vessel (top part of the lid). The exact value of the air pressure at this boundary is not relevant because only pressure differentials determine the air velocities in the vessel. These pressure differentials exclusively depend on the value of the source/sink term  $\frac{\epsilon_a}{\bar{P}_a} \frac{\partial P_a}{\partial t}$  which may be different for successive one-hour intervals.

The three lines in Fig. 7.9 (bottom-left) represent calculated concentrations with the two-dimensional numerical model using a grid size varying from 5 mm by 40  $\mu\text{m}$  in the opening of the foil, to 8 cm by 16 cm at the bottom of the vessel. The solid line denotes a calculation in which the foil is in direct contact with the sand surface. As mentioned before, there was a small air-layer (plenum) between foil and sand surface, with increasing thickness from the centre of the foil (direct contact with the sand) to the rim of the vessel (thickness about 1 cm). Considering the unknown exact plenum thickness distribution over the sand surface and other uncertainties (e.g. leakage along the foil), it was decided to model a relatively simple plenum. By doing so, one obtains more insight in the influence of such a plenum without very detailed modelling. Therefore, an air-filled space with a constant thickness of 0, 2 and 8 mm between the foil and the

<sup>7</sup>As the control-volumes are homogeneous with respect to the air-filled porosity in the 'fixed-interface' method, the integration of Eq. 7.10 over a control-volume  $G$  (as in Eq. 3.3) results in a simple expression for the source/sink term. A drawback is however a changing permeability from one nodal point to another between two different media. A mean permeability is calculated here according to a procedure recommended by Patankar [1980].



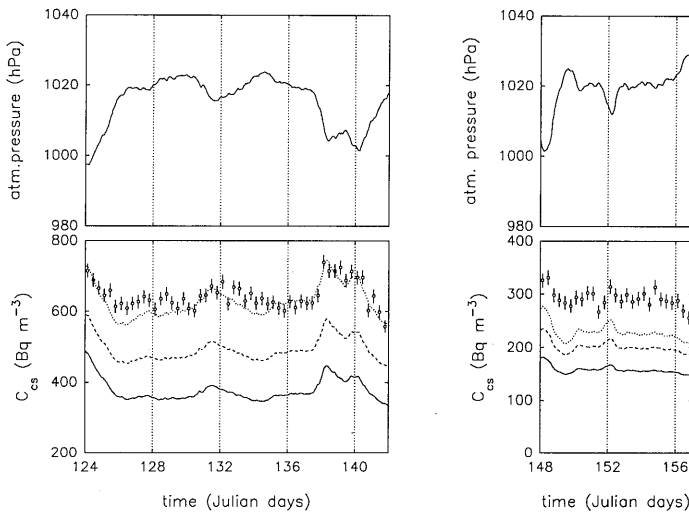


Figure 7.10: Results of the experiment with damaged foil and withdrawal of air at a flow rate of  $2.5\text{ l h}^{-1}$  (left part) and  $5\text{ l h}^{-1}$  (right part) via the perforated box. See also Fig. 7.9.

sand surface was modelled. The calculated crawl-space radon concentrations for these conditions are presented by the solid, dashed and dotted line in Fig. 7.9. It is seen that such an air-filled space has a considerable effect on the radon concentration. This is explained by an increased diffusivity in the plenum below the foil (differs a factor 5 with the diffusivity in the sand). It causes a larger diffusive flux towards the 5 cm opening in the foil, mainly from regions in the plenum near rim of the vessel. The results show that an effective plenum thickness between 2 and 8 mm represents the situation in the vessel quite well. This observation is supported by experimental and modelling results for a case where the ventilation flow through the crawl-space is turned off, see right part of Fig. 7.9. Also a rather impressive outcome of this latter experiment is the almost perfect agreement between experimental and modelling results considering the dynamic influence of the barometric pressure fluctuations. The results partly validate the extension made in the radon transport model for describing the influence of atmospheric pressure fluctuation for highly permeable porous media.

### 7.3.6 Damaged foil with suction of air from the sand

The results of the experiment in which air is withdrawn from the perforated box at a flow rate of  $2.5\text{ l h}^{-1}$  (unventilated crawl space) is presented in Fig. 7.10 (left part), together with two-dimensional numerical calculations with the three different plenum thicknesses.

The average measured radon concentration is almost three times higher than in the corresponding experiment without an opening in the foil. In the previous experiment a smaller increase of 75% was observed due to the presence of the 5 cm diameter opening. This may be explained by the difference in reduced diffusive flux through openings in and along the foil. In the corresponding experiment with undamaged foil, the air velocity in

the small openings was large enough to reduce the diffusive flux through these channels. This reduction seems much smaller in magnitude in the present experiment due to the relatively smaller air velocity in and below the opening in the centre of the foil.

The results in Fig. 7.10 (left part) show a difference between measured values and model calculations. Calculated concentrations are somewhat lower than the measured values assuming a 'correct' plenum thickness between 2 and 8 mm. These observations are reinforced by an experiment in which a larger air-flow of  $5 \text{ l h}^{-1}$  is induced through the sand column. The results of this experiment, presented in the right part of Fig. 7.10, show a 20-40% difference between calculations and measurements. It is remarkable that the calculations are lower, the more so since the disagreement for the corresponding experiment with undamaged foil is exactly reversed (see left part of Fig. 7.7).

Leakage along the foil near the rim of the vessel (due to an imperfect seal) may cause the discrepancies. These direct flow channels serve as a bypass for air-flow from the crawl space to the sand. As a result, the air velocity in the central 5 cm diameter opening is reduced, allowing a larger diffusive flux towards the crawl space. However, calculations with a slightly smaller air velocity through the central opening do not show a large increase of the crawl-space radon concentration. In order to increase the calculated concentrations (experiment with  $5 \text{ l h}^{-1}$ ) to the measured values, a 30-40% lower air velocity in the central opening is required. With an estimated typical length of 10 cm (underneath the tape) and an estimated *combined* surface area of several  $\text{cm}^2$  for the openings near the rim, their resistance to air-flow is expected to be much larger than for the central opening, thus not allowing a 30-40% decrease of air velocity. Moreover, if the size of the openings would be such that the necessary reduction of air velocity is accounted for, their influence must have been noticed in the preceding experiments. This is clearly not the case. On the other hand, a smaller air-flow through the central opening may be related to the direct contact between the opening and the sand. Because the openings along the foil near the rim of the vessel are connected to air-layer below the foil, the combined resistance to air flow of the central opening and the underlying sand may yet be large with respect to the leakages along the foil. Nevertheless, because of insufficient knowledge of the leakages along the foil, a well-founded cause of the disagreement can not be given.

### 7.3.7 Damaged foil with supply of air to the sand

The final experiment concerned a measurement with supply of air to the perforated box at a flow rate of  $2.5 \text{ l h}^{-1}$ . As in the corresponding experiment with undamaged foil, the advective radon flux into the crawl space is dominating over the diffusive

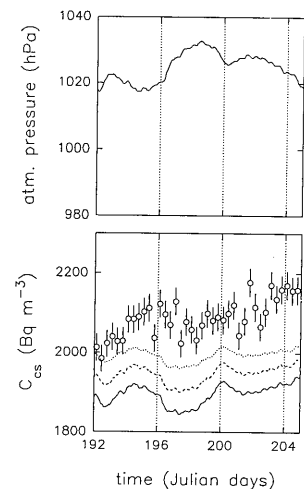


Figure 7.11: Results of the experiment with damaged foil and supply of air at a flow rate of  $2.5 \text{ l h}^{-1}$  to the perforated box. See also Fig. 7.9.

flux. Openings in the foil, which only increase the diffusive entry into the crawl space, have a nearly negligible effect on the total radon entry into the crawl space. The results that are presented in Fig. 7.11 indicate the validity of this supposition. The measured concentrations are approximately  $2000 \text{ Bq m}^{-3}$  in both experiments (compare with bottom-right part of Fig. 7.7), with slightly higher values in the experiment with damaged foil. It is also seen that the plenum thickness has a minor effect on the crawl-space radon concentration.

## 7.4 Conclusions and discussion

The experiments with the vessel have shown that the crawl-space radon concentration can be reduced by covering the crawl-space floor with a polyethylene foil. The comparisons between calculated concentrations and measured values indicate that the independently measured radon-diffusion coefficient of the foil represents the diffusion coefficient of a much larger piece of foil. The measured value of  $(1.02 \pm 0.02) \cdot 10^{-11} \text{ m}^2 \text{ s}^{-1}$  and a thickness of  $233 \mu\text{m}$  are such that the crawl-space radon concentration is reduced by at least one order of magnitude if the radon entry is only governed by diffusive transport through the foil. For the experiments in which these conditions are simulated, the agreement between calculations and measurements is within 10%.

Such conditions may not prevail in practice, i.e. pressure differences are exerted over the foil in most practical situations. These pressure differences may be due to either atmospheric pressure variations or to a steady under (or over) pressure of the crawl space with respect to outside. The latter may be caused by temperature differences (stack effect) or by an active system for (de)pressurising the crawl space.

The influence of barometric pressure variations on radon transport into the crawl space has been observed in all 'foil experiments' with the radon vessel. The influence is most notable for experiments in which diffusive transport (although low in magnitude) through and along the foil is dominating over steady advective transport. High crawl-space radon concentrations are observed during an atmospheric pressure drop due to the expansion of pore-air in the sand resulting in convective transport of radon-rich air towards the crawl space. During an atmospheric pressure rise the crawl-space radon concentration is diluted by entry of radon-poor ambient air, while crawl-space air is flowing to the sand through small openings along - and in - the foil. An important consequence of the air exchange between the crawl space and pore space of the sand due to barometric pressure fluctuations is the increased average crawl-space radon concentration (for the present geometry about 60%).

Since crawl-spaces are usually at a lower pressure with respect to outside, there may be a continuous advective transport from soil to crawl space. The experiments in which these conditions were simulated in the radon vessel indicate only a small effect of having the sheets of foil on the sand surface. Under these conditions, advective transport of radon towards the crawl space is dominating over diffusive transport. As a consequence, the relative importance of the barrier function of the foil for diffusive transport is strongly diminished. Considering the vessel experiments with forced advective transport from the sand to the crawl space, the agreement between calculations and measurements is also within 10%.

To reduce advective radon entry, such a continuous transport may be counteracted by depressurisation of the region below the foil. This mitigation technique was also investigated with the vessel by withdrawing pore-air from the sand at 1.6 m below the

sand surface (a shallower suction depth is more likely to be used in practice). This countermeasure was found to be very effective for reducing radon entry into the crawl space. The model calculations however overestimate the measurements with 20% for a situation with intact foil. This result suggests the presence of pinholes in the foil. On the other hand, for a situation with a damaged foil, the calculations *underestimate* the measurements with a factor 1.2-1.4. The cause of these discrepancies could not be identified precisely, but they may be due to uncontrolled leakage along the foil.

For practical purposes, it should be noted that this type of countermeasure (sub-membrane suction technique) is only effective if the whole surface area below the foil is at a lower pressure with respect to the upper side of the foil. The removal of soil-gas from below the foil should be equally spread over the total surface area to accomplish this. The experiments with the radon vessel indicate that a net flow density of only  $1 \text{ l h}^{-1} \text{ m}^{-2}$  surface area is sufficient if the foil is not damaged. In practice, this value may not be adequate because a larger volume of the soil may be influenced by atmospheric pressure variations. Moreover, holes, fissures or cracks in - and along - the foil have a strong negative effect on the mitigative impact. Air is transported along these openings without much pressure loss, resulting in a reduced pressure difference over the foil in the neighbourhood of the openings. The extension of such a pressure-field disturbance not only depends on the dimensions of openings in the foil but also on the permeability of the soil and how well the foil is in contact with the soil surface. The presence of a small air-layer (plenum) between foil and soil surface allows a horizontal air-flow below the foil, giving a more wide-ranging disturbance of the pressure field. This strongly reduces the mitigative effect of the foil. Therefore, it is important to ascertain that no holes, loose seams, fissures and such are present in the foil, especially if a sub-foil depressurisation technique is applied. A direct contact between foil and soil surface is recommended because it inhibits a wide disturbance of the pressure field below the foil in the unfavourable case of damages or openings in the foil. In practice, application of a completely airtight foil seems achievable. A problem is however formed at the perimeter of a house where the foil must be attached to the crawl-space wall. It is recommended to develop airtight attachment techniques for optimal mitigative performance of the foil.

In the light of the above mentioned condition that a net flow from crawl space to soil is necessary for reducing the crawl-space radon concentration, it is important to note that a crawl space is usually at a lower pressure with respect to outdoors. This pressure differential may induce an air-flow through the soil below the foundation of the house from outdoor to the crawl space. Results obtained by Andersen et al. [1996] show that this air-flow is about  $1.5 \text{ m}^3 \text{ h}^{-1}$  for the research house in Roden (normal conditions; 1.5 Pa depressurisation of the crawl space), corresponding with an air-flow density of  $16 \text{ l h}^{-1} \text{ m}^{-2}$ . So, if a sub-membrane suction technique is applied, the flow rate at which soil-gas is removed from below the foil should at least be as large as the steady flow towards the crawl space. The required flow might thus be much larger than the earlier mentioned value of  $1 \text{ l h}^{-1} \text{ m}^{-2}$ .

Another point of interest concerns the three orders of magnitude discrepancy between the measured value of the radon-diffusion coefficient of the foil and the value necessary in the model calculations to reproduce the observed crawl-space radon concentration in the research house [Andersen et al., 1996]. The authors give two explanations for the observed discrepancy: leaks in the foil and mixing flows created by fans located in the crawl space. With a simple calculation they estimated that a leakage-area density of  $10^{-3} \text{ m}^2$  per square meter could account for the observed difference. The radon-vessel experiments

show that a leakage-area density of  $6 \cdot 10^{-4} \text{ m}^2 \text{ m}^{-2}$  increases the diffusive radon entry rate by a factor three at most. On the basis of these results it seems unrealistic that a two times larger leakage-area density would increase the diffusive entry by three orders of magnitude. This shows that the leakage area of the foil in the research house must (even) have been larger than estimated or that the mixing flows created by the fans indeed diluted the sub-foil region to a large extent.

In conclusion, the experiments with a sheet of foil on top of the sand column in the vessel have shown that radon transport from the sand into the crawl space can be reasonably well described by model calculations using independently measured parameters for the sand as well as for the foil. Part of these calculations were done with the two-dimensional numerical model that was extended with a numerical approach to simulate the dynamic influence of atmospheric pressure fluctuations on air transport in highly permeable porous media. The good agreement between model and experiment validate this numerical approach in which the continuity equation for air transport is reduced to a steady-state diffusion equation with a source/sink term. Large differences between measured and expected concentrations as found in several studies concerning real houses, were not observed.



# Chapter 8

## Experiments with a ground-water level

### 8.1 Introduction

In the preceding chapters it was demonstrated that various experiments with dry sand in the vessel could be well described by the radon transport equations as presented in chapter 2, using values of parameters determined in separate experiments. As a consequence, a next step in complexity may be attempted: wetting the sand. In this chapter the experiments with a wetted sand column in the vessel will be described. The water level in the vessel was set at different heights by either supplying water through an inlet in the bottom or removing excess water through an outlet in the bottom.

Unfortunately, the adopted strategy of increasing the complexity step by step in the validation process by modifying one quantity in the transport process breaks down in these experiments. Introduction of water to the pore space of the sand inevitably increases the complexity of the radon-transport processes to a larger extent because several input parameters in the effective radon-transport equation are simultaneously influenced by the presence of water. These parameters (quantities) comprise the partition-corrected porosity  $\beta$ , the emanation coefficient  $\eta$  and bulk diffusion coefficient  $D$ . As the fraction of water saturation  $m$  of the pore space<sup>1</sup> of the sand varies with the height above the water table, the value of these quantities will also depend on the height in the vessel.

The situation is even further complicated by the dependence of the moisture-content distribution above the water table on preceding conditions in the sand (hysteresis effect). In addition, as a result of the spatial distribution of pore water near the air-filter of a radially inserted probe, different flow patterns are induced in the sand by the sampling of pore air. As this may influence the radon concentration of the air sample, one might question whether a pore-air radon concentration is measured corresponding with the true concentration at the probe height. Therefore, information about the air permeability of the sand as function of pore-water fraction is also required.

First, in section 8.2, the experiments are described for determining the water-retention characteristics of the sand. Section 8.3 covers the experimental set-up and results of measurements of the bulk radon-diffusion coefficient as function of the pore-water fraction of the sand. Subsequently, the effect of a changing permeability with height in the vessel on the measured radon concentration is discussed in section 8.4. Results of experiments

---

<sup>1</sup>The alternative term 'pore-water fraction' or 'moisture content' is also used in this thesis. Notice that in the literature, the moisture content is often given as the mass fraction of water per dry solid material.

with the vessel and corresponding model calculations are covered in section 8.5. Finally, conclusions are drawn in section 8.6.

## 8.2 Water-retention characteristics

Knowledge of the moisture content as function of height in the sand is mandatory for modelling radon transport in the vessel. Since water is attracted by the sand particles by adhesion to the solid surfaces and by capillary binding, the sand above the water table will adsorb water. The water table is defined as the level at which the pressure in the water phase equals the atmospheric pressure, and corresponds to the water level in a fictitious borehole. However, the total sand column will not be completely saturated with water since the weight of the water column above the water table counteracts the adhesive and capillary forces of the sand. In hydrostatic equilibrium (no water movement), the gravitational forces exactly counterbalance the capillary and adhesive forces. Consider for example the downward gravitational force acting on a water column of height  $h$  above the water table in a cylindrical pore of radius  $r$  (m). The gravitational force is given by  $\rho_w g h \pi r^2$  with  $\rho_w$  the density of water and  $g$  the acceleration due to gravity. In hydrostatic equilibrium, this force is counterbalanced by the upward capillary force which, for a cylindrical pore, may be expressed as  $2\pi r \sigma \cos \phi$  where  $\sigma$  ( $\text{J m}^{-2}$ ) is the surface tension of water and  $\phi$  is the contact angle between the water and solid phase. The maximum rise  $h_m$  (m) of the water in such a capillary is therefore found by equating both forces:

$$h_m = \frac{2\sigma \cos \phi}{\rho_w g r}. \quad (8.1)$$

When the sand is considered to exist of non-overlapping and non-interconnected cylindrical pores with different radii, one sees that the sand will remain completely saturated in a zone above the water table corresponding with the maximum capillary rise of the largest pores, called the ground-water zone. At larger heights the larger pores will loose their water while smaller pores will remain saturated. This is usually called the capillary zone. The result is a continuously decreasing moisture content with increasing distance above the water table. At even larger heights there can also be pore water that does not originate from capillary rise of the ground water (for example remaining rain-water or water left behind after a large drop of the ground-water table). This region is called the hang-water zone. It should be mentioned that a cylindrical capillary is of course a crude approximation or model for the pore space in sand. It is however thought that such a model can qualitatively be applied to the capillary binding of water in sand.

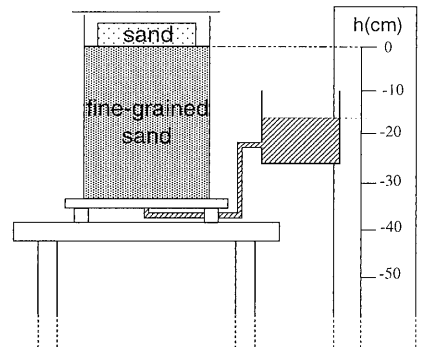


Figure 8.1: Schematic sketch of the instrument (sand-box method) for measuring the pore-water fraction of soil samples as function of moisture tension.



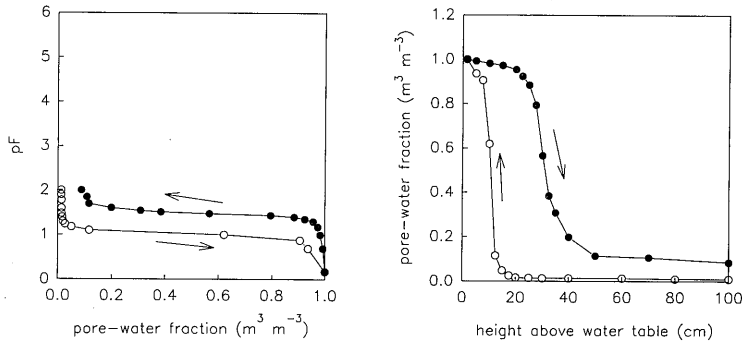


Figure 8.2: Water-retention characteristics for the sand in the vessel. The pF-value (10 base logarithm of the moisture tension in cm water column) as function of the pore-water fraction (left part) and pore-water fraction as function of the distance above the water table (right part). Open and closed markers denote experimental data obtained with a decreasing and increasing moisture tension, respectively (directions are indicated by an arrow). Solid lines connect data points.

The pore-water fraction of the sand as function of height above the water table was measured using the so-called sand-box method<sup>2</sup> [Van der Heij and Peerlkamp, 1961]. This 'water-retention instrument', sketched in Fig. 8.1, consists of a stainless-steel cylinder (height 35 cm, diameter 20 cm) filled with very fine-grained material<sup>3</sup>. The bottom of the cylinder has an opening through which water may enter or leave the fine-porous column via a flexible tube connected to a water reservoir that can be set between heights of -100 cm to 0 cm relative to the upper surface of the column. On this surface, a stainless-steel container can be placed that holds a sand sample (diameter 15 cm, height  $\approx$ 5 cm) resting on a tightened fine metal gauze<sup>4</sup> braced around the bottom of the container. Since the fine-grained sand remains fully saturated for the lowest position of the water reservoir, the suction pressure exerted on the water in the coarse-grained sample exactly corresponds with the height difference between the water level in the reservoir and the surface of the fine-grained sand column. In addition, as a result of having a saturated column, the contact-area between water in the sand sample and water in the fine-grained sand is maximised, and the time necessary to reach hydrostatic equilibrium is minimised. The suction pressure exerted on the water in the coarse-grained sand sample is usually called the moisture tension and is often expressed in terms of centimetres of water column, corresponding with the distance between the water level in the reservoir and the surface of the fine-grained sand column. In the (coarse-grained) sand column in the vessel, this corresponds with the distance above the water table.

<sup>2</sup>Based on the same principles is the often-used porous-membrane or porous-plate technique [Childs, 1969; Hillel, 1980].

<sup>3</sup>Synthetic sand, particle size circa  $73\mu\text{m}$ ; Eijkelkamp Agricultural Equipment, Giesbeek, The Netherlands.

<sup>4</sup>Stainless steel gauze, mesh size  $44\mu\text{m}$ , wire thickness  $35\mu\text{m}$ , Metaalgaasweverij Dinxperlo BV, The Netherlands.

The water content of the sand was determined by weighing in a series of measurements with the water reservoir set at successively lower positions (increasing moisture tension, starting at 0 cm) with an initially saturated sand sample and in a series with the reservoir set at successively higher positions (decreasing moisture tension, starting at -100 cm) with an initially dry sand sample. The results of these measurements are presented in Fig. 8.2.

The right part of this figure shows the moisture content as function of the height above the water table. Generally, such correlations are presented with the logarithm (10 base) of the moisture tension as function of the moisture content, and are usually referred to as the water-retention curve or pF-curve, as shown in the left part. The open markers denote data which are obtained by gradually decreasing (indicated with an arrow) the moisture tension on initially dry sand. The reversed procedure is applied for the experimental data denoted by closed markers. The data in Fig. 8.2 clearly indicates that the moisture content is subject to hysteresis. The hysteresis is a real effect and the datapoints can be well reproduced in repetitive experiments. A significant difference is the height above the water table at which the moisture content changes quickly. From dry to saturated at approximately 10 cm and from saturated to dry at circa 30 cm above the water table. In addition, dry sand remains dry up to a moisture tension of about 20 cm, while the pore-water fraction of initially wet sand is still about 10% at 70 cm above the water level. This hysteresis is among others due to the shape of the pores with changing wide and narrow passages and a different contact-angle for an advancing and receding water front [Pel, 1995]. The shape of the measured pF-curve for an increasing water tension resembles that for coarse-grained sand (particle size 210-2000  $\mu\text{m}$ ) [Woesten et al., 1987].

### 8.3 Radon diffusion coefficient

The experimental set-up used to measure the radon-diffusion coefficient in the sand as function of moisture content is nearly identical to the instrument used for measuring the diffusion coefficient of the polyethylene foil (see section 7.2), and is schematically shown in Fig. 8.3 (scintillation flasks and pm-tubes are not depicted). In the present case, the two compartments are separated by the cylindrical sample container described in the previous section, holding a 4.9 cm thick, 15 cm diameter sand sample. The analytical model describing the count rate in both scintillation flasks with a slab of sand as separating medium is discussed in appendix B.

Several experiments were carried out for a range of moisture contents, varying from room-dry to fully saturated. The

water content of the sand was regulated by placing the sample on the fine-grained sand in the water-retention instrument at different moisture tensions. For each experiment, the analytical expression for the count rate in each compartment was fitted to the data with the bulk radon-diffusion coefficient in the sand, the radon-source strength in the lower

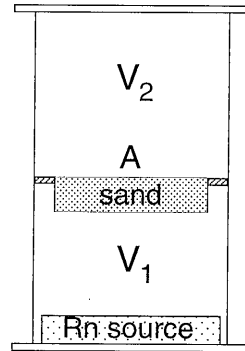


Figure 8.3: Sketch of the instrument for measuring the moisture-dependent radon diffusion coefficient in sand.

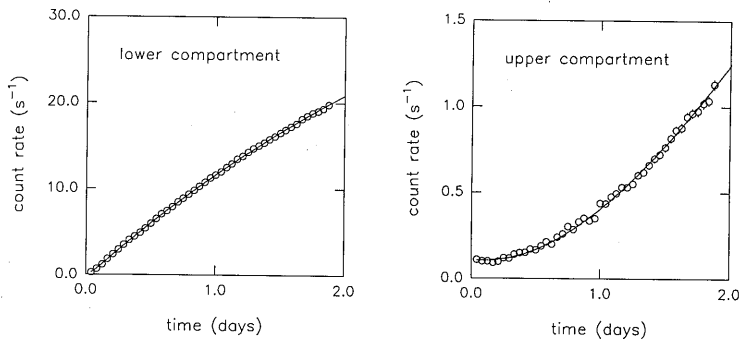


Figure 8.4: Measured count rate ( $\text{s}^{-1}$ ) in one-hour intervals as a function of time (markers) for the two compartments with in between a 4.9 cm sand sample with a moisture content of 79%. Solid lines represent a least-squares fit to the data. Note the different scale of the vertical axis.

compartment, and the initial radon concentration as free parameters. As an example, the measured count rate in each interval as function of time for the experiment with a moisture content of 79% is shown in Fig. 8.4 for the lower (left part) and upper (right part) compartment. Results of the least-squares fit ( $D = (1.164 \pm 0.010) \cdot 10^{-8} \text{ m}^2 \text{ s}^{-1}$ ,  $\chi_{\text{red}}^2 = 1.0$ ) to the data is indicated by solid lines. Clearly visible is a much slower increase in the upper compartment due to the 'barrier function' of the sand. Further, the S-shaped ingrowth curve (when extrapolated) in the upper compartment is remarkably different in shape from the exponential ingrowth usually seen for radon (as in the lower compartment). The absolute concentrations in the upper compartment as well as the shape of the ingrowth curve are determined by the diffusive flux through the sample. The fitting procedure, requiring consistency between both and also with the measured concentrations in the lower compartment, yields quite accurate values for the diffusion coefficient for relatively short measuring times.

The measured diffusion coefficient as function of moisture content for 14 experiments is shown in Fig. 8.5. As expected, the diffusion coefficient decreases with increasing water content, while the rate of decrease becomes faster at higher moisture contents. The decrease at low moisture contents is mainly due to a decreasing air-filled porosity. At higher moisture contents, the increasing number of water blockages in the pore space inhibits most of the diffusive transport through air-filled parts, causing a faster decreasing diffusion coefficient. For room-dry sand, the bulk diffusion coefficient is measured at  $(2.42 \pm 0.11) \cdot 10^{-6} \text{ m}^2 \text{ s}^{-1}$ , in good agreement with the value  $(2.39 \pm 0.08) \cdot 10^{-6} \text{ m}^2 \text{ s}^{-1}$  inferred from the porosity, tortuosity and diffusion coefficient in air (uncertainty of the latter not taken into account), as used for modelling the vessel experiments with room-dry sand, see section 5.3. It should however be remarked that the measured value is rather sensitive to a correction introduced in the analysis which accounts for a time lag in the measurements, see appendix B. As this concerns a first-order correction, which is only relevant at low pore-water fractions, a systematic off-set estimated  $<10\%$  may yet be present.

For a fully water-saturated sample, a bulk diffusion coefficient of  $(1.67 \pm 0.03) \cdot 10^{-10} \text{ m}^2 \text{ s}^{-1}$  is found, about 2.5 times higher than the expected value of  $6.6 \cdot 10^{-11} \text{ m}^2 \text{ s}^{-1}$

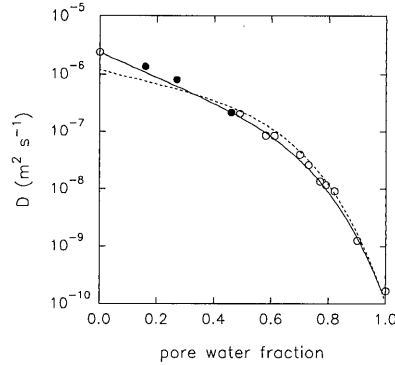


Figure 8.5: Measured bulk radon-diffusion coefficient (open and closed markers indicate a situation with an increasing and decreasing pore-water fraction, respectively) as function of pore-water fraction. Error bars are within markers. Solid and dashed line represent the fitted correlation function Eq. 8.3 and a correlation function developed by Rogers and Nielson [1991a] (Eq. 8.2), respectively.

(Eq. 2.36 with  $\epsilon_a = 0$ ,  $L = 0.26$ ,  $\epsilon_w = 0.34$ ,  $\tau_w = 0.64$  and  $D_w = 1.2 \cdot 10^{-9} \text{ m}^2 \text{ s}^{-1}$ ). This might be due to enclosed air in the sample or to diffusion along the interface between sand and the cylindrical wall of the container. Air-filled parts in or along the sand may have been introduced by a deformation of the sand matrix when the container is lifted. The weight of the sand namely stretches the tightened fine metal gauze on which the sand is resting (estimated vertical displacement about 1 mm at the centre).

For modelling purposes, a continuous expression for the dependence of the diffusion coefficient on moisture content is required. In this respect, it is interesting to compare the data set with an empirical function developed by Rogers and Nielson [1991a] for predicting the radon-diffusion coefficient in soil as function of, among others, the pore-water fraction. This function, based on more than one thousand diffusion-coefficient measurements on soil samples, is given by:

$$D = \epsilon\beta D_a \exp(-6m\epsilon - 6m^{14}\epsilon), \quad (8.2)$$

where  $m$  is the pore-water fraction (Eq. 2.7). This function, shown by a dashed line in Fig. 8.5, only approximates the diffusion coefficient in sand because each type of soil exhibits a different behaviour, based on differences in porosity, tortuosity, pore size distribution etc. The disagreement between the data and the correlation function at low moisture contents is due to approximating the tortuosity by the porosity in the correlation function. This appears to be inappropriate for coarse-grained sand. Therefore, an alternative empirical function was developed that resembles Eq. 8.2 but which represents the measured data better for low moisture contents. The function,

$$D = \epsilon\tau_a D_a \exp(a_1(m + m^5)), \quad (8.3)$$

was fitted to the data with  $a_1$  as free parameter and is shown by a solid line in Fig. 8.5 ( $a_1 = -4.99 \pm 0.04$ ). Consistency with the previously defined diffusion coefficient

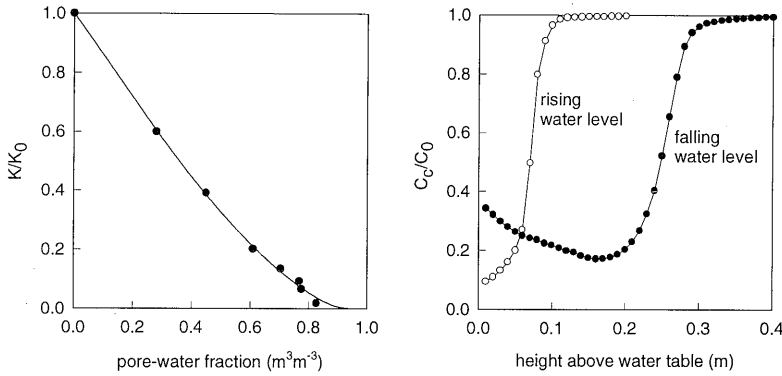


Figure 8.6: Left part: Measured air permeability (markers) of the sand as function of pore-water fraction. Error bars are within markers. Solid line represents the correlation function given by Eq. 8.4. Right part: Ratio of sampled and true radon concentration (both calculated numerically) in the vessel at the probe height as function of the distance (m) between the water table and the probe in a situation with a rising (open markers) and falling (closed markers) water level. Lines connect data points.

(Eq. 2.36) is obtained for dry sand by the constraint<sup>5</sup>  $D(m = 0) = \epsilon\tau_a D_a$ . The fit is seen to describe the data fairly well, but the empirical expressions as Eq. 8.3 are not yet the best achievable ones. Since we lack a physics-based function and qualitatively Eq. 8.3 describes the data quite well, a further optimisation of the empirical description was not attempted. An additional consideration was that the estimated uncertainties in each measured diffusion coefficient are probably too low (the reduced chi-square of the fit is high:  $\chi_{\text{red}}^2 = 214$ ). This is thought to be due to neglecting the effect of variations in the experimental procedures and set-up, e.g. rearrangement of the sand-grains when the sample is slowly wetted or when it is transferred from the water-retention instrument to the radon-transparency set-up, or evaporation of pore water. At this stage it is not possible to better quantify the uncertainties and since we have no better alternative, the correlation function Eq. 8.3 is used for modelling radon transport in the vessel.

## 8.4 Sampling technique - influence of pore water

An experimental difficulty which is encountered in the experiments with a water level is related to the radon concentration of the air samples taken from the vessel. The main question is whether this concentration is representative for the undisturbed pore-air radon concentration at the probe height. The same question could have been posed for the vessel experiments with dry sand, but the influencing factors are small in that case. With (homogeneous) dry sand, the 'active' volume of pore air, i.e. that part of the pore-air space that is being sampled, is nearly elliptically distributed around the air-filter of a probe. As a consequence, about as much air is taken from above the probe as from below. In case

<sup>5</sup>The corresponding constraint for  $m = 1$  is not fulfilled. This is however not of importance because of the extremely low diffusion coefficient at  $m = 1$ .

a vertical concentration gradient exists (e.g. an equilibrium diffusive radon-concentration profile), the higher concentration coming from below the probe is counterbalanced by the lower concentration coming from above. As a result, it is likely that a representative radon concentration is measured.

With moisturised sand, the situation is more complex due the presence of pore water. In case of an equilibrium moisture profile, the sand below a probe will contain more water than above if the probe is in the transition range from saturated to dry sand. As a higher pore-water fraction is accompanied by a lower air permeability, relatively more air will be sampled from above the probe, giving rise to a systematic underestimation of the actual radon concentration. Moreover, this underestimation is augmented by a steeper pore-air concentration gradient, caused by the limited radon solubility in water (radon concentration in the air phase is about 4 times higher than in the water phase, see Eq. 2.27). To estimate the systematic error introduced by this 'asymmetric' sampling, the transport processes during sampling may be simulated with the numerical model. This requires additional knowledge on the air-permeability as function of pore-water fraction.

The moisture-dependent air permeability was determined using the same sand sample as in the water-retention and diffusion experiments. In each experiment, the pressure drop across the slab of sand was measured at different flow rates. A linear fit to the data set  $(Q, \Delta P)$ , where  $Q$  is the air-flow rate ( $\text{m}^3 \text{s}^{-1}$ ) and  $\Delta P$  is the pressure difference, yields the permeability  $K(m)$  at moisture content  $m$ . The results, normalised with respect to the permeability  $K_0$  of dry sand ( $\approx 6 \cdot 10^{-11} \text{ m}^2$ ) and depicted in the left part of Fig. 8.6, show an almost linearly decreasing relative permeability to about 70% water saturation. This type of dependence has been observed for various soil types [Stonestrom and Rubin, 1989; McCarthy and Brown, 1992]. For modelling radon transport, the following (fitted) correlation function is used:

$$K(m) = K_0 \exp\left(\frac{1.372m - 1.0057m^3}{m - 1}\right), \quad (8.4)$$

shown by a solid line in Fig. 8.6 (left part). This correlation function satisfies the constraints  $K(0) = K_0$  and  $K(1) = 0$ .

### Numerical simulations

To model the radon-transport processes during sampling, the geometry of the air-filter in the probe head and surrounding sand must be 'translated' into a computational grid with a cylindrical coordinate system. Although the air-filter is cylindrical, the horizontal orientation of the probes prohibits use of this vertical cylindrical coordinate system of the vessel. It was therefore chosen to approximate the shape by modelling the head as a 1 cm thick, 6 cm diameter, cylindrical disc with an non-permeable bottom and top side, shown in Fig. 8.7. The intake of air occurs at the cylinder wall only, which has the same surface area as the air-filter. The disc is situated at 1 m depth in the centre of the

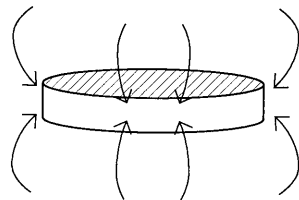


Figure 8.7: Cylindrical model representation of the perforated probe head. The intake of pore-air surrounding the disc takes place through the cylinder wall only.

The disc is situated at 1 m depth in the centre of the

sand column with the water table at greater depth. The boundary conditions for the pressure field imply zero pressure at the sand surface, a negative pressure at the cylinder wall and a no-flux condition at other boundaries. The pressure field is corrected such that the steady air-flow into the 'probe' is  $1 \text{ l min}^{-1}$  to simulate practical sampling conditions. For the concentration field, the boundary conditions imply zero radon concentration at the surface of the sand column and a no-diffusion condition at all other boundaries. The radon flux entering the disc perimeter therefore has an advective component only. The diffusive component can be neglected because the Peclet number ( $\frac{vL}{D}$  with air velocity  $v$ , disc radius  $L$  as typical distance and diffusion coefficient  $D$ ) for transport near the cylinder wall is large ( $> 100$ ). The effluent radon concentration from the probe  $C_{\text{eff}}(t)$  ( $\text{Bq m}^{-3}$ ) is evaluated as the ratio between the radon activity entering the disc per unit time and the accompanied air-flow:

$$C_{\text{eff}}(t) = \frac{\iint \frac{C}{\mu} \frac{dP}{dr} dA}{\iint \frac{K}{\mu} \frac{dP}{dr} dA}, \quad (8.5)$$

where the surface integral is taken over the cylinder wall. Since in the sampling procedure the first 0.5 l of air is discarded and the second 0.5 l is used for determining the radon concentration, the calculated concentration  $C_c$  ( $\text{Bq m}^{-3}$ ) of the air sample is evaluated as the average effluent concentration in the time interval from 30 to 60 s:

$$C_c = \frac{1}{30} \int_{30}^{60} C_{\text{eff}}(t) dt. \quad (8.6)$$

As initial concentration field, the (calculated) equilibrium radon-concentration profile in the sand with pure diffusive transport is taken. Furthermore, the height-dependent moisture content of the sand is inferred from the measured water-retention characteristics (linear interpolation between data points, see Fig. 8.2), the bulk diffusion coefficient is calculated using Eq. 8.3, the air permeability is calculated with Eq. 8.4, the emanation coefficient is assumed to be constant and a time step  $\Delta t$  of 1 s is chosen (a smaller time step does not yield significantly different concentrations).

The numerical simulations were carried out with a rising and falling water level and with the water table between 1 cm and 40 cm (with steps of 1 cm) below the disc. The calculated sampled radon concentration, normalised with respect the undisturbed initial pore-air radon concentration at the position of the probe, is plotted in Fig. 8.6 (right part) as function of the distance between the water table and the probe for a rising (open markers) and falling (closed markers) water level. These results show that for a rising water level, a representative sample is obtained if the water level is at a distance  $> 10$  cm below the probe. On the other hand, due to hysteresis in water retention of the sand, a representative sample is only obtained for a falling water level if this distance is  $> 30$  cm. The underestimation at smaller distances can be severe. For example, at a distance of 18 cm (falling water table), the sampled concentration is more than a factor 5 lower than the true concentration. At even smaller distances the probe head is located in a region with a smaller radon concentration gradient, resulting in a somewhat improved estimation of the undisturbed value.

### Comparison with alternative sampling technique

To verify whether a representative sample is indeed obtained when the water table is at 30 cm below the probe (falling water level), a comparison with an alternative sampling

technique was made. Therefore, a hollow small-diameter stainless-steel probe with a perforated tip<sup>6</sup> was placed vertically in the sand column until a depth of 1.2 m, i.e. at an effective height of 0.66 m, corresponding with the height of one of the horizontal probes. In the sampling procedure with the small-diameter probe the first 120 ml of air was discarded while the second 270 ml was used for determining the radon concentration. Since the extracted volume is only 40% of the one sampled with a horizontal probe, the influence of extracting radon-poor air from above the probe should be less.

The two sampling techniques were first compared in a situation with room-dry sand and without a concentration gradient in the sand column (lid at lowest position and the polyethylene foil on the sand surface). As the measured radon concentrations were identical, it may be concluded that the techniques were not hampered by systematic differences. In addition, a similar test was conducted with room-dry sand but with a concentration gradient in the sand (steady-state conditions with a downward air-flow of  $0.41 \text{ min}^{-1}$ ). Again the two concentrations were the same, indicating that both suction points were at the same depth. Finally, in a situation with the water table at a depth of 1.5 m (30 cm below the probes, falling water level) the two techniques again revealed no differences in measured concentration. Therefore, next to a numerical verification, it has been shown by experiment that the sampling technique with the horizontally inserted probes yields a representative pore-air radon concentration if the distance between the water table and the probe is  $>30$  cm. The situation with a rising water level has not been studied experimentally. Based on the numerical simulations only, the same is assumed to be valid for a distance  $>10$  cm. In comparing the measured radon concentrations in the sand with calculated values, only the measurements taken at positions above the mentioned distances above the water table will therefore be taken into account.

## 8.5 Experiments with the radon vessel

In the experiments with a ground-water table, steady-state pore-air radon concentration profiles were measured. The water table was consecutively set at 160, 120, 80, 40 and 0 cm below the sand surface at  $z = 1.86$  m (rising water level), which will be referred to as experiment RL160, RL120, RL80, RL40 and L0, respectively. At each level, equilibrium pore-air radon concentrations at the position of the probes located above the water table were measured. After the experiment with a completely saturated sand column, the experiments were repeated with the water table sequentially set at 40, 80, 120 and 160 cm below the sand surface (falling water level), established by removal of excess water through an outlet at the bottom of the vessel. For convenience, these experiments will respectively be referred to as FL40, FL80, FL120 and FL160. All experiments were carried with a 50-cm crawl space, ventilated with an air-flow of  $0.251 \text{ min}^{-1}$ . The radon concentration in the crawl space was measured quasi continuously. Radon concentrations in the water phase were not measured.

Fig. 8.8 shows the measured equilibrium pore-air radon concentration as function of height  $z$  (m) for the different levels of the water table. Markers of identical shape denote two profiles measured with the same water table. Open and closed markers designate a rising and falling water level, respectively. The horizontal dashed lines with perpendicularly a short vertical bar indicate the height of the water level for the several profiles. A difference in radon-concentration level up to about 15% is clearly

<sup>6</sup>Same probe as used for determining the homogeneity of the sand column, see section 4.4.



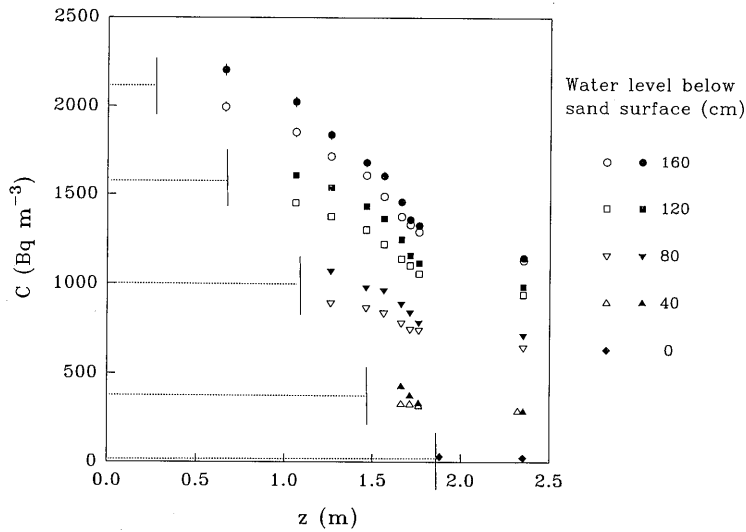


Figure 8.8: Results of the experiments with a ground-water table in the radon vessel. Equilibrium pore-air radon concentration  $C$  ( $\text{Bq m}^{-3}$ ) as function of effective height  $z$  (m) in the vessel with different (constant) levels of the water table, indicated with a dashed line. Open markers denote data obtained with a rising water level and closed markers denote data obtained with a falling water level.

noticed between two profiles measured with an equal water table but different preceding conditions (i.e. rising and falling water level). Higher concentrations are measured with a falling water level, probably related to hysteresis of the water retention of the sand. This phenomenon can be understood by a combination of effects. Assuming an equal number of radon atoms distributed over a pore-space region, the pore-air radon concentration will be higher when pores contain more water as a consequence of having a four times higher concentration in the air-filled pore space than in the water-filled pore space. In addition, the dependence of the emanation coefficient on moisture content probably plays an important role as well: a higher pore-water fraction is generally associated with a higher emanation coefficient, see Fig. 4.12. Since at a certain height above the water table the pore-water fraction is higher for a falling than for a rising water level, consequently higher concentrations are expected in the experiments with a falling water level.

A counteracting effect is expected from the fact that radon produced in the nearly-saturated region at 10-25 cm above the water table with a falling water level may not enter the upper regions of the column due to an extremely low diffusion coefficient in the nearly-saturated zone. Consequently, lower concentrations are expected in the air-filled pore space above the transition zone with a falling water level. On the other hand, because the diffusion coefficient in the unsaturated zone is lower with a falling water level than with a rising water level, the diffusive loss of radon into the crawl space is diminished, resulting in higher concentrations in the air-filled pore space of the sand

just above the ground-water zone. It should be mentioned that for the same reason the concentration just below the sand surface might as well become lower because of a lower crawl-space radon concentration (being the result of a decreased diffusive entry). The latter effect is however not observed in the experiments.

Recapitulating: in comparing the conditions with a falling and rising water level for an equal water-table height, the radon concentration in the air-filled pore space is expected to be *higher* with a falling water table as a result of:

- The partitioning of radon between air and water. For a constant number of radon atoms and since the concentration in the air phase is larger than in the water-phase, a higher pore-water content corresponds with a higher pore-air radon concentration.
- The radon emanation coefficient. This coefficient is larger for higher water contents.

and is expected to be *lower* for a falling water level as a result of:

- The further rise of the ground-water (and nearly-saturated) zone. Radon produced in this region hardly enters the air-filled pore space above.

One effect may as well increase as decrease the radon concentration in the air-filled pore space for a falling water level, depending on the position in the sand under consideration. This relates to:

- The radon diffusion coefficient in the unsaturated zone. Radon diffusion decreases with increasing moisture content. The loss of radon into the crawl space is therefore lower, giving *higher* concentrations in the sand just above the ground-water zone. On the other hand, the smaller diffusive entry into the crawl space results in a lower crawl-space radon concentration, corresponding with *lower* concentrations in the sand just below the sand surface.

These considerations show that the pore-air radon concentrations are determined by a complex interplay between the various position-dependent parameters. It is therefore difficult to even qualitatively explain the differences in radon-concentration level between two profiles measured with the same water table.

To analyse the data more quantitatively and also for comparing the results with expected concentrations, one-dimensional numerical model calculations are expedient. The experiments with a rising water level will first be discussed, followed by the experiments with a falling water level.

### 8.5.1 Model calculations: experiments with a rising water level

The first difficulty encountered in the calculations for a rising water level is a difference between the moisture conditions in the water-retention instrument and in the sand of the radon vessel. The moisture-content distribution that was measured independently with the set-up described in section 8.2 with a decreasing water tension indicates a pore-water fraction of 1.2% at moisture tensions in the range of 30 - 100 cm water column. It is however conceivable that this water entered the sand by condensation of water vapour present in the (partly-sealed) void space above the water-saturated fine-grained sand in the water-retention instrument. The true water content in the vessel at heights >30 cm above the water table may therefore be lower than 1.2%. The pore-water fraction might for example be 0.12%, corresponding with the value estimated for room-dry sand. As

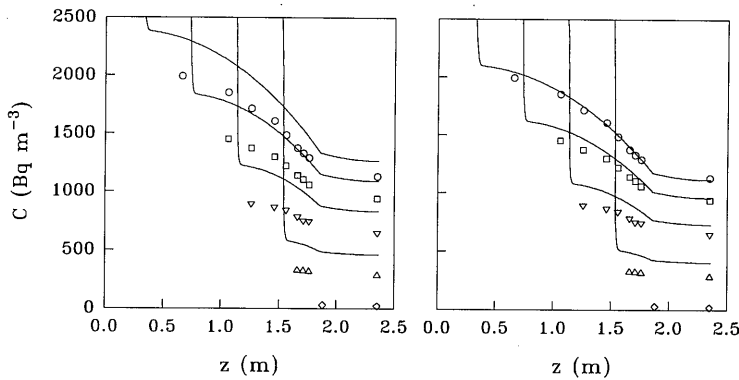


Figure 8.9: Experimental data (markers) and calculated pore-air radon concentrations  $C$  ( $\text{Bq m}^{-3}$ ) (lines) using the independently measured moisture-content distribution for a rising water level (see Fig. 8.2). The calculations in the left and right part of the figure are obtained with an emanation coefficient of 0.25 and 0.22, respectively.

in the experiments with room-dry sand, the main difficulty is actually caused by the sensitivity of the emanation coefficient to the moisture content for nearly-dry sand. As shown in Fig. 4.12, the emanation coefficient varies between 0.22 and approximately 0.25 at a moisture content ranging from 0.12% to  $\approx 0.4\%$ . This sensitivity introduces an uncertainty of  $\approx 15\%$  in the radon production rate of the sand. In the model calculations, at first instance, the independently measured moisture-content distribution is used in the calculations, i.e. a moisture content  $> 1\%$  is assumed at any position in the sand. Therefore, although the measured emanation coefficient is varying somewhat in this range of moisture content ( $> 1\%$ ), a constant emanation coefficient of 0.25 is assumed for the complete sand column.

The results of the one-dimensional model calculation for a rising water level, utilising the fitted correlation function for the bulk diffusion coefficient (Eq. 8.3) are presented in the left part of Fig. 8.9. In contrast to the results obtained with room-dry sand presented in chapter 5 and 6, it is seen that all calculated concentrations overestimate the measured values. The relative difference is about 15% for the concentration profile measured with the water table at 160 cm below the sand surface. With the water table at 40 cm below the sand surface, the calculated concentrations are however about 80% higher than measured. These differences are very large in comparison with those observed in modelling the experiments with room-dry sand.

Not shown in Fig. 8.9 are the results of calculations with a completely saturated sand column. In this situation, the radon concentration was not only measured at the top of the crawl space but also just above the surface of the sand by sampling with a piston. The measured concentration at the top,  $28 \pm 5 \text{ Bq m}^{-3}$ , and above the sand surface,  $30 \pm 2 \text{ Bq m}^{-3}$ , are in reasonable agreement with a numerical calculation using the literature value for the radon-diffusion coefficient in water, giving values of 27 and

$28 \text{ Bq m}^{-3}$  at the top and bottom of the crawl space, respectively<sup>7</sup> (assuming a radon concentration of  $5 \text{ Bq m}^{-3}$  for the ventilation air entering the crawl space). So, it is rather surprising to observe a good correspondence between measurements and calculations in case of a saturated column, whereas the correspondence is poor for the experiment with the water table at a depth of only several tens of centimetres.

In the light of the uncertainty associated with the radon production rate, the large disagreement between model and experiment might be caused by a too high value of the emanation coefficient in the model calculations. It is therefore interesting to examine the effect of taking a lower emanation coefficient in the calculations. The lowest possible value is 0.22 because the pore-water fraction of the sand at heights  $>30 \text{ cm}$  above the water table must at least have been higher than in the experiments with room-dry sand<sup>8</sup>. As a first attempt, the emanation coefficient is set to 0.22 and, for convenience, assumed to apply for the complete sand column. The results, depicted in the right part of Fig. 8.9, show that the radon-concentration profile for the lowest water table (RL160) is rather well reproduced by the calculations. On the other hand, as could be expected, discrepancies remain for the experiments with a higher water table. As this suggests a physical effect that has more influence at high water tables, the question arises whether the measured moisture-content distribution truly represents the situation in the vessel. The transition from saturated to dry sand may occur at a larger distance above the water table than indicated by the independently measured moisture-content distribution. The agreement between model and experiment would be improved if such a larger distance is used in the calculations, especially for the water table at  $40 \text{ cm}$  depth. This, because the volume of sand contributing to the radon concentration in the pore-gas phase in the unsaturated part of the column is reduced in the case of a transition at larger height.

To test the hypothesis of a different water-content distribution in the sand in the vessel than assumed in the calculations, a hard-plastic cylindrical drum (diameter  $50 \text{ cm}$ , height  $80 \text{ cm}$ , open top and closed bottom) was filled with the classified filter sand. Water was slowly added to the sand via a small-diameter plastic tube connected to a feed-through at the bottom of the drum. The other side of the tube was connected to a water reservoir of which the water level was kept at about  $60 \text{ cm}$  below the sand surface. After two weeks of allowing the pore-water content to reach a steady-state distribution, the sand column was carefully excavated. Samples were taken at regular depth intervals for analysing the water content, determined by weighing the samples before and after drying. It should be mentioned that during the excavation it was noted that the sand close to the cylinder wall of the drum contained less water than at the centre of the drum. The water apparently raised a larger distance at the centre than near the cylinder wall. This might be caused by a better compaction of the sand in the centre of the column.

To minimize the heterogeneity, the samples were taken from the inner  $30 \text{ cm}$  of the sand column because this part was visually observed to be rather homogeneously filled with water. Because the value of the porosity is required for calculating the pore-water fraction, this quantity was derived from a saturated sample taken from the bottom of the drum. The measured value of 0.395 (a high porosity, probably a result of simply pouring the sand into the drum) is more than 15% larger than the value assumed for

<sup>7</sup>If the measured diffusion coefficient in saturated sand is used ( $1.67 \cdot 10^{-10} \text{ m}^2 \text{ s}^{-1}$ , see section 8.3), the calculated concentrations in the crawl space are about  $42 \text{ Bq m}^{-3}$ . This further indicates that the true diffusion coefficient in saturated (and undisturbed) sand is probably somewhat lower than measured with the radon-transparency set-up.

<sup>8</sup>Assuming the emanation coefficient does not decrease with an increasing moisture content, see section 4.5.5.

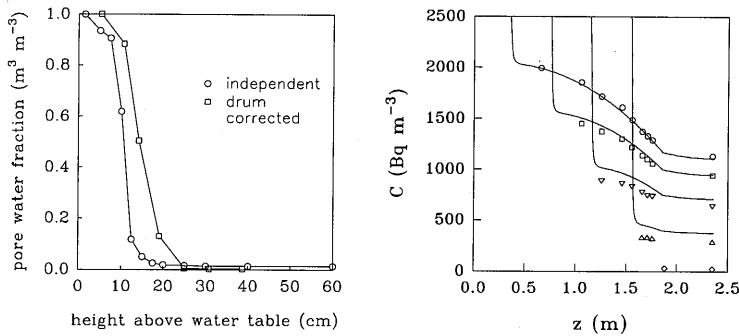


Figure 8.10: Left part: measured pore-water content as function of height above the water table in the sand in the cylindrical drum (squares), corrected for the difference between porosity of the sand in the drum and in the vessel. Lines connect data points. For comparison, the data obtained with the water-retention instrument, see Fig. 8.2, is also shown (circles). Right part: measured (markers) and calculated pore-air radon concentrations  $C$  ( $\text{Bq m}^{-3}$ ) (lines) using the measured moisture-content distribution in the drum and an emanation coefficient of 0.22.

the sand in the vessel. Since the capillary-suction pressure scales with the radius of a (cylindrical) pore, see Eq. 8.1, a correction is necessary to account for the effect of a larger porosity, such that the corrected pore-water distribution better applies to the situation in the vessel. As a first-order correction, the capillary-suction pressure is multiplied by the square root of the ratio of porosities<sup>9</sup> (8% correction). The corrected results are shown in the left part of Fig. 8.10 (square markers). It is seen that the transition from saturated to dry sand indeed occurs at a larger distance above the water table, namely at about 15 cm. The cause of the difference with the earlier measured water-retention curve is not clear. It might be that the fine stainless-steel mesh wrapped around the bottom of the sample container hindered the transport of water into the sand resting on the mesh or that measurements on small samples are not really representative for larger volumes due to boundary effects.

The results of model calculations including the measured water-content distribution in the drum and an emanation coefficient of 0.22 are shown in right part of Fig. 8.10. The influence of using this water-content distribution is noted by somewhat lower calculated concentrations, in particular for the experiments with a high water table. However, fairly large discrepancies remain. For the experiment with the water table at 40 cm depth a difference of about 35% is still observed. On the other hand, the experiment with the lowest water table (RL160) is almost perfectly reproduced. A better agreement for high water tables would be obtained if the transition from saturated to dry sand is modelled at an even larger distance above the water table. Considering the visually observed decreasing pore-water content with radius in the drum, the transition from saturated to dry sand in the vessel is more likely to occur at a larger distance from the water table,

<sup>9</sup>The porosity scales with the square of the radius when the pore space is considered to consist of straight (non-overlapping) cylindrical pin-holes.

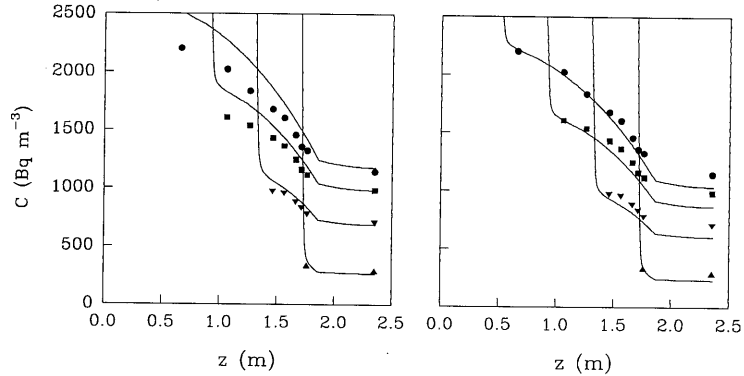


Figure 8.11: Experimental data (markers) and calculated pore-air radon concentrations  $C$  ( $\text{Bq m}^{-3}$ ) (lines) using the independently measured moisture-content distribution for a falling water level (see Fig. 8.2). The calculations in the left and right part of the figure are obtained with an emanation coefficient of 0.25 and 0.22, respectively.

being in favour of the agreement between model and experiment<sup>10</sup>.

### 8.5.2 Model calculations: experiments with a falling water level

As a starting point, the experiments with a falling water level are modelled using the independently measured moisture-content distribution with an increasing water tension and an emanation coefficient of 0.25. The results of these calculations are shown in the left part of Fig. 8.11. Note that the measured radon concentrations at a distance  $<30$  cm above the water table have been deleted, in view of the expected unreliable values of the concentrations as discussed in section 8.4. The calculations overestimate the measured concentrations for low water tables but reproduce the data for high water tables quite well. This is opposite to the results obtained with a rising water table. It is in fact rather surprising to observe a poor agreement between model and experiment for the FL160 and FL120 profile because the water content in the whole sand column is  $>9\%$  (hang-water or field capacity). In other words, the radon-emanation coefficient is relatively well defined in comparison with the previous experiments with a rising water level. So, there seems to be no reason to attempt a lower emanation coefficient in the calculations than the value of 0.25, measured in the range of pore-water contents  $>1\%$ . Yet, the fit to the FL160 and FL120 experiment would be greatly improved if the value for room-dry sand is used. To examine the result, the calculations using this value (0.22) of the emanation coefficient are shown in the right part of Fig. 8.11. As expected, the FL160 and FL120 profiles are much better reproduced while the agreement for the other two profiles is not reduced.

<sup>10</sup>One might ask why the moisture-content distribution was not measured in the vessel itself. The reason is that the initial condition for a rising water level, i.e. a room-dry sand column, is difficult to obtain once the sand has been wetted. The decision for remeasuring the moisture-content distribution was made just after the sand in the vessel had been saturated.

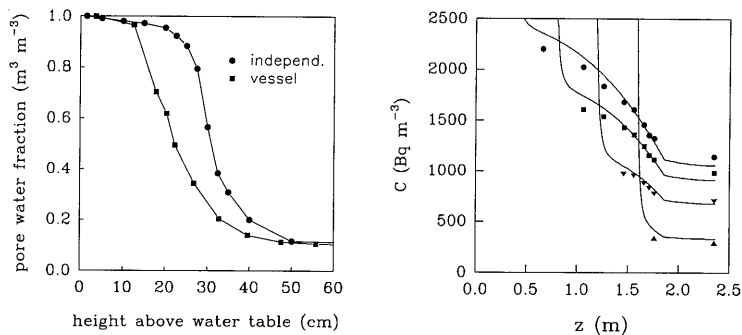


Figure 8.12: Left part: Measured pore-water content as function of height above the water table in the sand in the vessel (squares). Data is normalised such that the pore-water content of the sample taken at about 4 cm above the water table is set to unity. Lines connect data points. For comparison, the data obtained with the water-retention instrument, see Fig. 8.2, is also shown (circles). Right part: Measured (markers) and calculated pore-air radon concentrations  $C$  ( $\text{Bq m}^{-3}$ ) (lines) using the measured moisture-content distribution in the vessel and an emanation coefficient of 0.22.

Nevertheless, since the agreement between the measured and modelled *crawl-space* radon concentrations is somewhat worse, the maximum discrepancy is larger than 10% for each experiment.

At this point, it becomes relevant to refer to a previous remark concerning the possible occurrence of a systematic error in determining the water-retention characteristics of the sand. If the fine metal mesh of the container in the water-retention instrument indeed hampered the water transport, a systematic error may also have been present in the measurements with a falling water level (increasing moisture tension). It was therefore decided to measure the pore-water content distribution in the sand of the vessel. Because these measurements destruct the homogeneity of the sand column, they were not conducted before all vessel experiments were concluded. After first having saturated the complete sand column, the water level in the vessel was set at 80 cm below the sand surface. After about two weeks, 9 cm diameter core samples were taken at about 0.5 m from the centre of the sand column, opposite of the section with the horizontal probes, at depth intervals of approximately 8 cm using a hollow steel tube. These samples were weighted before and after drying. The results of the measurements are presented in the left part of Fig. 8.12. It is seen that the transition from dry to saturated sand occurs at a *smaller* distance (difference about 10 cm) above the water table than measured with the water-retention instrument. This again indicates the presence of a systematic error in the independent measurements. Normally, the sand-box method is used with a thin cloth as separating material between the coarse-grained sand in the sample container and the fine-grained sand in the box, instead of a fine stainless steel mesh. A metal mesh was used to be able to brace the mesh tightly around the bottom of the sample container, allowing the container to be transferred without significantly rearranging the sand grains caused by the stretching of the mesh.

The results of model calculations including the *in situ* measured water-content distribution in the vessel and an emanation coefficient of 0.22 are shown in the right part of Fig. 8.12. With respect to the calculations presented in the right part of Fig. 8.11, it is seen that the calculated concentrations have increased somewhat due to a decreased volume of (nearly) water-saturated sand above the water table, i.e. the amount of sand contributing to the radon concentration in the air-filled pore space has become larger. By using the *in situ* measured moisture-content distribution in the calculations, the correspondence between model and experiment improves considerably for the crawl-space radon concentrations and remains almost unchanged regarding the concentrations in the sand. The agreement is within 10% for the FL160, FL120 and FL80 experiment. A discrepancy of 15%-30% (calculations being higher) is however still observed for the FL40 experiment.

### 8.5.3 Discussion

It is remarkable that for both series of experiments, and especially for a falling water level, a reasonable agreement is observed between measurements and calculations if the emanation coefficient is set to 0.22: a 14% lower value than indicated by independent measurements. A fact is that a lower radon-production rate in the pore-air space of the sand is required to reasonably match the calculations with experiment. However, a lower radon-production rate in the pore space can also be attained by assuming a higher porosity. In this perspective it is important to mention that the core-sample measurements also provided a mean for determining the porosity of the sand in the vessel. Assuming that the sample taken from the largest depth was completely saturated with water, a porosity of 0.365 (uncertainty estimated  $<0.005$ ) was inferred for the sand at approximately 75 cm depth. This value is 7% larger than the value assumed in all previous model calculations presented in chapter 5, 6, 7 and this chapter. The consequences of using a larger porosity for the modelling results that were presented in the previous chapters will be reviewed in chapter 9. The attention in this chapter will be confined to the experiments with a ground-water level.

The influence of a different porosity on the radon-production rate in the pore space of the sand,  $\frac{S}{\epsilon}$ , is elucidated by considering the expression in basic parameters:

$$\frac{S}{\epsilon} = \frac{\eta \rho_b \lambda C^{Ra}}{\epsilon} = \frac{\eta(1 - \epsilon)}{\epsilon} \cdot \rho_s \lambda C^{Ra}. \quad (8.7)$$

It may be verified that the combination of emanation coefficient and porosity ( $\eta = 0.22$ ,  $\epsilon = 0.34$ ) which describes most experiments with the vessel quite well, is, as far as the pore radon-production rate is concerned, equivalent to the combination ( $\eta = 0.245$ ,  $\epsilon = 0.365$ ). In other words, it seems that if the value of the emanation coefficient obtained from independent measurements ( $\approx 0.25$ ) and the value of the *in situ* determined porosity are used in the calculations, the agreement with experiment will remain satisfying. Unfortunately, this is not the case. The results of calculations using the combination ( $\eta = 0.245$ ,  $\epsilon = 0.365$ ) and the moisture-content distributions as measured in the drum and in the vessel (and a 7% larger bulk radon-diffusion coefficient due to a larger porosity) are presented by solid lines in Fig. 8.13 for a rising (left part) and falling (right part) water level. The calculated values are larger compared with the modelling results using the combination ( $\eta = 0.22$ ,  $\epsilon = 0.34$ ) as presented in Figs. 8.10 and 8.12. The reason for this increase is that the total air-filled volume in the vessel has not increased by 7%



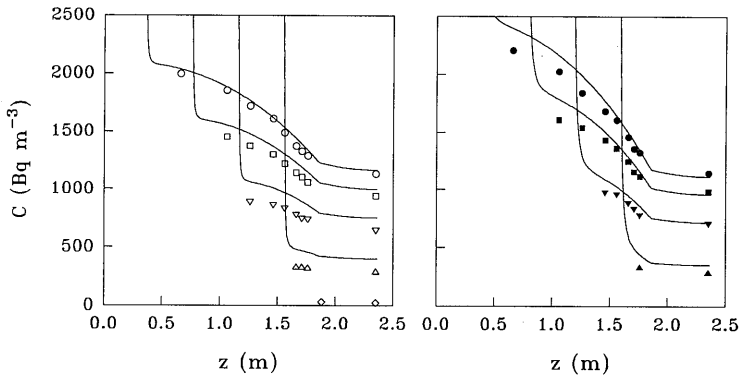


Figure 8.13: Results of calculations and measurements for a rising water level (left part) and falling water level (right part). Solid lines represent modelling results using the parameter set ( $\eta = 0.245$ ,  $\epsilon = 0.365$ ).

because of a constant crawl-space volume. As a result, the agreement between model and experiment is even reduced. So, using a set of parameters in the calculations that are thought to represent the true situation in the vessel as good as possible (i.e. *in situ* measured porosity and moisture-content distribution; independently measured emanation coefficient) does not yield an agreement with the imposed limit of 10% between model and experiment.

It seems that a lower emanation coefficient than measured independently is yet necessary in the calculations for obtaining a better agreement for a porosity of 0.365. A lower actual emanation coefficient in the sand of the vessel than measured independently may be related to the fact that the porosity of the sand in the closed cylinders, which were used in the separate experiments for determining the emanation coefficient, see section 4.5.5, was higher ( $\approx 0.4$ ) than the porosity of the sand in the vessel. It is known that radon atoms obtain a recoil energy of about 86 keV when they are formed in the decay of radium, and therefore may bury themselves in adjacent sand grains (and remain in the solid material) if the distance between the grains is small (recoil range in water and air is  $0.1 \mu\text{m}$  and  $63 \mu\text{m}$ , respectively [Nazaroff et al., 1988]). The larger distances between sand grains in the cylinders may thus have resulted in a higher emanation coefficient than the one applicable to the sand of the vessel. The hypothesis of a porosity-dependent emanation coefficient was not further examined.

On the other hand, to match the calculations with experiment, a lower emanation coefficient can not be the only adaptation. Inspection of the results presented in Fig. 8.13 shows that a lower production rate would deteriorate the agreement for the crawl-space radon concentration in the FL160 and FL120 experiments. This indicates that the assumption of a homogeneous column with respect to porosity and emanation coefficient might be invalid for these experiments. As the experiments with a rising water level are concerned, the discrepancies may also be caused by a different moisture-content distribution in the drum and that in the vessel.

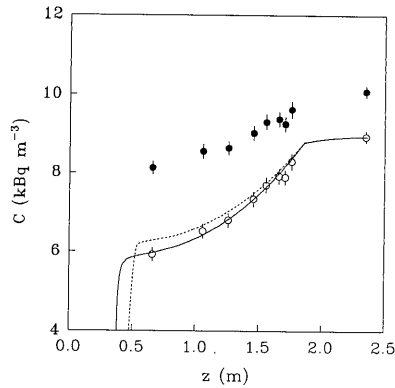


Figure 8.14: Measured (filled markers) radon concentrations  $C$  ( $\text{kBq m}^{-3}$ ) as function of height in the vessel for the experiments with the water table at 160 cm depth and a radon source ( $\approx 42 \text{ kBq}$ ) in the crawl space. Error bars indicate relative experimental uncertainties ( $1\sigma$ ). Open markers indicate the contribution of the radon source only by subtracting from the measured values the concentrations obtained without a source (see e.g. Fig. 8.8). Lines represent numerical results using the measured moisture-content distribution in the vessel (solid line) and the independently measured distribution (dashed line).

### Additional experiment

The analysis of the experiments with a ground-water level indicate that the agreement between model and experiment strongly depends on the value of the emanation coefficient. In addition, the possible variation of the emanation coefficient with height in the vessel complicates the comparison with calculations as well. It was therefore decided to conduct an experiment in which the influence of radon produced by the sand is minimised. Since the number of relevant parameters is decreased in such an experiment, other possible causes for the disagreement between model and experiment may appear more clearly.

In this experiment, a radon source ( $\approx 42 \text{ kBq}$ ) was placed in the crawl-space with the water table (falling level) at 160 cm depth<sup>11</sup>. Steady-state radon concentrations were measured in the sand and in the crawl space. The measured concentrations are shown by filled markers in Fig. 8.14. As opposed to previous results, the maximum concentrations are seen to occur in the crawl space and, as a result, the measured concentrations decrease with depth in the sand. Depending on the height in the vessel, the concentrations are 4 to 10 times higher than in the corresponding experiment without a radon source. The measured concentrations in the latter experiments were subtracted from the measured concentrations with a radon source to obtain the contribution of the radon source only, as indicated by open markers in Fig. 8.14. Note that this profile represents the situation in the vessel if the sand would *not* produce any radon.

Because the expected concentrations are independent of the porosity<sup>12</sup> of the sand

<sup>11</sup>Only one water-table height could be studied due to the limited amount of time.

<sup>12</sup>The differential equation for transport in the sand (of radon produced by the source in the crawl space) is given by  $\epsilon \tau_a D_a e^{-4.99(m+m^2)} \frac{d^2 C}{dz^2} - \epsilon(1-m+Lm)\lambda C = 0$ , which, divided by  $\epsilon$ , is independent of

in this case, the only parameter that determines the radon-concentration profile is the moisture-content distribution<sup>13</sup>. The results of model calculations (normalised with respect to the measured radon concentration in the crawl space because the radon-source strength is not precisely known) using the measured moisture-content distribution in the vessel are shown by a solid line in Fig. 8.14. The agreement with experiment is very satisfying. A calculation in which the independently measured moisture-content distribution is used, indicated by a dashed line in Fig. 8.14, shows a poorer agreement. These results indicate that the moisture-content distribution as inferred from the core-sample measurements in the vessel probably represents the undisturbed situation in the vessel well. They also demonstrate that the differences between model and experiment, at least for the FL160 experiment, are most probably caused by the value of the pore radon-production rate in the sand (porosity and/or emanation coefficient), which may also depend on the height in the vessel.

## 8.6 Conclusions

The experiments with a water level set in the radon vessel have shown that radon transport in moisturised sand is much more complicated than in room-dry sand. The higher complexity is mainly due to a varying moisture content and diffusion coefficient in the sand above the water table, and by the dependence of the water-content distribution on preceding conditions (hysteresis effect). In the radon-vessel experiments, steady-state pore-air radon-concentration profiles were determined in a situation with the lid installed. This was carried out for two sets of four different water-table heights: one set covering the experiments in which the water table was established by introducing water via the bottom of the vessel into initially dry sand (rising water level), and the other set covering the experiments in which excess water was removed via the bottom of the vessel from an initially saturated sand column (falling water level).

The moisture-content distribution and the hysteresis were measured independently using the so-called sand-box method. Also the radon-diffusion coefficient was measured independently as function of pore-water fraction using an instrument specially designed for this purpose. With these data and other previously measured parameters of the sand such as the (moisture-dependent) emanation coefficient, porosity, tortuosity and density, expected concentrations were calculated and compared with measured values. In general, these calculations significantly overestimated the measured values.

Because water influences the radon concentration in the sand in a variety of ways, a number of attempts were made to investigate the cause of the overestimation. For example, the agreement could be improved by using a lower emanation coefficient (corresponding with the one used for room-dry sand) in the model simulations, but differences remained. It was therefore decided to measure the moisture-content distribution in the radon vessel for a falling water level and in a sand-filled drum for a rising water level. As both measurements indicated a different distribution than obtained with the sand-box method, it was shown that a systematic error probably influenced the results obtained with this experimental technique. An experimental procedure for determining the moisture-content distribution in the vessel also provided a method for determining the porosity of the sand. This indicated a 7% higher value than assumed previously, corresponding with a nearly

---

porosity.

<sup>13</sup>The tortuosity is also of importance. Its value is however well defined.

12% lower pore radon-production rate in the sand. The results of model calculations using this value for the porosity, the moisture-content distributions as measured in the vessel and the drum, and the independently measured emanation coefficient, were still found to disagree more than 10% for most of the radon-concentration profiles. All calculated concentrations were again overestimating the measured values.

For the set of experiments with a rising water level, the agreement is within 10% for low water tables (depth >1 m) but about 20% and 40% for a water-table depth of 80 cm and 40 cm, respectively. The maximum differences for a falling water level are of the order of 15% for each of the four profiles. The cause of these discrepancies could not be precisely identified. For the experiments with a rising water level, it is thought that the moisture-content distribution in the vessel differs from the one measured in the drum. For the experiments with a falling and rising water level, it might be that the independently measured emanation coefficient is somewhat higher than in the vessel. This may be caused by a difference in porosity of the sand samples that were used in the emanation-coefficient measurements and the sand in the vessel. However, the value of this parameter can not be chosen such that all profiles are well reproduced by the calculations.

It is concluded that most experiments with a ground-water level can not be reproduced within the imposed limit of 10% by model calculations using either a set of independently measured parameters or a set which is partly based on *in situ* measured parameters such as the porosity and the moisture-content distribution with a falling water level. It is believed that the disagreement between model and experiment is due to a relatively poor knowledge of the radon emanation coefficient and of the moisture-content distribution with a rising water level. A position-dependent emanation coefficient is the next most plausible cause for the observed disagreement. The need for such a position-dependent emanation coefficient tells us that either the situation in wetted soil is, for the relatively simple experimental set up, very difficult to deal with and/or we are lacking enough knowledge on the physical processes that influence radon transport in moisturised sand.

# Chapter 9

## Assessment, conclusions and general discussion

In this chapter, the set of experiments conducted with the radon vessel will be reviewed in section 9.1. This section will mainly deal with the consequences of using knowledge that was gained in a later stage of the investigation in the analysis of earlier conducted experiments. Conclusions are drawn in section 9.2. Next, in section 9.3, the Dutch situation with respect to indoor radon is discussed. In the light of a recent investigation in houses showing that the contribution of porous building materials to the indoor radon concentration is larger than that of the soil [RIVM., 1997], transport of radon in building materials will be shortly discussed. Also, radon transport in the soil under a house for the Dutch situation is considered. These matters are discussed with the experience gained in this study as main point of departure. Finally, an outlook and recommendations for future research are given in section 9.4.

### 9.1 The vessel experiments with room-dry sand in retrospect: an assessment

In the final stage of this study, i.e. in the experiments with moisturised sand, more knowledge was gained about some parameters of the sand that are of importance for describing the experiments with the radon vessel. The consequences of using these new insights in the analysis of the earlier conducted experiments with room-dry sand will be shortly addressed. General conclusions are drawn in the following section.

A main finding in this context concerns the porosity,  $\epsilon$ , which was found to be  $0.365 \pm 0.005$  (estimated uncertainty) at 75 cm depth in the vessel, 7% higher than assumed previously (0.34). In addition, the experiments with a falling water level indicated that the emanation coefficient of wet sand is probably somewhat lower in the vessel than measured in the separate experiments. This is possibly related to a lower porosity of the sand in the vessel than of the sand used for determining the emanation coefficient  $\eta$ . If the dependence of emanation coefficient on porosity truly applies to the sand, the emanation coefficient of room-dry sand should accordingly be lower than assumed previously. However, using a higher porosity as well as a lower emanation coefficient in the model simulations of the experiments with room-dry sand results in a poorer agreement between model and experiment. That a set of input parameters which improves the wet-sand results leads to a worse agreement between model and experiment

in room-dry sand is of course an unwanted - and strange - outcome. At this point it is relevant to revert to a difficulty that was already mentioned in section 5.2 about the value of the emanation coefficient that should be used in modelling the experiments with room-dry sand.

The previous value of  $\eta$  was inferred from assuming equilibrium between moisture conditions in the sand of the vessel and the surrounding air (30% rel. humidity), corresponding with a moisture content in the sand of  $m = 0.12\%$ . This was in fact a crude estimate because the sand had been saturated one year before as part of the filling procedure. There were no measurements upon which the value of the moisture-content of the sand was based, nor were calculations done to estimate the effect of evaporation of remaining hang-water after the column had been drained. It is possible that the (average) moisture content was higher than 0.12%, corresponding with a higher emanation coefficient than the previously assumed value of 0.22. Moreover, as shown in Fig. 4.12, a low moisture content of 0.4% already corresponds to an emanation coefficient of  $\approx 0.25$ . In other words, the value of the emanation coefficient in the sand of the vessel can actually have been anywhere between approximately 0.20 and 0.25, corresponding with the extremes of having a moisture content of 0.12% and some dependence on porosity, and a moisture content  $>0.4\%$  and no dependence on porosity. So, if the calculations for room-dry sand are redone to investigate the influence of a higher porosity, the emanation coefficient may be chosen freely within the range 0.20 - 0.25. In this light, it could be that the previously estimated value of the emanation coefficient, in combination with an underestimated porosity, rather coincidentally yielded a good agreement between model and experiment.

The effect of using a higher porosity was checked for several experiments conducted with room-dry sand. The result is that no unique value of the emanation coefficient was found such that all experiments are as well reproduced by the calculations as before. Fortunately, most of the experiments are described by the model calculations within the limit of 10% if an intermediate value of 0.235 is assumed for the emanation coefficient. An exception is formed by experiments without the lid installed on the vessel of which the (previous) results are shown in Fig. 5.2 for pure diffusive transport and in Fig. 6.2 for a downward air-flow in the vessel. For these experiments, the calculated radon concentrations using the 'improved' parameter set ( $\eta = 0.235$ ,  $\epsilon = 0.365$ ) are somewhat *lower* than the previous ones with  $\eta = 0.22$  and  $\epsilon = 0.34$ . This gives a larger disagreement with the data, especially at large depths in the vessel ( $< 15\%$ ). On the other hand, the calculated concentrations in the experiments with an upward air-flow in the vessel, shown in Fig. 6.8 for steady-state conditions and, for example, in Fig. 6.11 for a pulsated air flow, are hardly changed by using the 'improved' parameter set. So, the value of 0.235 for the emanation coefficient appears to be an optimal compromise for keeping the overestimations in the experiments with pulsated upward advective transport and the underestimations in the experiment with pure diffusive transport or downward advective transport within bounds<sup>1</sup>.

This assessment shows that the emanation coefficient for 'room-dry' sand has to be somewhat higher (0.235) than assumed previously (0.22) in order to maintain a good agreement between calculations and experiment if a 7% larger porosity (0.365) is used in the calculations. As a consequence, the (average) moisture content of the room-dry sand

<sup>1</sup>The 'foil experiments', discussed in chapter 7, are disregarded here because the observed differences in some of these experiments were already higher than 10% and because these experiments are less well-defined due to uncontrolled leakage along - and through - the foil.

was probably somewhat higher than assumed previously (0.12%).

## 9.2 Conclusions

With respect to the main goal of this study, i.e. to validate a model for radon transport in sand, the experiments conducted with the radon vessel may be subdivided in three series, covering transport in room-dry sand, diffusive transport in sand with a ground-water level, and radon entry into the space under the lid when the sand surface is covered by a sheet of polyethylene foil. Conclusions will be drawn for each series in separate sections. Finally, main findings are presented in section 9.2.5. First, the attention is concentrated on the determination of the input parameters for the transport model.

### 9.2.1 Input parameters

As much as possible, the input parameters for the transport model, which are the radon emanation coefficient, tortuosity, porosity, radium content, specific density of the sand, radon-diffusion coefficient and moisture content were obtained from independent measurements. This is an important aspect of the validation process. It is of major interest to know whether the relevant transport parameters of a porous medium as found *in situ* can be based on measurements on relatively small samples in the laboratory.

Some of the measurements, specifically dealing with the determination of parameters that play a role in moisturised sand, will be discussed in section 9.2.3. Results of measurements for determining the input parameters necessary for modelling radon transport in room-dry sand are outlined below.

- The specific density  $\rho_s$  of the sand could be determined precisely by weighing:  $\rho_s = 2634 \pm 10 \text{ kg m}^{-3}$ .
- Also the tortuosity  $\tau$  could be determined accurately using electrical conductivity measurements:  $\tau = 0.640 \pm 0.010$ .
- The radium content was measured using gamma-ray spectroscopy (the accurateness of this value is irrelevant for this validation):  $C^{Ra} = 3.68 \pm 0.13 \text{ Bq kg}^{-1}$ .
- The emanation coefficient was measured with a closed-can method and a 'flush and adsorb method' as function of the fraction of water saturation of the pores. This indicated a sharp rise in emanation coefficient from 0.13 to  $\approx 0.28$  as the pore water fraction is increased from zero to only 0.5%. For higher moisture contents, the emanation coefficient scatters somewhat around a value of 0.25.
- The porosity  $\epsilon$  was inferred from the mass increase of a small sand sample due to water saturation. It was observed that saturating and drying the sample several times compacted the sand notably: the porosity dropped from 0.38 to 0.33. Since the vessel had been gradually filled with sand in layers of 15-20 cm and the water level had been raised and lowered a few times after each layer, it was estimated that such compaction probably also took place in the vessel. The porosity was estimated at  $0.34 \pm 0.01$ , at the low end of the measured range.
- Another quantity, which was not measured but taken from literature, concerns the molecular diffusion coefficient for radon in air. A value of  $1.1 \cdot 10^{-5} \text{ m}^2 \text{ s}^{-1}$  was used,

a best compromise of values (between  $1.0 \cdot 10^{-5}$  and  $1.2 \cdot 10^{-5} \text{ m}^2 \text{ s}^{-1}$ ) cited in the literature.

- The radon-adsorption coefficient was determined by measuring the effluent radon concentration from a column of sand in which a high pore-air radon concentration was established initially. This indicated that, for room-dry and moisturised sand, adsorption of radon to solid surfaces may be neglected.
- The homogeneity of the sand column was assessed by measuring the pressure field in the sand. Based on these measurements, it was estimated that deviations from the ideal homogeneous situation are less than 10%. The maximum allowed differences in the validation process between modelled and measured radon concentrations in the vessel were therefore also set at 10%.

### 9.2.2 Experiments with room-dry sand

The data obtained in the experiments with room-dry sand were compared with results of model calculations using the set of input parameters as given in the previous paragraph and assuming a homogeneous sand column. A difficulty was however encountered by the sensitivity of the radon emanation coefficient in the range of moisture contents from 0% to  $\approx 0.5\%$ . The difficulty originates from the fact that the value of the moisture content of the sand is not precisely known. As a result, the value of the emanation coefficient had to be estimated. As a starting point, it was assumed that the water content of the whole sand column is in equilibrium with the moisture conditions of the surrounding air. This corresponds to a moisture content of 0.12% and an emanation coefficient of 0.22.

The comparison using these initial values showed a good agreement between calculational and experimental results, with maximum differences  $< 10\%$ . It was therefore concluded that the experiments had shown that it is possible to model radon transport in room-dry sand accurately based on independently measured parameters.

In a later stage of the study, the porosity of the sand in the vessel was however measured with an *in situ* technique, see section 8.5.2. As this indicated a  $(7.0 \pm 1.4)\%$  higher value than was estimated initially, the compaction as observed during wetting and drying a small sand sample apparently did not occur in the vessel. The pressure on the sand grains in the vessel due to sand laying on top may have counteracted the forced compaction to a high value. The model simulations using the higher value of porosity showed that the emanation coefficient must then be somewhat higher than 0.22 to match the calculations with the data. The need for a higher emanation coefficient showed that the average moisture content of the sand probably exceeded 0.12%. As a consequence, the assumption of having equilibrium moisture conditions in the sand with respect to the surrounding air appeared to be invalid. An emanation coefficient of 0.235 was found to be an optimal value as to match the calculations with the data reasonably well. The overall agreement was however slightly reduced with respect to the former set of input parameters.

As it is better to rely on an *in situ* measured porosity, the previous conclusion about the reproducibility has to be reconsidered. This, because the rigidity of the validation is reduced when a parameter is optimised in order to reproduce the data, and secondly, the agreement between model and experiment has slightly decreased. It is therefore concluded that, using the 'improved' set of input parameters, the experiments with room-dry sand are *generally* reproduced by model calculation within the imposed limit



of 10%. Underestimations of 15% at maximum are occasionally observed at large depths in the vessel. Possible causes for these discrepancies are inhomogeneities in the sand column, especially with respect to the emanation coefficient, remaining pore water at large depth or a lower true molecular diffusion coefficient for radon in air than assumed in the modelling.

### 9.2.3 Experiments with a ground-water level

In the experiments with a ground-water level in the vessel two conditions were distinguished based on the manner in which the water table was established. In one case the water table was established by slowly adding water to the sand column via the bottom (rising water level) and in the other case by slowly removing excess water from the sand column, also via the bottom (falling water level). These procedures were followed because the moisture content depends on preceding conditions. Knowledge on the pore-water content in the sand as function of height above the water table was obtained by measuring this dependence using the so-called sand-box method. The results of these measurements indicated a sudden transition from saturated to dry sand at about 10 cm above the water table for a rising water level and a slower transition from dry to saturated sand at approximately 30 cm above the water table for a falling water level. Also the bulk radon-diffusion coefficient was measured as function of moisture content. Results of these measurements showed that the diffusion coefficient decreases with increasing water content with the rate of decrease being faster at higher moisture contents.

The initial model calculations using these parameters strongly suggested that the moisture-content distribution as inferred from the sand-box measurements poorly represents the true situation in the vessel. This hypothesis was tested by measuring the moisture-content distribution *in situ*, i.e. in the vessel, for a falling water level, and in a separate smaller column of sand for a rising water level. These measurements indeed indicated that a systematic error influenced the results of the sand-box method.

Model calculations using the measured pore-water content distributions in the vessel and the separate small sand column, as well as the *in-situ* measured porosity improved the agreement considerably. However, the calculations do not match with the data as well as in the experiments with room-dry sand. For a rising water level, a slight overestimation is seen for the water-table at large depths, whereas a 40% overestimation is observed for shallow water-table depths. There are two possible explanations for the discrepancy: the emanation coefficient might have been lower in the dry part of the sand column (same difficulty as was encountered with room-dry sand: the moisture content is not precisely known in the dry part of the sand column), and/or, the pore water might have risen somewhat further upwards in the vessel than measured in the smaller separate sand column. This can be a result of side effects that were visually observed in the smaller column. The large overestimation of radon concentrations at shallow water-table depths strongly supports the suggestion of a further rise of ground-water.

For a falling water level, the situation is better defined from a modelling point of view because the moisture-content in the complete column was  $\geq 9\%$  (field capacity), corresponding with a relatively well-defined emanation coefficient. Nevertheless, also in this set of experiments the calculations overestimate the data up to 20% in the sand column. On the other hand, the 'crawl-space' radon concentrations are well described. Since all input parameters are precisely known for the experiments with a falling water level, the disagreement suggests that the assumption of a homogeneous sand column may

be too strict. In this light it should be remarked that the experiments with room-dry sand already indicated possible heterogeneities. Note, however, that in these experiments an *underestimation* is observed at large depths, whereas with moisturised sand and a falling water level an *overestimation* is seen at corresponding positions in the vessel. This indicates that an inhomogeneous sand column probably can not account for all the observed discrepancies between model and experiment. For room-dry sand, the conditions in the sand could have been such that the pore radon-production rate was higher at large depths. On the contrary, for wetted sand and a falling water level there is, on basis of the present knowledge, no reason for having a *lower* pore radon-production rate at large depths. This shows that the situation in wetted soil is, for the relatively simple experimental set up, already very complicated to deal with. It might also be that the transport model as presented in chapter 2 does not provide a complete description of the transport processes. If this is true, we are lacking knowledge of the physical processes that influence radon transport in moisturised sand.

#### 9.2.4 Experiments with a foil covering the sand surface

The last set covers experiments with a sheet of polyethylene foil covering the sand surface, carried out with an intact - or 'undamaged' - foil and with a 'damaged' foil, meaning that a 5 cm diameter opening was cut out the centre. These experiments were conducted with a 9 cm crawl space and two flow conditions: without a forced air-flow through the sand column, and with a small downward and upward air-flow induced by (de)pressurising the perforated box at 1.63 m depth in the sand. For modelling purposes, in line with the strategy of using independently measured quantities, the thickness and radon-diffusion coefficient of the foil were measured independently. This indicated a thickness of  $233 \pm 2 \mu\text{m}$  and a diffusion coefficient of  $(1.02 \pm 0.04) \cdot 10^{-11} \text{ m}^2 \text{ s}^{-1}$ .

The 'undamaged foil' experiments were analysed using a simplistic mass-balance model for the radon concentration in the crawl space which included the influence of air-flows induced by barometric pressure fluctuations. Without flow and with an upward forced air-flow through the sand, the calculations were seen to describe the data fairly well. However, the experiments with a downward air flow show a 20% *overestimation* of the calculations. This may be caused by openings along the foil or by small pin-holes in the foil. The diffusive flux through such openings into the crawl space is namely strongly reduced during advection-dominated transport; an effect that is not incorporated in the simple mass-balance model.

In the corresponding 'damaged foil' experiments, the central opening in the foil increased the average crawl-space radon concentrations. The relative increment was observed to be largest for the experiments with a downward air-flow. For a quantitative analysis, the two-dimensional numerical model was used, extended to simulate the barometric pressure induced air-flows in the vessel. A satisfying agreement between model and experiment was observed in the cases without flow and with an upward air-flow in the sand. However, the calculations for the experiment with a downward air-flow *underestimated* the data with 20%-40%. A well-founded explanation for this discrepancy could not be given, although it may be caused by leakage along the foil and by an oversimplification in the model of the region just below the foil.

The influence of barometric pressure variations was observed in all experiments with the foil. The effect is most notable for experiments without a forced air-flow through the sand, i.e. when diffusion through the foil is the dominating transport mechanism.

Higher crawl-space radon concentrations were observed during an atmospheric pressure drop. Due to the expansion of pore-air in the sand below the foil a flow of radon-rich air is induced towards the crawl space. During an atmospheric pressure rise the crawl-space radon concentration is diluted by entry of radon-poor ambient air. An important consequence of the air exchange between the crawl space and pore space of the sand due to barometric pressure fluctuations is the increased average crawl-space radon concentration with respect to conditions with a constant air pressure (pumping effect).

In conclusion, the foil experiments showed that radon transport from the sand into the crawl space can be reasonably well described using independently measured parameters for the sand and the foil. The differences remain within 10%, except for the experiments with a downward air-flow, in which case the differences are 40% at maximum. It is thought that these differences are caused by the presence of poorly-defined leakages along the foil, possibly by pin-holes in the foil, and by a simplified representation in the model of the air-layer between the sand surface and the foil.

### 9.2.5 Main findings

In overviewing all the experiments with the radon vessel, it has been demonstrated that the research strategy of starting the validation with a simple porous medium as sand has proven to be a good choice. This, because the transport processes in this simple medium already turned out to be complex and difficult to model in some cases. With sand, the difficulties and problems, although not all were solved and/or investigated further, were still traceable. This might not have been the case if the investigation was started with a more complex material such as concrete.

The vessel experiments have shown that, within the uncertainties of the experimental conditions, diffusive and two-dimensional (pulsated) combined diffusive and advective transport in room-dry sand and into a crawl space can be reproduced by model calculations on the basis of known transport processes and *independently* measured parameters. Occasionally, differences between model and experiment are seen of 15% at maximum which are thought to be due to remaining pore-water, a lower molecular diffusion coefficient than modelled, a position-dependent emanation coefficient and/or porosity.

The situation is more complex if water is added to the sand column. The experiments with a ground-water table in the vessel showed that this situation is difficult to deal with. The shape of the measured concentration profiles are well described, but numerical differences between calculated and measured values larger than 10% are generally observed. The same uncertainty in the parameters as mentioned in the previous paragraph may of course also effect the experiments with a ground-water table. The reversed discrepancies however suggest that we still lack some knowledge of the processes that influence radon transport in moisturised sand.

The experiments with room-dry sand and a foil on the sand surface are reasonably well reproduced by calculations on the basis of measured parameters of the sand as well as the foil. Large discrepancies (<40%) are only seen in case a forced air-flow is induced from the crawl space into the sand. These are probably caused by uncontrolled and poorly defined radon transport through, along and just below the foil. The experiments indicated that coverage of the crawl-space floor with a foil can be an effective mitigation technique if the air-flows are always directed from the crawl space into soil.

The investigations with the radon vessel have provided us more information on the

processes that influence radon transport in soil. The attention was however limited to sand, a simple porous medium. Yet, the present knowledge and insights gained in this study may contribute to the analysis of more complex radon transport in other porous materials and to the understanding of the real situation in houses. It may also contribute, by calculating the effectiveness of countermeasures, to the reduction of the indoor radon concentration. In the following section, these matters are discussed in more detail.

### 9.3 General discussion

With respect to the main goal of radon research, i.e. to lower the radon concentration in the indoor environment, it needs to be mentioned that our present understanding of the radon transport processes that are responsible for the entry of radon into the indoor environment is still incomplete for the Dutch situation. An important question that should be addressed is how the knowledge gained in this study can help to better understand the situation in, under and/or around a dwelling. That we do not fully understand the situation in practice at the moment will be elucidated first.

The recent national survey 'Landelijk onderzoek naar radon in woningen' on radon in 1500 dwellings built after 1984 in the Netherlands [RIVM., 1997], showed for the living room: 1) an average contribution from building materials to the radon concentration of 70%; 2) an average radon concentration of  $30 \text{ Bq m}^{-3}$ ; and 3) an average incoming ventilation stream from outdoors of  $80 \text{ m}^3 \text{ h}^{-1}$  ( $1\sigma$ :  $50 \text{ m}^3 \text{ h}^{-1}$ ). The survey thus indicates an absolute contribution of  $0.7 \cdot 30 = 21 \text{ Bq m}^{-3}$  from building materials. With a simple calculation it will be shown that the expected *absolute* contribution of the building materials to the indoor radon concentration is much lower.

Let us consider a living room with an 'average' volume of  $4 \times 8 \times 2.5 = 80 \text{ m}^3$ . Based on above-mentioned results of the survey, the average ventilation rate for this room can be estimated at  $1 \text{ h}^{-1}$  ( $1\sigma$ :  $0.6 \text{ h}^{-1}$ ). Let us further assume that the walls, floor and ceiling are made of concrete. For simplicity, we neglect the presence of windows. To calculate the contribution of the concrete to the radon concentrations in the room, we base the value of the radon exhalation rate on measurements of the *diffusive* exhalation rate of normal concrete used in the Netherlands. The measured range, (2.2 - 3.7)  $\text{Bq m}^{-2} \text{ h}^{-1}$  [Put and Van der Graaf, 1996], indicates an average value of  $3.0 \text{ Bq m}^{-2} \text{ h}^{-1}$ . It should be remarked that the exhalation rate of normal concrete is relatively high compared to other frequently used building materials in the Netherlands. So, in this simple model the contribution from building materials will certainly not be underestimated as a result of taking only one material into consideration. Based on the above-mentioned average values, the radon concentration in the living room, originating from the concrete, can be calculated<sup>2</sup> at nearly  $5 \text{ Bq m}^{-3}$ , which is more than 4 times lower than determined in the national survey. Moreover, if the maximum exhalation rate of concrete would be used in combination with a one standard deviation lower ventilation rate ( $0.4 \text{ h}^{-1}$ ), an extreme case, the contribution from the concrete is still only  $15 \text{ Bq m}^{-3}$ .

This simple calculation shows that, if we rely on the results obtained in the national survey, i.e. that building materials contribute 70%, transport processes may exist that are not accounted for in our simple model. A first 'candidate' in this perspective concerns advective transport through building materials. In other words, the measured diffusive

<sup>2</sup>The total area of the concrete is  $2 \cdot 8 \cdot 2.5 + 2 \cdot 4 \cdot 2.5 + 2 \cdot 4 \cdot 8 = 124 \text{ m}^2$ , corresponding with a radon-source strength of  $124 \cdot 3.0 = 372 \text{ Bq h}^{-1}$ . The living room is ventilated once per hour, so in equilibrium  $372 \text{ Bq}$  is distributed over  $80 \text{ m}^3$ , corresponding with a radon concentration of  $4.7 \text{ Bq m}^{-3}$ .

exhalation rate from building materials might not be a good measure of the exhalation rate of these materials in real houses. In the forthcoming, we will shortly examine, using radon-transport theory presented in chapter 2, whether advective transport may result in significantly higher exhalation rates.

Advective transport through building materials takes place as a result of pressure differences that exist over a porous medium. In case of a house, they may be induced by wind, temperature differences between in- and outdoor and over walls, barometric pressure fluctuations and/or forced ventilation. In general, these pressure differences are very small, i.e. in the range 0 – 10 Pa. The magnitude of advection not only depends on the pressure gradient, but also on the permeability of the porous medium at hand, the air-filled porosity and the radon-adsorption coefficient. Moreover, if we want to calculate the ratio  $E(\text{adv})/E(\text{dif})$  between the combined diffusive and advective exhalation rate and the diffusive exhalation rate, the quantity of interest, additional knowledge is needed of the diffusion coefficient. As such a great deal of information is required before the effect of advection can be estimated, the attention will be limited by varying the two most important parameters only.

Results of one-dimensional calculations of the ratio  $E(\text{adv})/E(\text{dif})$  as function of permeability  $K$  and effective diffusion coefficient  $D_e$  (the latter by varying the radon adsorption coefficient  $k_a$  in Eq. 2.43; the bulk diffusion coefficient  $D$  is ‘fixed’ by  $\epsilon\tau D_a$ ) for a slab of porous medium with thickness 15 cm, porosity 0.2, tortuosity 0.64, moisture content 0, density  $2300 \text{ kg m}^{-3}$  and a pressure difference of 5 Pa over the slab are shown in Fig. 9.1. It is seen that, depending on permeability and diffusivity, the exhalation ratio  $E(\text{adv})/E(\text{dif})$  varies between 1 and 3. Advection might therefore be important, but one has to realise that a low  $D_e$  is usually not accompanied by a high  $K$  and vice versa. For normal (intact) concrete, with a permeability of the order of  $10^{-16} \text{ m}^2$  [Nielson et al., 1997; Renken and Rosenberg, 1995], the effect of advection is probably negligible (measured effective diffusion coefficients for concrete given in the literature cover the range as presented in Fig. 9.1, see also next footnote). Other materials, such as masonry, generally have a higher permeability. Nielson et al. [1997] measured permeabilities for masonry of the order of  $5 \cdot 10^{-11} \text{ m}^2$  and effective diffusion coefficients of about  $2 \cdot 10^{-6} \text{ m}^2 \text{ s}^{-1}$ . Based on these values the effect of advection in masonry is expected to be small as well. These calculations indicate that, in general, advective transport through building materials is not expected to increase the exhalation rate to a great extent<sup>3</sup>.

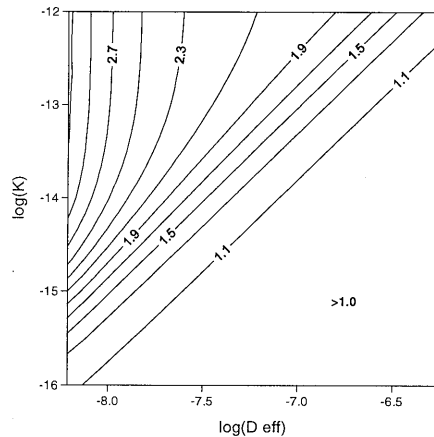


Figure 9.1: Contour plot of the exhalation ratio  $E(\text{adv})/E(\text{dif})$  for a slab of material as function of effective diffusion coefficient  $D_e$  and permeability  $K$ .

<sup>3</sup>It should be mentioned that Knudsen diffusion can be important in concrete due to the small pore sizes. Then, the bulk diffusion coefficient  $D$  is lower than  $\epsilon\tau D_a$  (neglecting pore water for the moment). The measured range of effective diffusion coefficients might therefore be a result of differences in  $D$  instead

Apparently, the first obvious 'candidate' can not account for the differences between the simple model and results of the survey. Other causes may be:

- Time-dependent effects such as pressure pulses due to wind, atmospheric pressure fluctuations, and varying moisture conditions in the building materials (and soil).
- Preferential flow paths through cracks, fissures, joints, holes etc. These flow paths may not only increase advective transport but also diffusive transport.
- The presence of a cavity wall. If there is air exchange between the cavity wall and the living room, the exhalation surface of the walls as 'seen' in the living room can be three times larger (one side towards the living room and two sides in the cavity wall). This may triple the radon-source strength.
- Also radon originating from the soil may enter the cavity wall and emerge in the living room, formerly called the 'the third entry route' [De Meijer, 1992]. It would appear that this radon originates from building materials.
- Inhomogeneities in the walls. Masonry, for example, may have a higher exhalation rate than the sum of the measured one-dimensional exhalation rate from the individual blocks (e.g. bricks) and joints (mortar). This is the case when radon is more easily transported in one of the constituents.

As these matters have not yet been investigated on a large scale, it may be concluded that our present knowledge with respect to radon entry is insufficient to account for the observed indoor radon concentrations in the Netherlands.

The question remains how the knowledge gained in this study can help to better understand the situation in practice. The previous discussion mainly focussed on building materials because they are the most important source of indoor radon in the Netherlands<sup>4</sup>. It should however not escape one's attention that earlier studies showed that soil is probably the main contributor in case high indoor radon concentrations are observed [Put, 1989]. The soil should therefore not be ignored in future research; one might throw out the baby with the bathwater if, e.g., the Dutch government would set limits to the maximum allowed indoor radon concentration. Both soil and building materials should therefore remain the subject of our attention.

In comparing soil and building materials, it should be realised that these media have different characteristics and may contribute to the indoor radon concentration in a different manner. A main contrast concerns the typical scales that are involved: several meters in soil and several centimeters in building materials. The required experimental techniques and analysing methods are therefore different in some cases. On the other hand, the mathematical modelling of radon transport in both media is in principle similar.

of  $\beta (k_a)$ . In that case, the ratio  $E(\text{adv})/E(\text{dif})$  should have been calculated by varying  $D$  and fixing  $k_a$ . This alters the results significantly. For  $k_a = 0$  the '1.1 contour line' in Fig. 9.1 is shifted upwards at low  $D_e$ , intersecting the  $y$ -axis at  $\log(K) = -14.5$ . So, the effect of advection on the exhalation rate is even smaller when less radon is adsorbed to solid surfaces. On the other hand, in the literature  $D_e$  is often given as  $D/\epsilon$  where  $D$  and  $\epsilon$  are measured separately and radon adsorption is ignored. The value of  $D/\beta$ , the definition of  $D_e$  as used in this study and in Fig. 9.1, might be much lower if radon is strongly adsorbed. As a consequence, the range of  $D_e$ , as defined by Eq. 2.43, might shift to lower values than shown in Fig. 9.1, corresponding with a larger relative influence of advection. However, the first mentioned influence (a smaller effect of advection as a result of Knudsen diffusion) is probably more important.

<sup>4</sup>In the forthcoming, the clause 'in the Netherlands' will be omitted as long as the Dutch situation is meant.

In the following, issues that may be further investigated using the modelling techniques, in particular the validated 2D numerical model, presented in this thesis are elucidated below on a point by point basis with soil and building materials only being distinguished when necessary:

**Barometric pressure fluctuations.** These probably affect the soil to a larger extent than building materials. With the extension made in the 2D-model in chapter 7, their influence in more realistic situations can be studied as long as the pressure pulse is transported at a relatively large velocity in the soil ( $>1 \text{ mm s}^{-1}$ ).

**Pressure fields in the soil.** Pressure gradients under a house may be of importance. Usually the house and the crawl space are at a lower pressure than outside. As a result, a small air-flow will run from outside into the soil, further underneath the footer of the house, and emerge in the crawl space. Such a pressure regime may considerably increase the radon exhalation rate from the soil into the crawl space. This has been observed both in the vessel and in the research house in Roden [Aldenkamp and Stoop, 1994].

**Preferential flow.** Cracks, fissures and macro-pores in the soil and building materials (which may also contain transits) have a low resistance to air-flow and therefore may augment transport of radon-rich pore gas into the crawl space or into the indoor environment. It depends on many factors whether cracks are important for radon entry [Schery and Siegel, 1986]. Results of a study on radon transport in a fractured Danish soil type suggest that the radon exhalation rate is not altered by the presence of fractures for typical pressure gradients under a house [Hoff, 1997]. Radon transport in one or two well-defined cracks or macro-pores may be simulated with the 2D-model (the perforated box in the vessel can be considered as a large crack or cavity). More specialised models are required for simulating several - or a network of - cracks.

**Ground water.** The influence of a shallow ground-water table, specific for the Dutch situation, may be studied in connection with pressure gradients in the soil.

**Radon adsorption.** Adsorption of radon to the solid phase can be significant in building materials and other soils than sand. The theory presented in chapter 2 forms the basis for further investigations in this field.

**Inhomogeneous media.** As indicated previously, in masonry the transport processes are affected by different properties of the constituents. Since this transport should be described in three dimensions, the 2D model can only be used as an approximation. The model outlined in chapter 4 can be extended to simulate 3D transport. Unfortunately, the method of finding the solution (solving the set of equations with a direct method) becomes too inefficient to apply and one should turn to either more advanced techniques or to the (delicate) ADI (Alternating-Direction Implicit) method [Ames, 1977; Van der Spoel, 1993].

## 9.4 Outlook and recommendations for future developments

The main question that inevitably emerges, concerns the line of research that should be followed in the future and/or actions that should be taken to reach the final goal, i.e. to lower the radon concentration in the indoor environment. The radon vessel experiments and the above general discussion made clear that our knowledge is still incomplete and that numerous topics in the field of radon remain to be investigated. Future research should focus on these 'unexplored areas' in order that effective countermeasures can be developed.

### 9.4.1 Identifying the source of indoor radon

In first instance, it is recommendable to investigate in more detail which processes are responsible for the (unexplained) entry of radon into the indoor environment. All the processes pointed out previously (see page 144) may play a role, but it is conceivable that one or two of these are dominating, or that a totally unexpected cause emerges. Besides, for houses with a high radon concentration, it is certainly advisable to pay attention to the influence of the soil as well and to identify which processes are determining the entry of soil-gas radon into these houses. At one hand, part of the research may be conducted in the laboratory. On the other hand, *in situ* investigations are probably unavoidable to identify the source of indoor radon. Both types of research are necessary simultaneously to identify the source of indoor radon in the Netherlands at short notice.

In the light of the discussion in section 9.3, it is recommended that *in situ* studies focus on the radon exhalation rate from the building materials first. Considering the extremely large discrepancy between the expected and measured average radon concentration in the living room, it is sufficient to start such investigations in merely one or a couple of 'average' houses, i.e. houses with an average ventilation rate, average radon concentration in the living room and a 70% contribution from building materials. One might choose these houses from the set that was investigated in the latest national survey. To measure the *combined* diffusive and advective exhalation rate *in situ*, new techniques have to be developed. The technique may be based on measuring the radon concentration in a open-faced chamber pressed with the open side against a surface, with the air pressures in- and outside balanced at any time by controlled supply of (radon-free) air into - and removal of air from - the chamber.

In these *in situ* studies it is recommended to measure the exhalation rate of the walls, ceiling and floor of the living room under normal conditions first. It is also advisable to conduct several exhalation measurements at different positions to 'map' each complete surface. To verify whether the measured exhalation rates can account for the contribution of building materials to the indoor radon concentration, measurements of the ventilation rate, radon concentration in the living room, the crawl space and outdoors, and the infiltration rate from crawl space to the living room should be conducted. In a later stage, similar experiments with the living room at underpressure and overpressure may provide more information on the advective radon-exhalation component, as in the diagnostic method developed by Aldenkamp and Stoop [1994]. In addition, tracer-gas experiments may be used to identify the infiltration from compartments that have been disregarded so far, viz. the cavity wall.

Simultaneous with these investigations, laboratory research should focus on the



diffusive and combined advective and diffusive radon exhalation rate of building materials. It is recommended to start with simple conditions and to increase the complexity gradually. In this respect one might start with studying pure diffusive exhalation by placing bricks, concrete blocks and/or mortar in a closed chamber and measuring the radon-exhalation rate under different conditions (ventilation rate, temperature, humidity). This may first be done with a single block and later with a stacked configuration, possibly with mortar between the blocks. To measure the combined diffusive and advective exhalation rate, a pressure difference should be exerted over the material. This may be realized by placing the (stacked) block(s) between two compartments being at different air-pressures. A requirement concerning these experiments is that no air - and radon - leakage along the material should occur. Therefore, glues or resins with a low radon-diffusion coefficient and gas permeability should be used that fix the outer sides of the block(s) to a leak-tight frame. The aim of these measurements merely comprehends an assessment of the exhalation rate under different conditions; an in-depth knowledge of the processes responsible for the exhalation rate is relevant at second instance. The results of these studies may reveal which processes and/or conditions play a role in real houses. As such, it may also indicate where to concentrate the attention on in the *in situ* studies and speed up the identification process.

#### 9.4.2 Basic research

At second instance, with the eye on the development of countermeasures against radon entry, the transport processes need to be well understood. A sound scientific basis can probably only be reached with detailed research under controlled and well-defined circumstances. The radon vessel experiments presented in this thesis form part of such a strategy. By this study, more certainty has been obtained with respect to our understanding of radon transport in soil. Since it is limited to sand, it is advisable to extend the knowledge by conducting similar experiments with a soil type that better represents realistic conditions. Moreover, as this study showed that transport in moisturised sand can not be reproduced within the imposed limits by using either a set of independently measured parameters or a set containing some *in situ* measured parameters, possibly as a result of heterogeneities, it is advisable that in such future studies the attention is also directed towards development and application of techniques to measure the parameters (porosity and moisture content in particular) as a function of position in the soil.

As far as building materials are concerned, the exhalation-rate measurements described in section 9.4.1 may already help in improving the fundamental understanding. It is recommended that a transport model for building materials will be developed and validated, first based on these measurements, in the same way as was carried out for the sand. This will certainly be a laborious task. Concrete, for example, is made of several different materials and may be fabricated using different mixing ratios and procedures. The variation of the properties influencing radon transport is therefore large. Moreover, some of the quantities that are necessary in the transport model are not easily measured. Especially if cracks would appear to be important, it is difficult to characterise these preferential flow paths and to translate them into a mathematical model (this also applies to soil). It seems therefore sensible to start the validation with a simple building material, a choice that proved to be not too prudent for soil. An even further simplification can be attained by first studying the constituent materials individually. This research strategy is

presently being contemplated at the KVI.

It is stressed that basic research remains necessary so that effective countermeasures can be developed. As radon is concerned, there are numerous topics towards which the attention can be directed. It seems therefore wise to confine the range of possibilities by focussing on subjects that are relevant for practical situations. The choice of topics should therefore preferentially be made depending on the outcome of studies directed at identifying the source of indoor radon. Nevertheless, considering the expected complexity that is involved in the validation of radon transport in building materials and more realistic soils, it seems sensible not to postpone such validation studies. After all, the gained knowledge may also help in the search of relevant transport mechanisms in houses.

Thus far, we have solely been focussing on radon transport in soil and building materials as porous media. The oil and gas industry faces similar problems in understanding the behaviour in (porous media) reservoirs. Not all their work, however, is accessible and we have not been able to benefit from their expected experience. It is therefore hypothesized that in turn the research at the oil and gas industry may benefit as well from a better understanding of radon transport.

### 9.4.3 Radon mitigation

Finally, at third instance, (cost-) effective radon mitigation methods and/or new building techniques need to be developed and tested. It should be mentioned that measures have already been tested which, based on former insights, were directed at preventing entry of radon from the crawl space into the living rooms and at lowering the crawl-space radon concentration by, respectively, lowering the effective leakage area of the ground floor and increasing the natural ventilation rate of the crawl space. Since we nowadays know that most of the indoor radon originates from building materials, it is not so surprising that these measures did not significantly lower the indoor radon concentration. One should however not forget that soil is probably an important source in houses with a high radon concentration. The previously mentioned countermeasures may therefore be effective in these houses. Therefore, the further development of measures against entry of soil-gas radon should not be abandoned. In this light, coverage of the crawl-space floor with a membrane in combination with sub-membrane suction seems a good candidate for being an effective mitigation technique.

Because the development of effective countermeasures can not be undertaken before sufficient knowledge has been gained of the transport processes that are responsible for the entry of radon into 'normal' houses, such activities can probably not be undertaken soon. It should nevertheless be remarked that, if 70% originates from building materials in most houses, the indoor radon concentration can simply be reduced by utilising materials that intrinsically produce less radon. Assuming that natural materials such as concrete, gypsum, sandstone and brick will also be used in future dwellings, one might concentrate the attention at developing materials with a low radon emanation coefficient or radium content. As the former parameter is concerned, this requires basic research on the radon emanation processes. The radium content depends on the type of raw natural materials that are used in the manufacturing. Unfortunately, removal of radium from these raw materials is yet practically impossible.

Another interesting mitigation method concerns the use of building materials that strongly adsorb radon. In this light, one might think of applying (natural) zeolites or other radon-adsorbing substances as a supplement for building materials or as an upper

layer. Zeolites adsorb radon due to their large specific surface area. An advantage of this method is the possibility to use secondary raw materials (e.g. slag from the artificial-fertilizer and iron industry, fly-ash), which usually have a higher radium content, in the manufacturing of building materials. Further research in this field is required to find out to what extent this technique can lower the radon exhalation rate.

In conclusion, radon transport in porous media remains a challenging research topic that, in consideration of the final aim of reducing the radiation exposure to humans in the interior environment, deserves our further attention and may have applications beyond the present goal.



# Appendix A

## Time-dependent diffusive transport in a rectangle

The differential equation for two-dimensional time-dependent diffusive radon transport in a homogeneous isotropic medium in cartesian coordinates  $(x, y)$  is given by:

$$\frac{\partial C}{\partial t} = D_e \left( \frac{\partial^2 C}{\partial x^2} + \frac{\partial^2 C}{\partial y^2} \right) - \lambda C + \frac{S}{\beta}, \quad (\text{A.1})$$

where  $D_e$  is the effective diffusion coefficient (Eq. 2.43). The medium is assumed to exist in a rectangle  $(0 \leq x \leq a; 0 \leq y \leq b)$ . The boundary conditions imply zero radon concentration at three sides of the rectangle ( $x = 0$ ,  $x = a$  and  $y = b$ ) and a Neumann boundary condition (no radon flux) at the remaining side ( $y = 0$ ):

$$C = 0 \quad x = 0; 0 \leq y \leq b; t > 0, \quad (\text{A.2})$$

$$C = 0 \quad x = a; 0 \leq y \leq b; t > 0, \quad (\text{A.3})$$

$$C = 0 \quad y = b; 0 \leq x \leq a; t > 0, \quad (\text{A.4})$$

$$\frac{\partial C}{\partial y} = 0 \quad y = 0; 0 \leq x \leq a; t > 0. \quad (\text{A.5})$$

As initial condition, zero radon concentration is imposed:

$$C = 0 \quad t = 0; 0 \leq x \leq a; 0 \leq y \leq b. \quad (\text{A.6})$$

In the first step to find  $C(x, y, t)$ , the method of Laplace transformation [Crank, 1956] is used. Suppose  $f(t)$  to be a known function of  $t$  for positive values of  $t$ . Then the Laplace transform  $\bar{f}(p)$  of  $f(t)$  is defined as:

$$\bar{f}(p) = \int_0^{\infty} e^{-pt} f(t) dt, \quad (\text{A.7})$$

where  $p$  is a number sufficiently large to make the integral converge. The Laplace transform of differential equation A.1 is then:

$$D_e \left( \frac{\partial^2 \bar{C}}{\partial x^2} + \frac{\partial^2 \bar{C}}{\partial y^2} \right) - (p + \lambda) \bar{C} + \frac{S}{\beta p} = 0, \quad (\text{A.8})$$

and the boundary conditions are:

$$\bar{C}(0, y) = 0, \quad (\text{A.9})$$

$$\bar{C}(a, y) = 0, \quad (\text{A.10})$$

$$\bar{C}(x, b) = 0, \quad (\text{A.11})$$

$$\frac{\partial \bar{C}(x, 0)}{\partial y} = 0. \quad (\text{A.12})$$

Further, it is assumed that the solution  $\bar{C}(x, y)$  of Eq. A.8 can be written as the sum of two terms [Carslaw and Jaeger, 1959]:

$$\bar{C}(x, y) = \bar{C}(x) + \bar{V}(x, y), \quad (\text{A.13})$$

in which  $\bar{C}(x)$  represents the solution of the problem:

$$D_e \frac{\partial^2 \bar{C}}{\partial x^2} - (p + \lambda)\bar{C} + \frac{S}{\beta p} = 0, \quad (\text{A.14})$$

with boundary conditions  $\bar{C}(0) = \bar{C}(a) = 0$ . The solution of this problem is:

$$\bar{C}(x) = \frac{S}{\beta p(p + \lambda)} \left( 1 - \cos(k_x x) + \frac{(\cos(k_x a) - 1) \sin(k_x x)}{\sin(k_x a)} \right), \quad (\text{A.15})$$

where

$$k_x^2 = \frac{-(p + \lambda)}{D_e}. \quad (\text{A.16})$$

Since the inhomogeneous term  $\frac{S}{\beta p}$  has been incorporated in Eq. A.14, a homogeneous problem remains for  $\bar{V}$ , given by:

$$D_e \left( \frac{\partial^2 \bar{V}}{\partial x^2} + \frac{\partial^2 \bar{V}}{\partial y^2} \right) - (p + \lambda)\bar{V} = 0, \quad (\text{A.17})$$

with boundary conditions:

$$\bar{V}(0, y) = 0, \quad (\text{A.18})$$

$$\bar{V}(a, y) = 0, \quad (\text{A.19})$$

$$\bar{V}(x, b) = -\bar{C}(x), \quad (\text{A.20})$$

$$\frac{\partial \bar{V}(x, 0)}{\partial y} = 0. \quad (\text{A.21})$$

This homogeneous problem has been solved with the method of separation of variables [Kreyszig, 1988]. By writing  $\bar{V}(x, y) = X(x)Y(y)$ , the solution  $\bar{V}(x, y)$  of the problem is given by:

$$\bar{V}(x, y) = \sum_{m=1}^{\infty} (A_m \sin(k_y y) + B_m \cos(k_y y)) \sin\left(\frac{m\pi x}{a}\right), \quad (\text{A.22})$$

with

$$k_y^2 = k_x^2 - \left(\frac{m\pi}{a}\right)^2, \quad (\text{A.23})$$

and  $A_m, B_m$  are constants which can be found by substitution of Eq. A.22 in the boundary conditions. With Eq. A.21 it follows immediately that  $A_m = 0, m = 1, 2, \dots$ . With Eq. A.20 and using Fourier theory, the constant  $B_m$  can be expressed as:

$$B_m = -\frac{2}{a \cos(k_y b)} \int_0^a \bar{C}(x) \sin\left(\frac{m\pi x}{a}\right) dx. \quad (\text{A.24})$$

The final step is to calculate the inverse transformation of  $\bar{C}(x, y)$ . In general [Crank, 1956], if a transform  $\bar{y}$  has the form:

$$\bar{y} = \frac{f(p)}{g(p)}, \quad (\text{A.25})$$

where  $f(p)$  and  $g(p)$  are polynomials in  $p$  which have no common factor, the degree of  $f(p)$  being lower than that of  $g(p)$ , and if

$$g(p) = (p - a_1)(p - a_2)\dots(p - a_m), \quad (\text{A.26})$$

where  $a_1, a_2, \dots, a_m$  are constants which may be real or complex but must all be different, then the function  $y(t)$ , which transform is  $\bar{y}(p)$ , is given by:

$$y(t) = \sum_{r=1}^m \frac{f(a_r)}{g'(a_r)} e^{a_r t}. \quad (\text{A.27})$$

Here  $g'(a_r)$  denotes the value of  $\frac{dg(p)}{dp}$  when  $p = a_r$ . Eq. A.27 still holds for  $m = \infty$  [Carslaw and Jaeger, 1959].

This procedure, operated on  $\bar{C}(x, y)$  as to find  $C(x, y, t)$ , gives:

$$C(x, y, t) = \frac{S}{\beta\lambda} \left[ \left( 1 - \cosh\left(\frac{x}{\ell}\right) + \frac{(\cosh\left(\frac{a}{\ell}\right) - 1) \sinh\left(\frac{x}{\ell}\right)}{\sinh\left(\frac{a}{\ell}\right)} \right) + \frac{2a^2}{\pi} \sum_{m=1}^{\infty} \frac{((-1)^m - 1) \cosh\left(\frac{y}{\ell_m}\right) \sin\left(\frac{m\pi x}{a}\right)}{m(a^2 + (m\pi\ell)^2) \cosh\left(\frac{b}{\ell_m}\right)} - \frac{2\lambda}{\pi} \sum_{m=1}^{\infty} \sum_{j=1}^{\infty} \frac{(-1)^j (j - \frac{1}{2}) H_{jm}}{p_{jm} \left( (j - \frac{1}{2})^2 + \left(\frac{bm}{a}\right)^2 \right)} \cos\left(\frac{(j - \frac{1}{2})\pi y}{b}\right) \sin\left(\frac{m\pi x}{a}\right) e^{p_{jm} t} \right], \quad (\text{A.28})$$

with  $\ell$  the diffusion length:

$$\ell = \sqrt{\frac{D_e}{\lambda}}, \quad (\text{A.29})$$

and

$$\ell_m = \frac{a\ell}{\sqrt{a^2 + (m\pi\ell)^2}}, \quad (\text{A.30})$$

$$H_{jm} = \frac{-2((-1)^m - 1)}{m\pi} - \frac{\cos(k_{jm}a - m\pi) - 1}{k_{jm}a - m\pi} + \frac{\cos(k_{jm}a + m\pi) - 1}{k_{jm}a + m\pi} + \frac{\cos(k_{jm}a) - 1}{\sin(k_{jm}a)} \left( \frac{\sin(k_{jm}a - m\pi)}{k_{jm}a - m\pi} - \frac{\sin(k_{jm}a + m\pi)}{k_{jm}a + m\pi} \right), \quad (\text{A.31})$$

$$k_{jm}^2 = \left( \frac{(j - \frac{1}{2})\pi}{b} \right)^2 + \left( \frac{m\pi}{a} \right)^2, \quad (\text{A.32})$$

and

$$p_{jm} = -D_e k_{jm}^2 - \lambda. \quad (\text{A.33})$$

In the comparison with the 2D numerical model, only the first fifty terms in the series in Eq. A.28 were calculated. This results in a much smaller truncation error than the error introduced by the numerical model.



# Appendix B

## The radon-transparency instrument: mathematical formalism

In this chapter analytical expressions are derived for the radon concentration and measured count rate as function of time in both compartments of the radon-transparency set-up. In short, the set-up (schematically shown in Figs. 7.1 and 8.3) consists of two leak-tight compartments separated by e.g. a slab of sand or a sheet of foil. Radon is produced in the lower compartment and may enter the upper compartment by diffusion through the sand or foil (no pressure differences are applied over the separating medium). The alpha activity in both compartments is measured with scintillation flasks positioned in front of a photomultiplier tube. At the start of an experiment, lower and upper compartment are flushed with radon-poor ambient air as to create an initial condition with a low radon concentration in both compartments. After stopping the air-flow, the alpha activity in both compartments is measured by registering the number of pulses as function of time in a selected time interval.

### B.1 Radon concentration

We start by considering the time-dependent multi-phase equation for one-dimensional radon transport in the (homogeneous) slab of sand<sup>1</sup> (Eq. 2.32) where radon production in the sand may be neglected ( $<0.2\%$ ) with respect to the production rate of the radon source in the lower compartment. Imposing a one-dimensional coordinate system ( $z$ ) along the vertical axis of the set-up with  $z = 0$  being the bottom surface of the sand and  $z = d$  the upper surface, this equation is written as (neglecting advection and using  $C$  instead of  $C_a$  for the pore-air radon concentration):

$$\beta \frac{\partial C}{\partial t} = D \frac{\partial^2 C}{\partial z^2} - \beta \lambda C \quad 0 \leq z \leq d. \quad (\text{B.1})$$

Further, it is assumed that radon is well mixed in both compartments. Since radon is produced in the lower compartment by a source of strength  $S_s$  ( $\text{Bqs}^{-1}$ ) and 'leaves' the compartment by decay and diffusion into the sand, the boundary condition for this compartment ( $z = 0$ ) is written as (compare with Eq. 5.3):

$$V_1 \frac{\partial C}{\partial t} = AD \left. \frac{\partial C}{\partial z} \right|_{z=0} - \lambda CV_1 + S_s \quad z = 0; t > 0, \quad (\text{B.2})$$

---

<sup>1</sup>Sand will be referred to in the derivation, but may as well be a sheet of foil.

where  $V_1$  ( $\text{m}^3$ ) is the volume of the lower compartment and  $A$  ( $\text{m}^2$ ) is the surface area of the lower (and upper) surface of the sand. For the upper compartment with volume  $V_2$  ( $\text{m}^3$ ) we may write:

$$V_2 \frac{\partial C}{\partial t} = -AD \left. \frac{\partial C}{\partial z} \right|_{z=d} - \lambda CV_2 \quad z = d; t > 0. \quad (\text{B.3})$$

As initial condition (at first instance), zero radon concentration is imposed in the whole set-up:

$$C = 0 \quad 0 \leq z \leq d; t = 0. \quad (\text{B.4})$$

The method of Laplace transformation [Crank, 1956], see also appendix A, is used to find the concentration as a function of time and height. The Laplace transform of differential equation B.1 is given by:

$$p\bar{C} = \frac{D}{\beta} \frac{d^2 \bar{C}}{dz^2} - \lambda \bar{C}, \quad (\text{B.5})$$

and the Laplace-transformed boundary conditions by:

$$p\bar{C} = \left. \frac{D}{h_1} \frac{d\bar{C}}{dz} \right|_{z=0} - \lambda \bar{C} + \frac{S_s}{pV_1} \quad z = 0, \quad (\text{B.6})$$

$$p\bar{C} = - \left. \frac{D}{h_2} \frac{d\bar{C}}{dz} \right|_{z=d} - \lambda \bar{C} \quad z = d, \quad (\text{B.7})$$

with

$$h_1 = \frac{V_1}{A} \quad \text{and} \quad h_2 = \frac{V_2}{A},$$

the effective height of the lower and upper compartment, respectively. The solution of differential equation B.5, using both boundary conditions, is given by:

$$\bar{C} = \frac{S_s}{pV_1} \left( \frac{\cos(kz)}{\frac{DkR_1}{h_1R_2} + p + \lambda} - \frac{\sin(kz)}{\frac{Dk}{h_1} + (p + \lambda)\frac{R_2}{R_1}} \right), \quad (\text{B.8})$$

in which

$$R_1 = (p + \lambda) \cos(kd) - \frac{Dk}{h_2} \sin(kd), \quad (\text{B.9})$$

$$R_2 = (p + \lambda) \sin(kd) - \frac{Dk}{h_2} \cos(kd), \quad (\text{B.10})$$

and

$$k^2 = \frac{-\beta(p + \lambda)}{D}. \quad (\text{B.11})$$

Applying the procedure described on page 153 for obtaining the inverse transformation  $C(z, t)$  of  $\bar{C}$ , gives:

$$C(z, t) = \frac{S_s}{\lambda V_1} \left[ \frac{\left( \sinh\left(\frac{d}{\ell}\right) + \frac{\beta \ell}{h_2} \cosh\left(\frac{d}{\ell}\right) \right) \cosh\left(\frac{z}{\ell}\right) - \left( \cosh\left(\frac{d}{\ell}\right) + \frac{\beta \ell}{h_2} \sinh\left(\frac{d}{\ell}\right) \right) \sinh\left(\frac{z}{\ell}\right)}{\beta \ell (h_1^{-1} + h_2^{-1}) \cosh\left(\frac{d}{\ell}\right) + \left( 1 + \frac{\beta^2 \ell^2}{h_1 h_2} \right) \sinh\left(\frac{d}{\ell}\right)} - \frac{h_1 \exp(-\lambda t)}{h_1 + h_2 + \beta d} + \lambda \sum_{n=2}^{\infty} \left( \frac{(R_2 \cos(k_n z) - R_1 \sin(k_n z)) \exp(p_n t)}{\frac{Dk_n}{h_1} (R_1 + p_n R_3) + (p_n + \lambda) (R_2 + p_n R_4) - \frac{\beta p_n}{2h_1 k_n} R_1 + p_n R_2} \right) \right], \quad (\text{B.12})$$

where

$$R_3 = \left( \frac{\beta d}{2h_2} + 1 \right) \cos(k_n d) + \left( \frac{\beta}{2h_2 k_n} - \frac{k_n d}{2} \right) \sin(k_n d), \quad (\text{B.13})$$

$$R_4 = \left( \frac{\beta d}{2h_2} + 1 \right) \sin(k_n d) - \left( \frac{\beta}{2h_2 k_n} - \frac{k_n d}{2} \right) \cos(k_n d), \quad (\text{B.14})$$

and where  $k_n$  ( $n = 2, 3, \dots$ ) are the positive roots (with  $k_2$  being the first) of

$$\left( k^2 - \frac{\beta^2}{h_1 h_2} \right) \tan(kd) - \beta k (h_1^{-1} + h_2^{-1}) = 0. \quad (\text{B.15})$$

and according to Eq. B.11:

$$p_n = -\frac{Dk_n^2}{\beta} - \lambda. \quad (\text{B.16})$$

It was stated earlier that a zero radon concentration is assumed at  $t = 0$ . As we actually have a non-zero radon concentration  $C_0$  initially, the term:

$$C_0 \exp(-\lambda t) \quad (\text{B.17})$$

is finally added to Eq. B.12 for a realistic description of the experimental conditions.

It should be remarked that in the case of a nearly water-saturated sand sample, the radon production in the sand may not be ignored when considering the concentration in the upper compartment. The small value of the bulk radon diffusion coefficient ( $\approx 1 \cdot 10^{-10} \text{ m}^2 \text{ s}^{-1}$  for a fully saturated sample) inhibits transport of radon from the lower to the upper compartment in the first few days of the experiment. As a result, for these experiments the previous derivation must be complemented with a description in which production in the sand is accounted for and in which production in the lower compartment is ignored. Mathematically, this is expressed as:

$$\beta \frac{\partial C}{\partial t} = D \frac{\partial^2 C}{\partial z^2} - \beta \lambda C + S \quad 0 \leq z \leq d, \quad (\text{B.18})$$

where  $S$  is given by Eq. 2.34 (notice  $S_s$  has other units) and with boundary conditions:

$$\frac{\partial C}{\partial t} = \frac{AD}{h_1} \frac{\partial C}{\partial z} \Big|_{z=0} - \lambda C \quad z = 0; t > 0, \quad (\text{B.19})$$

$$\frac{\partial C}{\partial t} = -\frac{AD}{h_2} \frac{\partial C}{\partial z} \Big|_{z=d} - \lambda C \quad z = d; t > 0, \quad (\text{B.20})$$

$$C = 0 \quad 0 \leq z \leq d; t = 0. \quad (\text{B.21})$$

The solution, found using similar procedures as given above, is given by:

$$C(z, t) = \frac{S}{\beta \lambda} \left[ \frac{\left( \cosh\left(\frac{d}{\ell}\right) + \frac{\beta \ell}{h_2} \sinh\left(\frac{d}{\ell}\right) - 1 \right) \sinh\left(\frac{z}{\ell}\right) - \left( \frac{\beta \ell}{h_1} + \sinh\left(\frac{d}{\ell}\right) + \frac{\beta \ell}{h_2} \cosh\left(\frac{d}{\ell}\right) \right) \cosh\left(\frac{z}{\ell}\right)}{\beta \ell (h_1^{-1} + h_2^{-1}) \cosh\left(\frac{d}{\ell}\right) + \left( 1 + \frac{\beta^2 \ell^2}{h_1 h_2} \right) \sinh\left(\frac{d}{\ell}\right)} \right. \\ \left. + 1 + \left( \frac{h_1 + h_2}{h_1 + h_2 + \beta d} - 1 \right) \exp(-\lambda t) \right. \\ \left. - \lambda \sum_{n=2}^{\infty} \left( \frac{\left( \left( \frac{Dk_n}{h_1} + R_2 \right) \cos(k_n z) - (R_1 - p_n - \lambda) \sin(k_n z) \right) \exp(p_n t)}{\frac{Dk_n}{h_1} (R_1 + p_n R_3) + (p_n + \lambda) (R_2 + p_n R_4) - \frac{\beta p_n}{2h_1 k_n} R_1 + p_n R_2} \right) \right], \quad (\text{B.22})$$

where  $k_n$ ,  $p_n$ ,  $R_1$ ,  $R_2$ ,  $R_3$ , and  $R_4$  are given by their previous definitions. The influence of incorporating production in the sand on the fitted diffusion coefficient decreases fast with decreasing moisture content. The effect is circa 25% for a water-saturated sample (thickness 4.9 cm) and less than 4% for a pore-water content of 90%.

## B.2 Count rate

The count rate measured with the two scintillation flasks depends on the alpha activity in the measuring volume (energy window of radiation monitors is such that pulses due to beta and gamma activities are not registered). As the alpha activity is determined by the concentrations in the scintillation flask of  $^{222}\text{Rn}$  and its alpha-emitting progeny  $^{218}\text{Po}$  and  $^{214}\text{Po}$  (see Fig. 1.1), the count rate is also dependent on the efficiency of the flask for detecting an alpha particle emitted in the decay of  $^{222}\text{Rn}$ ,  $^{218}\text{Po}$  or  $^{214}\text{Po}$ .

In the previous section an expression for the radon concentration in a compartment was derived. In simplified form, this expression for the radon concentration  $C_1(t)$  in a compartment can be written as:

$$C_1(t) = \sum_{i=0}^{\infty} A_i \exp(p_i t) \quad t \geq 0, \quad (\text{B.23})$$

where the subscript '1' is a reference to radon and where  $p_0 = 0$ ,  $p_1 = -\lambda$ , and  $p_i$  ( $i = 2, 3, \dots$ ) is given by Eq. B.16. The coefficients  $A_i$  ( $i = 0, 1, \dots$ ) follow from the solution, i.e. Eq. B.12 complemented with Eqs. B.17 and B.22 (notice that coefficient  $C_0$  in Eq. B.17 is comprised in  $A_1$ ). The concentrations of radon progeny  $^{218}\text{Po}$ ,  $^{214}\text{Pb}$  and  $^{214}\text{Po}$ , respectively denoted as  $C_2(t)$ ,  $C_3(t)$  and  $C_4(t)$  (with corresponding decay constants  $\lambda_2 = 3.78 \cdot 10^{-3} \text{ s}^{-1}$ ,  $\lambda_3 = 4.31 \cdot 10^{-4} \text{ s}^{-1}$  and  $\lambda_4 = 5.81 \cdot 10^{-4} \text{ s}^{-1}$ ) are found from the set of differential equations describing the rate of change of concentration of each of these nuclides:

$$\frac{dC_2(t)}{dt} - \lambda_2 C_2(t) = \lambda_2 C_1(t) \quad t \geq 0, \quad (\text{B.24})$$

$$\frac{dC_3(t)}{dt} - \lambda_3 C_3(t) = \lambda_3 C_2(t) \quad t \geq 0, \quad (\text{B.25})$$

$$\frac{dC_4(t)}{dt} - \lambda_4 C_4(t) = \lambda_4 C_3(t) \quad t \geq 0. \quad (\text{B.26})$$

$$(\text{B.27})$$

The solution of differential equation B.24 is given by:

$$C_2(t) = \exp(-\lambda_2 t) \int_0^t \exp(\lambda_2 t) \lambda_2 C_1(t) dt + C_2(t_0) \exp(-\lambda_2 t), \quad (\text{B.28})$$

where  $C_2(t_0)$  is the  $^{218}\text{Po}$  concentration at  $t = 0$ . Using Eq. B.23, Eq. B.28 can be written as:

$$C_2(t) = \lambda_2 \sum_{i=0}^{\infty} \frac{A_i}{\lambda_2 + p_i} (\exp(p_i t) - \exp(-\lambda_2 t)) + C_2(t_0) \exp(-\lambda_2 t). \quad (\text{B.29})$$

The expressions for  $C_3(t)$  and  $C_4(t)$  are found with a similar procedure, starting from the basic solutions:

$$C_3(t) = \exp(-\lambda_3 t) \int_0^t \exp(\lambda_3 t) \lambda_3 C_2(t) dt + C_3(t_0) \exp(-\lambda_3 t), \quad (\text{B.30})$$

$$C_4(t) = \exp(-\lambda_4 t) \int_0^t \exp(\lambda_4 t) \lambda_4 C_3(t) dt + C_4(t_0) \exp(-\lambda_4 t). \quad (\text{B.31})$$

As the experimental set-up is flushed for more than three hours before an experiment is started, we have secular equilibrium between radon and its progeny. As a consequence, the activity concentrations at  $t = 0$  can be written as:

$$C_4(t_0) = C_3(t_0) = C_2(t_0) = C_1(t_0) = C_0. \quad (\text{B.32})$$

The number of counted pulses  $N_j$  in time bin  $j$  (from  $t_{j-1} = (j-1)\Delta t$  to  $t_j = j\Delta t$ ,  $j = 1, 2, \dots$ ), where  $\Delta t$  is the time interval at which the number of pulses are registered, is obtained by integrating the alpha activity in the measuring volume  $V_m$  of a scintillation flask from time  $t_{j-1}$  to  $t_j$ :

$$N_j = V_m \int_{t_{j-1}}^{t_j} (\xi_1 C_1(t) + \xi_2 C_2(t) + \xi_4 C_4(t)) dt + N_{bck} \quad j = 1, 2, \dots \quad (\text{B.33})$$

where  $\xi_1$ ,  $\xi_2$  and  $\xi_4$  denote the efficiency for detecting an alpha particle emitted in the decay of  $^{222}\text{Rn}$ ,  $^{218}\text{Po}$  and  $^{214}\text{Po}$ , respectively, and where  $N_{bck}$  is the number of background pulses within the interval  $\Delta t$ .

Finally, referring to Fig. 8.3, a typical experimental artefact should be addressed. As mentioned before, both volumes are assumed to be well mixed at all times. In reality, the mixing in both volumes is driven by radon diffusion in free air. As a result, the radon concentration as seen by both scintillation cells (into which radon has to diffuse too) lags the real concentration near the surfaces of the sand sample. For the lower compartment, this time lag is expected to be small because the distance from the radon source to the lower sand surface nearly equals the distance from the source to the scintillation cell. However, for the upper compartment the time lag is significant due to the 8 cm (vertical) separation between the upper sand surface and the cell. A numerical test case with two scintillation cells 8 cm apart indicates a time lag of 1500 s between the respective count rates. This time lag is therefore used for the upper compartment in the analyses of the diffusion experiments. The effect of this correction is considerable for dry sand (20%) but small for pore-water contents  $>0.5$  ( $<3\%$ ).

### B.2.1 Detection efficiencies

The relative detection efficiencies  $\xi_2/\xi_1$  and  $\xi_4/\xi_1$  were determined in an experiment where a high radon concentration was established in a scintillation flask (without radon initially) and the number of pulses were registered in intervals of 10 min during a period of 3 h. The number of pulses  $N_j$  in each interval in such an experiment is given by:

$$N_j = \xi_1 V_m \int_{t_{j-1}}^{t_j} \left( C_1(t) + \frac{\xi_2}{\xi_1} C_2(t) + \frac{\xi_4}{\xi_1} C_4(t) \right) dt + N_{bck} \quad j = 1, 2, \dots, \quad (\text{B.34})$$

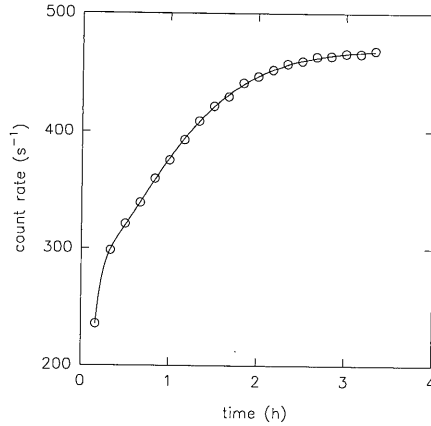


Figure B.1: Count rate ( $\text{s}^{-1}$ ) in 10 min time intervals measured with a scintillation flask in which a high radon concentration is introduced at  $t = 0$ . Solid line represents a least-squares fit to the data with the initial radon concentration and relative detecting efficiencies for alpha-emitting radon progeny with respect to radon as free parameters.

where the radon concentration is given by:

$$C_1(t) = C_{in} \exp(-\lambda_1 t) \quad t \geq 0, \quad (\text{B.35})$$

and where the progeny concentrations are obtained by evaluating the expressions as given by Eqs. B.28, B.30 and B.31 with  $C_4(t_0) = C_3(t_0) = C_2(t_0) = C_1(t_0) = 0$  and  $C_1(t)$  given by Eq. B.35. A least-squares fit of Eq. B.34 to the data (for simplicity the uncertainty in the number of detected pulses is approximated by  $\sqrt{N_j}$ ), see Fig. B.1, with  $\xi_2/\xi_1$ ,  $\xi_4/\xi_1$  and the initial radon concentration  $C_{in}$  as free parameters resulted in  $\xi_2/\xi_1 = 1.15 \pm 0.03$  and  $\xi_4/\xi_1 = 1.333 \pm 0.018$  (external errors) with  $\chi_{\text{red}}^2 = 1.3$ . The detection efficiency for radon,  $\xi_1$ , is not a relevant parameter for determining diffusion lengths in a sand sample because the production rate of the radon source in the lower compartment is also fitted in the procedure, i.e. the concentration in the upper compartment *relative* to the concentration in the lower compartment is of importance only. Nevertheless, to obtain reasonably realistic values for the source strength in the lower compartment and initial radon concentration, its value was inferred from a comparison between the measured count rate with a scintillation flask and a 'standard' Lucas cell used in the radon vessel experiments. This resulted in  $\xi_1 = 0.43$ .

# Bibliography

- Ackers J.G. Concentratie van radionucliden in bouwmaterialen en grondsoorten, 1985. Rapportnr. RD-E/8505 - 246 (in Dutch).
- Ackers J.G. Gemeten radon emanatiefactoren van bouwmaterialen, 1989. Rapportnr. RD-E/8901 - 271 (in Dutch).
- Åkerblom G., Andersson P., and Clavensjö B. Soil gas radon - a source for indoor radon. *Rad. Prot. Dos.*, 7:49-54, 1984.
- Aldenkamp F.J. and Stoop P. *Sources and Transport of Indoor Radon - Measurements and Mechanisms*. PhD thesis, Rijksuniversiteit Groningen, The Netherlands, 1994.
- Ames W.F. *Numerical methods for partial differential equations*. Academic Press, 1977.
- Andersen C.E. *Entry of Soil Gas and Radon into Houses*. PhD thesis, Risø National Laboratory, DK-4000, Roskilde, Denmark, 1992.
- Andersen C.E., Koopmans M., and De Meijer R.J. Identification of advective entry of soil-gas into a crawl space covered with sheets of polyethylene foil. Technical Report Risø-R-876(EN), Risø National Laboratory, DK-4000, Roskilde, Denmark, 1996. In corporation with Kernfysisch Versnellend Instituut, Zernikelaan 25, 9747 AA, Groningen, The Netherlands.
- Andersen C.E., Sogaard-Hansen J., and Majborn B. Soil-gas and radon entry into a simple test structure: Comparison of experimental and modelling results. *Rad. Prot. Dos.*, 56:151-155, 1994.
- Anderson D.A., Tannehill J.C., and Pletcher R.H. *Computational Fluid Mechanics and Heat Transfer*. Hemisphere Publishing Corporation, 1984.
- Arvela H. Seasonal variation in radon concentration of 3000 dwellings with model comparisons. *Rad. Prot. Dos.*, 59:33 - 42, 1995.
- Bear J. Eight lectures on mathematical modelling of transport in porous media. In Bear J. and Buchlin J.M., editors, *Modelling and Applications of Transport Phenomena in Porous Media*. Kluwer Academic Publishers, 1991. Lecture Series presented at the van Karman Institute for Fluid Dynamics, Rhode-Saint-Genèse, Belgium, 1987.
- Beleidsstandpunt radon, 1994. Vergaderjaar 1993-1994, 21483, Ministerie van VROM, SDU, 's Gravenhage (in Dutch).
- Bird R.B., Stewart W.E., and Lightfoot E.N. *Transport Phenomena*. John Wiley & Sons, 1960.

- Broecker W.S. and Peng T.H. Gas exchange rates between air and sea. *Tellus*, 26:21-35, 1974.
- Carnahan B., Luther H.A., and Wilkes J.O. *Applied numerical methods*. John Wiley & Sons, 1969.
- Carslaw H.S. and Jaeger J.C. *Conduction of Heat in Solids*. Oxford University Press, 1959.
- Childs E.C. *Introduction to physical basis of soil water phenomena*. John Wiley & Sons Ltd., London, 1969.
- Clements W.E. and Wilkening M.H. Atmospheric pressure effects on  $^{222}\text{Rn}$  transport across the earth-air interface. *J. Geophys. Res.*, 79(33):5025-5029, 1974.
- Clever H.L. *Krypton, Xenon and Radon - Gas Solubilities*, volume 2 of *Solubility Data Series*. Pergamon Press, 1979.
- Crank J. *The mathematics of diffusion*. Clarendon Press Oxford, 1956.
- Darcy H.P.G. Les Fontaines Publiques de la Ville de Dijon. Librairie de Corps Imperiaux des Ponts et Chaussées et de Mines; Paris, 1856. (in French).
- De Meijer R.J. Infiltratie van radon in woningen, 1992. Reeks stralenbescherming, nr. 50A (in Dutch).
- Edwards J.C. and Bates R.C. Theoretical evaluation of radon emanation under a variety of conditions. *Health Phys.*, 39:263-274, 1980.
- Emsley J. *The Elements*. Clarendon Press Oxford, 1989.
- Ennemoser O., Oberdorfer E., Brunner P., Schneider P., Purtscheller F., Stingl V., and Ambach W. Mitigation of indoor radon in an area with unusually high radon concentrations. *Health Phys.*, 69(2):227-232, 1995.
- Gadd M.S. and Borak T.B. Partitioning of  $^{222}\text{Rn}$  entry into a structure surrounded by soil. *Health Phys.*, 67(1):53 - 59, 1994.
- Garbesi K. and Sextro R.G. Modelling and Field Evidence of Pressure-Driven Entry of Soil Gas into a House through Permeable Below-Grade Walls. *Env. Sci. Techn.*, 23: 1481 - 1487, 1989.
- Garbesi K., Sextro R.G., Fisk W.J., Modera M.P., and Revzan K.L. Soil-Gas Entry into an Experimental Basement: Model Measurement Comparisons and Seasonal Effects. *Env. Sci. Techn.*, 27(3):466 - 473, 1993.
- Hakl J., Hunyadi I., and Tóth-Szilágyi. Radon permeability of foils measured by SSNTD technique (non-equilibrium approach). *Nucl. Tracks Radiat. Meas.*, 19(1-4):319-320, 1991.
- Haraya K. and Hwang S. Permeation of oxygen, argon and nitrogen through polymer membranes. *J. Membrane Sci.*, 71:13-27, 1992.



- Henschel D.B. Indoor radon reduction in crawl-space houses: a review of alternative approaches. *Indoor Air*, 2:272–287, 1992.
- Hillel D. *Fundamentals of Soil Physics*. Academic Press, New York, 1980.
- Hirst W. and Harrison G.E. The diffusion of radon gas mixtures. *Proc. Roy. Soc. London*, A 169:573–586, 1939.
- Hoff A. *Radon Transport in Fractured Soil: Laboratory Experiments and Modelling*. PhD thesis, Risø National Laboratory, DK-4000, Roskilde, Denmark, 1997.
- Jha G., Raghavayya M., and Padmanabhan N. Radon permeability of some membranes. *Health Phys.*, 42(5):723 – 725, 1982.
- Klinkenberg L.J. Analogy between diffusion and electrical conductivity in porous rocks. *Bul. Geol. Soc. Am.*, 62:559–564, 1951.
- Kreyszig E. *Advanced engineering mathematics*. John Wiley & Sons, 1988.
- Krishnaswami S. and Seidemann D.E. Comparative study of  $^{222}\text{Rn}$ ,  $^{40}\text{Ar}$ ,  $^{39}\text{Ar}$  and  $^{37}\text{Ar}$  leakage from rocks and minerals: Implications for the role of nanopores in gas transport through natural silicates. *Geochim. Cosmochim. Acta*, 52:655–658, 1987.
- Labeled V., Rannou A., and Tymen G. Study of  $^{222}\text{Rn}$  permeation through polymer membranes: application to continuous measurement of  $^{222}\text{Rn}$  in water. *Health Phys.*, 63(2):172–178, 1992.
- Loureiro C.O. *Simulation of the Steady-state Transport of Radon from Soil into Houses with Basements under Constant Negative Pressure*. PhD thesis, Lawrence Berkeley Laboratory, Berkeley, CA, USA, 1987.
- Lucas H.F. Improved low-level alpha scintillation counter for radon. *Rev. Sci. Instrum.*, 28:680, 1957.
- Mason E.A. and Malinauskas A.P. *Gas transport in porous media: the dusty-gas model*. Elsevier, 1983.
- McCarthy K.P. and Brown K.W. Soil Gas Permeability as Influenced by Soil Gas-Filled Porosity. *Soil Sci. Soc. Am. J.*, 56(4):997–1003, 1992.
- Meschendorp J.G. Properties of porous media: measurements on, and modelling of permeability and tortuosity. Master's thesis, Rijksuniversiteit Groningen, 1994. KVI report R-76.
- Nazaroff W.W. Predicting the rate of  $^{222}\text{Rn}$  entry from soil into the basement of a dwelling due to pressure-driven flow. *Rat. Prot. Dos.*, 24:199 – 202, 1988.
- Nazaroff W.W. and Doyle S.M. Radon entry into houses having a crawl space. *Health Phys.*, 48(3):265 – 281, 1985.
- Nazaroff W.W., Moed B.A., and Sextro R.G. Soil as a Source of Indoor Radon: Generation, Migration, and Entry. In Nazaroff W.W. and Nero A.V., editors, *Radon and its Decay Products in Indoor Air*, pages 57–112. John Wiley & Sons, 1988.

- Nero A.V. and Nazaroff W.W. Characterising the source of radon indoors. *Rat. Prot. Dos.*, 7:23 – 39, 1984.
- Nielson K.K., Rogers V.C., Holt R.B., Pugh T.D., Grondzik W.A., and De Meijer R.J. Radon penetration of concrete slabs, cracks, joints and sealants. *Health Phys.*, 73(4): 668 – 678, 1997.
- Nielson K.K., Rogers V.C., Rogers V., and Holt R.B. The RAETRAD model of radon generation and transport from soils into slab-on-grade houses. *Health Phys.*, 67(4):363 – 377, 1994.
- Osborne M. and Harrison J. An overview of indoor radon risk reduction in the United States. *J. Radioanal. Nucl. Chem.*, 161(1):265–272, 1992.
- Osborne M.C., Moore D.G., Southerlan R.E., Brennan T., and Pyle B.E. Radon reduction in crawl space houses. *J. Environ. Engin.*, 115(3):574–589, 1989.
- Patankar S.V. *Numerical heat transfer and fluid flow*. Hemisphere Publ. Cor., 1980.
- Pel L. *Moisture transport in porous building materials*. PhD thesis, Technische Universiteit Eindhoven, Eindhoven, The Netherlands, 1995.
- Put L.W. Radonconcentraties in een twintigtal woningen, 1989. Reeks Stralenbescherming, nr. 50E, 1992 (in Dutch).
- Put L.W. and Van der Graaf E.R. Invoerparameters voor radontransportmodellen: een literatuurstudie, 1996. report R92 (in Dutch).
- Put L.W., Veldhuizen A., and De Meijer R.J. Radonconcentraties in Nederland, 1986. Reeks Stralenbescherming, nr. 14 (in Dutch).
- Renken K.J. and Rosenberg T. Laboratory measurements of the transport of radon gas through concrete samples. *Health Phys.*, 68(6):800–808, 1995.
- Revzan K.L., Fisk W.J., and Sextro R.G. Modeling radon entry into Florida slab-on-grade houses. *Health Phys.*, 65(4):375–385, 1993.
- RIVM . Landelijk onderzoek naar radon in woningen, 1997. Concerns preliminary results; brochure (in Dutch). Final result will be published in report nr. 610058006.
- Robinson A.L. and Sextro R.G. The influence of a subslab gravel layer and open area on soil-gas and radon entry into two experimental basements. *Health Phys.*, 69(3):367–377, 1995.
- Rogers V.C. and Nielson K.K. Correlations for predicting air permeabilities and  $^{222}\text{Rn}$  diffusion coefficients of soils. *Health Phys.*, 61(2):225–230, 1991a.
- Rogers V.C. and Nielson K.K. Multiphase radon generation and transport in porous materials. *Health Phys.*, 60(6):807–815, 1991b.
- Rogers V.C. and Nielson K.K. Generalized Source Term for the Multiphase Radon Transport Equation. *Health Phys.*, 64(3):324–326, 1993.

- Schaap L.E.J.J. Effecten van maatregelen ter beperking van de natuurlijke achtergrondstraling in woningen, 1996. Eindrapportage Statego 17, rapportnummer R43029A3.LS (in Dutch).
- Schery S.D., Gaeddert D.H., and Wilkening M.H. Factors Affecting Exhalation of Radon From a Gravelly Sandy Loam. *J. Geophys. Res.*, 89(D5):7299-7309, 1984.
- Schery S.D. and Siegel D. The Role of Channels in the Transport of Radon From the Soil. *J. Geophys. Res.*, 91(B12):12366-12374, 1986.
- Schery S.D. and Whittlestone S. Desorption of Radon at Earth's Surface. *J. Geophys. Res.*, 94(D15):18297-18303, 1989.
- Søgaard-Hansen J. and Damkjær A. Determining  $^{222}\text{Rn}$  diffusion lengths in soils and sediments. *Health. Phys.*, 53(5):455-459, 1987.
- Stonestrom D.A. and Rubin J. Air Permeability and Trapped-Air Content in Two Soils. *Water Resour. Res.*, 25(9):1959-1969, 1989.
- Swedjemark G.A. and Mäkitalo A. Recent Swedish experiences in  $^{222}\text{Rn}$  control. *Health Phys.*, 58(4):453-470, 1990.
- Tanner A.B. Radon migration in the ground: a review. In Adams J.A.S. and Lowder W.M., editors, *The Natural Radiation Environment*, pages 161-190. The University of Chicago Press, 1964.
- Tanner A.B. Radon Migration in the Ground: A Supplementary review. In Gesell T.F. and Lowder W.M., editors, *Natural Radiation Environment III*, pages 5-56. USDOE Rept. CONF-780422, NTIS, 1980.
- Tritton D.J. *Physical fluid dynamics*. Clarendon Press Oxford, 1988.
- Tsang Y.W. and Narasimhan T.N. Effects of periodic atmospheric pressure variation on radon entry into buildings. *J. Geophys. Res.*, 97(B6):9161-9170, 1992.
- Vaas L.H., Kal H.B., De Jong P., and Slooff W. (eds). *Basisdocument radon*. Rijksinstituut voor Volksgezondheid en Milieuhygiëne (RIVM), Bilthoven, The Netherlands, 1991. Rapport nr. 710401012 (in Dutch).
- Van den Berg G.P. Radonkoncentraties in 9 woningen in Beijum (Groningen), 1990. Rapport NWU-33 (in Dutch).
- Van den Ham E.R., Winder C., and Ackers J.G. Verkennend onderzoek naar de kosten-effectiviteit van maatregelen ter beperking van natuurlijke achtergrondstraling in de woning, 1991. Reeks stralenbescherming, nr. 49 (in Dutch).
- Van der Graaf E.R. Orientation of the radon vessel and determination of the positions of the multi-functional measuring probes. Technical Report RV-03, KVI, Zernikelaan 25, 9747 AA, Groningen, The Netherlands, 1992.
- Van der Graaf E.R., Cohilis P., Ten Have R., De Meijer R.J., and Stapel C. Pressure fields in sand. Technical Report RV-05, KVI, Zernikelaan 25, 9747 AA, Groningen, The Netherlands, 1992.

- Van der Graaf E.R., Cozmuta I., and Van der Spoel W.H. Calibration of the KVI instrument to measure radon exhalation rates from building materials under controlled conditions. Technical Report R-99, KVI, Zernikelaan 25, 9747 AA, Groningen, The Netherlands, 1997. In preparation.
- Van der Graaf E.R., De Meijer R.J., and Put L.W. Toepassing van een folie op de bodem van de kruipruimte in combinatie met een bodemafzuigstelsel als maatregel tegen radoninfiltratie in woningen. Technical Report R-95, KVI, Zernikelaan 25, 9747 AA, Groningen, The Netherlands, 1997. (In Dutch).
- Van der Graaf E.R., Heijs S., De Meijer R.J., Put L.W., and Mulder H.F.H.M. A facility to study transport of radon in soil under controlled conditions. *Rad. Prot. Dos.*, 45: 223-226, 1992.
- Van der Graaf E.R., Heijs S., De Meijer R.J., Put L.W., and Mulder H.F.H.M. The choice of soil type for radon vessel experiments. Technical Report RV-04, KVI, Zernikelaan 25, 9747 AA, Groningen, The Netherlands, 1993. Revised version.
- Van der Graaf E.R., Van der Spoel W.H., and De Meijer R.J. Radon transport in building materials, progress until July 1995. Technical Report R-88, KVI, Zernikelaan 25, 9747 AA, Groningen, The Netherlands, 1995.
- Van der Graaf E.R., Witteman G.A.A., Ten Have R., De Meijer R.J., Put L.W., Van der Spoel W.H., and Elmegeerhi M. Determination of the relative efficiencies of seven Pylon model AB-5 portable radiation monitors and 23 Lucas cells. Technical Report R-42, KVI, Zernikelaan 25, 9747 AA, Groningen, The Netherlands, 1994. Revised version.
- Van der Grinten J.G.M. *An experimental study of shock-induced wave propagation in dry, water-saturated, and partially saturated porous media*. PhD thesis, Technische Universiteit Eindhoven, Eindhoven, The Netherlands, 1987.
- Van der Heij D. and Peerlkamp P.K. *Kennis van grond en bodem*. Wolters - Groningen, The Netherlands, 1961.
- Van der Spoel W.H. Modelling of radon transport in the KVI radon vessel. Master's thesis, Eindhoven University of Technology, Eindhoven, The Netherlands, 1993. KVI report R-76, KVI, Zernikelaan 25, 9747 AA Groningen, The Netherlands.
- Van der Spoel W.H. Radondoorslaapbaarheid van een Tonzon bodemfolie. Technical Report R69, KVI, Zernikelaan 25, 9747 AA, Groningen, The Netherlands, 1994. (In Dutch).
- Ward D.C., Borak T.B., and Gadd M.S. Characterization of  $^{222}\text{Rn}$  entry into a basement structure surrounded by low-permeability soil. *Health Phys.*, 65(1):1-11, 1993.
- Woesten J.H.M., Bannink M.H., and Beuving J. *Waterretentie -en doorlatendheidskarakteristieken van boven -en ondergronden in Nederland: de Staringreeks*. Instituut voor Cultuurtechniek en Waterhuishouding (ICW), Wageningen, 1987. STIBOKA-rapport 1932 (in Dutch).
- Wojcik M. Measurement of radon diffusion and solubility constants in membranes. *Nucl. Instr. Methods Phys. Res.*, B61:8-11, 1991.

---

Wolfs F., Hofstede H., De Meijer R.J., and Put L.W. Measurements of radon-daughter concentrations in and around dwellings in the northern part of the Netherlands; a search for the influences of building materials, construction and ventilation. *Health Phys.*, 47(2):271-279, 1984.



# Publications

Part of this thesis is based on the following publications:

## Chapter 5 and 6:

*Measurements on, and modelling of diffusive and advective radon transport in a homogeneous column of sand.*

W.H. van der Spoel, E.R. van der Graaf and R.J. de Meijer.

Proceedings of the International Workshop "Indoor Air, An Integrated Approach".

Ed. L. Morawska, N.D. Bofinger, M. Maroni; 1995.

## Chapter 5:

*Diffusive transport of radon in a homogeneous column of dry sand.*

W.H. van der Spoel, E.R. van der Graaf and R.J. de Meijer.

Health Physics 72(5): 765 - 777; 1997.

## Chapter 6:

*Combined diffusive and advective transport of radon in a homogeneous column of dry sand.*

W.H. van der Spoel, E.R. van der Graaf and R.J. de Meijer.

Health Physics 74(1); 1998.

## Chapter 7:

*Foil coverage of a crawl-space floor: measurements and modelling of radon entry.*

W.H. van der Spoel, E.R. van der Graaf and R.J. de Meijer.

Accepted for publication in Health Physics.

Other publications:

*Measurements on and modelling of diffusive and advective radon transport in soil.*

E.R. van der Graaf, G.A.A. Witteman, W.H. van der Spoel, C.E. Andersen and R.J. de Meijer.

Radiat. Prot. Dosim., 56, 167-170, 1994.

*Radon transport in soil: Measurements on and modelling of diffusive and advective transport in a homogeneous column of sand.*

E.R. van der Graaf, G.A.A. Witteman, W.H. van der Spoel and R.J. de Meijer.

Annales de l'Association Belge de Radioprotection, 91, 335-350, 1994.

*Radon transport in soil.*

W.H. van der Spoel, E.R. van der Graaf and R.J. de Meijer.

Radiation protection research action. Euratom. Nuclear fission safety programme 1992-94; Final report EUR 16769 vol. 3, 3083-3093; 1997.

*Radon transport in building materials.*

E.R. van der Graaf, W.H. van der Spoel and R.J. de Meijer.

Radiation protection research action. Euratom. Nuclear fission safety programme 1992-94; Final report EUR 16769 vol. 3, 3124-3133; 1997.

*Modelling of radon transport in porous media.*

E.R. van der Graaf, W.H. van der Spoel and R.J. de Meijer.

To be published in the proceedings of the 7th Tohwa University International Symposium "Radon and Thoron in the Human Environment", Fukuoka, Japan; 1997.



# Nederlandse samenvatting

## Inleiding

In vrijwel alle natuurlijke materialen wordt het radioactieve edelgas radon gevormd uit sporen uranium die zich daarin bevinden. Als het materiaal een poreuze structuur heeft kan dit gas gemakkelijk via de vele kleine luchtgevulde gaatjes uit het materiaal ontsnappen. Radon bindt zich namelijk niet aan andere stoffen. Het transport van radon in zand, een poreus materiaal, vormt het onderwerp van dit proefschrift.

Poreuze materialen waaruit radon kan ontsnappen zijn de bodem en bouwmaterialen als beton, gips, en baksteen. De binnen- en buitenlucht bevatten daarom (een zeer kleine hoeveelheid van) dit onzichtbare en reukloze radioactieve gas. De radonconcentraties in de binnenlucht zijn echter hoger omdat binnen meer natuurlijk materiaal in de directe omgeving (vloeren, plafonds en muren) aanwezig is. Bovendien vormt een gebouw een enigszins afgesloten geheel waarin radon zich kan ophopen. Door inademing bevat ook de lucht in onze longen radongas.

Radioactieve stoffen kunnen verschillende soorten straling uitzenden. Radon en vervalproducten zenden alfadeeltjes uit. In feite zijn dit heliumdeeltjes (ontstaan van de elektronen) die met een grote snelheid worden uitgestoten. Net als een kogel kan zo'n alfadeeltje schade aanrichten bij botsing met andere materie. Daarom kunnen alfadeeltjes in onze longen schade toebrengen aan het levende weefsel. Het gevolg van deze schade is kans op longkanker. De vervalproducten van radon brengen overigens de meeste schade toe omdat zij zich hechten aan het longweefsel en daar, in direct contact met het weefsel, verder vervallen onder uitzending van alfadeeltjes.

In de Nederlandse woningen vervalt er per liter binnenlucht gemiddeld elke halve minuut een radondeeltje. In de buitenlucht zijn de radonconcentraties circa 10 maal lager. Op basis van deze concentraties wordt het aantal overlijdensgevallen in Nederland als gevolg van longkanker veroorzaakt door radon, op ongeveer 800 per jaar geschat. De Nederlandse overheid wil in de toekomst een limiet stellen aan de hoeveelheid straling, grotendeels afkomstig van radon, die mensen binnenshuis mogen ontvangen. Om effectieve en efficiënte maatregelen te kunnen treffen die een verlaging van de radonconcentratie bewerkstelligen, is inzicht vereist in de processen die verantwoordelijk zijn voor het binnentreden van radon in huizen. In de wetenschap wordt inzicht vaak verwoord in een model met als doel de processen wiskundig te beschrijven.

Kennis van radoninfiltratie in woningen kan en moet op verschillende niveaus en manieren worden verkregen. Enerzijds kan de distributie van radon in woningen worden bestudeerd *nadat* het gas uit een poreus materiaal is ontsnapt. De hoeveelheid radon die uit een materiaal (muren, bodem onder een huis) komt, ook wel de exhalatiesnelheid of bronsterkte genoemd, wordt dan als een gegeven beschouwd. Anderzijds kan men zich richten op het gedrag van radon *in* het poreuze materiaal zelf en de processen bestuderen die verantwoordelijk zijn voor de exhalatiesnelheid.

Een andere tweedeling is mogelijk door onderscheid te maken tussen onderzoek binnen en buiten het laboratorium. Buiten het laboratorium spreekt men ook wel van *in situ* onderzoek. Een voordeel van *in-situ* metingen is dat er inzicht wordt verkregen in processen die zich voordoen in realistische situaties. Een sterk nadeel is dat de omstandigheden hierbij niet goed gecontroleerd kunnen worden. In woningen hebben factoren als temperatuur, vochtigheid, regenval en wind invloed op het proces van radoninfiltratie. Bij onderzoek binnen het laboratorium kunnen de omstandigheden goed worden gecontroleerd, wat de mogelijkheid biedt systematisch te werk te gaan. Zo kan de temperatuur worden gevarieerd terwijl alle andere grootheden constant worden gehouden. Op deze manier kan de invloed van verschillende grootheden op radoninfiltratie- en transport stap voor stap worden onderzocht. Een nadeel is de lagere realiteitswaarde bij het bekijken van sterk vereenvoudigde situaties. Het is echter wel mogelijk meer realistische omstandigheden na te bootsen.

Het onderwerp van dit proefschrift betreft een laboratoriumonderzoek naar het gedrag van radon in een poreus materiaal waarbij de omstandigheden goed zijn gecontroleerd en gedefinieerd. Het doel van dit onderzoek is het toetsen van een (grotendeels bestaand) model dat het transport van radon in poreuze materialen beschrijft. Dit wil zeggen dat aan de hand van proeven wordt nagegaan of het model de werkelijkheid goed beschrijft. Voor deze toetsing moet de invloed van allerlei factoren nauwkeurig bekend zijn. Het vergaren van deze kennis is op zich al een omvangrijke taak. Het is dan ook verstandiger de omstandigheden zo te kiezen dat de invloed van deze factoren gemakkelijk te bepalen is. Tevens is het zinvol het aantal factoren te beperken. Laboratorium-omstandigheden en een eenvoudig natuurlijk poreus medium als zand zijn in dit opzicht optimale keuzes. Aangezien er complexere natuurlijke materialen dan zand bestaan, moet het onderzoek worden gezien als een eerste stap in het toetsingsproces.

## Radon transport

Er zijn een viertal processen die het transport van radon in een poreus materiaal (medium) beïnvloeden:

1. **Productie.** Radon wordt gevormd tijdens het radioactieve verval van radium dat als vervalproduct van uranium in alle natuurlijke materialen voorkomt. Een deel van het gevormde radon komt in de poriën terecht waarin transport kan plaatsvinden.
2. **Verval.** Een radondeeltje kan op elk moment vervallen maar na gemiddeld vier dagen is nog de helft van het oorspronkelijke aantal radonatomen over: de halveringstijd. Door het verval (radon verdwijnt) kunnen de concentraties niet onbeperkt toenemen.
3. **Diffusie.** In feite is diffusie de vermenging die automatisch optreedt als gevolg van het kris-kras door elkaar heen bewegen van de deeltjes in een gas en, in mindere mate, in een vloeistof. Dit resulteert in een netto transport van deeltjes van gebieden met hoge, naar gebieden met lage concentraties. Er wordt ook wel gezegd dat diffusie de concentratieverschillen opheft. Het is te vergelijken met warmtetransport. Stel dat een uiteinde van een metalen staaf warmer is dan het andere uiteinde. Door warmtegeleiding daalt de temperatuur aan de warme zijde en stijgt deze aan de koude zijde. Uiteindelijk zal de temperatuur overal in de staaf gelijk zijn en de temperatuurverschillen opgeheven. Een dergelijk proces vindt

plaats bij een gasgevulde buis waarin de concentraties aan beide uiteinden in eerste instantie verschillen. Door diffusie dalen de hoge concentraties en nemen de lage concentraties juist toe. Uiteindelijk zal de concentratie overal gelijk zijn. Diffusie van radon in poreuze media vindt voornamelijk plaats in de gasgevulde poriën.

4. **Advectie.** Bij advectie wordt radon door het poreuze medium meegenomen met een gasstroom. Deze stroming wordt veroorzaakt door (lucht)drukverschillen. Het is te vergelijken met het roken van een sigaret. Bij het nemen van een trek, is de druk in de mond lager dan buiten en stroomt er lucht door de sigaret (poreus medium) de mond in. Ondertussen neemt deze luchtstroom allerlei (schadelijke) gassen met zich mee. Deze gassen worden dan advectief getransporteerd.

Luchtdrukverschillen in en rondom een huis worden veroorzaakt door wind, veranderingen van de barometrische luchtdruk, mechanische ventilatie, en temperatuurverschillen. Een ventilator die lucht afzuigt naar buiten brengt de woning op onderdruk mits er geen lucht (actief) wordt toegevoerd. Een ander voorbeeld: in een verwarmd huis stijgt de warme lucht naar boven en verdwijnt daar deels naar buiten. De luchtdruk in het onderste gedeelte van het huis is dan lager dan buiten. Dit veroorzaakt niet alleen een inwaartse luchtstroom via de gevels maar ook via de bodem en de kruipruimte. Welk transportproces het sterkst is, diffusie of advectie, hangt van veel factoren af. Diffusie treedt in alle gevallen op, advectie alleen bij verplaatsing van de lucht door het poreuze medium.

## Onderzoeksopzet

Om het transport van radon in zand te onderzoeken is een cilindrisch roestvrijstalen vat gebouwd met een diameter en hoogte van twee meter. Een schematische afbeelding staat op blz. 38. Het vat is volledig gevuld met zand waarvan de korreltjes weinig in grootte van elkaar verschillen. Water kan aan het zand worden toegevoegd en afgevoerd via afsluitbare openingen in de bodem van het vat. Tijdens het vullen met zand werd getracht overal in de zandkolom een gelijke structuur te verkrijgen door, na elke laag van circa 20 cm dikte, het waterniveau in het vat enkele malen op en neer te bewegen. De bovenkant van het vat kan worden afgesloten met een in hoogte instelbaar deksel. De ruimte die daarmee onder het deksel ontstaat kan worden gezien als een kruipruimte.

Om ook advectief transport te kunnen onderzoeken is op een diepte van circa 1,6 m in het zand een ronde doos over bijna de gehele horizontale dwarsdoorsnede van de zandkolom geplaatst. De boven- en onderzijde van de doos bestaan uit geperforeerde metalen platen bedekt met een fijn metaal gaas. Het zand kan hier niet doorheen. De platen zijn gemonteerd op een funderingsrooster met een grote luchtdoorlatendheid in alle richtingen. Via een smalle buis die via de bodem van het vat verbonden is aan het centrum van de doos kan lucht worden toe- en afgevoerd. De doos verdeelt de lucht over een groot oppervlak waardoor de snelheid en richting van de luchtstroom in de porieruimte vrijwel onafhankelijk is van de plaats in de zandkolom. De lucht verdwijnt, of komt het vat binnen, via een kleine opening in het deksel.

Met behulp van holle naalden die op negen verschillende hoogtes radiaal tot het midden van het vat gestoken zijn, kan porielucht uit het centrum van de zandkolom worden onttrokken. Door deze lucht over te brengen in een luchtdicht flesje waarvan op één na alle wanden bedekt zijn met een materiaal dat licht uitzendt als het door alfadeeltjes wordt getroffen. Aan de onbedekte kant bevindt zich een fotobuis waarmee

de lichtflitsjes worden geregistreerd. Door het tempo te meten waarin alfadeeltjes in dit flesje lichtflitsen maken, wordt de radonconcentratie bepaald. Zo kan op elk tijdstip de radonconcentratie als functie van de hoogte, een zogenaamd radonprofiel, worden gemeten.

Als onderzoekstrategie werd een stap voor stap methode toegepast. In eerste instantie werd een zo eenvoudig mogelijk situatie bekeken (droog zand zonder deksel op het vat, geen luchtstroming) waarna de complexiteit stap voor stap werd vergroot. Na iedere stap volgde een serie metingen en een toetsing van het transportmodel aan de meetresultaten. Hiertoe werden de gemeten radonprofielen in het vat vergeleken met de uitkomsten van modelberekeningen.

## Eigenschappen van het zand

De radontransportprocessen (behalve verval) zijn afhankelijk van de eigenschappen van, en omstandigheden in het zand. Grootheden als porositeit, homogeniteit, vochtgehalte, tortuositeit, diffusie- en adsorptiecoëfficiënt, radiumgehalte, en emanatiecoëfficiënt zijn van belang in het model. Deze grootheden zijn zoveel mogelijk bepaald aan de hand van aparte metingen met kleine hoeveelheden zand. Als voornaamste reden kan worden aangemerkt dat het moeilijk is (of onmogelijk) de eigenschappen van het zand ter plekke in het vat te bepalen zonder de structuur van het zand te verstoren. De grootheden en de resultaten van de metingen worden puntsgewijs toegelicht:

- **Porositeit.** De verhouding van het volume tussen de korreltjes (porieruimte) en het totale volume is de porositeit. Deze is bepaald door de hoeveelheid water te meten nodig voor de verzadiging van een zandmonster met bekend volume. Het bleek dat na enkele malen verzadigen en drogen de porositeit daalde: het zand klonk in. Omdat tijdens het vullen van het vat het zand ook afwisselend werd verzadigd en gedroogd, werd de porositeit geschat op de waarde die het zandmonster bezat nadat dit proces enkele malen was doorlopen.
- **Homogeniteit.** Een belangrijk aspect van het transportmodel is dat wordt uitgegaan van een zandkolom met overal dezelfde porositeit. De juistheid van deze veronderstelling is (in het vat) nagegaan door lucht toe te voeren aan de geperforeerde doos waardoor een opwaartse luchtstroom in het zand wordt verkregen. De luchtdruk in de doos is onder deze omstandigheden iets hoger dan aan het oppervlak van het zand. Als het droge zand overal dezelfde porositeit heeft, neemt de luchtdruk lineair toe met de diepte in het zand. Uit metingen van de luchtdruk in het zand als functie van de positie in het vat werd geschat dat de variaties in de porositeit kleiner zijn dan 10%. Op basis hiervan werden de toegelaten verschillen tussen modelberekeningen en meetresultaten ook op 10% gesteld.
- **Watergehalte.** Deze grootte is een maat voor de verzadiging van de porieruimte met water: 0% is droog en 100% is volledig verzadigd. De diffusie-, adsorptie- en emanatiecoëfficiënt zijn afhankelijk van het vochtgehalte. Voor een modelvalidatie moeten deze afhankelijkheden bekend zijn. Daarnaast moet rekening worden gehouden met de oplosbaarheid van radon in water. Bij kamertemperatuur is de radonconcentratie in de porielucht ongeveer vier maal groter dan in het poriewater. Kennis van het vochtgehalte als functie van de hoogte in de zandkolom is ook vereist als een waterniveau in het vat is ingesteld. Hier komen we later op terug.

- **Tortuositeit.** De invloed van de vorm van de porieruimte op het transport in deze ruimte wordt bepaald door de tortuositeit. Het gegeven dat de radondeeltjes niet rechtdoor kunnen maar bij transport om de zandkorreltjes heen moeten is in deze grootheid verwerkt. Ook is het effect van vernauwing en verbreding van de poriën opgenomen. De tortuositeit is bepaald met elektrische geleidbaarheidsmetingen aan zandmonsters verzadigd met een zoute oplossing. De gevonden waarde komt waarschijnlijk goed overeen met die voor het zand in het vat. In het onderzoek is de tortuositeit alleen van belang voor diffusief transport in droog zand.
- **Diffusiecoëfficiënt.** De 'snelheid' van het diffusief transport wordt bepaald door de diffusiecoëfficiënt. Een grotere diffusiecoëfficiënt resulteert in een snellere vermenging en vereffening van concentratieverschillen. De diffusiecoëfficiënt voor radon in lucht en in water zijn door anderen eerder gemeten en is daarom bekend uit de wetenschappelijke literatuur. In (droog) zand moet wel rekening worden gehouden met een diffusievertraging omdat de deeltjes om de korreltjes heen moeten en omdat de poriegrootte niet constant is: de tortuositeit speelt een rol. Ook als radon aan het oppervlak van de korreltjes blijft plakken wordt het diffusieproces vertraagd (zie volgende alinea). Daarnaast is het aantal getransporteerde deeltjes afhankelijk van de porositeit. In vochtig zand is de situatie een stuk complexer en kan de diffusiecoëfficiënt in het zand niet uit deze basale grootheden worden berekend. De diffusiecoëfficiënt is daarom gemeten als functie van het vochtgehalte. Omdat diffusie in water veel trager verloopt dan in lucht, neemt de diffusiecoëfficiënt af met toenemend vochtgehalte.
- **Adsorptiecoëfficiënt.** Radon kan ook (tijdelijk) aan het oppervlak van een vaste stof blijven plakken. De mate waarin dit plaatsvindt wordt aangeduid met de adsorptiecoëfficiënt. Adsorptie verlaagt de radonconcentraties in de porielucht en heeft daarom een reducerend effect op diffusief en advectief transport. Metingen hebben echter aangetoond dat radonadsorptie in het zand te verwaarlozen is.
- **Radiumgehalte.** De hoeveelheid radium per kilogram stof is bepaald door de intensiteit van bepaalde gamma-straling te meten die door een bekende hoeveelheid zand wordt uitgezonden. Radium, dat alleen in de zandkorreltjes voorkomt, en enkele van de stoffen die tijdens het radioactief verval ontstaan, zenden deze relatief eenvoudig meetbare straling uit. Per seconde en per kilogram zand vervallen ongeveer vier radiumdeeltjes en vormen zo radon.
- **Emanatiecoëfficiënt.** Een deel van het gevormde radon blijft in de zandkorreltjes, en een deel komt in de porieruimte terecht. De laatste fractie wordt aangeduid met de emanatiecoëfficiënt. Deze grootheid is gemeten als functie van het vochtgehalte van het zand. Het bleek dat de emanatiecoëfficiënt het laagst is voor droog zand. Toevoeging van een klein beetje water tot een vochtgehalte van 0,5% doet de emanatiecoëfficiënt bijna verdubbelen. Daarna is deze vrijwel constant als functie van het vochtgehalte. Een verklaring hiervoor is dat in droog zand een zojuist gevormd radondeeltje (het heeft dan een snelheid) zich in een tegenoverliggend zandkorreltje kan boren en daarin achterblijven. Dit gebeurt minder vaak bij aanwezigheid van water in de poriën omdat het gevormde radondeeltje in water sterk wordt afgeremd.

## Experimenten

De experimenten met het vat kunnen grofweg in drie categorieën worden onderverdeeld. In volgorde van complexiteit zijn dat de experimenten met 1) droog zand met alleen diffusief en gecombineerd diffusief en advectief transport; 2) droog zand met een folie op het zandoppervlak; en 3) bevochtigd zand met alleen diffusief transport. De term 'droog zand' wordt hier gebruikt maar in feite is er sprake van zand met een laag vochtgehalte.

### Droog zand

De experimenten met droog zand begonnen met het onderzoeken van puur diffusief transport. In een aantal gevallen werd de zandkolom eerst doorgespoeld met buitenlucht om overal in de poriën een zeer lage radonconcentratie te krijgen. Meteen daarna werd de radonconcentratie in het zand als functie van de hoogte en de tijd gevolgd. Dit is uitgevoerd met het deksel op verschillende hoogtes. Tevens is het effect nagegaan van kruipruimteventilatie op het radonconcentratieprofiel.

De daaropvolgende experimenten met advectie werden grotendeels uitgevoerd door een constante luchtstroom in het zand teweeg te brengen door aan- of afvoer via de geperforeerde doos en de tijdonafhankelijke radonprofielen te meten voor verschillende constante debieten van de luchtstroom. Naast deze experimenten werden er ook een aantal uitgevoerd waarbij de luchtstroom werd gepulseerd, d.w.z. gedurende gezette tijden achter elkaar werd aan- en uitgezet. De radonconcentraties werden hierbij op twee verschillende hoogtes in het vat als functie van de tijd gemeten.

De meetresultaten werden vergeleken met de uitkomsten van modelberekeningen. Daartoe namen we aan dat het vochtgehalte van het zand in balans was met de vochtigheid van de omgevingslucht, hetgeen neerkomt op een vochtgehalte van 0.12% en een emanatiecoëfficiënt van 0.22. Helaas is de emanatiecoëfficiënt sterk afhankelijk van het vochtgehalte voor deze relatief droge condities. Een kleine variatie in het vochtgehalte, mogelijk als functie van de positie in het zand, geeft een grote variatie in de emanatiecoëfficiënt. Het zou geen probleem voor de modeltoetsing opleveren als het vochtgehalte in het vat nauwkeurig kan worden bepaald maar dit was helaas niet het geval. Ondanks deze onzekerheden kwamen alle modelberekeningen, gebruik makend van een constante emanatiecoëfficiënt, binnen 10% overeen met de meetresultaten.

Aan het einde van het onderzoek werd de porositeit van het zand in het vat gemeten. Omdat deze metingen de homogeniteit van het zand verstoren werden ze niet eerder uitgevoerd. De gemeten porositeit bleek 7% hoger te zijn dan eerder op basis van aparte metingen aan een klein zandmonster was bepaald. Blijkbaar was het zand in het vat minder ingeklonken dan geschat. Toepassing van deze 'nieuwe' porositeit in de modelberekeningen liet een verslechtering van de overeenkomst met de meetresultaten zien. Wordt echter rekening gehouden met de onzekerheden in het vochtgehalte en de daaruit voortvloeiende onzekerheden in de emanatiecoëfficiënt, dan leidt dit nog niet tot verwerping van het model. Een 7% hogere emanatiecoëfficiënt in de berekeningen doet de verslechtering namelijk grotendeels teniet. Het vochtgehalte was waarschijnlijk toch iets groter dan 0.12%. Desondanks geeft toepassing van de hogere porositeit en een aangepaste emanatiecoëfficiënt een minder goede overeenkomst tussen model en experiment. De grootste verschillen liggen in de orde van 15%. Dit wordt waarschijnlijk veroorzaakt door een inhomogene verdeling van het watergehalte. Doordat het zand alleen aan het oppervlak kon drogen is het zand dichtbij de bodem vermoedelijk vochtiger geweest.

## Droog zand met folie

Een volgende onderzoekstap werd gemaakt door het radontransport te bestuderen waarbij het oppervlak van het zand is bedekt met een radonremmend polyethyleen folie. Toepassing van een dergelijk folie op de bodem van een kruipruimte in woningen kan een maatregel zijn tegen radoninfiltratie via de kruipruimte naar de woning. Bij deze experimenten werd de tijdsafhankelijke radonconcentratie in de ruimte onder het deksel gemeten onder verschillende condities: met en zonder advection in het zand (de lucht stroomt dan langs kieren en gaten in en rondom het folie) en met en zonder een kunstmatig aangebrachte ronde opening (diameter 5 cm) in het midden van het folie. In navolging van de gehanteerde onderzoekstrategie zijn de eigenschappen van het folie (dikte en diffusiecoëfficiënt voor radon) met aparte metingen bepaald.

De modelberekeningen voor de experimenten met intact folie zijn overigens van een andere aard dan in de vorige serie experimenten omdat alleen het transport van en naar de kruipruimte daarin wordt beschouwd. Tevens werd daarin de invloed van schommelingen in de barometrische luchtdruk opgenomen. Bij een stijging van de luchtdruk stroomt er namelijk buitenlucht via het deksel het vat binnen en, via openingen in en langs folie, verder het zand in. Het omgekeerde proces vindt plaats bij een luchtdrukdaling. Deze luchtstromen tussen het zand en de kruipruimte resulteren in advectief radontransport dat niet verwaarloosd mag worden. Het model beschrijft de metingen zeer goed, behalve wanneer lucht via de doos wordt afgezogen. De modeluitkomsten zijn dan ongeveer 20% te hoog. Dit wordt waarschijnlijk veroorzaakt door de aanwezigheid gaten in en/of langs het folie.

In de berekeningen voor de experimenten met een opening in het folie werd tevens het transport in de zandkolom gemodelleerd. De invloed van luchtdrukschommelingen op het radontransport in het zand werd in het model verdisconteerd. Ook voor deze experimenten bleek de overeenkomst tussen model en experiment goed, behalve wanneer lucht via de doos wordt afgezogen. In tegenstelling tot de resultaten met intact folie, blijken de modeluitkomsten 20% tot 40% *lager* dan de meetresultaten. Dit lijkt niet logisch, maar ook hier geldt dat de afwijkingen kunnen worden veroorzaakt door lekken langs het folie.

We kunnen concluderen dat het transport van radon tussen het zand en de kruipruimte redelijk goed beschreven kan worden op basis van de gemeten eigenschappen van het zand en het folie. In sommige gevallen worden relatief grote afwijkingen tussen experiment en model gevonden maar dit is, gezien de onzekerheden omtrent de lekken langs het folie, geen reden om aan het transportmodel te twifelen.

## Bevochtigd zand

In de laatste serie metingen werd het effect van grondwater op het diffusief radontransport bestudeerd. Een grondwaterniveau werd ingesteld door water, via de bodem van het vat, het zand in of uit te laten lopen. Het grondwaterniveau is de positie van de waterspiegel in een fictief boorgat in het zand. Niveaus van 0, 40, 80, 120 en 160 cm diepte werden op twee verschillende manieren bereikt: door water toe te voegen aan droog zand (stijgend peil) en door water weg te laten lopen (dalend peil) uit verzadigd zand. Voor elk niveau werden dus twee situaties bestudeerd. Beide gevallen onderscheiden zich door een verschillende verdeling van het vochtgehalte boven het grondwaterniveau. Vanuit een situatie met verzadigd zand blijft, na het laten wegllopen van een deel van het water, meer vocht achter in het zand boven het grondwaterniveau dan bij toevoeging van water aan

droog zand tot op hetzelfde niveau. Voor beide uitgangssituaties en elk grondwaterniveau werd het tijdonafhankelijke radonconcentratieprofiel in de porielucht gemeten.

De vochtverdeling in het zand is apart gemeten met een standaard techniek waarbij een zandmonster op een waterverzadigde fijn-poreuze kolom wordt geplaatst. Door de druk in het water te variëren kunnen de verschillende posities boven het grondwaterniveau, voor beide uitgangssituaties, worden gesimuleerd.

De gemeten waterverdelingen en relaties tussen het vochtgehalte en de diffusie- en emanatiecoëfficiënt werden gebruikt in de modelberekeningen. De uitkomsten van deze berekeningen weken aanzienlijk af van de meetresultaten. Een opmerkelijk punt is dat de 7% hogere porositeit bij deze experimenten juist wel een betere overeenkomst opleverde. De verschillen bleven echter relatief groot en wezen in de richting van een andere vochtverdeling in het zand. Dit is nagegaan door de verdeling in het vat voor een dalend peil te meten, en in een kleinere kolom zand voor een stijgend peil. Beide metingen wezen inderdaad op een andere vochtverdeling. Voor een stijgend peil bleek het zand boven het grondwaterniveau vochtiger en voor een dalend peil juist droger. Hiermee was aangetoond dat de methode met de fijn-poreuze kolom geen betrouwbare resultaten oplevert.

De uitkomsten van de modelberekeningen waarin de 'nieuwe' waterverdelingen werden gebruikt lieten echter nog steeds afwijkingen zien ten opzichte van de metingen. Voor een stijgend peil overschatten de berekeningen de gemeten radonconcentraties met 5% tot 40%. De grootste verschillen vinden we voor een grondwaterniveau op 40 cm diepte. De reden kan zijn dat de gemeten vochtverdeling in de kleinere kolom zand ook niet goed overeenkomt met de situatie in het vat.

Voor een dalend peil zijn de verschillen maximaal 15% en zijn afhankelijk van de hoogte in het vat. Dit geeft aan dat de zandkolom mogelijk niet homogeen was met betrekking tot de porositeit en/of emanatiecoëfficiënt. Een andere mogelijkheid is dat het model niet alle transportprocessen (correct) beschrijft. In het laatste geval is onze kennis omtrent radontransport in vochtige materialen onvolledig.

## Conclusies

De laboratoriumproeven met het vat hebben aangetoond dat, binnen de onzekerheid van de gecontroleerde omstandigheden, radontransport in (kamer)droog zand en radonexhalatie uit het zand bevredigend door een transportmodel worden beschreven uitgaande van bekende transportprocessen en onafhankelijk gemeten eigenschappen van het zand. De omstandigheden zijn echter een stuk complexer wanneer water aan het zand is toegevoegd. De verschillen tussen de modelberekeningen en de metingen zijn in dit geval zodanig dat we moeten vaststellen dat het model niet alle processen adequaat beschrijft die in vochtig zand kunnen optreden en/of dat de veronderstelling dat de kolom in het model als homogeen beschouwd mag worden niet gerechtvaardigd is.

Het proefschrift heeft dus niet geleid tot een volledige beschrijving van alle processen maar heeft wel laten zien dat een systeem van lucht, korrels zand, water en radon dat door de korrels wordt geproduceerd, redelijk nauwkeurig kan worden beschreven. Het proefschrift geeft een basis voor de beschrijving van complexe situaties zoals die zich voordoen in de bodem rond een huis of in bouwmaterialen.



# Curriculum vitae

- 18 november 1968 geboren te Ridderkerk
- 1987 diploma VWO  
Dongemond College, Raamsdonksveer
- 1991 stage fysische oceanografie  
Marine Research Institute, Reykjavik (IS)
- 1993 diploma Technische Natuurkunde  
Technische Universiteit Eindhoven
- 1993 - 1997 promotieonderzoek  
Environmental Radioactivity Research and Consultancy Group  
Kerfysisch Versneller Instituut, Groningen



# Nawoord

Dit proefschrift had uiteraard niet tot stand kunnen komen zonder de medewerking en ondersteuning van veel mensen. Ik bedank iedereen die zijn of haar steentje hebben bijgedragen, op welke manier dan ook. Op deze plaats zou ik graag een aantal personen in het bijzonder willen bedanken voor hun inzet.

Allereerst wil ik mijn directe begeleider Emiel van der Graaf bedanken voor zijn nimmer tanende interesse voor allerlei discussies. Zijn kalmte, kennis van zaken, hulp bij de experimenten, didactische vaardigheden en humor waardeer ik zeer. Ook de prettige tijd die we hebben doorgebracht in Montreal en Rome zal me lang bijblijven. Mijn promotor Rob de Meijer bedank ik in de eerste plaats voor zijn aanbod, ruim vier jaar geleden tijdens mijn afstuderen, om het radononderzoek aan het KVI als promovendus voort te zetten. Ik ben hem erkentelijk voor de goede, vaak niet voor de hand liggende, suggesties voor experimenten en voor zijn kritische blik op al het schrijfwerk. Ik wil tevens mijn tweede promotor, prof. Van Dongen, bedanken voor de nauwkeurigheid waarmee hij het proefschrift heeft nagekeken en zijn waardevolle suggesties voor verbeteringen.

Ik bedank de leden van de kerncommissie, prof.dr. M.J.A. de Voigt en prof.dr. A. van der Woude, voor het doorlezen van het proefschrift en voor hun waardevolle voorstellen ter verbetering.

Op het experimentele vlak heb ik veel ondersteuning gekregen van Ron ten Have en Tjalling Nijboer. Ron ben ik dankbaar voor de technische assistentie, ook op computergebied, die hij altijd bereid was te verlenen. Tjalling bedank ik voor al zijn 'elektronische' bijdragen. Daarnaast wil ik Margit Goosen van de vakgroep Fysische Geografie in Haren bedanken voor haar 'bodemkundige' adviezen. Mijn speciale dank gaat ook uit naar Johan Messchendorp die als afstudeerder de tortuositeitsmetingen heeft verricht en daarnaast uitkomsten van het numerieke model heeft vergeleken met die van een Eindige Elementen programma. Verder ben ik dank verschuldigd aan Madito Witteman aan wie de mooie resultaten van de eerdere experimenten met het radonvat zijn toe te schrijven.

I would like to thank Claus Andersen for giving me the opportunity to work for two months at RISØ National Laboratory in Denmark and for his supervision during the project. It was a very fruitful and instructive period with many pleasant discussions.

Verder ben ik de medewerkers van de verschillende afdelingen van het KVI zeer erkentelijk voor hun bijdragen. Zonder hen was het onderzoek zeker niet mogelijk geweest. Ik bedank de fijnmechanische werkplaats voor het ontwerpen en maken van de instrumenten, de vacuümdienst en de tekenkamer voor de technische ondersteuning, alsook het softwarehuis. Rob Kremers bedank ik voor de hulp bij de keuze van meet- en regelapparatuur.

Rianne Swinkels ben ik dankbaar voor de vele secretariële klussen die ze voor me heeft willen doen. Ik bedank Marjan de Ruiter voor de hulp bij allerlei bijkomende zaken en voor het nakijken van de nederlandse samenvatting. Fred van Os ben ik dankbaar voor

het ontwerp van het omslag.

De vier jaren op het KVI heb ik als zeer plezierig ervaren. De fijne en gezellige samenwerking met (oud-) collega's Ilka, Cees, Louis, Joop, Gerald, Albert, Lars en Han, en kamergenoten Ioana, Ronald, Patrick en Pieter zal me lang heugen. Ik bedank ook alle andere KVI medewerkers voor de fijne werksfeer.

Ten slotte ben ik veel dank verschuldigd aan alle vrienden en familie die mij hebben bijgestaan tijdens de totstandkoming van dit proefschrift. Ik wil Frank bedanken voor zijn bijzonder inspirerende en opgewekte discussies. Janine, bedankt voor de steun die je me altijd hebt willen geven en voor het vertrouwen dat je in me hebt gesteld. Zonder jou zou het leven een stuk minder aantrekkelijk zijn!

Wim





# STELLINGEN

behorende bij het proefschrift

## RADON TRANSPORT IN SAND: A LABORATORY STUDY

1. Bij een overgang tussen twee verschillende poreuze media stellen Rogers en Nielson als voorwaarde dat de grootheid  $j/\epsilon$  continu is, waarbij  $j$  ( $\text{Bq m}^{-2} \text{s}^{-1}$ ) de radonactiviteitsflux per oppervlakte-eenheid van het materiaal is en  $\epsilon$  de porositeit. Bij een overgang dient echter  $j$  continu te zijn.

V.C. Rogers and K.K. Nielson, *Health Phys.* 60(6):807 (1991)

2. De diffusielengte voor radon in dun folie is geen inzichtelijke maat om aan te geven in welke mate het folie doorlatend is voor radon.

*Dit proefschrift*

3. Gezien het gebrek aan kennis omtrent de radoninfiltratie in Nederlandse woningen, is het onwaarschijnlijk dat een infiltratiemodel beschikbaar komt binnen de termijn waarop de overheid een stralingsprestatienorm voor verblijfsruimten wenst in te voeren.

4. Metingen van  $^{210}\text{Pb}$  in kustsedimenten laten grote variaties in de tijd zien die ruwweg overeenkomen met het  $^{210}\text{Pb}$ -gehalte in regenwater. Metingen van  $^{210}\text{Pb}$  in zowel regenwater als kustsediment kunnen daarom gebruikt worden om variaties over korte termijnen van sedimentatiesnelheden vast te stellen.

5. Uit recente onderzoeksresultaten<sup>(1)</sup> blijkt dat de verantwoording van het onderzoek in het kader van het STRATEGO-programma, naar maatregelen tegen radoninfiltratie uit de kruipruimte, berustte op de onjuiste veronderstelling dat de radonconcentratie in de kruipruimte ongeveer tienmaal hoger is dan de radonconcentratie in de woonkamer.

(1) *Landelijk onderzoek naar radon in woningen*, informatiebrochure voorlopige resultaten, Rijksinstituut voor Volksgezondheid en Milieu (RIVM) (1997)

6. Verder onderzoek naar de invloed van vocht op radontransport in poreuze media is alleen zinvol als de omstandigheden in het materiaal beter gecontroleerd kunnen worden dan mogelijk was met de proefopstelling gebruikt bij dit onderzoek.

*Dit proefschrift*

7. Met de intrede van home-shopping via het internet gaan we een stap terug in de tijd: de melkboer komt weer aan huis.

8. Voor een stringente toetsing van een model voor radontransport in poreuze media, dient de moleculaire diffusiecoëfficiënt voor radon in lucht nauwkeuriger bekend te zijn.

*Dit proefschrift*

9. Ondanks aanwijzingen dat de wisselwerking van zonne-activiteit en kosmische straling aanzienlijke invloed heeft op het aardse klimaat, wordt deze component in de politieke discussie over klimaatverandering stelselmatig buiten beschouwing gelaten.

N. Calder, *De grillige zon*, Segment (1997)

10. Uitgaande van het standpunt dat geen enkele plant -of diersoort op aarde nadelige gevolgen mag ondervinden van menselijke activiteiten, dienen we het verbruik van fossiele brandstoffen te beperken, de transitie naar toepassing van duurzame energiebronnen op korte termijn te realiseren, en een limiet te stellen aan het energieverbruik per hoofd van de bevolking.

H-P. Dürr, *Living with An Energy Budget: The 1.5 Kilowatt Society*. International conference on environment and society, La Habana, Cuba (1997)

11. Het verzoek van de overheid om zuinig met energie om te gaan, weerspiegelt zich niet in de inspanning die zij levert voor een optimale regeling van het verkeer bij verkeerslichtgeregelde kruisingen.
12. 'Milleniumprobleem' is een misleidende term voor de problematiek rond de overgang van het jaartal '99' naar '00' in computersoftware. 'Eeuwprobleem' zou een betere benaming zijn.
13. Als Jezus nu zou leven, zou hij een veelgevraagde talkshow-gast zijn.
14. Waarschijnlijk zal slechts één land, Luxemburg, aan alle normen kunnen voldoen voor toetreding tot de Economische en Monetaire Unie<sup>(1)</sup>. Dit illustreert dat de 'éénwording van Europa' voor meer dan één uitleg vatbaar is.

(1) *Intermediair* 1-2:17 (1998)

Groningen, februari 1998

Wim van der Spoel